Hereditary Sensory Neuropathy Type 1 secondary to *SPTLC1/2* mutations: pathogenesis and treatment

Umaiyal Kugathasan

UCL Institute of Neurology

PhD Supervisors:

Professors Mary Reilly and Linda Greensmith

Thesis submitted for the degree of Doctor of Philosophy

University College London

2020

Declaration

I, Umaiyal Kugathasan, confirm that the work presented in this thesis is my own. Where information has been derived from other sources, I confirm that this has been indicated in the thesis.

Abstract

Hereditary Sensory Neuropathy Type I (HSN1) secondary to *SPTLC1/2* mutations is a rare, slowly progressive sensory-motor neuropathy, leading to profound sensory loss and variable, but often severe, motor deficits. The genes *SPTLC1/2* encode for Serine Palmitoyltransferase, an essential enzyme in de-novo sphingolipid biosynthesis. *SPTLC1/2* mutations alter its substrate specificity, leading to the synthesis and accumulation of atypical metabolites, 1-deoxysphinigolipids (1-deoxySLs).

1-DeoxySLs have been postulated to be neurotoxic however the underlying pathomechanism has not been elucidated. L-serine oral supplementation is a potential therapeutic candidate but the lack of responsive outcome measures is an obstacle in carrying out a definitive clinical trial. The first objective of this thesis was to determine if 1-deoxySLs are neurotoxic and to investigate the mechanism of their toxicity using two in-vitro neuronal models: 1) mouse primary motor and DRG neurons and 2) human iPSC derived sensory neurons. The second objective was to identify a responsive outcome measure by carrying out a natural history study.

1-deoxySL treatment resulted in dose dependent neurotoxicity in both in-vitro models. Findings in the mouse in-vitro model suggest mitochondrial and ER dysfunction as possible mediators of 1-deoxySL toxicity. Probing further into ER dysfunction using SH-SY5Y cells suggests 1-deoxySLs cause early ER stress leading to the activation of the unfolded protein response. In the HSN1 iPSC derived sensory neurons there was increased production of 1-deoxySLs and early cell loss but no functional or structural ER and mitochondrial defects in these neurons at 5 months.

Assessments used in the natural history study included CMT Neuropathy score version 2, nerve conduction studies, quantitative sensory testing, computerised myometry, intra-epidermal nerve fibre density (thigh), MRI determined calf intramuscular fat accumulation, plasma 1-deoxySLs and patient based questionnaires. MRI determined calf muscle fat fraction showed validity and high responsiveness over 12 months and will be useful in HSN1 clinical trials.

Impact Statement

Applications of the research relevant to patient care

HSN1 is slowly progressive, lifelong condition, which over time causes significant disability due to profound sensory loss and resultant sensory complications and weakness. HSN1 patients require long-term intensive support. There is currently no treatment for HSN1 secondary to *SPTLC1/2* mutations. One of the key obstacles in undertaking a clinical trial in slowly progressive neuropathies is the lack of responsive outcome measures. In a rare condition like HSN1, limited patient numbers and marked phenotypic heterogeneity, require the outcome measure to be highly sensitive to change. The HSN1 natural history study has shown that MRI determined calf fat fraction is highly responsive over 12 months and could be used in a clinical trial. This study has also highlighted the limitations of using assessments such as nerve conduction studies, quantitative sensory testing and intra-epidermal nerve fibre density measures as outcome measures in progressive neuropathies.

As the result of these findings, a grant application is currently underway, led by Professor Reilly, for a double blind placebo controlled trial of L-serine in HSN1. The lessons and knowledge gained from using MRI determined fat fraction in an effective clinical trial in a rare inherited neuropathy like HSN1 will be useful in future clinical trials in a range of neuromuscular diseases.

A better understanding of the clinical phenotype will help with earlier diagnosis and counselling of patients.

Applications of the research relevant to academic colleagues

The development of a human iPSC derived sensory neuron model will provide a platform for investigating the effects of endogenous 1-deoxysphingolipids. Research on this model has continued in Professor Bennett's lab, Oxford with further phenotyping of the HSN1 iPSC derived sensory neurons and evaluation of the effects of L-serine supplementation on these neurons. This model can also be used to gain a better understanding of the sphingolipid biosynthetic pathway.

The in-vitro mouse model using primary motor neuron and DRG cultures provides another model that can be used to investigate the neurotoxic effects of 1-deoxysphingolipids. This model, in conjunction with the iPSC model, can be used to assess the reproducibility of pathomechanisms and can suggest phenotypes (both in-vivo and in-vitro) that can be tested in transgenic mouse models in potential pre-clinical trials.

There is emerging evidence that raised levels of 1-deoxysphingolipids are found in other diseases, including non-neurological diseases, and that they play a role in the pathogenesis. One such disease is diabetes. Better understanding of sphingolipid metabolism will enable manipulation of aberrant pathways for therapeutic use in diseases other than HSN1 which have considerably higher levels of prevalence.

Applications of the research relevant to Industrial Partners

The human iPSC derived sensory neuron model of HSN1 can be used in large scale studies of small molecule libraries with the potential for both biological insights and therapeutics.

Acknowledgements

Firstly, I must thank the patients who took part in the natural history study. I am truly grateful for the time they gave up for the study which included two long gruelling days of intense testing. It was a humbling experience meeting them. They are an inspiring group of people who met the challenges of their neuropathy with ingenuity, unending determination and humour.

I would like to thank my two supervisors, Professors Mary Reilly and Linda Greensmith. I thank Prof Reilly for giving me this opportunity and for her supervision, invaluable clinical teachings and inspiring work ethics. I thank Prof Greensmith for welcoming me into her lab, her supervision on the lab project and her guidance on thesis writing.

I am grateful to so many people who have helped me throughout the PhD years and who are responsible for many memorable moments. I thank Matilde for all her help with the natural history study, especially in obtaining the ethics approval. I would not have been able to carry out the primary motor neuron and DRG cultures without Bernadett's tutoring. I am grateful to Bernadett for putting up with a novice medic like me and my endless queries and lab disasters. The iPSC work would not have been possible without the tutoring of the iPSC extraordinaire, Alex Clark. I have only admiration for the endless patience, perseverance and magic touch that he has with iPSC derived neurons. I am also extremely grateful to Professor Bennet for giving me the opportunity to work with iPSC derived neurons in his lab and for his supervision. I have learnt a great deal from the incredible group of postdocs (Iulia, Andreas, John, Greg, Jorge, Annina, Simon and Steve) in his lab and I had the opportunity to witness clinicians and scientists working together cohesively and seamlessly to produce amazing research.

I am grateful to my fellow comrades in the MRC fellows' room (Alex Horga, Enrico, Pedro, Karen, Helen, Matt and Aisling) for keeping me sane and reminding me there was more to life than DRGs. I would also like to thank the team at Prof. Greensmith's lab (Emma, Charlotte, Barney, Mhoriam, Bilal, Ching-Hua, Leoni and especially Jim) for always being ready to lend a hand or trouble shoot a failed experiment. I would like to thank the formidable duo, Mariola and Iwona for all their help, especially in assisting with the skin

biopsies and for their practical no-nonsense advice. I would also like thank Jacky for her continued support and patience during this PhD.

Last, but not least, I would like to thank my husband, Mohan whose selflessness, patience and support had no bounds. Words cannot describe my gratitude- I would not have survived this PhD without him.

Table of Contents

List of Figures

List of Tables

Abbreviations

AraC	Cytosine β-D-arabinofuranoside
ATF3	Activating Transcription Factor 3
ATF6	Activating Transcription Factor 6
ATP	Adenosine triphosphate
BDNF	Brain-derived neurotrophic factor
BiP	Binding immunoglobulin protein
BNB	Blood nerve barrier
BSA	Bovine serum albumin
CDT	Cold Detection Threshold
CGRP	Calcitonin Gene Related Peptide
CHOP	C/EBP homologous protein
CMAP	Compound Muscle Action Potential
CMT	Charcot-Marie-Tooth Disease
CMTES	Charcot Marie-Tooth Examination Score
CMTSS	Charcot Marie-Tooth Symptom Score
CMTNSv2	Charcot Marie-Tooth Neuropathy Score version 2
CMTNSv2-R	Rasch modified version of Charcot Marie-Tooth Neuropathy Score version 2
CPT	Cold Pain Threshold
CSF	Cerebrospinal Fluid
DAPI	4’,6-Diamidino-2-phenylindole dihydrochloride

1-DeoxymethylSA	1-Deoxymethylsphinganine
1-DeoxySA	1-Deoxysphinganine
1-DeoxymethylSO	1-Deoxymethylsphingosine
1-DeoxySO	1-Deoxysphingosine
1-dSL	1-Deoxysphingolipids
DIV	Days in-vitro
DMA	Dynamic Mechanical Allodynia
DMEM	Dulbecco's modified Eagle's Medium
DMSO	Dimethyl sulfoxide
DRG	Dorsal root ganglia
EDTA	Ethylenediaminetetraacetic acid
ER	Endoplasmic reticulum
EtOH	Ethanol
FBS	Foetal Bovine Serum
FF	Fat fraction
GDNF	Glial derived Neurotrophic Factor
HBSS	Hank's balanced salt solution
HEK cells	Human Embryonic Kidney cells
HPT	Heat Pain Threshold
HSN1	Hereditary Sensory Neuropathy Type 1
IB4	Isolectin B4
IP^3R	Inositol 1,4,5-triphosphate receptor

IEFND	Intra-epidermal Nerve Fibre Density
iPSC	Induced Pluripotent Stem cell
IQR	Inter-quartile range
IRE1α	Inositol-requiring enzyme 1 alpha
KSR	Knockout serum replacement
MDT	Mechanical Detection Threshold
MEF	Mouse Embryonic Fibroblast cells
MPT	Mechanical Pain Threshold
MRI	Magnetic Resonance Image
NGF	Nerve Growth Factor
NF200	Neurofilament 200 (high molecular weight-200kD)
NMDAR	N-methyl-D-aspartate receptor
NPSI	Neuropathic Pain Symptom Inventory
NT3	Neurotrophin 3
PBS	Phosphate buffered saline
PDI	Protein Disulphide Isomerase
PERK	Protein kinase R-like ER kinase
Phgdh	3-phosphoglycerate dehydrogenase
Phospho-IRE1α	Phosphorylated Inositol-requiring enzyme 1 alpha
PPT	Pressure Pain Threshold
QST	Quantitative Sensory Testing
ROCK	Rho associated coiled -coin containing protein kinase

ROI	Region of interest
SA	Sphinganine
SEM	Standard Error of the Mean
SF-36v2	Short Form Health Survey version 2
SF-36v2-PC	SF-36v2-Physical Component
SNAP	Sensory Nerve Action Potential
SPT	Serine palmitoyl transferase
SO	Sphingosine
SRM	Standardised Response Mean
SSR	Sympathetic skin response
TG	Thapsigargin
TMRM	Tetramethylrhodamine methyl ester
TEM	Transmission Electron Microscopy
TRK A/B/C	Tropomycin-receptor -kinase A/B/C
TSL	Thermal Sensory Limen
UPR	Unfolded Protein Response
VDT	Vibration Detection Threshold
WDT	Warm Detection Threshold
WUR	Wind-Up Ratio

1. Introduction

1.1 Peripheral Neurons

The peripheral nervous system (PNS) is split into the somatic and autonomic systems. The somatic PNS consists of afferent sensory fibres and efferent motor fibres. Each spinal nerve is formed of two roots: (1) ventral root which consists of motor neuron axons and (2) dorsal root which contains the sensory fibres. The autonomic nervous system is responsible for internal organ homeostasis. The neurogenesis and maintenance of sensory and motor neurons involves a complex interplay of a multitude of intrinsic and extrinsic factors. This section focuses only on sensory and motor neurons as these are the predominant neuronal types affected in HSN1.

1.1.1 Sensory Neurons

Development

The dorsal root, as it emerges from the intervertebral neural foramina, forms the dorsal root ganglion (cell bodies of the peripheral sensory neurons). The peripheral sensory neurons in the dorsal root ganglia (DRG) transmit sensory information from the skin, bones, visceral organs and muscles and are sub-classified into (i) proprioceptors which sense body positions (ii) low threshold mechanoreceptors which sense touch, pressure and vibration (iii) thermoreceptors which detect innocuous cold or warm temperatures (iv) nociceptors which are activated by pain inducing high threshold stimuli and (v) pruriceptors which respond to itch inducing compounds (Liu and Ma, 2011).

Somatic sensory neurons are derived from the neural crest cells (NCCs). Following specific inductive signals, the neural crest cells delaminate from the dorsal neural tube and migrate along a ventral pathway and coalesce into DRG at regular intervals in the anterior half of each somite, adjacent to the neural tube (Marmigère and Ernfors, 2007). During this migration, sensory neurogenesis occurs in three successive waves. The first wave of neurogenesis involves a third of the NCCs and has limited cell division, producing on average 3.1 neurons. These cells give rise to large myelinated DRG neurons (Aβ- fibre

neurons) which include proprioceptors and mechanoreceptors (Marmigère and Ernfors, 2007). The second wave of neurogenesis involves the remaining NCCs and these on average produce 35.9 neurons each and lead to the formation of non-myelinated or thinly myelinated DRG neurons (C-fibre and Aδ fibre neurons respectively), all of which initially express tropomyosin-receptor-kinase A (TrkA) receptors. These neurons will become nociceptors, thermoreceptors, pruriceptors and C-fibre low threshold mechanoreceptors (detect gentle touch). The third wave of neurogenesis occurs much later with the cells involved originating from the boundary cap (cellular structure at boundary between PNS and CNS) and constitutes 5% of almost exclusively TrkA expressing DRG neurons (Marmigère and Ernfors, 2007).

Sensory neurogenesis is controlled by two pro-neural transcription factors Neurogenin 1 (Ngn1) and Neurogenin 2 (Ngn2). These early differentiation programmes are switched off by two homeobox class transcription factors, Brn3a and Islet1 which are expressed by all sensory neurons (Liu and Ma, 2011). The diversification into neuronal types is therefore orchestrated by transcription factors which not only induce and maintain expression of different growth factor receptors but also control their timely suppression to drive segregation into unique types.

Diversification into sensory neuronal types

Sensory neuron types can be delineated by the expression of neurotrophic factor receptors, tropomycin-receptor-kinase A (TrkA), TrkB, TrkC, Met and Ret receptor tyrosine kinases, which serve as receptors for the neurotrophins [nerve growth factor (NGF), brain-derived neurotrophic factor (BDNF) and neurotrophin 3 (NT3)], hepatocyte growth factor (HGF) and glial-derived neurotrophic factor (GDNF) family ligands respectively (Lallemend and Ernfors, 2012). These receptors are vital for cell survival, peripheral innervation of appropriate targets and expression of ion channels and receptors which determine the functional properties of the different sensory neurons. Large diameter DRG neurons conveying mechanoreception express Ret and/or TrkB (e.g. Neurofilament 200 positive neurons) whereas large proprioceptive neurons express TrkC. Small and medium sized neurons, most of which are nociceptors, express TrkA, Met and /or Ret (Lallemend and Ernfors, 2012).

Nociceptive neurons, which express TrkA, undergo two distinct differentiation pathways that lead to the formation of peptidergic and nonpeptidergic nociceptors. During development, about half the nociceptors switch off TrkA expression and begin to express Ret and become non-peptidergic neurons (Woolf and Ma, 2007). Most of these neurons bind isolectin B4 (IB4). The remaining nociceptors retain TrkA expression and become peptidergic neurons which also express calcitonin gene related peptide (CGRP) and substance P (SP).

Each sensory neuron type exhibits stereotypical termination patterns in the spinal cord as well as peripherally, either in specialised end organ structures or as free nerve endings. Individual sensory modalities are determined by the expression of unique set of channels and receptors. For example, TRPV1, a type of Transient receptor potential (TRP) ion channel, responds to heat, protons, toxins and capsaicin and activation of the receptor produces a painful burning sensation (Liu and Ma, 2011). There are various subtypes of low threshold mechanoreceptors. Meissner's corpuscles are an example. These are encapsulated nerve endings and respond to low frequency vibration (Jenkins and Lumpkin, 2017). DRG neurons are pseudo-unipolar with one axon that bifurcates into two separate branches. Myelinated nerve fibres consist of a single axon that is enveloped by a series of schwann cells (Geuna *et al.*, 2009; King, 2013). Adjacent schwann cells join at nodes of Ranvier and each schwann cell encapsulates the axon with concentric layers of schwann cell plasma membrane forming the myelin sheath. Unmyelinated nerve fibres are composed of several nerve axons enveloped as a group by a single schwann cell. In cutaneous nerves and dorsal spinal roots, unmyelinated fibres constitute about 75% of the axons (Geuna *et al.*, 2009).

1.1.2 Somatic Motor Neurons

Lower motor neuron cell bodes are located in specific brainstem nuclei and in the ventral horn of the spinal cord. They can be classified into three groups according to their target innervation: (i) branchial (located in the brainstem and innervate branchial arch derived muscles of the face and neck), (ii) visceral (belong to the autonomic nervous system and control smooth muscle and glands) and (iii) somatic (located in the Rexed lamina IX in the brainstem and the spinal cord and innervate skeletal muscles) (Stifani, 2014). The somatic motor neurons are further sub-divided into three types: (i) alpha motor neurons (innervate

extrafusal muscle fibres which are the main mediators of muscle contraction), (ii) beta motor neurons (innervate both extrafusal and intrafusal muscle fibres thereby control both muscle contraction and responsiveness of sensory feedback from muscle spindles respectively) and (iii) gamma motor neurons (exclusively control the sensitivity of muscle spindles) (Stifani, 2014).

In embryogenesis, following neurulation, the gradient expressions of several inductive signals are responsible for the dorso-ventral and rostro-caudal patterning of the neural tube. Sonic Hedgehog, a secreted glycoprotein, plays a critical role in motor neuron generation via its action in two temporally distinct phases. In the early signalling period, it induces neural plate precursors to become ventralised and in the late signalling phase, it drives the ventralized precursors into becoming motor neurons (Patani, 2016). Further specification of motor neurons enables the co-ordinated movement of distinct muscle groups (Davis-dusenbery *et al.*, 2014). Motor neuron precursors have unique subsets of transcription factors where each transcription factor has a distinct role in motor neuron specification. The motor neurons sub-types are further organised into discrete columns which extend along the rostro-caudal axis of the neural tube, reflecting their developmental origins and future function. Retinoic acid signalling plays a key role at this stage, contributing to diversification of motor neuron sub-types and the spinal cord columnar organisation (Patani, 2016).

1.1.3 Blood Nerve Barrier (BNB)

The BNB is located at the innermost layer of the perineurium and at the endoneurial microvasculature (Kanda, 2013). The main mode of transperineurial passage of substances is the paracellular pathway. This is regulated by belts of intercellular tight junctions (Reinhold and Rittner, 2020). The endothelial cells of the endoneurial vessels are normally non-fenestrated with adjacent endothelial cells being connected by continuous tight junctions (Kanda, 2013). However, the endothelial tight junctions are more permeable than those of the perineurium (Mizisin and Weerasuriya, 2011). These tight junctions are fairly leaky at birth and tighten gradually (Reinhold and Rittner, 2020). The BNB plays a critical role in protecting the endoneurial homeostasis. The endothelial cells forming the BNB express various receptors and transporters which play a role in importing essential compounds and eliminating toxic metabolites (Kanda, 2013). Impairment in BNB function

could therefore result in the entry of toxic compounds and immunoglobulins leading to neuronal damage.

The DRG consist of neuron rich region (NRR) and fibre rich region (FRR) and their respective epi-/perineurium. The blood DRG barrier is considerably more permeable than the BNB and the NRR contains a 7 fold higher density of capillaries (Reinhold and Rittner, 2020). Whilst the FRR shares many features of the BNB, the NRR is markedly different. It enables more contacts between neurons and blood, thus allowing more molecular exchange (Reinhold and Rittner, 2020).

As nerve fascicles approach sensory and motor end organs, the number of concentric perineural layers decreases (Mizisin and Weerasuriya, 2011). Although ultrastructural evidence is limited, it is likely that there is an open ended perineural sleeve for simple sensory formations/arborizations in connective tissue as well as naked nerve ending in intra-epidermal innervation (Mizisin and Weerasuriya, 2011). In rat motor neurons, the perineural sleeve ends just before it reaches the motor endplate where at its termination, the perineurium is open-ended (Burkel, 1967). The peripheral terminations of both sensory and motor neurons are therefore sites of increased blood-nerve exchange. Another key site with reduced blood nerve barrier properties is at the spinal root (Kanda, 2013).

1.1.4 Growth factor dependency of mature sensory and motor neurons

In sensory neurons, neurotrophins (NGF, BDNF, NT3, NT4) exert target dependent retrograde survival effect through binding and activation of high affinity tyrosine kinase receptors (Gould and Oppenheim, 2011). Studies of NGF and TrkA deficient mice show a complete absence of nociceptive sensory neurons (Klein, 1994). Similarly, different sub-types of motor neurons, respond to distinct neurotrophic factors (GDNF, ciliary neurotrophic factor-CNTF, insulin-like growth factor-IGF, hepatocyte growth factor-HGF, vascular endothelial growth factor-VEGF) or combinations of neurotrophic factors (Gould and Oppenheim, 2011). The neurotrophic heterogeneity is also the result of different sensory and motor neurons expressing unique combinations of neurotrophic receptors depending on target innervation, position and maturational stage of the neurons (Davidson *et al.*, 2012).

1.2 Genetic Neuropathies

Genetic neuropathies encompass a broad spectrum of diseases. The diseases range from those where the neuropathy is the sole or predominant feature of the disease to those where the neuropathy is a component of a multisystem disease, for example the mitochondrial disorder SANDO (Sensory Ataxia Neuropathy Dysarthria and Ophthalmoplegia).

The genetic neuropathies in which the neuropathy is the predominant or sole feature are collectively referred to as Charcot-Marie-Tooth (CMT) disease and related disorders (Rossor *et al.*, 2015). Within this group, there is again a spectrum ranging from neuropathies which are solely or predominantly motor, called distal hereditary motor neuropathies to hereditary sensory neuropathies, where there is purely or predominantly sensory involvement. CMT, a sensory-motor neuropathy, lies along the middle of this spectrum.

CMT is the commonest inherited neuromuscular disorder with an overall European prevalence estimated at 10-28 per 100000 (Pareyson *et al.*, 2017). The prevalences of distal hereditary motor neuropathy and hereditary sensory neuropathy are considerably less with distal hereditary motor neuropathy having a reported prevalence of 2.14 per 100000 (Pareyson *et al.*, 2017). CMT is a clinically and genetically heterogenous group of disorders characterised by sensory loss, weakness and muscle wasting, starting in the feet and later slowly progressing in a length dependent manner to involve the upper limbs. The advent of techniques to study nerve neurophysiology and pathology in the latter half of the 20th century, has enabled classification of CMT into two main sub-types: CMT1 (demyelinating) and CMT2 (axonal) based on upper limb motor conduction velocities (MCV). Demyelinating is defined as MCV below 38m/s and axonal as MCV greater than 38m/s (Harding and Thomas, 1980).

The genetic era of inherited neuropathies began with the discovery of the duplication in the short arm of chromosome 17 containing the peripheral myelin protein 22 gene as the cause of CMT1A. Since then, the field of inherited neuropathies has witnessed an explosion of gene discovery which has paved the way for understanding the molecular basis of many forms of CMT and related disorders. This has been facilitated by the evolution in genetic techniques from “first generation” sanger sequencing to next generation sequencing (NGS)

which allows multiple parallel sequencing of either targeted genes (panels), only the protein coding sequences (whole exome sequencing, WES) or the whole genome (whole genome sequencing). With advances in NGS, this technique has become increasingly more affordable and more practical in terms of timescale. The genetic advances have broadened the phenotypic spectrum of CMT and related diseases. They have also highlighted the complexity of genetic neuropathies whereby mutations in a single gene can have different clinical phenotypes and the limitations of the clinical features traditionally used to distinguish between acquired and inherited neuropathies (Rossor *et al.*, 2013).

1.3 The Hereditary Sensory (Autonomic) Neuropathies

In 1975, Dyck (Dyck, 1975) proposed a descriptive classification of hereditary peripheral neuropathies and introduced the term Hereditary Sensory Neuropathy (HSN). They concluded that there were at least 4 varieties of hereditary sensory neuropathies: a dominantly inherited variety (HSNI), a congenital sensory neuropathy (HSN II), familial dysautonomia (HSN III) and a congenital insensitivity to pain (HSN IV).

It was further subdivided in 1993 by Dyck *et al.* (1993) and in the presence of prominent autonomic features in some subtypes, it was renamed hereditary sensory autonomic neuropathy. This classification still largely stands today even following the discovery of causal genes (Auer-Grumbach, 2008) (Table 1.1). HSN is becoming the preferred term again due to the lack of prominent autonomic features in most of the sub-types. The presence of severe motor involvement in some cases creates a source of confusion by blurring the boundaries between HSN and CMT**.** For example, CMT 2B was initially classified as CMT due to the presence of severe distal weakness. However, the phenotype also includes severe sensory disturbance and ulcerations and hence could be included among the HSNs (Vance *et al.*, 1996).

The HSNs are a rare group of clinically heterogeneous disorders, ranging from phenotypes with pure sensory involvement, through phenotypes with variable motor involvement to almost pure autonomic neuropathies (Table 1.1). The molecular mechanisms that underlie HSNs are equally diverse and include disturbances in axonal transport, ion channel function and neuronal development.

1.3.1 Epidemiology

Within the United Kingdom, HSN1 secondary to mutations in *SPTLC1* is the commonest HSN (Davidson *et al.*, 2012), with most having the p.Cys133Trp mutations due to a founder effect in the United Kingdom (Nicholson *et al.*, 2002). However, in a European cohort (Rotthier *et al.*, 2009), mutations in RAB7 and NTRK1 (both 7%) were found to be the commonest mutations whilst mutations in *SPTLC1* was the third most common (2%). In both studies, where patients fitting the HSN phenotype were recruited, a genetic diagnosis was not possible in the majority (mutation frequency 14-19%) indicating that further HSN genes are yet to be identified.

Sub-Type	OMIM	Inheritance	Gene/ locus	Protein/mechanism	Clinical Features
HSN1A	162400	AD	*SPTLC1*	Encodes a subunit of Serine Palmitoyltransferase which catalyses the first step in de-novo sphingolipid biosynthesis. Mutations alter substrate specificity	Sensory-motor neuropathy (sensory predominant), lancinating pain, ulcero-mutilating complications
HSN1B	608088		*3p22-p24*		Sensory neuropathy with chronic cough and gastro-oesophageal reflux. Sensorineural hearing loss and lancinating pain frequently reported. (Spring *et al.*, 2005)
HSN 1C	613640		*SPTLC2*	Encodes a subunit of Serine Palmitoyltransferase. Mutations alter substrate specificity	Sensory-motor neuropathy (sensory predominant), lancinating pain, ulcero-mutilating complications
HSN1D	613708		*ATL1*	Encodes Atlastin-1, a dynamin-related GTPase which plays a part in the formation of tubular endoplasmic reticulum (ER) network and in axon elongation.	Sensory-motor neuropathy (sensory predominant), ulcero-mutilating complications, brisk reflexes common, cases with spasticity reported. Allelic with Hereditary Spastic Paraplegia SPG3A (Guelly *et al.*, 2011; Leonardis *et al.*, 2012)
HSN1E	614116		*DNMT1*	Member of the DNA methyltransferases which maintain patterns of methylated cytosine residues in mammalian genome.	Sensory neuropathy (infrequent motor involvement), sensorineural deafness and dementia (onset 30-40's) (Klein *et al.*, 2011).
HSN1F	615632		*ATL3*	Paralogue of ATL1. Mutations have a disruptive effect on ER structure.	Sensory neuropathy, distal lower limb bone destruction, ulcero-mutilations (Kornak *et al.*, 2014). Brisk reflexes reported (Fischer *et al.*, 2014)

Sub-Type	OMIM	Inheritance	Gene/ locus	Protein/mechanism	Clinical Features
CMT2B	600882		*RAB7*	Encodes a small Ras related protein, Rab-7, which is a Rab GTPase. This family of proteins has a major role in intracellular vesicle formation and transport and endosomal membrane tethering and fusion	Sensory-motor neuropathy, early motor involvement, ulcero-mutilating complications (Verhoeven *et al.*, 2003).
HSN2A	201300		*HSN2/ WNK1*	Nervous tissue specific exon of WNK1 which encodes a serine-threonine protein kinase. High level of expression of HSN2 containing isoforms in DRG cell bodies and axons.	Sensory neuropathy with mild or no motor involvement. Ulcero-mutilating complications. Mild/no autonomic dysfunction. Onset in early childhood/adolescent (Lafrenie *et al.*, 2004) .
HSN2B	613115		*FAM134B*	Member of ER resident receptors that bind to autophagy modifiers and facilitate ER degradation by autophagy (Khaminets *et al.*, 2015)	Exclusive or predominant sensory neuropathy, frequent severe ulcero-mutilating complications. Early onset (Kurth *et al.*, 2009).
HSN2C	614213	AR	*KIF1A*	Encodes a motor protein involved in anterograde transport of synaptic vesicle precursors along the axon.	Sensory-motor neuropathy. Early onset (1st decade). Mild autonomic involvement (Rivière *et al.*, 2011).
HSN2D	243000		*SCN9A*	Voltage gated sodium channel (Nav1.7). Loss of function mutations.	Sensory-motor neuropathy (sensory predominant). Associated with hyposmia, hearing loss and autonomic dysfunction (hypohydrosis/anhydrosis). Onset: infancy-adulthood (Yuan *et al.*, 2013).

Sub-Type	OMIM	Inheritance	Gene/ locus	Protein/mechanism	Clinical Features
HSN3	223900		*IKBKAP*	Component of Elongator, transcription elongation factor complex. Most are splice site mutations which results in premature truncated protein	Familial dysautonomia/Riley–Day Syndrome. Decreased sensitivity to pain and temperature, autonomic dysfunction (cardiovascular instability, gastrointestinal and respiratory dysfunction), absence of fungiform papillae of the tongue and scoliosis (Slaugenhaupt *et al.*, 2001). High carrier frequency in individuals of Ashkenazi or Eastern European Jewish extraction.
HSN4	256800		*NTRK1*	Neurotrophic Tyrosine Kinases receptor type 1 which encodes a high affinity nerve growth factor receptor Trk-A. Trk-A activation is required to support neurite outgrowth and survival of sympathetic ganglia neurons and nociceptive neurons in dorsal root ganglia	Congenital Insensitivity to Pain with Anhydrosis (CIPA). Lack of normal responses to pain, self-mutilating behaviour, anhydrosis, episodic fevers and mental retardation (Indo *et al.*, 1996; Indo, 2001).
HSN5	608654		*NGFβ*	Encodes Nerve Growth Factor beta. Belongs to the neurotrophin family of proteins which regulate neuronal survival, development and function	Loss of pain and temperature sensation, ulcero-mutilations, variable autonomic involvement and lack of mental retardation (Einarsdottir *et al.*, 2004).
HSN6	614653		*DST*	Encodes dystonin, which is member of family of proteins that bridge cytoskeletal filament networks.	Neonatal onset of hypotonia, respiratory difficulties, autonomic dysfunction , severe psychomotor retardation, distal contractures and early death (Edvardson *et al.*, 2012).

Sub-Type	OMIM	Inheritance	Gene/ locus	Protein/mechanism	Clinical Features
HSN7	615548	AD	*SCN11A*	Encodes voltage gated sodium channel (Nav 1.9). Possible gain of function mutation resulting in excess sodium influx and cell depolarization at rest	Congenital pain insensitivity, self-mutilations, multiple painless fractures, mild muscular weakness, delayed motor development and autonomic dysfunction (Leipold *et al.*, 2013).
HSN8	616488	AR	*PRDM12*	Encodes a family of transcriptional regulators. PRDM12 is expressed in nociceptors and their progenitors and participates in the development of sensory neurons	Congenital insensitivity to pain, large fibre sensory modalities mostly normal. Minor autonomic dysfunction (reduced sweating). (Chen *et al.*, 2015)
HSN with spastic paraplegia	256840	AR	*CCT5*	Chaperonin containing T-complex polypeptide1 subunit which is involved in the folding of cytoskeletal proteins	Sensory neuropathy, ulcero-mutilating complications and spastic paraplegia (Bouhouche *et al.*, 2006).
HSN and dementia		AD	*PRNP*	Encodes the prion protein.	Presenting with chronic diarrhoea in the 30s followed by autonomic failure, length dependent axonal predominantly sensory neuropathy and cognitive decline noted in the 40s or 50s. (Mead *et al.*, 2013)

Table 1.1 Classification of Hereditary Sensory Neuropathies (HSN)

OMIM: online Mendelian Inheritance in Man, *SPTLC1/2*: Serine Palmitoyl Transferase Long Chain base unit 1/base unit 2, *ATL1*: Atlastin GTPase 1, *DNMT1*: DNA Methyltransferase 1, *ATL3*: Atlastin GTPase 3, *RAB7*: RAS related GTP binding protein, *WNK1*: WNK lysine deficient protein kinase 1, *FAM134B*: Family with

sequence similarity 134, member B, *KIF1A*: Kinesin family member 1A, *SCN9A*: Sodium channel, voltage gated, type 9, α, *IKBKAP*: Inhibitor of k light polypeptide gene enhancer in B cells, kinase complex–associated protein, *NTRK1*: Neurotrophic tyrosine kinase, receptor, type 1, *NGF*: Nerve growth factor (b polypeptide), *DST*: Dystonin, *SCN11A*: Sodium channel, voltage gated, type 11, α, *PRDM12*:PRDI-BF1 and RIZ homology domain containing protein 12, *CCT5*: Cytosolic chaperonin-containing complex peptide-1, PRNP: Prion Protein, AR; autosomal recessive, AD: autosomal dominant

1.4 Hereditary Sensory Neuropathy Type 1 (HSN1) secondary to *SPTLC1/SPTLC2* mutations

1.4.1 Historical note

An early report of a phenotype resembling HSN1 dates back to 1852 by Nélaton who described familial neurotrophic plantar ulcers in three out of six brothers (Nélaton M, 1852). Hicks, in 1922, described a London family of 34 members, spread over 4 generations ,10 of whom had symptoms suggestive of HSN1 (relatively painless foot ulcers noted in early adulthood, later lancinating pain and deafness) (Hicks, 1922). Denny-Brown, in 1951, reviewed one of the cases from the same family (third generation) (Denny-Brown, 1951). From post-mortem findings, he concluded that this was a degenerative condition of the dorsal root ganglia. Since then, many other families have been reported with a phenotype consistent with HSN1.

1.4.2 Identification of the gene

The HSN1 locus was mapped to chromosome 9q22.1-q22.3 region following genome wide linkage screen in four large Australian kindreds (Nicholson *et al.*, 1996). Using fine linkage mapping this region was narrowed down further to a stretch of 3-4Mb (Blair *et al.*, 1997). The *SPTLC1* gene was one of seven genes encoding identified proteins in this linked region (Bejaoui *et al.*, 2001).*SPTLC1* along with *SPTLC2* and *SPTLC3* encode for separate subunits of the enzyme serine palmitoyltransferase (SPT). The *SPTLC1* gene comprises 15 exons spanning approximately 85kbp. In 2001, two groups discovered three missense mutations in the *SPTLC1* gene, each changing a conserved amino acid. Bejaoui *et al.* (2001) analysed the full DNA sequence of *SPTLC1* in 8 different HSN1 families and detected mutations in 2 different nucleotides of codon 133 (C133Y- German origin and C133W- Canadian origin) in exon 5 in 2 out of 8 families. Dawkins *et al.* (2001) discovered three mutations in 11 different HSN1 families: 8 families (most families were of English or Australian with English extraction) carried the C133W mutation, 2 families (Australian with

English/Scottish extraction) carried the V144D mutation on exon 6 and one family (Austrian/German origin) carried the C133Y mutation.

Nicholson *et al.* (2002) found that three Australian families of English extraction and four English families had the same mutation (C133W), same chromosome 9 haplotype and the same phenotype. Based on this, they concluded that the Australian and English families may have a common founder. Houlden *et al.* (2006) found a common haplotype across the *SPTLC1* gene and in flanking markers in six English HSN1 families suggesting a founder effect. Based on the size of the conserved haplotype, they estimated that the mutation occurred approximately 900-1600 years ago.

Two further mutations in *SPTLC1* were discovered in 2009. Rautenstrauss and Neitzel (Rautenstrauss and Neitzel , 2009) described a female patient with age of onset at 50 years. Her predominant symptom was distal, symmetric hyperaesthesia with no motor involvement detected on nerve conduction studies or EMG. She had a heterozygous missense mutation p.C133R. Up to this point, all the missense mutations reported in *SPTLC1*, were located within a 12 amino acid segment encoded by exons 5 and 6. Rotthier *et al.* (2009) reported a patient (French-Gypsy origin) with a de novo missense mutation downstream of this segment, p.S331F, with a severe congenital phenotype associated with microcephaly, severe growth retardation, vocal cord paralysis and sleep apnoea requiring non-invasive ventilation. Within the same study, they discovered another sequence variant in *SPTLC1,* p.A352V, in a patient with the typical phenotype of HSN but the pathogenicity of the variant could not be verified at that time as DNA from family members were not available for segregation analysis and the target amino acid is not well conserved in evolution. Both these mutations (S331F and A352V) were later proved to be pathogenic with functional studies assessing Serine Palmitoyltransferase (SPT) activity in-vitro and the presence of raised levels of plasma 1-deoxysphingolipids (1-deoxysphingolipids will be discussed in more detail in section 1.4.3) in patients with these two mutations (Rotthier *et al.*, 2011).

Another sequence variant, p.G387A, was identified in twin sisters with a phenotype consistent with HSN1 (Verhoeven *et al.*, 2004). Hornemann *et al.* (2009a) later demonstrated that this mutation was not pathogenic but instead a rare non-synonymous SNP. In-vitro studies showed that G387A mutation did not result in a change in SPT activity

and that G387A mutant can reverse the phenotype of a *SPTLC1* deficient cell line. Furthermore, this sequence variant was found in a homozygous state in an asymptomatic relative.

Mutations in *SPTLC2* were first described in 2010. *SPTLC2* gene comprises 12 exons spanning approximately 110kbp on chromosome 14q24.3-q31. Rotthier *et al.* (2010) reported three heterozygous missense mutations in *SPTLC2*: p.V359M (Austrian), p.G382V (German/Austrian) and p.I504F (Czech Republic). V359M and G382V mutations have the typical HSN phenotype but I504F is atypical with early age of onset (5 years) and anhydrosis. All three mutations were associated with raised plasma levels of 1-deoxysphinganine (1-deoxySA). Another mutation in *SPTLC2,* p.A182P, was later identified (Murphy *et al.*, 2013). Two female patients were identified with the age of onset younger than typical for HSN1. More recently, two mutations in *SPTLC2* (p.S384F and p.R183W) have been described which have similar phenotypes: late onset, slower progression and no lancinating pain (Ernst *et al.*, 2015; Suriyanarayanan *et al.*, 2016). The latest reported mutation in *SPTLC2,* has the typical HSN1 phenotype (Suriyanarayanan *et al.*, 2019).

As yet, no mutations have been identified in *SPTLC3.* A summary of the currently known mutations in *SPTLC1* and *SPTLC2* is shown in Table 1.2.

Variant	Age of onset	Clinical Features	Identified
SPTLC1			
p.C133W	Adolescent-adult	Predominant sensory neuropathy, ulceromutilations, lancinating pain	Bejaoui 2001 Dawkins 2001
p.C133Y	Adolescent-adult	Predominant sensory neuropathy, ulceromutilations, lancinating pain	Bejaoui 2001 Dawkins 2001
p.C133R	Adult (50)	Predominant sensory neuropathy	Rautenstrauss 2009
p.V144D	Adolescent-adult	Predominant sensory neuropathy, ulceromutilations, lancinating pain	Dawkins 2001
p.S331F	Congenital to early onset	Congenital: Insensitivity to pain, ulcerations, motor involvement, severe growth and mental retardation, microcephaly, vocal cord paralysis Early onset: Insensitivity to pain, ulcerations, motor involvement, juvenile cataracts	Rotthier 2009 Rotthier 2011
p.S331Y	Infant	Growth retardation, severe diffuse muscle wasting and hypotonia, prominent distal sensory deficit and bilateral juvenile cataracts	Auer-Grumbach 2013
p.A352V	16yrs	Predominant sensory neuropathy, lancinating pain. No ulceromutilations	Rotthier 2009
SPTLC2			
V539M	52yrs	Predominant sensory neuropathy, ulceromutilations	Rotthier 2010
p.G382V	adult	Predominant sensory neuropathy	Rotthier 2010
p.I504F	5yrs	Sensory neuropathy, ulceromutilations, anhydrosis	Rotthier 2010
p. A182P	1st decade	Predominant sensory neuropathy, ulceromutilations, prominent motor involvement	Murphy 2013
p.S384F	4th-5th decade	Sensory motor neuropathy (predominant sensory), ulceromutilations Macular telangiectasias, pyramidal signs	Ernst 2015 Triplett 2019
p.R183W	5th decade	Sensory-motor neuropathy	Suriyanarayanan 2016
p.N177D	2nd-6th decade	Sensory-motor neuropathy, ulcerations	Suriyanarayanan 2019

Table 1.2 Summary of the currently known *SPTLC1* and *SPTLC2* mutations

(Adapted from Rotthier et al.(2011)*)*

1.4.3 Clinical features

There is a large variability in the clinical presentation of HSN1 (Table 1.2). In the typical HSN1 phenotype, the onset is usually between the second to the fifth decades of life with slow progression thereafter (Rotthier *et al.*, 2012). A large study performed by Houlden *et al.*(2006) looking at 8 HSN families showed age of onset varying between 12-70 years with one patient still asymptomatic at the age of 89. Recently, mutations in *SPTLC1* (Rotthier *et al.*, 2009) and *SPTLC2* (Rotthier *et al.*, 2010) have been described which have congenital/early childhood onset (Table 1.2).

Pes cavus, pes planus and/or hammer toes may be present since childhood (Auer-Grumbach *et al.*, 2003). The initial symptoms are loss of pain and temperature sensation distally in the lower limbs which gradually progresses up the limbs. An early but transient period of hyperpathia can also be seen (Rotthier *et al.*, 2012). There is a length dependent dissociated sensory loss where pain and temperature sensations are affected earlier and more severely than joint position sense and vibration (Auer-Grumbach *et al.*, 2003; Houlden *et al.*, 2006). Painless ulcerations that are slow to heal are a frequent feature and can lead to complications such as osteomyelitis and amputations. Another common symptom, which is relatively unique, is the brief episodes of spontaneous lancinating pain in the limbs, (Auer-Grumbach *et al.*, 2003). There is considerable variation in motor weakness, ranging from no weakness to severe weakness (Houlden *et al.*, 2006). Variable autonomic involvement has been reported. Some studies have reported that there is no autonomic involvement (Geraldes *et al.*, 2004; Houlden *et al.*, 2006) whereas others have reported that there is frequent autonomic involvement consisting mainly of disturbances in sweating (Auer-Grumbach *et al.*, 2003; Davidson *et al.*, 2012; Rotthier *et al.*, 2012).

Houlden *et al.* (2006) noted that females had older age of onset and a milder phenotype. Another finding in the study is the earlier age of onset and often more severe disease phenotype in successive generations. The earlier age of onset could reflect closer monitoring of these individuals. The team also reported that there was significant variation in the phenotype within family members, which suggests that additional acquired factors as well as genetic factors contribute towards the clinical presentation.

With advances in genetic diagnosis, the phenotypic spectrum of HSN1 has broadened (Table 1.2). Mutations at the same locus on *SPTLC1,* S331F and S331Y, are associated with early onset severe phenotypes (Rotthier *et al.*, 2009, 2011; Auer-Grumbach *et al.*, 2013). Rotthier *et al.* (2009) described a severe congenital phenotype in a HSN1 patient with S331F mutation. The clinical features include congenital insensitivity to pain, microcephaly, severe growth retardation, vocal cord paralysis, bilateral cataracts, gastro-oesophageal reflux and sleep apnoea requiring non-invasive ventilation. Later, atypical phenotypes were also seen in patients with mutations in *SPTLC2.* I504F and A182P mutations were associated with early onset and anhidrosis was noted in patients with the I504F mutation (Rotthier *et al.*, 2010; Murphy *et al.*, 2013). Macular telangiectasias and pyramidal signs have also been noted in two generations of a single family with S384F mutation (Triplett *et al.*, 2019).

1.4.4 Neurophysiological findings

The most detailed neurophysiological assessment of HSN1 patients can be found in the study by Houlden *et al.* (2006). Overall, the findings showed a length dependent axonal sensory-motor (sensory>motor) peripheral neuropathy. Sensory potentials were absent in the lower limbs but were often recordable in the upper limbs. Motor studies showed greater variability between patients. Motor responses were often reduced in amplitude or absent in the lower limbs and normal or only moderately reduced in the upper limbs. Motor conduction velocities ranged from normal, to intermediate slowing (35-50m/s) to definitely in the demyelinating range (≤35m/s). Demyelinating features were most clearly seen in male patients.

Geraldes *et al.* (2004) described one patient (one out of three males from a family with the C133Y mutation) who had intermediate slowing of ulnar and peroneal motor studies. Dubourg *et al*. (2000), reported on a single patient from a large family with HSN1 phenotype with linkage to HSN-I locus on 9q22.1–q22.3 who had an ulnar motor nerve conduction velocity clearly in the demyelinating range at 31m/s with compound muscle action potential of 2.6mV. More recently, patchy motor conduction slowing has been reported in patients with *SPTLC2* mutations (Rotthier *et al.*, 2010; Murphy *et al.*, 2013; Triplett *et al.*, 2019).

1.4.5 Pathological findings

Denny-Brown (1951) performed a post mortem examination of a member of the family (third generation) described by Hicks (Hicks, 1922). This showed primary degeneration of dorsal root ganglia in a length dependent pattern. There was considerable loss of fibres in the dorsal columns and great loss of ganglion cells with severe degeneration of both the peripheral and central parts of the dorsal nerve roots. The ventral nerve roots were intact throughout. There was a diffuse perineural fibrotic connective tissue in the ganglia. In Hicks'a family and similar cases, the diagnosis was thought to be syringomyelia because of the sensory dissociation. However, there was no evidence of deformity of the cord in this autopsy.

Lindahl *et al*. (2006) described similar autopsy findings in a genetically confirmed HSN1 patient (T399G mutation) with symptom onset around the age of 68. The spinal cord showed moderate loss of myelinated nerve fibres from the dorsal column. There was moderate loss of dorsal root ganglion cells with evidence of satellite cell proliferation and scattered residual nodules of Nageotte. The sural nerve and the cutaneous branch of the radial nerve were moderately fibrotic and almost completely depleted of myelinated nerve fibres. The loss of peripheral nerve fibres was much more than would be expected for age. There was no significant abnormality of the vagus, coeliac or other sympathetic ganglia.

Sural nerve biopsies in the study by Houlden *et al.* (2006) (6 in total, 3 from the same family) were similar to each other. They were very few remaining myelinated fibres and the presence of stacks of flattened Schwann cell processes suggests there is also unmyelinated axon loss. There was very little to suggest regenerative activity. There were equivocal demyelinating features: teased myelinated nerve fibre preparation from the sural nerve of one patient showed two fibres possibly undergoing primary (segmental) demyelination. Electron microscopy revealed that numerous unmyelinated axons still remained and there were no abnormal inclusions in any cell type. The team also performed an autopsy on a male patient who died at the age of 81 with symptom duration of 49 years. There was mild to moderate loss of dorsal root ganglia neurons and the sites of ganglion cell degeneration were marked by nodules of Nageotte. The dorsal spinal roots were mildly fibrotic and

depleted of myelinated fibres. The anterior horn cells appeared to be well preserved at all levels and the ventral roots were relatively well preserved. The sympathetic trunk, superior and coeliac ganglia and the vagus nerve appeared normal. Sural nerve biopsy of a 62 year old patient with *SPTLC2* mutation (R183W), 12 years after symptom onset showed subtotal loss of myelinated fibres with the number of non-myelinated fibres being relatively preserved in all nerve fascicles (Suriyanarayanan *et al.*, 2016).

1.5 Exploration of the pathomechanism

1.5.1 Serine Palmitoyltransferase (SPT)

Sphingolipid biosynthesis

SPT belongs to a family of pyridoxal 5-phosphate (PLP)-dependent α-oxoamine synthases (POAS): SPT requires pyriodoxal 5 phosphate as a co-factor (Hanada, 2003). It catalyses the first and rate limiting step of de-novo sphingolipid biosynthesis. The first step is the condensation of serine with palmitoyl CoA (Figure 1.1). SPT strictly uses L-serine as its amino acid substrate and competition analysis of SPT activity with serine analogues (L-alanine, L-serinamide, D, L-serinol and L-serine methylester) indicated that all of the hydroxyl, carboxyl and amino groups of L-serine are needed for the recognition of the amino acid substrate by SPT (Hanada *et al.*, 2000). SPT is located on the outer membrane of the endoplasmic reticulum (Mandon *et al.*, 1992).

Interestingly, a recent study by Wei *et al.* (2009) demonstrated that in addition to the endoplasmic reticulum, the subunit 1 of SPT was also localised in focal cell adhesions and played a role in cell morphology. Knock down of SPT1 mRNA caused cell rounding. The localisation of SPT in focal adhesions disappeared when cells grew to confluence and reappeared when cells were induced to proliferate and spread to refill gaps made by scratch wound healing assay.

The de-novo pathway for sphingolipid biosynthesis can vary between species however the entry point catalysed by SPT is conserved across species (same in plants, fungi, bacteria and mammals) (Lowther *et al.*, 2012). Sphingolipids are lipids that contain sphingoid bases as a structural back bone. They are ubiquitous components of eukaryotic lipid membranes. Sphingosine is the most abundant of the sphingolipids with sphinganine being the second

most abundant. The sphingolipids are associated with a vast number of cellular processes ranging from mediating cell stress responses, regulating actin cytoskeleton to roles in cell survival (Hannun and Obeid, 2008). As well as having a single entry point, there is only one exit pathway mediated by sphingosine -1-phosphate (S1P) lyase which metabolises sphingosine -1-phosphate.

The sphingolipid biosynthetic pathway in its entirety is hugely complex (Hannun and Obeid, 2008). The individual components are intimately connected to each other providing a mechanism of regulating lipid production by interconnected network of positive and negative feedback. These pathways can occur in parallel, further adding to the complexity. Finally, as these lipids have hydrophobic properties, they are restricted to biological membranes. Sphingolipid metabolism is highly compartmentalised to avoid potential futile cycles of opposite anabolic and catabolic reactions (Lone *et al.*, 2019). Hence, sub-cellular and sub-membranous localisation of specific reactions also adds to the complexity. Where there is a lack of specific transport mechanisms, the site of generation of the sphingolipids will dictate the site of action. Another thing to bear in mind is that the cellular levels of the various bioactive sphingolipids vary greatly. For example, ceramide is often found in concentrations that are more than an order of magnitude higher than that of sphingosine. Therefore, small changes in ceramide levels can have profound changes in the level of sphingosine. A comprehensive understanding of the sphingolipid biosynthesis therefore requires integration of information in different planes and makes the task of predicting the effects of perturbations of a single component of the pathway very difficult.

SPT expression

In keeping with the ubiquitous presence of sphingolipids in eukaryotic lipid membranes, SPT activity is detected in many tissue types (Dickson *et al.*, 2000) however the level of expression varies between tissues (Weiss and Stoffel, 1997). SPT tissue distribution analysed in 3 month old mice by northern blot analysis revealed the highest expression in lungs and kidneys and lowest expression in muscle. Specific expression in peripheral nerves was not studied (Weiss and Stoffel, 1997). SPT activity is also determined by the

developmental stage of the tissue. Longo *et al*. (1997) assayed SPT activity in rat lung microsomes during foetal, neonatal and adult stages of development. SPT activity steadily increased from day 17 gestation to the neonatal period where the highest values of activity were detected. The activity plateaued in the adult lung.

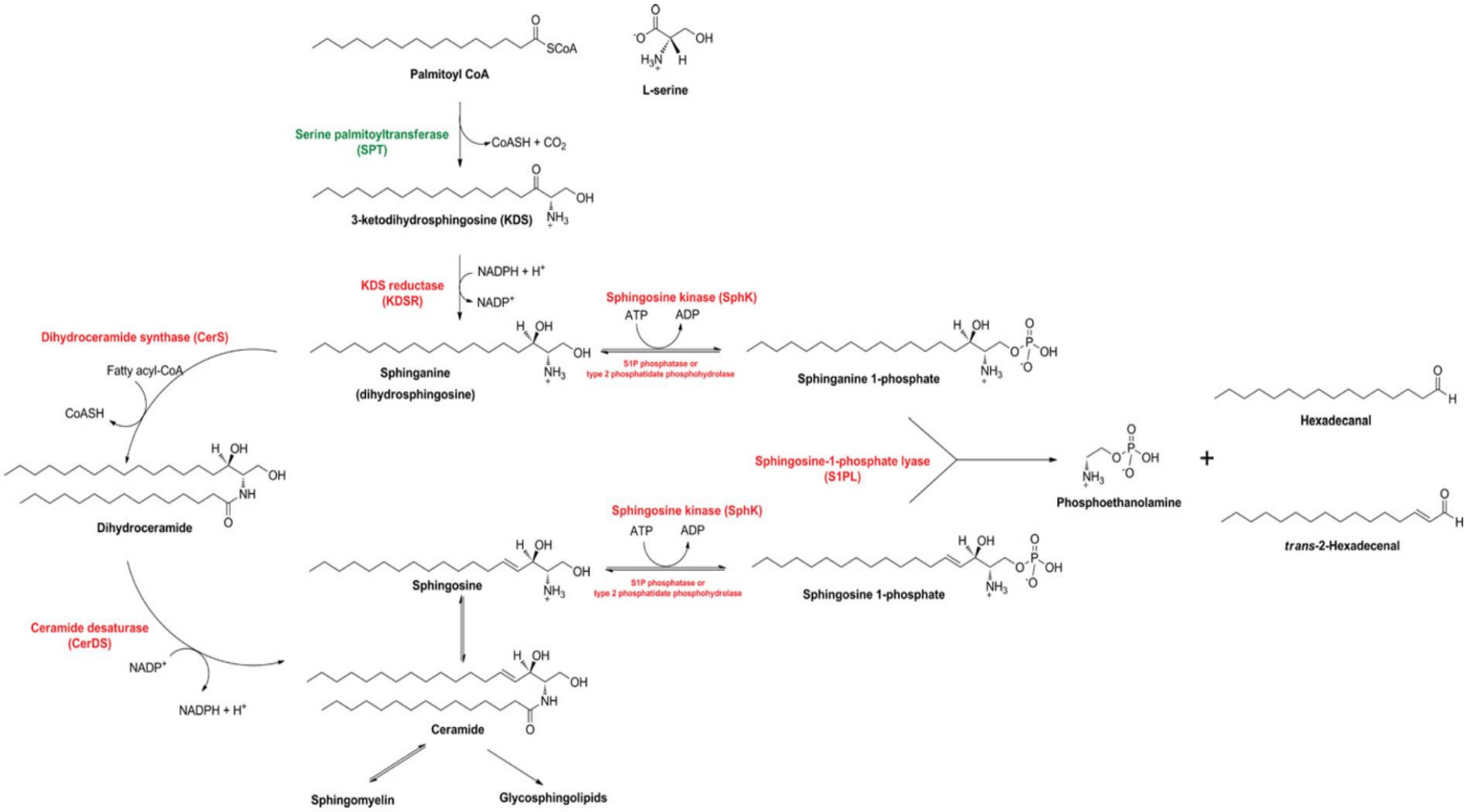
Palmitoyl CoA
L-serine
Serine palmitoyltransferase (SPT)
CoASH + CO2
3-ketodihydrosphingosine (KDS)
KDS reductase (KDSR)
NADPH + H+
NADP+
Sphingosine kinase (SphK)
ATP
ADP
S1P phosphatase or type 2 phosphatidate phosphohydrolase
Sphinganine (dihydrosphingosine)
Sphinganine 1-phosphate
Dihydroceramide synthase (CerS)
Fatty acyl-CoA
CoASH
Dihydroceramide
Sphingosine-1-phosphate lyase (S1PL)
Phosphoethanolamine
Hexadecanal
trans-2-Hexadecenal
Sphingosine
Sphingosine 1-phosphate
Ceramide desaturase (CerDS)
Ceramide
Sphingomyelin
Glycosphingolipids

Figure 1.1 De-novo sphingolipid biosynthetic and degradation pathway in mammals (from Lowther *et al.*, 2012)

There is a single entry point which is catalysed by serine Palmitoyltransferase, SPT (green), which is conserved amongst different species and a single exit point which is catalysed by sphingosine -1-phosphate lyase (S1PL). The other major enzymes in the pathway are labelled in red. Steps up to the point of ceramide synthesis occur exclusively at the ER. The downstream individual steps are compartmentalised within different organelles and are mostly reversible except for the last step catalysed by sphingosine-1-phosphate lyase.

SPT structure and regulation of its activity

Genetic analysis in yeast has shown that eukaryotic SPT consists of a heterodimer of 2 related subunits, LCB1 and LCB2 (Nagiec *et al.*, 1994) which is in keeping with other PLP-dependent α-oxoamine synthases (POAS). SPTLC1 and SPTLC2 are their mammalian counterparts. It is thought the heterodimer comprises a non-PLP-binding LCB1/SPTLC1 subunit and a PLP binding LCB2/SPTLC2 subunit (Lowther *et al.*, 2012). There has been no analysis of the PLP binding capacity of the two subunits as yet but the inability of the LCB1/SPTLC1 to bind the co-factor PLP has been inferred from sequence homology/alignment studies. LCB2/SPTLC2 has all the residues required for PLP binding and catalysis which are conserved among the POAS. LCB1/SPTLC1 has none of these residues (Lowther *et al.*, 2012). However, LCB2 is not expressed in the absence of LCB1 (Nagiec *et al.*, 1994).

A third mammalian subunit, SPTLC3 was identified by Hornemann *et al.* in 2006 (Hornemann *et al.*, 2006) which shows 68% homology to the SPTLC2 subunit and contains a PLP consensus motive. Quantitative real time PCR revealed that its expression was variable between different human tissues. Relative to SPTLC1 and SPTLC2, high levels of expression were seen in heart, kidney and placenta and low levels in brain and muscle. The same study demonstrated that over-expression of SPTLC3 in HEK293 cells, which otherwise have very little endogenous SPTLC3, led to a 2- to 3-fold increase in cellular SPT activity (similar increase seen with SPTLC2 over-expression but no increase noted with SPTLC1 over-expression). Silencing of SPTLC3 expression resulted in a significant reduction of cellular SPT activity. A later study by the same group has shown that SPTLC3 incorporated SPT has different substrate specificity and leads to the formation of different metabolites (C_{16}-sphinganine and C_{16}-sphingosine) (Hornemann, Penno, Rütti, *et al.*, 2009). These metabolites constitute a significant proportion of human plasma sphingolipids (15%).

The current consensus is that in eukaryotes such as yeasts and humans, SPT is a membrane bound heterodimer consisting of a SPTLC1 subunit associated with either a SPTLC2 or SPTLC3 subunit (Rotthier *et al.*, 2010) . In bacteria, it is a cytoplasmic homodimer. Yard *et al.* (2007) were the first to describe the structure of the bacterial (*Sphingomonas paucimobilis*) SPT at 1.3 Å resolution. The structure consists of a

symmetrical homodimer with two active sites. Models of the human SPTLC1/SPTLC2 heterodimer were created from the bacterial structure using bioinformatic tools. This model provides clues as to how the common mutations in *SPTLC1* can affect the activity of the enzyme. For example, the model predicts that the C133W mutation will result in a steric clash between Trp133 and the carbonyl oxygen of the active site lysine residue which anchors the PLP cofactor.

Hornemann *et al.* (2007) proposed a different model to the heterodimer. On pull down assays using lysates from HEK-293 cells and human placenta tissue, they demonstrated that all three subunits (SPTLC1-3) co-precipitated indicating that all three subunits are located within a simple complex. They proposed that SPT is not a dimer but a higher organised complex composed of three subunits (SPTLC1, SPTLC2 and SPTLC3) where the stoichiometry between SPTLC2 and SPTLC3 may vary depending on tissue specific expression.

A curious finding by Gable *et al.* (2000) and the subsequent discoveries have completely changed the view of SPT as a simple heterodimer. Gable et al discovered that a third gene, *TSC3,* was needed in addition to LCB1 and LCB2, for optimal de-novo sphingolipid synthesis in yeast. *TSC3* encodes a 80 amino acid membrane bound protein (Tsc3p) that co-immunoprecipitates with LCB1 and/or LCB2. Tsc3 mutant cells have reduced SPT activity but Tsc3p expression is not necessary for LCB1/LCB2 expression, stability or membrane localisation.

Since then several studies have found that there is a non-linear relationship between the level of expression of LCB1/LCB2 in over-expression models and SPT activity (Han *et al.*, 2009). For example, Han *et al*. (2004) noted that although co-expression of SPTLC1 with SPTLC2 subunit in mammalian cells increases SPT activity, the increased activity does not correlate with the levels of subunit expression. In addition, co-expression of LCB1 and LCB2 subunits from a variety of higher eukaryotes in yeast did not confer activity comparable to that measured in the organisms of origin (Han *et al.*, 2009). In 2009, two proteins, small subunit SPTa (ssSPTa) and small subunit SPTb (ssSPTb) were discovered (Han *et al.*, 2009) which enhance the activity of mammalian SPT (>10 fold) expressed in either yeast or mammalian cells. This results in the creation of different isoenzymes (SPTLC1+SPTLC2 or

SPTLC1+SPTLC3 combined with either ssSPTa or ssSPTb). The combination of SPTLC1+SPTLC2+ssSPTa led to the most enhancement in SPT activity. Given the fact that all three of these proteins co-purify, this led the team to conclude that these subunits were integral components of the SPT complex. When each SPT isoenzyme was expressed in either yeast or CHO cells lacking endogenous SPT activity, characterization of their in vitro enzymatic activities, and long-chain base (LCB) profiling revealed differences in substrate preferences (different chain length acyl-CoAs) between them and as a consequence, production of different chain length sphingoid bases.

It has been known for some time that SPT is homeostatically regulated by intracellular levels of sphingolipids. Mandon *et al.* (1991) demonstrated that murine cerebellar cells (microsomes) when treated with sphingosine of different alkyl chain lengths, had a concentration and time dependent decrease in SPT activity. Van Echten-Deckert *et al*. (1997) studied the effects of four different methyl-branched sphingosine analogues as well as cis-sphingogsine and 1-deoxysphingosine on sphingolipid biosynthesis in primary cultured neurons. Addition of all compounds led to a reduction in sphingolipid biosynthesis which paralleled the reduction in SPT activity. However, until recently, the mechanism underlying this regulation was unknown.

In yeast, Orm1/2 (genes *ORM1* and *ORM2*) have been discovered to associate with SPT and negatively regulate its activity. Their mammalian orthologues are the three ORMDL isoforms (ORMDL 1/2/3). Orm proteins belong to a family of transmembrane endoplasmic reticulum proteins. Absence of Orm1 and Orm2 proteins in yeast led to the accumulation (4.8 fold increase) of sphingolipids when compared to controls (Han *et al.*, 2010). This rise was abolished in the presence of myriocin which blocks SPT activity. In the same study, western blot analysis revealed that Orm2 co-immunoprecipitates with LCB1 and LCB2 indicating a physical interaction between the proteins. The mammalian ORMDLs also form a stable complex with SPT as measured by immunoprecipitation (Davis *et al.*, 2018).

Breslow *et al* (2010) also had similar findings using human cells. In addition, they discovered another protein, Sac1, in yeast. Sac1, a phosphoinositide phosphatase, was involved in the formation of the SPT complex and played a role in regulating its activity. Absence of Sac1 leads to increased de-novo sphingolipid production and resistance of

LCB1/2 to the inhibitor myriocin. Absence of both Sac1 and ORM1/2 is lethal. Their combined immunoprecipitation studies with mass spectrometry has revealed that Orm proteins bind with Sac1 thereby creating what is now called the “SPOTS” (Serine Palmityoltrasferase-Orm1/2-Tsc3-Sac1) complex. They also proposed a phosphorylation based feedback regulation of sphingolipid production in yeast whereby increased levels of downstream sphingolipids leads to hypophosphorylation of Orm1 and Orm2. The hypophosphorylated Orm1/Orm2 can then bind to the SPT complex and inhibit SPT activity. In support of this theory, they discovered that Orm1 and Orm2 contain several phosphorylation sites. Mutations at these sites lead to a significant reduction in sphingolipid production and the inability to phosphorylate maintains the attachment of Orm1/2 to the SPT complex. Finally, they noted that the level of Orm1/2 phosphorylation is determined by levels of downstream sphingolipids. Gururaj *et al.* (2013) have also found evidence in support of this feedback mechanism. Both Orm1 and Orm2 underwent rapid hypophosphorylation upon acute treatment with downstream SPT products. Mammalian ORMDLs are not regulated via this phosphorylation mechanism as they lack the stretch of amino acids located on the amino terminus which contains the phosphorylation sites. The level of association of the mammalian ORMDLs with SPT is the same in both high and low sphingolipid conditions indicating that ORMDL regulation of SPT is mediated by a conformational change in the ORMDL/SPT complex rather than by a regulated association of ORMDL with SPT or by changes in expression levels of either of these two proteins. Davis *et al.* (2019) have demonstrated a strict stereospecificity in the ability of ceramide to induce ORMDL dependent inhibition of SPT. Since stereospecificity is a hallmark of direct ligand binding, this suggests that ceramide directly binds to the ORMDL/SPT complex rather than exerting an effect by altering the lipid environment of the complex.

A recent study suggests that there is another regulator of SPT (Cantalupo *et al.*, 2015). In endothelial cells, Nogo-B (membrane protein of the endoplasmic reticulum primarily located in vasculature) directly interacted with SPT subunits, inhibited their function and led to increased production of nitric oxide. This raises the question of whether there are other tissue specific regulators of SPT.

Diet, especially during development, can affect SPT activity. Rotta *et al.* (1999) analysed SPT activity in hypothalamic microsomal fractions of rats pre and postnatally

undernourished (protein restricted) from 21 days gestation to 21 days postnatal. SPT activity was significantly lower in the undernourished rats when compared to the control group. Various biological and chemical stimuli have been shown to upregulate SPT activity transcriptionally and post-transcriptionally (Linn *et al.*, 2001; Hanada, 2003; Hannun and Obeid, 2008). Such stimuli include cytokines, ultraviolet B radiation, heat stress, chemotherapy (e.g. etoposide, daunorubicin).

Over the past few years there has been a dramatic expansion in the understanding of the sphingolipid biosynthetic pathway and its key enzyme, SPT. An important point to bear in mind is that increased flux through this de-novo sphingolipid biosynthetic pathway does not necessarily lead to an increase in downstream components unless further metabolic transformation is limited/saturated or inhibited (Hannun and Obeid, 2008). It is becoming increasingly clear that full understanding of the impacts of any perturbation in this pathway cannot be achieved by studying individual reactions in isolation or by compartmentalisation.

1.5.2 Effects of *SPTLC1/SPTLC2* mutations on SPT function

The early molecular background of HSN1 is confusing and contradictory. Initially, an increase in glucosyl ceramide synthesis (ceramide metabolite) was reported in cultured lymphoblasts from HSN1 patients (175% of that seen in controls) , with a possible pathomechanism being ceramide induced apoptosis (Dawkins *et al.*, 2001). This was thought to reflect increased SPT activity and mutations were proposed to have a (toxic) gain of function.

However, since then, corresponding mutations in various cell types have shown a decrease in SPT activity (Bejaoui *et al.*, 2002; Gable *et al.*, 2002). Evidence from mouse models suggests that haploinsufficiency is not the cause of the disease. Homozygous SPTLC1 knockout and SPTLC2 knockout mice are not viable however heterozygous SPTLC1 and SPTLC2 knockout mice are viable. They have marked reduction in SPT activity however no neuropathy was documented (Hojjati *et al.*, 2005; Eichler *et al.*, 2009). This favoured the emerging theory that these mutated SPTLC1 subunits competed with the wild-type subunits for SPTLC2 binding, forming inactive complexes and creating a dominant negative effect. Gable *et al.* (2002) were the first to propose this idea. Their study demonstrated that HSN1

like substitutions in yeast LCB1 catalytically inactivated SPT when co-expressed with wild-type alleles and also that the mutant protein (lcbp1) retains its ability to interact with the wild-type lcbp2 protein. Bejaoui *et al.* (2002) probed further and showed that overproduction of mutant LCB1C133Y or LCB1C133W subunits in CHO (Chinese Hamster Ovarian) cells inhibited SPT activity despite the presence of wild-type LCB1 subunits.

However, reduced SPT activity by itself was not a sufficient explanation for the pathomechanism in HSN1. Reduced SPT activity is not associated with decreased total sphingolipids. Dedov *et al.* (2004) noted that despite a 44% reduction in SPT activity in EBV transformed lymphocytes from HSN1 patients with C133W mutation, the lipid composition, cell proliferation and apoptosis were unchanged when compared to control cell lines. The reduction in activity of the SPT is suggestive of equal amounts of active and inactive enzyme and not consistent with a dominant negative effect. They also noted that there was an overlap in SPT activity between controls and patients with some controls having SPT activity levels lower than that of patients.

Similar findings were reported by McCampbell *et al.* (2005), who created transgenic mice that ubiquitously over-expressed either wild-type ($SPTLC^{WT}$ mice) or mutant SPTLC1 ($SPTLC1^{C133W}$ mice). The $SPTLC1^{C133W}$ mice had decreased SPT activity however there was no difference in lipid composition between the $SPTLC1^{C133W}$ mice and $SPTLC^{WT}$ mice. There was however an increase in a subset of ceramides (C16:0 and C18:0 fatty acids). These are precursors of glucosylceramide, previously reported to be elevated in HSN1 lymphoblasts (Dawkins *et al.*, 2001). The mutant mice developed age dependent sensory changes (noted at 10 months) where they were significantly more sensitive to thermal pain. There was no difference between the two groups to von Frey, pinprick or acetone (cold) stimuli. Unlike HSN1 patients, none of the mice developed ulcerative mutilations. In terms of motor involvement, hind leg hyperkinesis was noted at 6-8months but this remained stable and other measures of motor performance (e.g. rotarod) were normal up to 10 months (sacrificed at 10 months). The aged mice showed a loss of myelinated fibres in the ventral and dorsal roots with preservation of unmyelinated fibres. The g-ratio (the ratio of axon diameter to overall fibre diameter) was significantly increased in the ventral roots of the $SPTLC1^{C133W}$ mice reflecting myelin thinning but no difference was noted in the dorsal roots. There was no significant difference in the gross appearance of the DRG. There was also no

change in the large fibre neurofilament positive and peptidergic neurons however there was a significant reduction in the number of non-peptidergic IB4 positive cells.

There was also autonomic involvement. Autopsy performed on some of the mice showed exocrine pancreatic degeneration (acinar cells largely replaced by fatty infiltrates) with absence of neuritic staining in regions of the acinar cells. Gastro-intestinal transit assays showed reduced smooth muscle motility in SPTLC1^{C133W} mice with normal morphology of the smooth muscle wall suggesting that the delayed transit was related to neuronal dysfunction. Although there are some parallels between the HSN1 patients and this mouse model, there are several features unique to the mouse model such as the early autonomic involvement and the phenotype is considerably milder than that seen in patients at comparable ages.

Following on from the work of McCampbell *et al.*, Eichler *et al.* (2009) reported that the mutant SPTLC1 protein is not inherently toxic. The phenotype of the above mentioned SPTLC1^{C133W} mice was reversed when these mice were crossed with transgenic mice over-expressing wild-type SPTLC1. The team performed behavioural assays in older SPTLC1^{C133W} mice and noted that the hyperpathia previously reported at 10months disappeared at 12 months and by 14 months, the mice became hypopathic. By 14 months, these mice showed significant deficits in mechanical sensitivity (von Frey) and hotplate testing. At this age, significant deficits in motor function (rotarod) were also noted. The double transgenic mice showed no evidence of a neuropathy following detailed behavioural and morphological studies despite continuing the assessments to 22 months of age.

The pivotal finding in how the mutations in *SPTLC1/2* cause disease came in 2008 when Hornemann *et al*. (2008) reported on the accumulation of two atypical sphingolipids (1-deoxysphingolipids) in lymphoblasts of HSN1 patients and corresponding increase in 1-deoxysphingolipids (1-deoxySLs) in the plasma of HSN 1 patients. Penno *et al*. (2010) showed that in cultures of HEK293 cells expressing the mutant SPTLC C133W (HEK_{C133W}) and C133Y (HEK_{C133Y}), there was an accumulation of an unknown metabolite which was not observed when SPT activity was blocked by myriocin. Analysis with liquid chromatography-mass spectrometry revealed two distinct metabolites: 1-deoxysphinganine (1-deoxySA, m18:0) and 1- deoxymethylsphinganine (1-deoxymethylSA, m17:0). This was noted to occur

as a result of the shift in the SPT substrate specificity. Gable *et al*.(2010) showed that the mutant SPT enzyme in yeast only had a two-fold greater K_m (K_m = concentration of substrate at which the reaction achieves half Vmax which is the maximum rate of a reaction) for serine than wild-type enzyme (1.4 versus 0.75mM respectively) with V_{max} of 275 and1350pmol/mg/min respectively. However, the mutant SPT utilised L-alanine better than wild-type SPT. K_m and V_{max} of approximately 9.6mM and 110pmol/mg/min for mutant SPT. The wild-type SPT did not efficiently utilize alanine, precluding direct measures of enzyme kinetics. The K_i (inhibitor constant=concentration required to produce half maximum inhibition) for alanine inhibition of serine utilisation by the mutant enzyme is similar to that of wild-type SPT. This constellation of findings led the authors to speculate that the major effect of HSN1 mutation is not to facilitate L-alanine binding but to allow bound L-alanine to react with acyl-Co A substrate.

Bode *et al.* (2016) compared 17 SPT mutants, the majority of which were identified in HSN1 patients, for their enzymatic activity and substrate affinity. None of the mutations resulted in a reduced formation of canonical C_{18} sphingoid bases. Mutations resulting in typical HSN1 phenotypes *(*STPLC1p.C133W, p.C133Y and SPTLC2p.A182P, p.G382V, p.S384F) clustered around the active site whereas mutations *(*STPLC1p.S331F, p.S331Y and SPTLC2p.I504F) associated with a more severe phenotype were located on the surface of the protein. These three mutations also resulted in increased canonical activity as well as 1-deoxySL and C_{20}sphingolipid formation. It is possible that the more severe phenotype seen with these mutations is the result of altered interactions with the small subunits ssSPTa and ssSPTb. Mutation in ssSPTb has been linked with increased C_{20}sphingolipid formation and neurodegenerative changes in the eyes and brain of mutant mice (Zhao *et al.*, 2015).

1.5.3 1-Deoxysphingolipids

1-deoxySLs are evolutionarily conserved and have been found in fungal and lower invertebrate species (Lone *et al.*, 2019). 1-deoxySA was first isolated from the arctic clam *Spisula polynyma* as part of a screen for anti-cancer agent (Cuadros *et al.*, 2000). Originally named Spisulosine (ES-285), treatment with it led to reduction in cell growth and altered cell morphology with absence of actin stress fibres which are important for cell adhesion. It was

tested as an anti-cancer drug in several phase I trials and was associated with dose limiting adverse effects which included hepatic and neurological toxicity (sensory-motor neuropathy +/- associated with pain) (Schöffski *et al.*, 2011; Vilar *et al.*, 2012).

Almost a decade later, Penno *et al.* (2010) in their seminal paper published in 2010, probed further into the link between 1-deoxySLs and HSN1. They demonstrated that HSN1 mutations (C133W and C133Y) induced a shift in substrate specificity whereby the mutated SPT is able to use alanine and to lesser extent glycine instead of the canonical substrate serine to form 1-deoxySA and 1-deoxymethylSA respectively (Figure 1.2). Addition of alanine to the culture medium produced a 3-4 fold increase in 1-deoxySA without significantly altering the level of 1-deoxymethylSA. Conversely the addition of glycine produced a 10 fold increase in the level of 1-deoxymethylSA.

1-deoxySA and 1-deoxymethylSA lack the C_1 hydroxyl group and hence cannot be converted to higher sphingolipids such as phosphosphingolipids and glycosphingolipids or be degraded by the conventional pathway via sphingosine-1-phosphate lyase as this requires formation of a phosphoester bond at C_1. As a result, they accumulate. There is however limited N-acylation and desaturation of these two 1-deoxySLs by ceramide desaturase to form 1-deoxy-ceramide and 1-deoxymethyl- ceramide (Zitomer *et al.*, 2009). These in turn are converted to 1-deoxysphingosine (1-deoxySO) and 1-deoxymethylsphingosine (1-deoxymethylSO) by ceramidase. The ceramides synthesised in the ER are translocated to the Golgi to be converted into complex sphingolipids via either a ceramide transporter protein or in vesicles. Fluorescently labelled (dihydro)ceramide analogue was shown to be trafficked to the Golgi however the 1-deoxy(dihydro) ceramide did not localise to the golgi (Kok *et al.*, 2002). Therefore, the 1-deoxySLs do not appear to undergo the typical trafficking of traditional ceramides. Also, the position of the carbon-carbon double bond in 1- deoxySA is distinct from that of the canonical position and indicates that the metabolism of 1-deoxySA deviates from that of canonical sphingolipids (Steiner *et al.*, 2016). Interestingly, the glycine derived 1-deoxymethylSA seems to follow the traditional metabolic pathway.

A recent study by Alecu *et al*. (2017a) suggests that the notion of considering these 1-deoxySLs as “dead end metabolites” might not be strictly correct. They identified eight 1-

deoxySL downstream products which appear to be formed by the action of cytochrome P450 (CYP4A) enzymes. Inhibition and induction of these enzymes resulted in blocking and stimulating the formation of the downstream metabolites, respectively. However, compared to the canonical sphingolipid catabolism which occurs within minutes to hours, the conversion of 1-deoxySLs occurs over days. Nuclear receptor, peroxisome proliferator-activated receptor (PPARα) regulates the genes *CYP4A* and *CYP4F.* Fenofibrate, a clinically used PPARα agonist has been shown to lower plasma 1-deoxySLs in dyslipidemic patients (Othman *et al.*, 2015a).

Penno *et al*. (2010) showed that that the serum levels of 1-deoxySLs are elevated in all HSN1 patients (C133W, C133Y and V144D mutations). Low levels of 1-deoxySA is detected in wild type cells and plasma of control subjects but to a significantly lesser degree than in mutant cell lines.1-deoxymethylSA is only detected in mutant cell lines and plasma of HSN1 patients. They assessed the plasma 1-deoxySL levels in a large family with the C133W mutation and their data suggested a correlation between disease severity and plasma levels of 1-deoxySLs. Yeast cells and CHO-LysB cells expressing mutant SPTLC1 (C133W) were also found to have raised 1- deoxySL levels when compared to controls (Gable *et al.*, 2010). Raised 1-deoxySL levels were also found in HEK293 cells expressing mutant SPTLC2 (V359M, G382V and I504F) and HSN patient lymphoblastoid cell lines (SPTLC2 mutations G382V and I504F) (Rotthier *et al.*, 2010). Eichler *et al.* (2009) demonstrated that these 1-deoxySLs were significantly raised in the plasma and sciatic nerves of transgenic mice over-expressing mutant SPTLC1 (SPTLC1^{C133W} mice) when compared to their wild-type counterparts. In phenotypically uninvolved areas such as the brain, there was little or no accumulation of 1-deoxySLs.

Penno *et al*. (2010) also investigated if these deoxysphingolipids were neurotoxic. The 1-deoxySLs appear to be neurotoxic to avian in-vitro DRG and motor neuron cultures. 1-deoxySLs caused a dose-dependent reduction in neurite length at concentration ranges seen in the plasma of patients. 1-deoxySA was more toxic than 1-deoxymethylSA and DRGs were more vulnerable to the neurotoxic effects than motor neurons.

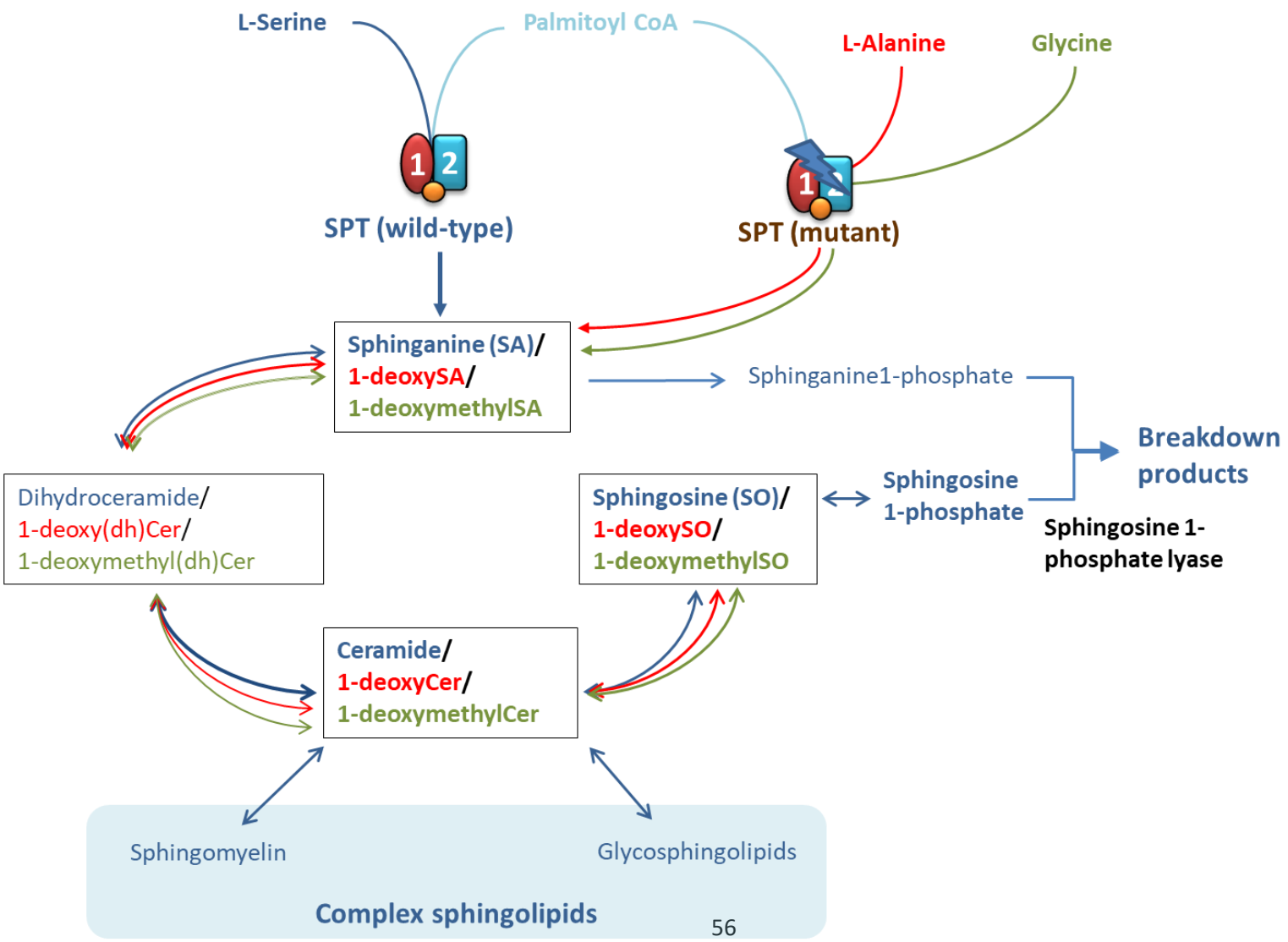
L-Serine
Palmitoyl CoA
L-Alanine
Glycine
1
2
SPT (wild-type)
SPT (mutant)
Sphinganine (SA)/
1-deoxySA/
1-deoxymethylSA
Sphinganine1-phosphate
Breakdown products
Dihydroceramide/
1-deoxy(dh)Cer/
1-deoxymethyl(dh)Cer
Sphingosine (SO)/
1-deoxySO/
1-deoxymethylSO
Sphingosine 1-phosphate
Sphingosine 1-phosphate lyase
Ceramide/
1-deoxyCer/
1-deoxymethylCer
Sphingomyelin
Glycosphingolipids
Complex sphingolipids

Figure 1.2: Abbreviated pathway for the biosynthesis of canonical sphingoid and 1-deoxysphingoid bases.

This diagram summarises the key steps of the biosynthesis of the traditional sphingoid bases produced from condensation of L-serine with palmitoyl-CoA in blue. Mutations in *SPTLC1* and *2* alter its substrate specificity, enabling the enzyme to use alanine and to a lesser extent glycine to form 1-deoxysphinganine and 1-deoxymethylsphinganine respectively. The analogous metabolic steps are shown in red for mutant SPT derived 1-deoxysphinganine and in green for mutant SPT derived 1-deoxymethylsphinganine. The 1-deoxysphingoid bases lack the C1-hydroxyl group of sphinganine which prevents the addition of a head group to form complex sphingolipids and also blocks their degradation as the essential catabolic intermediate sphingosine-1-phosphate cannot be formed.

The discovery of these atypical 1-deoxySLs led Garofalo *et al.* (2011) to undertake a treatment trial of L-serine on transgenic mice over-expressing SPTLC1 (C133W). They noted a suppression of 1-deoxySA production in HSN1 mutant HEK293 cells with increasing concentration of L-serine in the media (Figure 1.3). This indicated that the deoxysphingolipid production could in theory be overcome by increased systemic availability of L-serine.

Transgenic mice over-expressing mutant SPTLC1 (C133W) supplemented orally with L-serine led to a significant reduction in plasma 1-deoxySA levels within three days of treatment. No significant change was noted on behavioural assessments with 2 month supplementation of L-serine starting at 13 months of age. Long term supplementation (10 month duration) starting at 2 months of age resulted in a significant improvement in rotarod performance and a trend towards improved mechanical sensitivity (von Frey). Importantly however, no differences were seen on hotplate testing after short or long term treatment. L-serine treatment had no effect on axon density of myelinated sciatic nerves but led to two fold increase in the number of unmyelinated nerve fibres when compared to the untreated group. The group also performed a pilot study of oral L-serine supplementation in HSN1 patients (C133Y mutation). 14 patients were treated with either low or high dose L-serine (200 or 400mg/kg/d respectively) for 10 weeks. A significant lowering of plasma 1-deoxysphingolipid levels was seen in both groups (greater reduction seen in the higher dose group) with a nadir at 6 weeks. Neurological symptoms were not assessed due to the short duration of the treatment and no significant side effects were reported.

Fridman *et al*. (2019) have recently completed a randomised, placebo- controlled trial of L-serine (400mg/Kg) with open label extension in 18 patients with HSN1 in the United States. The primary end-point was the Charcot-Marie-Tooth Neuropathy Score (CMTNS). Secondary end-points used in the study were nerve conduction studies, autonomic function tests, intra-epidermal nerve fibre density measurements (distal leg and proximal thigh),and patient based questionnaires, Neuropathic Pain Scale and the 36-item Short Form health questionnaire (SF-36). The primary outcome, defined as the proportion of patients progressing more than 1 point on the CMTNS at 1 year, was not significantly different between the L-serine and placebo groups.

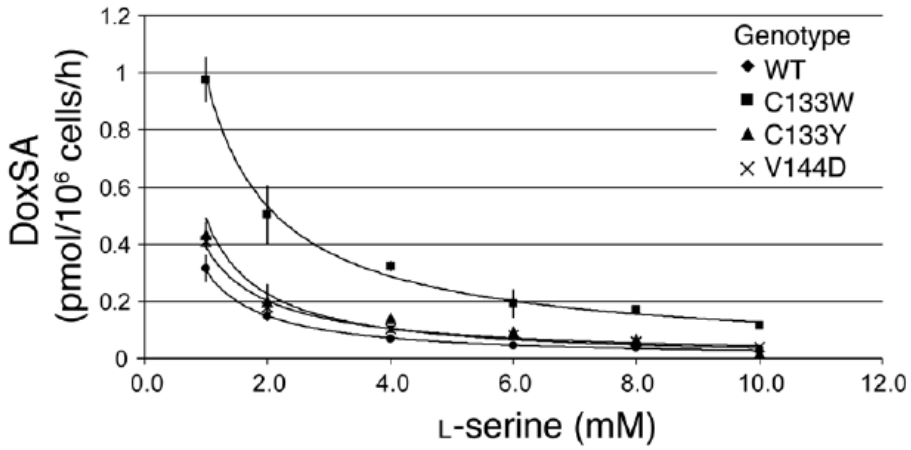

Figure 1.3 Kinetic characterisation of SPT (from Garofalo *et al.* 2011)

Suppression of 1-deoxySA (DoxSA) generation in SPTLC1 wild-type and HSN1 mutant expressing HEK293 cells at increasing L-serine medium concentrations (constant background of 2mM L-alanine)

However, it was reported that the L-serine group experienced an improvement in CMTNS relative to the placebo group (-1.5units, 95% CI:-2.8 to -0.1, p=0.03). No significant treatment effects were seen in the secondary end-points. There were also no significant adverse effects observed during the two years of the study.

1.5.4 Pathomechanism of 1-deoxysphingolipid induced neurotoxicity

Despite these rapid advances towards a possible treatment option for HSN1 patients, the exact pathomechanism underlying the neurotoxic effects of these 1-deoxySLs remains to be discovered.

Toxicity of 1-deoxySA varies greatly between different cell types. Fibroblasts can tolerate relatively high concentrations of 1-deoxySA whereas cells of neural origin are far more susceptible (Lone *et al.*, 2019). Glia are the main suppliers of L-serine to neurons in-vivo (Jun *et al.*, 2015). Glia in the peripheral nervous system tend to ensheath axon in a much lower ratio than in the CNS. This distinct environment of the peripheral sensory and motor neurons might lead to greater production of 1-deoxySLs due to alterations in the L-serine/L alanine ratio.

Different mechanisms for 1-deoxySL mediated toxicity have been proposed. Mechanisms suggested by early studies of 1-deoxySA as an anti-tumour agent include de novo ceramide synthesis and activation of PKCζ (protein kinase C which is involved in apoptotic responses) and caspases (3 and 12, involved in the execution phase of cell apoptosis) (Salcedo *et al.*, 2007; Sánchez *et al.*, 2008).

In in-vitro models of HSN1, studies have suggested that the 1-deoxySLs may mediate cellular toxicity via an ER stress response. It was observed that GADD153, an ER stress response protein, was induced in un-transfected CHO-LysB cells grown in 1uM 1-deoxySA and was increased in cells expressing mutant SPT (Gable *et al.*, 2010). Later studies have showed further evidence of ER involvement in the pathogenicity. Prolonged exposure of MEF (mouse embryonic fibroblasts) cells to toxic concentrations of 1-deoxySA induced splicing of X-box binding protein 1 (XBP1) and led to morphological changes of the ER (Alecu *et al.*, 2017b). XBP1 is an unfolded protein response (UPR) specific transcription

factor. Accumulation of unfolded/misfolded proteins, which can occur for various reasons (perturbations in ER homeostasis, oxidative stress, hypoxia, increased protein production) activates the adaptive cellular response, UPR (Cao and Kaufman, 2013). UPR increases the ER protein folding capacity, reduces global protein production and enhances ER associated degradation of misfolded proteins. SPTLC1 mutant lymphoblasts derived from HSN1 patients have decreased levels of BiP (ER stress marker) and ERO1-Lα (responsible for maintaining reduction potential of ER) (Myers *et al.*, 2014).

Mitochondria have also been suggested as potential molecular targets of the 1-deoxySLs. Mitochondria in SPTLC1 mutant lymphoblasts derived from HSN1 patients had altered morphology but no demonstrable alteration in function (Myers *et al.*, 2014). Another study using SPTLC1 mutant lymphoblasts has shown increased levels of ubiquinol-cytochrome c reductase core protein 1, which is an electron transport chain protein, in the mutant lines (Stimpson *et al.*, 2014). Alecu *et al.* (2017b) demonstrated that exogenous 1-deoxySA predominantly localises to the mitochondria and induces mitochondrial fragmentation and dysfunction in MEF cells. Exogenous 1-deoxySA also caused alterations in the morphology of mouse DRG neurons. Of note, the 1-deoxySA toxicity was rescued by inhibition of ceramide synthase activity and suggests that N-acylated deoxySA metabolite might be the agent causing the toxicity.

1-DeoxySLs could also have an impact on axonal growth. Jun *et al.* (2015) showed that DRG cultures from transgenic mice overexpressing the C133W mutant exhibited increased neurite length and branching with restoration of the normal growth patterns following L-serine supplementation or removal of L-alanine. This coincided with increased p-ERM expression in the neuronal growth cones. ERM proteins (ezrin/radixin/moesin) tether actin filaments to the cell membrane when phosphorylated and are important for neurotrophin mediated chemotactic growth in sensory neurons (Marsick *et al.*, 2012). Penno *et al.* (2010) however, observed a dose dependent reduction in neurite number and length following 1-deoxySL treatment in chick primary motor neuron and DRG cultures.

Structurally, 1 -deoxySLs differ from their canonical counterparts by the lack of C1 hydroxyl group and the double bond position. This could have implications for the biophysical

properties of membranes. Canonical ceramides are more miscible with sphingomyelin bilayers than 1-deoxyceramides (Jiménez-Rojo *et al.*, 2014). The presence of these 1-deoxyceramides could have a large impact on membrane structure and integrity.

Marshall *et al*. (2014) found a significant increase in lipid droplets in HSN1 patient derived lymphoblasts without a parallel increase in adipophilin which is involved in the regulation of lipid metabolism. They postulated that dysregulation of lipid metabolism might play role in the pathogenesis of HSN1. Similar accumulation of lipid droplets has not been reported in other studies using HSN1 in-vitro models.

Effects of 1-deoxySLs have also been evaluated in cortical neurons (primary neuronal cultures isolated from cerebral cortex of mouse embryos). Guntert *et al.* (2016) showed that as was the case with primary motor and DRG neurons, 1-deoxySLs were neurotoxic (mitotoxic, increased cell death, disruption of cytoskeleton structures) to cortical neurons. Metabolism to 1-deoxyceramide species was found to be largely responsible for 1-deoxySA mediated toxicity and resulted in NMDAR (N-methyl-D-aspartate receptor) activation. The toxicity can be significantly reduced by using NMDAR antagonists. The relevance of this cortical model findings for HSN1 is uncertain given that HSN1 is a disease of the peripheral sensory and motor neurons.

In addition to cortical neurons, 1-deoxySLs have been shown to be toxic to various other cell types: mouse embryonic fibroblasts (MEF), lymphoblasts, insulin producing cells (Zuellig *et al.*, 2014; Stimpson *et al.*, 2014; Esaki *et al.*, 2015; Alecu *et al.*, 2017b). It is unknown why the pathologically elevated 1-deoxySLs in HSN1 have a detrimental effect on solely/predominantly the peripheral sensory and motor neurons and in a length dependent manner.

1.6 Role of deoxysphingolipids outside HSN1

De novo sphingolipid biosynthesis occurs at the crossroad between fatty acid and amino acid metabolism. Serine is formed from the glycolytic intermediate, 3 phophoglycerate therefore de-novo sphingolipid biosynthesis is also closely related to carbon metabolism

(Lone *et al.*, 2019). Several studies have shown that 1-deoxySLS are elevated in metabolic diseases and could potentially act as biomarkers for metabolic control.

There is emerging evidence that deoxySLs may play a role in the pathogenesis of Type II diabetes. The link was first made in 2010 when diabetic patients were found to have increased levels of 1-deoxySLs (1-deoxySA and 1-deoxySO) (Bertea *et al.*, 2010). There were no differences in the other sphingoid bases between the diabetic patients and controls. This forms an interesting link since diabetic neuropathy and HSN1 phenotype share some similar characteristics. 1-deoxySLs have also been identified as predictive biomarkers for the incidence of type II diabetes in asymptomatic patients (Mwinyi *et al.*, 2017). 1-deoxySL levels are not significantly elevated in patients with type I diabetes (Wei *et al.*, 2014).

Recently, 1-deoxySLs were found to be cytotoxic for insulin producing Ins-1 cells (Zuellig *et al.*, 2014). Treatment of Ins-1 cells with 1-deoxySA resulted in a dose-dependent cytotoxicity. As in other cell types, metabolic conversion of 1-deoxySA to 1-deoxydihydroceramide appears to be responsible for the toxicity.1-deoxySA treatment also induced alterations in actin cytoskeleton and activated multiple key signalling pathways which include JNK (c-Jun N-terminal kinase-and MAPK [p38 mitogen-activated protein kinase]). JNK/MAPK mediate cell responses, including autophagy, to a wide range of stress insults. 1-deoxySLs therefore have the potential to exacerbate the disease course of type II diabetes. Othman *et al*. (2015b) evaluated the therapeutic potential of L-serine supplementation, in both a therapeutic and a preventative setting, in streptozotocin (STZ) induced rat model of diabetes. The diabetic rats had significantly increased levels of plasma 1-deoxySL levels. L-serine supplementation significantly reduced plasma 1-deoxySL levels in both treatment regimens and resulted in a significant improvement in mechanical sensitivity.

Patients with metabolic syndrome also have raised 1-deoxySL levels, with the levels being comparable to those found in patients with Type II diabetes (Othman *et al.*, 2012). The increase in 1-deoxySLs in metabolic disorders is caused by dysregulated carbohydrate and fatty acid metabolism instead of by mutant SPT. It has been suggested that elevated triglycerides could be triggering 1-deoxySL production in these metabolic disorders (Wei *et al.*, 2014). The expression of *Cyp4f* , which have been shown to play a part in 1-deoxySL

catabolism, is downregulated in instances of metabolic dysregulation (Lone *et al.*, 2019). This degradation pathway therefore offers a potential therapeutic target in patients with both HSN1 and metabolic syndromes/type II diabetes.

The formation of 1-deoxySLs is closely related to L-serine depletion. Deprivation of external L-serine in MEF cells lacking 3-phosphoglycerate dehydrogenase (Phgdh), which catalyses the rate limiting step in the formation of de-novo L-serine, results in the production of 1-deoxySLs (Esaki *et al.*, 2015). Genetic ablation of Phgdh in MEF cells led to reduced cell proliferation and activation of p38 MAPK and JNK in conditions of L- serine depletion (Esaki *et al.*, 2015). Survival of these MEF cells was reduced by p38 MAPK inhibition. As was the case in insulin producing cells, 1-deoxySA can activate p38 MAPK. It is possible that in situations of L-serine deficiency, 1-deoxySA production may be an adaptive response. Patients with primary serine biosynthetic defects have varied phenotypes which include intellectual disability, microcephaly, ichthyosis, seizures and peripheral neuropathy. They have also been shown to have significantly elevated deoxySLs, especially deoxydihydroceramides (Ferreira *et al.*, 2018). Patients with primary mitochondrial disorders (MERRF, POLG deletion, LHON, MELAS) were found to have significantly reduced levels of plasma serine and elevated levels of alanine and 1-deoxySLs (Ferreira *et al.*, 2018). This has led some to speculate whether elevated 1-deoxySLs play a role in the aetiology of the peripheral neuropathy seen in many primary mitochondrial disorders (Ferreira *et al.*, 2018).

Plasma 1-deoxySL levels are elevated in patients with glycogen storage disease type I and are associated with an altered plasma L-serine to Alanine ratio (Hornemann *et al.*, 2018). Continuous glucose monitoring in these patients revealed that the plasma 1-deoxySA concentration correlated with occurrence of hypoglycaemia. 1-deoxyceramides have been shown as potential biomarkers to assess progression of non-alcoholic fatty liver disease to non-alcoholic steatohepatitis (NASH) (Gorden *et al.*, 2015). Elevation of 1-deoxyceramides in NASH could be related to L-serine deficiency (Mardinoglu *et al.*, 2014).

Paclitaxel is one of the most commonly used chemotherapy agents however its use is often hampered by dose limiting painful peripheral neuropathy. Paclitaxel chemotherapy in patients with breast cancer caused a dose dependent increase in 1-deoxySLs and there was a correlation between the severity of neuropathy, especially motor neuropathy, and the

levels of 1-deoxyceramides (Kramer *et al.*, 2015). In a rat model of paclitaxel induced peripheral neuropathy, paclitaxel treatment led to a reduction in L-serine concentration in the dorsal root ganglia but not the sciatic nerve or spinal cord (Kiya *et al.*, 2011). In addition, paclitaxel treatment decreased the expression of Phgdh which on immunostaining was localised in satellite cells but not in DRG neurons. This demonstrates the important role played by glial cells in determining the susceptibility of neurons to 1-deoxySL mediated toxicity. Intra-peritoneal administration of L-serine improved paclitaxel induced mechanical allodynia/hyperalgesia and the reduction in sensory nerve conduction velocity.

1.7 Summary

HSN1 secondary to *SPTLC1/2* mutations is the commonest subtype of HSN and is phenotypically heterogenous. *SPTLC1/2* encode for separate subunits of the enzyme, SPT, mutations of which result in altered substrate specificity and the production of atypical metabolites, 1-deoxySLs.

1-deoxySL production in mammals occurs primarily under two, interlinked circumstances: mutations in SPT which alter substrate specificity, as in HSN1 or when there is metabolic dysfunction. Metabolic dysfunction can either be as a result of dyslipidaemia or due to perturbations in serine metabolism/ availability. Recent advances in biochemical analytical technologies have enabled the understanding of the canonical and atypical de-novo sphingolipid pathways. However, the targets and mode of action of these atypical 1-deoxySLs is yet unknown. As elevated 1-deoxySLs are found in various diseases with different clinical phenotypes, it is unlikely that their cellular toxicity can be attributed to a single effect. Site of production, accessibility to L-serine and elimination pathways will also determine the cell types affected. There is now emerging evidence that 1-deoxySLs might also have a physiological role. There is still a long way to go before the complex web of 1-deoxySLs is unravelled but further understanding of these conserved metabolites will have widespread impact.

1.8 Thesis overview

Overall, this thesis has two objectives. First, to investigate the pathomechanisms of 1-deoxySL mediated neurotoxicity using different cellular models. Second, to identify responsive outcome measures that can be used in a definitive therapeutic trial in HSN1.

Chapter 2 describes a series of experiments in a murine in-vitro model using primary motor and DRG neurons. The effects of exogenous application of 1-deoxySLs on cell survival, neurite outgrowth, ER stress response and mitochondrial function were investigated. Effects of 1-deoxySLs on the mediators of the ER unfolded protein response were further evaluated using SH-SY5Y (human neuroblastoma cell line) cells. Some of the results of this chapter were published in Neurobiology of Disease (Wilson *et al.*, 2018).

Chapter 3 focuses on a human iPSC derived (reprogrammed fibroblasts form HSN1 patients and control subjects) sensory neuron model of HSN1. Effects of endogenous and exogenous 1-deoxySLs on cell survival, neurite outgrowth and expression of caspase 3 (mediator of apoptosis) and markers of axonal injury were investigated. Effects of endogenous 1-deoxySLs on ER and mitochondrial structure and function were also assessed.

Chapter 4 describes the baseline cross-sectional profile of HSN1 patients in the natural history study and provides an in-depth phenotype of HSN1. Various assessments were used in the natural history study in order to capture the spectrum of deficits noted in HSN1 patients. These included Charcot-Marie-Tooth Neuropathy Score (CMTNS), nerve conduction studies, quantitative sensory testing, intra-epidermal nerve fibre density (upper thigh), computerised myometry, MRI determined calf fat fraction and patient based questionnaires (Neuropathic Pain Symptom Inventory and SF-36 version 2).

Chapter 5 covers the one year natural history study in HSN1. The responsiveness and validity of the individual assessments used in the study were evaluated. The results of Chapters 4 and 5 were recently published in the Journal of Neurology, Neurosurgery and Psychiatry (Kugathasan *et al.*, 2019).

Finally, Chapter 6 presents the overall conclusions and discusses areas for future research.

2. 1-Deoxysphingolipid (1-deoxySL) induced neurotoxicity in a mouse in-vitro model

2.1 Introduction

Plasma 1-deoxySL levels are raised in patients with HSN1. Prior to the start of this project, 1-deoxySL induced neurotoxicity had only been demonstrated in one in-vitro primary culture model of chicken primary motor neuron and dorsal root ganglia (DRG) cells by Penno *et al.* (2010). This study demonstrated a dose-dependent reduction in neurite number and neurite length with 24 hour 1-deoxySA treatment in DRG cultures and a less pronounced effect in motor neuron cultures. More recently, 1-deoxySL mediated toxicity has also been demonstrated in mouse primary DRG cultures in which 1-deoxySA causes a dose dependent reduction in longest neurite length and mitochondrial morphological abnormalities as well as mouse primary cortical neuron cultures where a dose dependent cytotoxicity was observed (Güntert *et al.*, 2016; Alecu *et al.*, 2017b). 1-deoxySL mediated toxicity has also been demonstrated in various cell lines including Mouse Embryonic fibroblasts (MEF), human SH-SY5Y cells (neuroblastoma line) and CHO-LyB cells (Gable *et al.*, 2010; Alecu *et al.*, 2017b).

Investigations into the mechanism underlying dSL toxicity have used one of two approaches: exogenous application of 1-deoxySLs or the endogenous production of 1-deooxySLs in cells expressing mutant SPT. Alecu *et al.* (2017b) investigated the sub-cellular localisation of exogenously applied 1-deoxySLs and the underlying pathomechanism of 1-deoxySL induced toxicity. By synthesising alkyne analogues of 1-deoxySA, they were able to determine their localisation within cells by fluorescence microscopy. Treatment of MEF cells with a non-toxic concentration of alkyne-deoxySA led to rapid uptake in the mitochondria (5 minutes after treatment) and to lesser extent in the Golgi body. After one hour, a minor degree of uptake was also seen in the ER. This delayed uptake in the ER coincides with the conversion of alkyne-deoxySA to deoxydihydroceramide and deoxyceramide metabolites as the enzyme (ceramide synthase) responsible for this conversion resides in the ER. With longer treatment periods of toxic concentration of alkyne-

deoxySA (24 hours), significant cell death and fragmentation of the mitochondria were observed. Co-treatment with fuminosin B_1, a ceramide synthase inhibitor, ameliorated the alkyne-deoxySA induced mitochondrial fragmentation. These findings led the authors to conclude that it was the downstream metabolites rather than 1-deoxySA that was responsible for the mitotoxicity, suggesting that the initial accumulation of 1-deoxySA in the mitochondria is not directly toxic to the mitochondria. With longer periods of 1-deoxySA treatment, they also observed morphological alterations in the ER, from a reticular pattern to enlarged and dense appearing sheets and ER stress. Güntert *et al.* (2016) used primary cortical neuronal cultures to investigate the effects of exogenous 1-deoxySLs. Following treatment for 24 hours with 2µM 1-deoxySA, they observed alterations in cytoskeletal regulators and associated proteins, with a reduction in the expression of IRSp53 (insulin receptor substrate 53, a target of RhoGTPases which are major modulators of cytoskeletal organisation and cell survival) and upregulation of phosphor-Ezrin (links plasma membrane to the actin cytoskeleton). In both of these studies described above, pathomechanisms have been investigated using doses and time points at which cell death occurs. However, it is unclear whether these findings are end stage processes or whether they reflect the initial mode of toxicity. Interestingly, both studies reported that co-treatment of 1-deoxySA with fuminosin B_1 ameliorated 1-deoxySA induced toxicity, providing a consensus that it is the downstream metabolites (1-deoxy-dihydroceramide/ 1-deoxyceramide) that are responsible for the toxicity rather than 1-deoxySA per se.

Several pathomechanisms of endogenous 1-deoxySL induced neurotoxicity have been proposed, based on results from a variety of non-neuronal in-vitro models. Gable *et al.* (2010) used yeast expressing human SPT and found increased GAD153/CHOP expression, a marker of ER stress, in yeast carrying the mutant SPT which was further enhanced when cultured in alanine enriched media. In the same study, increased GAD153/CHOP expression was seen in untransfected CHO-LyB cells treated with 1µM 1-deoxySA. In a study using HSN1 patient derived lymphoblasts (C133W and V144D mutations), increased lipid droplet formation was reported, without a corresponding increase in expression of adipophilin, a membrane associated protein present in mature lipid droplets and widely used as a marker for lipid droplets (Marshall *et al.*, 2014). This led the authors to conclude that there might be an underlying deregulation of lipid metabolism in cells expressing HSN1

mutations. The same group also observed abnormalities in mitochondrial ultrastructure and disruption of ER homeostasis including a reduction in the expression of BiP, an ER chaperone and ERO1-Lα which maintains the redox potential of ER, in HSN1 patient derived lymphoblasts. Stimpson *et al.* (2014) examined mitochondrial protein isolates from control and HSN1 patient (V144D) lymphoblasts and found an increased expression of ubiquinol -cytochrome C reductase core protein, an electron transport chain protein.

The effects of endogenously produced 1-deoxySLs have been examined in primary DRG cultures obtained from transgenic mice overexpressing the C133W SPT mutation (Jun *et al.*, 2015) and in a transgenic (C129W) drosophila model of HSN1 (Oswald *et al.*, 2015). Mutant DRGs from transgenic mice exhibited increased neurite growth and branching and increased expression of p-ERM, an actin crosslinking protein. L-serine supplementation or removal of L-alanine independently restored normal neurite growth patterns in the mutant DRGs. In the drosophila model, mutant sensory neurons were found to have impaired ER to golgi trafficking and reduced dendrite arborization. Co-expression of dominantly active form of Rab, an effector of ER to Golgi membrane trafficking, restored the nociceptive defect observed in transgenic mutant drosophila.

Despite these findings, the precise pathomechanism of 1-deoxySL induced toxicity in mammalian neurons remains unclear. Various mechanisms have been proposed, but two of the most prominent defects appear to include ER stress and mitochondrial dysfunction.

2.2 Aims

1) To determine whether 1-deoxySLs are toxic to mammalian (mouse) motor and DRG neurons by evaluating their effects on:

a) survival
b) neurite outgrowth (DRG neurons)

2) To determine if there is differential vulnerability to exogenously applied 1-deoxySLs within DRG subpopulations, i.e., small peptidergic sensory neurons and large myelinated sensory neurons.

3) To investigate the underlying pathomechanisms of 1-deoxySL neurotoxicity:

a) To determine if there is mitochondrial dysfunction in the initial stages of 1-deoxySL induced neurotoxicity
b) To determine if 1-dSL treatment induces ER stress and the activation of the unfolded protein response (UPR).
c) To determine if 1-deoxySLs alter ER or golgi morphology.

2.3 Materials and Methods

2.3.1 Animals used

C57BL/6J (Charles River Laboratories) wild-type mouse colonies were maintained by Dr. Bernadett Kalmar in accordance with the Animals (Scientific Procedures) Act 1986. For the motor neurone cultures, the pregnant mice were terminally anaesthetised with pentobarbitone (intra-peritoneal, 140mg/kg) under Schedule 1 as specified by the UK Animals Scientific Procedures Act 1986. For the DRG cultures, 5-8 day post-natal pups were sacrificed by Schedule 1 methods as outlined in the UK Animals Scientific Procedures Act 1986.

2.3.2 Primary mixed motor neuron cultures

Prior to the start of the culture, 13mm glass coverslips were coated with polyornithine (3µg/ml, Sigma) dissolved in Hanks Buffered Saline Solution (HBSS) and incubated at 37ºC overnight. The solution was then replaced with laminin (5µg/ml, Sigma) and incubated for a further 2 hours prior to use. All reagents stated below were obtained from Gibco by ThermoFisher Scientific unless otherwise specified.

Day 12.5-13.5 (E12/13) embryos were harvested from female mice by hysterectomy and placed in a petri dish containing chilled HBSS and 2% penicillin/streptomycin which was kept over an ice pack during the dissection. Individual embryos were transferred one at a time to a petri dish containing HBSS and 2% penicillin/streptomycin and placed under a dissecting microscope. The ventral horns of the spinal cord were dissected out according to the method described by Camu and Henderson (1992). This involved removing the head of the embryo and laying the body prone. The skin overlying the neural tube was removed and the neural tube was gently separated from the rest of the body. The dura mater with the attached DRGs was then removed, followed by the removal of the lateral/dorsal region of the spinal cord via scalpel dissection. The cords were then trypsinized (incubated for 10 minutes at 37ºC) in HBSS containing 0.025% bovine pancreatic trypsin (Sigma). The tissue was transferred into a solution containing 800µl of Leibovitz's L15 media, 100µl of 4% bovine serum albumin (BSA) 100µl of DNAase (1mg/ml) and gently triturated 3-4 times using a 1ml pipette. The supernatant was collected and another solution containing 900µl of Leibovitz's L15, 100µl of 4% BSA and 20µl of DNAase (1mg/ml) was added to the pellet.

This solution was triturated gently about 10 times and again the supernatant was collected. The supernatants were pooled and centrifuged for 5 minutes at x375g through a 4% BSA cushion (4% in Leibovitz's L15 media). The supernatant was discarded and the pellet re-suspended in 1ml of complete neurobasal medium containing 2% B27 supplement, 2% horse serum, 0.5mM glutaMAX, 0.05% 2 mercaptoethanol, penicillin/streptomycin (50 units per ml/50µg per ml) (all Invitrogen) and supplemented with 0.1ng/ml murine glial cell derived neurotrophic factor (GDNF), 0.5ng/ml human ciliary neurotrophic factor (CTNF) and 0.1ng/ml human brain derived neurotrophic factor (BDNF, all Peprotech).

Cell density of the suspension was estimated using a haemocytometer. Cells were plated onto 24 well plates with coated glass coverslips at a density of 5 $x10^4$ and cultured in 1ml volumes of complete neurobasal media under standard culture conditions (37ºC, 5% CO_2).

2.3.3 Primary dorsal root cultures

Glass coverslips were prepared as above but poly-D-lysine (100µg/ml) was used to coat the coverslips instead of polyornithine.

Mouse pups aged between 5 and 8 days were used. The DRGs were dissected using the technique described by Hall (Hall, 2006). This involved placing the pup dorsal surface up under a dissecting microscope and the limbs were fixed with pins. The back fur was soaked with 70% ethanol. A flap of dorsal skin was removed extending along the spine from the lower back to the neck. The vertebral column was cut through transversely near the base of the spine and the spinal canal was located. The vertebrae were cut through by inserting the tip of a small scissor into the spinal canal and cutting along to create a V-shape (cutting at 3 o'clock and 9 o'clock positions), working rostrally. Along the way, the dorsal piece of the vertebrae was peeled back to expose the spinal cord. The DRGs were isolated by pushing the spinal cord to one side to reveal the ventral roots leading to the DRGs. Both the ventral and dorsal roots were cut and the DRG was placed in a petri dish containing chilled HBSS containing 2% penicillin and streptomycin. The dish was kept over ice during the dissection. Lumbar, thoracic and cervical DRGs were removed. 30-35 DRGs were removed from each mouse. The dissociation protocol applied in this study was a modification of three previously described (Malin *et al.*, 2007; Owen and Egerton, 2012; Sun *et al.*, 2012). The harvested

ganglia were transferred into a falcon containing 3ml HBSS with 60u of Papain (Sigma) and incubated on a rotating incubator for 10 minutes at 37ºC. The solution was then centrifuged at x200g for one minute. The papain solution was removed and replaced with 2ml pre-warmed HBSS (with Calcium and Magnesium added) containing 0.1% collagenase type II and 1.5u/ml dispase and incubated for further 45 minutes in the rotating incubator at 37ºC. The solution was centrifuged again at x200g and the collagenase mixture removed. The pellet was re-suspended in 1ml of neurobasal media containing 2% B27 supplement, 1% foetal calf serum, 2mM GlutaMAX, 1% Penicillin and streptomycin and supplemented with 50ng/ml mouse nerve growth factor (NGF, Promega). The solution was gently triturated 4 times to dissociate the DRGs, taking care to maintain a constant slow speed of trituration to reduce the shear force applied to the cells in the suspension. The solution was allowed to settle. The supernatant was collected, and the pellet was re-suspended in 0.5ml of media. The above process was repeated twice and the supernatants were pooled together.

It was difficult to estimate accurately the density of the cells in the suspension using a haemocytometer. Some of the cells were too large to be sucked into the measuring grid. The DRGs from one pup were sufficient to provide adequate plating density for 8 wells of a 24well plate (each well contained cells from an average of 4 DRGs). Cells were plated onto 24 well plates with coated glass coverslips and cultured in 1ml volumes of complete neurobasal media under standard culture conditions (37ºC, 5% CO_2). For live-cell imaging cells were plated onto glass bottom dishes (35 mm petri dish with 14 mm microwell, MatTek) and cultured in 2ml culture media. For western blots, cultures were plated onto 6 well plates (approximately 16 DRGs per well).

2.3.4 Sphingolipid treatment

1mM sphingolipid-ethanol stock solutions were prepared for sphinganine (SA, molecular weight 301.51), 1-deoxysphinganine (1-deoxySA, molecular weight 285.51) and 1-deoxymethylsphinganine (1-deoxymethylSA, molecular weight 271.48) by dissolving these lipids in ethanol. All sphingolipids were obtained from Avanti Polar Lipids.

Both the motor and sensory neurons were cultured for 3-4 hours before the start of the treatment regime. Motor neuron and DRG cultures were treated with sphingolipids at a final concentration of 1µM (adding 1µl of stock to 1ml of culture media). Following the addition of

the sphingolipids to the culture, the plates were gently swirled to distribute the sphingolipids throughout the wells. Control cultures were treated with the ethanol (EtOH) vehicle (1µl of ethanol in 1ml of complete neurobasal media).

Four treatment durations were used for the motor neurons: 12 hours, 24 hours, 36 hours and 48hours. 12 hours, 24 hours and 48 hour treatment durations were used for DRGs. Due to the relatively short culture times, media changes were not necessary.

2.3.5 Immunocytochemistry

The motor neurons and DRG cells were fixed by the addition of 4% paraformaldehyde in phosphate buffered saline (PBS) for 20 minutes followed by a PBS wash. Before primary antibody labelling, the cells were permeabilised by incubating in blocking solution (5% goat/donkey serum in PBS) containing 0.1% Triton X-100 (PBST: Sigma) for one hour at room temperature. Cells were then washed with PBS and incubated overnight with the primary antibody (Table 2.1) at 4ºC. The cells were washed in PBS and the nuclear marker, 4',6-Diamidino-2-phenylindole dihydrochloride (DAPI, Sigma) was applied at a dilution of 1:1000 for 5 minutes. The cells were again washed and incubated in the secondary antibody (Table 2.1) at room temperature for 1.5hours. After three more PBS washes, the coverslips were mounted onto slides using mounting media (Glycerol/PBS solution at 4:1 ratio).

Culture	Blocking serum	Primary antibody	Secondary antibody	Manufacturer
Motor neuron	5% Goat serum	Rabbit β- III Tubulin 1:500	Goat anti-rabbit IgG Alexa molecular probes 568 1:1000	Covance MRB-435P
DRG (cell count)	5% Goat serum	Mouse β- III Tubulin 1:500	Goat anti-mouse IgG Alexa molecular probes 568	Covance MMS-435P
DRG (evaluating sensory neuron sub-populations)	5% Donkey serum	Mouse Neurofilament 200 1:100	Donkey anti-mouse IgG Alexa molecular probes 488	Iowa RT97
		Goat CGRP 1:200	Donkey anti-goat IgG Alexa molecular probes 568	AbDSerotec
DRG (Golgi)	5% Goat serum	Rabbit β-III Tubulin 1:500	Goat anti-rabbit IgG Alexa molecular probes 488 1:1000	Covance MRB-435P
		Mouse Giantin 1:500	Goat anti-mouse IgG Alexa molecular probes 568	Biolegend
DRG (ER)	5% Goat serum	Rabbit β-III Tubulin 1:500	Goat anti-rabbit IgG Alexa molecular probes 488 1:1000	Covance MRB-435P
		Mouse PDI 1:500	Goat anti-mouse IgG Alexa molecular probes 568	Enzo

Table 2.1 Commercial antibodies used for immunocytochemistry of primary motor neuron and DRG cultures

2.3.6 Microscopy and analysis of cell survival and neurite outgrowth

Images were taken using Leica inverted epifluorescence light microscope and Leica Application Suite software. Neuronal cell survival was measured by counting the number of beta III tubulin and DAPI co-stained positive cells present per field of view (x200 magnification used for motor neurons and x100 magnification used for sensory neurons). Ten fields of view, selected randomly, were examined per treatment condition for the individual experiments. Fields of view with significant clumping or mechanical distortion

were avoided. The cell counts were normalised to equivalent cell counts in the ethanol vehicle control.

Differential neuronal survival was evaluating by measuring neurofilament 200 (heavy chain) positive DRG neurons (large diameter, myelinated neurons) and Calcitonin Gene Related Peptide (CGRP) positive DRG neurons (small, unmyelinated peptidergic neurons). The cell counts were normalised to those obtained from cultures treated with the ethanol vehicle.

Neurite outgrowth measurements were performed on DRG neurons labelled with beta III tubulin in the 12hour treatment group. Individual neurites were traced to determine average neurite length for each sensory neuron. Neurite arborization area was measured by drawing a line which joined the ends of the neurites together. For both methods, the Leica Application Suite software was used. Only neurons with clearly identified neurites and where the whole neurite arborization could be clearly visualised were selected for analysis. Neurons from 10 randomly selected fields of view were used.

2.3.7 Mitochondrial membrane potential measurement

Primary DRG cultures 2-3 DIV (days in-vitro) were treated with 1µM sphingolipids for 2 hours prior to live cell imaging. The cultures were then washed twice with warmed recording media (156 mM NaCl, 10 mM HEPES, 10 mM D-glucose, 3 mM KCl, 2 mM $MgSO_4$, 2 mM $CaCl_2$, 1.25 mM KH_2PO_4, pH 7.35). Cells were loaded for 30 minutes at room temperature with tetramethylrhodamine methyl ester (TMRM) (20 Nm, ThermoFisher Scientific) in recording media supplemented with pleuronic acid F-127 (0.005%, ThermoFisher Scientific). TMRM is a cell-permeant potentiometric dye which becomes sequestered in the mitochondria because of the electrochemical gradient that exists between the mitochondria and the cytosol.

Immediately before live imaging, calcein blue AM dye (1µM, ThermoFisher Scientific), which acts as a viability probe, was added to the cells. Z stack images were taken on Zeiss Laser Scanning Microscope (LSM) 780 confocal microscope using ZEN LE Digital Imaging 2012 software. The cells were maintained at 37ºC and 5% CO_2 inside a stage top incubator. Z-stacks were taken at 1µm depth intervals using 40X oil objective. TMRM intensity

measurements (in arbitrary units) of mitochondria located within the cell bodies were measured. TMRM intensities were measured using ZEN 2 lite blue edition software and were taken as estimate readouts of mitochondrial membrane potential. Neuronal diameters were also measured by drawing around the cells highlighted by calcein blue AM on sections bisecting the nucleus.

2.3.8 Culture of SH-SY5Y cells

SH-SY5Y cells was used in the analysis of expression of proteins of ER stress and UPR following sphingolipid treatment. SH-SY5Y cell line (ECSCC catalogue number 94030304) is derived from female, human neuroblastoma cells. The cells were cultured in Dulbecco's modified Eagle's Medium (DMEM-12, Gibco) containing 2mM Glutamine, 1% Non-essential amino acids (NEAA), 15% Foetal bovine serum (FBS) and 1% penicillin/streptomycin (50 units per ml/50µg per ml). The cells were maintained in an incubator at 37ºC in a saturated humidity atmosphere of 5% CO_2.

The cells were passaged when about 90% confluent. The culture was split by washing the cells with PBS followed by the addition of 0.5ml warmed trypsin (0.25%)-EDTA in HBSS (Ca^2/Mg^2 free) and incubation in incubator for 1 minute. The flask was gently tapped to detach any remaining adherent cells. 0.5ml of culture medium was added to halt trypsin's enzymatic activity and cells were transferred to a falcon and centrifuged at 400g. The supernatant was removed and the pellet resuspended in 6 ml of culture media. 6 T75 flasks were filled with 15ml of culture medium and each flask seeded with 1 ml of the cell suspension. 24 hours later, the media was replaced with culture media containing 10µM all-trans retinoic acid (Sigma). The SH-SY5Y cells were cultured until 90% confluent. Media (containing trans-retinoic acid) was changed every 2 days. When 90% confluent, sphingolipid (1µM) treatment was initiated and treatment durations of 2 hours, 6 hours and 24 hours were used. At the end of the treatment regime, the cells were harvested for western blot experiments.

2.3.9 Western blot

Cell lysate preparation

DRG cultures were treated with 1 µM sphingolipids (SA, 1-deoxySA and 1-deoxymethylSA) and 1µM thapsigargin (positive control for ER stress, AdipoGen) 3-4 hours after plating into 6 well plates. After 24 hours of treatment, the cells were washed with ice cold PBS. 150µl of urea buffer (8M urea, 2% SDS and 20mM Tris Base, pH=7.07) and 1% Halt Protease and Phosphatase Inhibitor cocktail was added to each well and the plate kept on ice for one minute. The cells were scraped off with a cell scraper and transferred into an Eppendorf, held on ice and then stored at -20ºC.

For SH-SY5Y cultures in T75 flasks, 1ml of urea buffer and 1% Halt Protease and Phosphatase Inhibitor cocktail was added and the cells scraped off with a cell scraper.

Protein Assay

Protein standards were made by diluting 2mg of BSA (Sigma) in 1ml of urea buffer, Serial dilutions of this solution were carried out to obtain further BSA protein standards of 1, 0.5,0.25 and 0.125mg/ml. With DRG cultures, 5µl of cell samples and BSA protein standards were plated in triplicate onto a 96 well Falcon plate. With SH-SY5Y cultures, 10µl of cell sample were plated onto a 96 well plate. Protein assays were performed using the Bio-Rad Laboratories Protein Assay DC reagents A and B. 25µl of Bio-Rad reagent A followed by 200µl of Bio-Rad reagent B were added to each well. The plate was kept in the dark for 15 minutes at room temperature. The absorbance at an excitatory wavelength of 750nm was measured using a plate reading spectrophotometer. Absorbance measurements for the protein standards were used to produce a scatter graph of known protein concentrations against absorbance readouts. A best fit line was drawn and the equation of this line used to calculate the protein concentrations of the cell samples from their absorbance measurements.

Gel protein electrophoresis

A Protean Bio-Rad system was used to make 1mm thick, 10% polyacrylamide gels. The gels were immersed in running buffer (distilled water containing 0.025M TRIS, 0.192M glycine and 0.1% SDS). Cell sample buffers were prepared from the cell samples to contain 10µg of protein by mixing with 4x Laemmli sample (75%, Bio-Rad). β-Mercaptoethanol (10%) was added to these cell sample buffers. 8µl of a standard western ladder (Precision Plus Protein Western Standards, Bio-Rad), together with 15µl of sample buffer (30µl for DRG samples) for each condition were loaded into individual wells. A 160V was applied and the gel was run until the front just run off the gel (approximately 1 hour). The gel was then packed in a cassette containing sponges and blotting paper on either side and nitrocellulose membrane (all soaked in ice cold transfer buffer). The cassette was then placed in chamber containing ice cold transfer buffer (distilled water containing 0.025M TRIS, 0.192M glycine and 20% methanol), ice box and a magnetic stirrer. A potential difference of 100V was applied for 60 minutes. The nitrocellulose membrane was then removed and immersed in Ponceau C solution for 2 minutes to confirm the transfer of proteins.

The membrane was then immersed in a blocking solution (PBS containing 0.1% Tween 20 and 5% milk) for one hour. Primary antibody (in PBS 0.1% Tween 20 and 5% milk) was added next and left overnight at 4ºC (Table 2.2). The membrane was then washed three times with PBS-Tween before the application of the horse radish peroxidase (HRP) conjugated secondary antibody (1:1000 dilution) mixed with Strep Tactin- HRP conjugate (Bio-Rad, for detection of western ladder) for 2 hours at room temperature. The membrane was again washed three times with PBS-Tween. In-order to visualise the protein bands, the membrane was incubated in mixture of solution A and B (1:1, Supersignal West Pico Chemiluminescent substrate, ThermoFisher Scientific) and then exposed to Kodak X-ray film in a dark room. In later experiments, the protein bands were visualised using ChemiDoc Imaging system (Bio-Rad). The optical densities of the protein bands were quantified using the image analysis software, Image J.

Culture	Primary antibody	Concentration	Manufacture
DRG and SH-SY5Y cultures	Mouse monoclonal PDI	1:1000	Enzo (ADI-SPA-891)
	Rabbit polyclonal BiP (GRP78)	1:1000	Abcam (ab21685)
	Rabbit monoclonal PERK	1:1000	Cell Signaling (C33E10)
	Rabbit monoclonal IRE1α	1:1000	Cell Signaling (14C10)
	Rabbit polyclonal phospho-IRE1α	1:1000	Novusbio (NB100-2323)
DRG cultures	Rabbit monoclonal ATF6	1:1000	Novusbio NBP1-40256

Table 2.2 Commercial antibodies used for Western blots in this study

2.3.10 Statistical analysis

Statistical analysis was performed using SPSS 22.0 and GraphPad Prism version 7.0 software. Frequency distribution graphs of the data were visually inspected to determine if normally distributed. Motor neuron and DRG cell counts were normalised to vehicle (ethanol) control. Statistical significance for the relative cell counts, were determined using the non-parametric, One-sample Wilcoxon Signed Rank test. Neurite length and arborisation area for the various treatments are given relative to the ethanol and compared using the Kruskall-Wallis test and corrected for multiple comparisons with Dunn's test. Statistical significance for mitochondrial membrane potentials were determined using one-way Anova followed by post-hoc correction for multiple comparisons (Dunnett test). Statistical difference in western blot protein levels were determined using One-sample Wilcoxon Signed Rank test for DRG cultures and using Kruskall-Wallis test (corrected for multiple comparisons with Dunn's test) for SH-SY5Y cultures. Data are represented as mean ± standard error of the mean (SEM).

2.4 Results

2.4.1 Maturation of sensory and motor neurons in-vitro

Neurite outgrowth was faster in DRG cultures compared to motor neuron cultures. At 12 hours post-plating, elaborate neurite arborisations can be seen in the DRG cultures whereas only early sprouting of neurites can be seen in motor neuron cultures (Figure 2.1). By 24 hours after plating, dense network of neurites can be seen in DRG cultures (Figure 2.1). The differences in maturation may reflect the differences in age of the animals the primary cultures were obtained from: 12.5-13.5 day old mouse embryos for motor neuron cultures and 5-8 day old pups for DRG cultures.

2.4.2 1-DeoxySLs reduce DRG neuron survival

Primary DRG cultures were treated with 1μM sphingolipids at two different time points following plating, at either A) 3-4 hours post plating referred hereafter as 'early treatment', or B) 48 hours post plating, referred to as 'late treatment' (Figure 2.2A). For the early treatment paradigm, the treatment duration consisted of 12, 24 and 48 hours. In contrast, in the 'late treatment', the cells were treated for 48 hours only. The concentration of 1μM was chosen since a dose response experiment in a previous study in chick DRG cultures has shown that this concentration has deleterious effects on DRG cultures (Penno *et al.*, 2010). In these experiments the number of β-III tubulin positive cells were counted as neurons. Sensory neuron survival was determined by comparing the extent of sensory neuron survival in sphingolipid treated cultures relative to survival in vehicle (ethanol) treated cultures.

The effects of 'early treatment' with sphingolipids on sensory neuron survival is summarised in Figures 2.2B and C. There was a clear reduction in sensory neuron survival in cultures treated with 1-deoxySA and 1-deoxymethylSA. With 1-deoxySA treatment, a reduction in cell survival was seen after 12 hours of treatment and 82 ± 4% of neurons survived ($p=0.043$). With longer 1-deoxySA treatment durations, there was a further reduction in the number of surviving sensory neurons and 72 ± 3% of neurons survived at 24 hours, ($p=0.028$) and 31 ± 7% neurons survived at 48 hours ($p=0.043$). 1-deoxymethylSA was less neurotoxic and only caused a significant reduction in sensory neuron survival after 48 hours of treatment, when only 60 ± 6% of neurons survived ($p=0.043$). Treatment with the

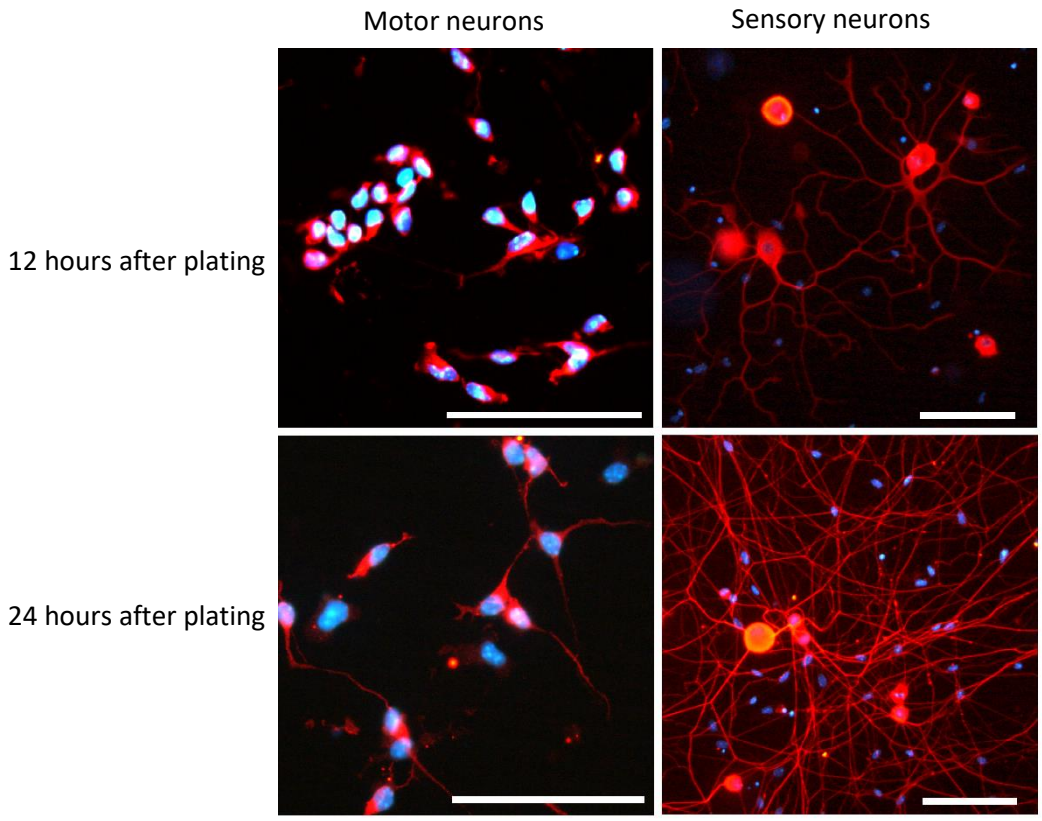

Figure 2.1 Maturation of motor and sensory neurons in-vitro

The images show primary motor and sensory (DRG) neurons in-vitro which have been immunostained for neuronal marker β-III Tubulin (red) and the nuclear marker DAPI (blue) at either 12 or 24hours after plating. The growth of neurites in-vitro was faster in the sensory neurons than in motor neurons. Complex neurite arborisations were seen in sensory neurons as early as 12 hours after plating. Scale bars = 100µm

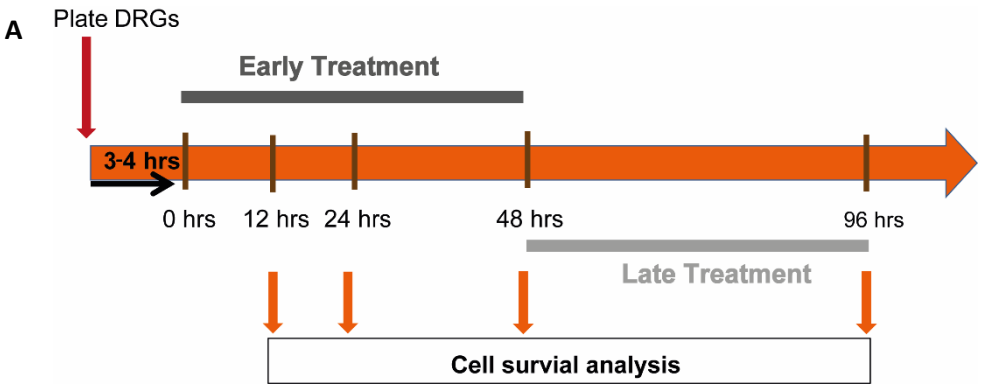
A
Plate DRGs
Early Treatment
3-4 hrs
0 hrs
12 hrs
24 hrs
48 hrs
96 hrs
Late Treatment
Cell survial analysis

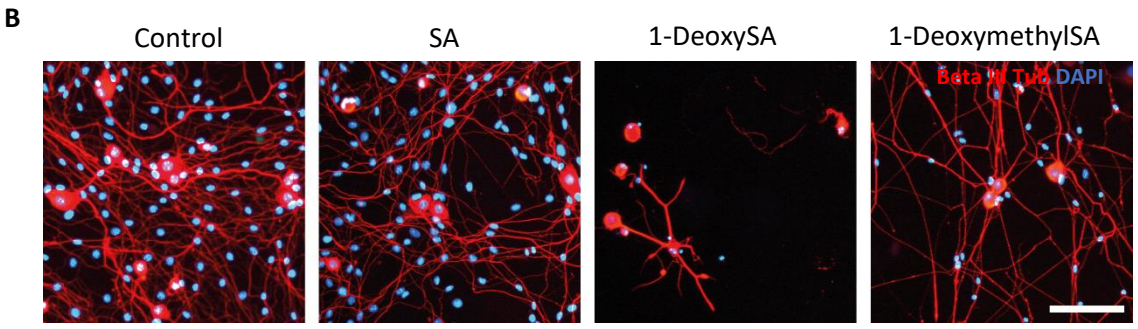
B
Control
SA
1-DeoxySA
1-DeoxymethylSA
Beta III Tub DAPI

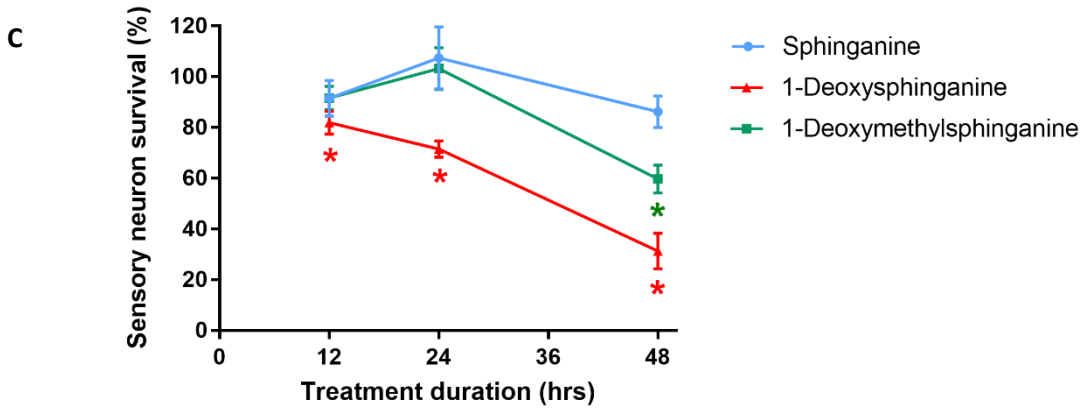
C
Sensory neuron survival (%)
120
100
80
60
40
20
0
0
12
24
36
48
Treatment duration (hrs)
Sphinganine
1-Deoxysphinganine
1-Deoxymethylsphinganine

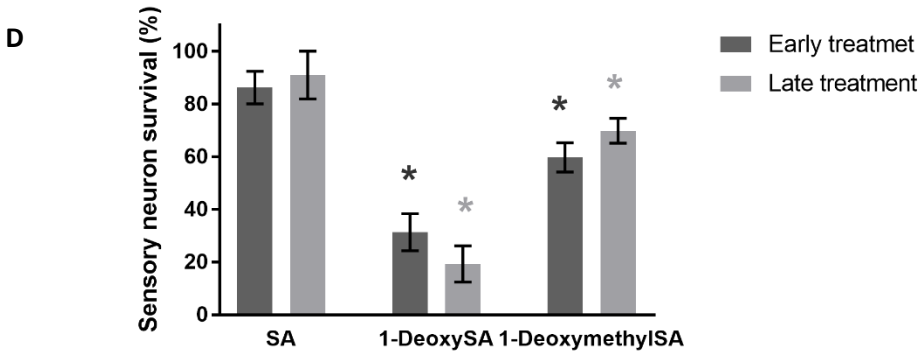
D
Sensory neuron survival (%)
100
80
60
40
20
0
SA
1-DeoxySA
1-DeoxymethylSA
Early treatmet
Late treatment

Figure 2.2 The effects of 1-deoxysphingolipids on sensory neuron survival in-vitro

A) A schematic showing the two sphingolipid treatment regimes. Early treatment started 3-4 hours after plating and the cells were fixed after 12, 24 and 48 hours of treatment. Late treatment was initiated 48 hours after plating and the cells were fixed after 48 hours of treatment. **(B)** Representative images of sensory neurons following 'early' treatment with 1μM sphinganine (SA), 1-deoxySA and 1-deoxymethylSA and vehicle control for 48 hours and immunostained for neuronal marker βIII Tubulin (red) and co-stained with nuclear marker DAPI (blue). Scale bar=200μm **(C)** The survival of sensory neurons treated 'early' with SA, 1-deoxySA and 1-deoxymethylSA for 12, 24 and 48 hours. 'Early' treatment with 1-deoxySA results in a significant death of DRGs by 12 hours. Treatment with 1-deoxymethylSA also decreases DRG survival but this only reaches significant after 48 hours of treatment. **(D)** The survival of sensory neurons following 'early' or 'late' treatment with sphingolipids. Early and late deoxysphingolipid treatments are equally cytotoxic with 1-deoxySA being more toxic than 1-deoxymethylSA in both cases. n=5-6 independent experiments. Sensory neuron survival is displayed as a percentage relative to ethanol vehicle control. For statistical comparison, each treatment group was compared to its ethanol vehicle control. *****$p<0.05$, Error bars=SEM.

normal enzymatic product, SA, did not cause any significant reduction in sensory neuron survival over the 48 hours of treatment however there appears to be a trend towards decreased sensory neuron survival with longer treatment duration of 48 hours.

Interestingly, following 48hours of treatment with 1-deoxySLs, the significant loss of sensory neurons was also accompanied by the loss of non-neuronal cells (DAPI positive/β-III tubulin negative cells) such as fibroblasts (Figure 2.2B)

'Late' treatment with sphingolipids for 48 hours has a similar pattern of toxicity to early treatment, with no significant difference (Figure 2.2D). Both 1-deoxySA and 1-deoxymethylSA 'late' treatments led to reduction in sensory neuron survival where 18 ± 8% ($p=0.028$) and 72 ± 5% ($p= 0.028$) of neurons survived, respectively.

2.4.3 1-DeoxySLs reduce motor neuron survival

Primary motor neuron cultures were treated with sphingolipids 3-4 hours after plating (Figure 2.3A) for treatment durations of 12, 24, 36 or 48 hours. The effects of early treatment with sphingolipids on motor neuron survival is summarised in Figure 2.3B and C. There was time dependent 1-deoxySA neurotoxicity, with 66 ± 4% of motor neurons surviving following 36 hours of treatment ($p=0.042$) and 61 ± 3% of neurons surviving following 48 hours of treatment ($p=0.043$). 1-deoxymethylSA appears to have delayed neurotoxicity when compared to 1-deoxySA with a significant reduction in motor neuron survival seen after 48 hours of treatment when 64 ± 6% neurons survived ($p=0.043$). However, following 48 hours of treatment, both 1-deoxySA and 1-deoxymethylSA caused a similar reduction in cell survival. Interestingly, both SA and 1-deoxymethylSA appeared to improve motor neuron survival initially at 24 hours so that 112 ± 3% ($p=0.042$) and 111 ± 3% ($p=0.043$) neurons survived respectively. As with DRG cultures, 48 hours of treatment with 1-deoxySLs caused a loss of non-neuronal cells in additional to motor neurons.

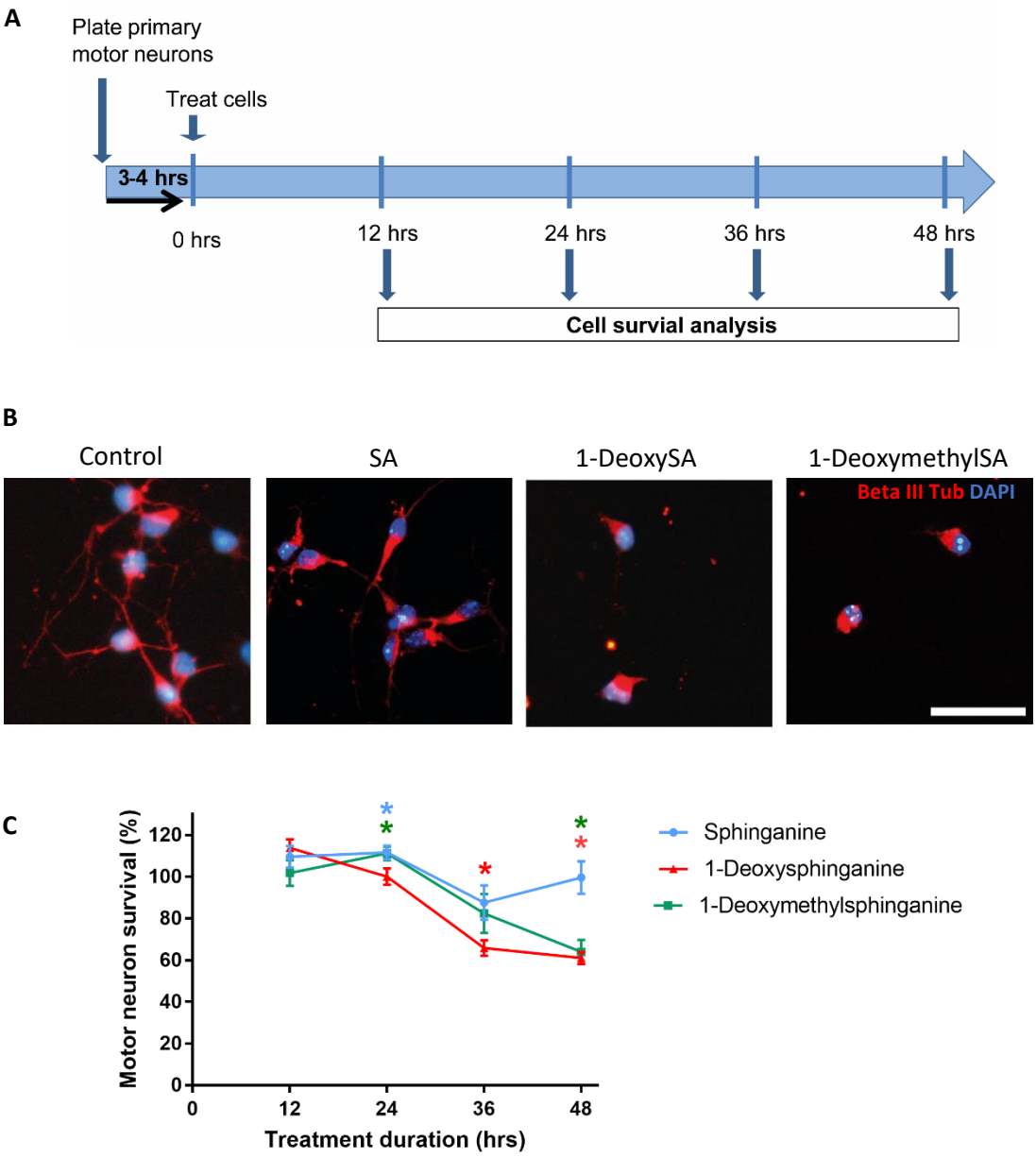

Figure 2.3 The effects of 1-deoxysphingolipids on motor neuron survival in-vitro

(A) The schematic shows the treatment protocol used. **(B)** Primary motor neuron cultures were treated for 48 hours with 1 μM sphingolipids (sphinganine (SA), 1-deoxySA and 1-deoxmethylSA) or vehicle control 3-4hours after plating. The neurons were then immunostained for β-III Tubulin (red) and stained with the nuclear marker DAPI (blue). Scale bar=50 μm **(C)** 1-DeoxySLs cause a time- dependent reduction in motor neuron survival (after 36 hours of treatment for 1-deoxySA and 48 hours for 1-deoxymethylSA). Motor neuron survival is shown as a percentage relative to ethanol vehicle control. n= 5 independent experiments. ***p*<0.05 Error bars =SEM.

2.4.4 Differential toxicity of 1-deoxySLs on DRG sub-types.

The purpose of this series of experiments was to determine if there is differential vulnerability to the deoxySLs in the different types of sensory cells. To differentiate between sensory neuron subtypes, DRG cultures were co-labelled with a marker for large myelinated sensory neurons (an antibody recognizing neurofilament 200) and a marker for small peptidergic nociceptors (an antibody recognizing Calcitonin Gene Related Peptide, CGRP). These two subtypes were chosen for study because in the HSN1 clinical phenotype there is a sensory dissociation whereby small fibre mediated nociception and temperature sensation are affected earlier and more severely than large, myelinated fibre mediated vibration and joint position sense (Auer-Grumbach *et al.*, 2003; Houlden *et al.*, 2006). The number of neurofilament 200 (NF200) and CGRP positive cells in each condition were counted and expressed as a percentage of the number of NF200 and CGRP positive cells, respectively, in the vehicle control group.

Representative images of DRG cultures stained for CGRP and NF200 following 'early' treatment with sphingolipids for 48 hours are shown in Figure 2.4A. In the CGRP positive neuronal sub-population, there was a time-dependent reduction in cell survival so that following treatment with 1-deoxySA, 57 ± 18% of neurons survived at 24 hours (p= 0.043) and 19 ± 6% survived at 48 hours (p=0.043) (Figure 2.4B). 1-deoxymethylSA was also toxic to this sub-population of neurons with 78 ± 5% (p=0.028) neurons surviving at 12hours and only 44 ± 14% (p=0.043) of neurons surviving after 48hours of treatment. In the NF200 positive neuronal sub-population, 1-deoxySA treatment also caused a significant reduction in cell survival but only following the longest treatment duration of 48 hours, when 41 ± 10% (p=0.043) of neurons survived (Figure 2.4C). 1-deoxymethylSA treatment caused an initial reduction in cell survival following 12 hours of treatment where 75 ± 7% (p=0.043) of neurons survived, however the cell numbers remained stable thereafter.

The small diameter, CGRP positive (peptidergic) sensory neurons appear more susceptible to 1-deoxySL mediated toxicity than the large, myelinated NF200 positive sensory neurons. The CGRP positive neurons showed signs of 1-deoxySA toxicity at an earlier time point of 24 hours compared to 48 hours for the NF200 positive cells. After 48 hours of 1-deoxySA treatment, there was a greater reduction in CGRP positive neurons compared to the neurofilament positive neurons. For both NF200 and CGRP positive neurons, 1-

deoxymethylSA appears to be less neurotoxic than 1-deoxySA. This milder toxicity is particularly apparent in NF200 positive large myelinated neurons.

2.4.5 Effects of sphingolipid treatment on early neurite outgrowth

For these experiments, the early treatment protocol was used, in which cells were exposed within 3-4hours of plating to 1µM sphingolipids for 12 hours, then fixed and stained for the neuronal marker beta III tubulin. The effects on neurite outgrowth was then determined by assessing two parameters: i) average neurite length for each sensory neuron and ii) average neurite arborisation area. The methods for assessing these parameters are illustrated in Figures 2.5B and 2.5D respectively and described in detail in the methods section, 2.3.6.

The average neurite length per sensory neuron was significantly reduced in all sphingolipid treatment groups and were found to be 199 ± 8µm with SA ($p<0.0001$), 203 ± 8µm with 1-deoxySA ($p=0.0001$) and 200 ± 8µm with 1-deoxymethylSA ($p<0.0001$), compared to the vehicle control which was 262 ± 11µm (Figures 3.5A and C). Individual neurite lengths per sensory neuron appeared more uniform in the vehicle (ethanol) control group, whereas in the sphingolipid treatment groups there was greater variation in neurite length and the branching pattern was less complex. These findings are better represented by measuring the overall neurite arborisation area, which is less influenced by individual neurite lengths. Sphingolipid treatment significantly reduced the neurite arborisation area from $1.361x10^5 \pm 1.290x10^4$ in vehicle control cultures to $8.655x10^4 \pm 8.848x10^3 \mu m^2$ in SA ($p=0.0006$), $7.730x10^4 \pm 8.001x10^3 \mu m^2$ in 1-deoxySA ($p<0.0001$) and $7.934x10^4 \pm 8.408x10^3 \mu m^2$ in 1-deoxymethylSA ($p<0.0001$) treated cells (Figure 3.5E). Assessment of the neurite arborisation area revealed a more dramatic reduction in neurite growth following sphingolipid treatment to 64% with SA, 57% with 1-deoxySA and 58% with 1-deoxymethylSA versus 76%, 78% and 76%, respectively, when average neurite length measurements were used. The reduction in neurite length and arborisation area caused by SA treatment was comparable to that caused by 1-deoxySL treatment.

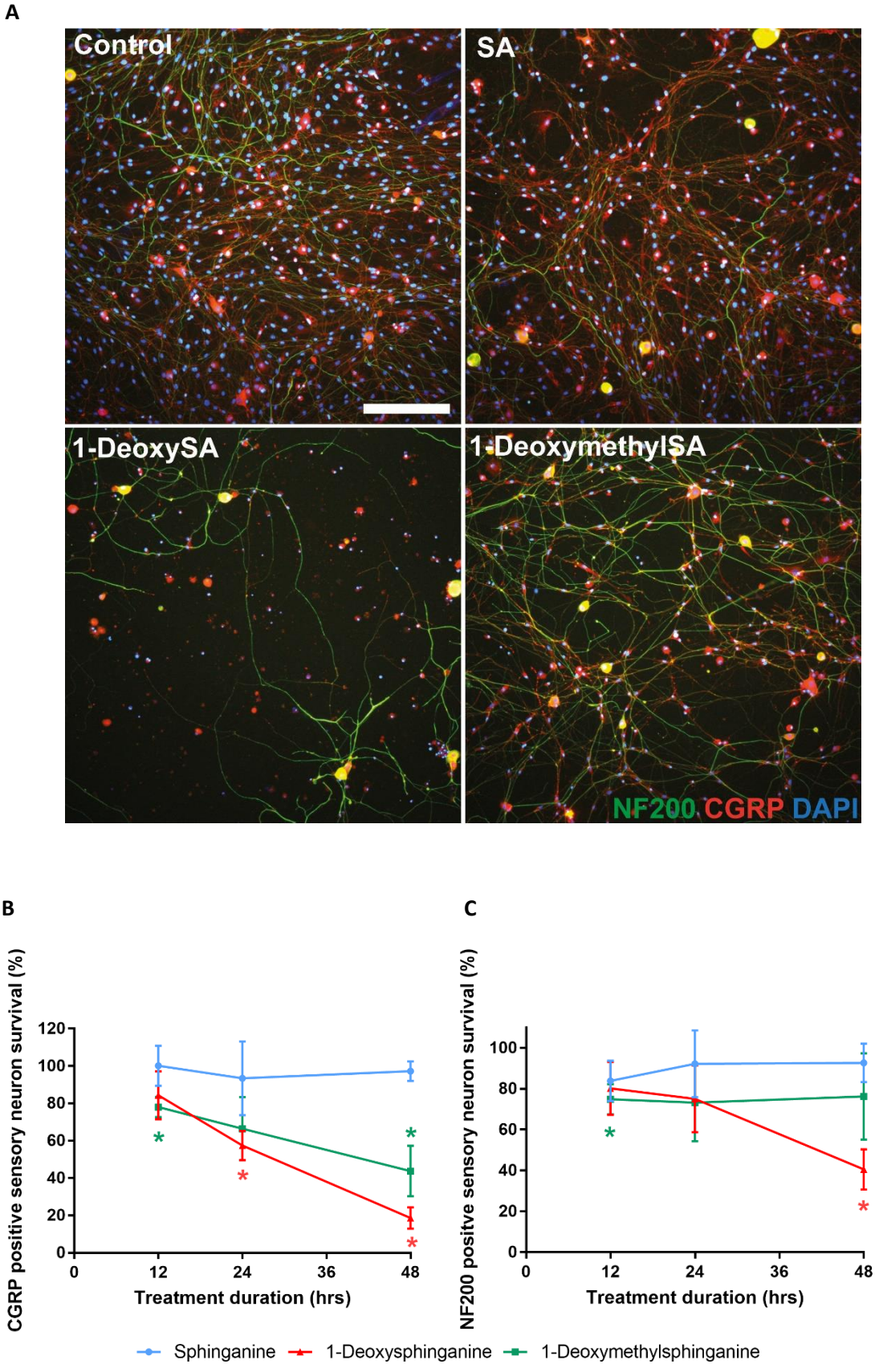
A
Control
SA
1-DeoxySA
1-DeoxymethylSA
NF200 CGRP DAPI
B
CGRP positive sensory neuron survival (%)
120
100
80
60
40
20
0
0
12
24
36
48
Treatment duration (hrs)
C
NF200 positive sensory neuron survival (%)
100
80
60
40
20
0
0
12
24
36
48
Treatment duration (hrs)
Sphinganine
1-Deoxysphinganine
1-Deoxymethylsphinganine

Figure 2.4 Differential toxicity of 1-deoxysphingolipids on sensory neuron sub-types.

(A) Primary DRG cultures were treated after 3-4hours of plating with 1μM sphingolipids (sphinganine (SA), 1-deoxySA and 1-deoxymethylSA or vehicle control (ethanol) for 48 hours. The cells were immunostained for markers of large myelinated neurons (NF200: green) and small peptidergic neurons (CGRP: red) and co-stained with the nuclear marker, DAPI (blue). Scale bar=100μm **(B)** The small CGRP positive (peptidergic) sensory neurons appear to be more vulnerable to 1-deoxySL induced neurotoxicity compared to the large **(C)**, myelinated NF200 positive neurons. Sensory neuron survival is shown as a percentage relative to vehicle control. n= 5-6 independent experiments. *p<0.05. Error bars=SEM

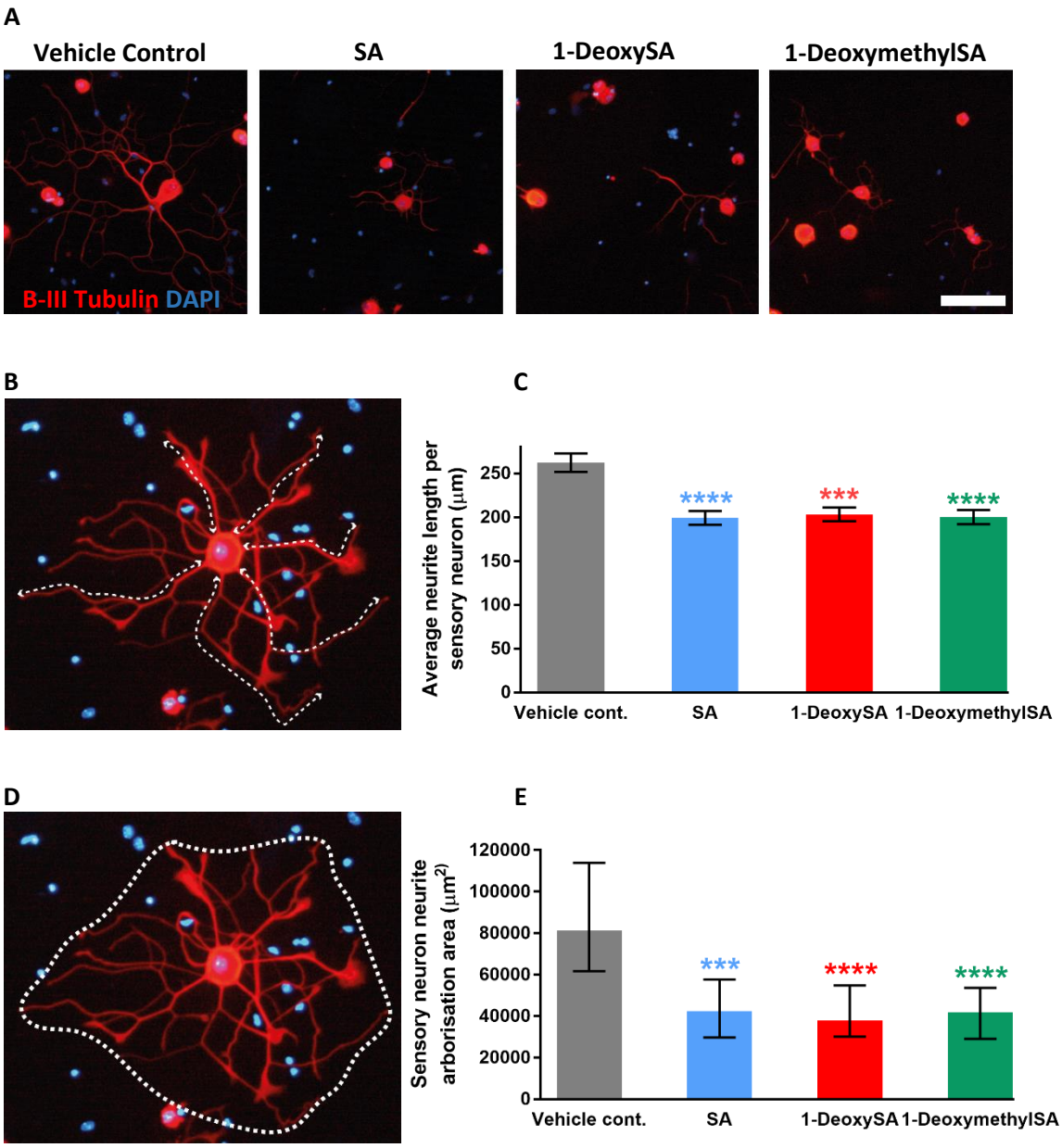

Figure 2.5 Treatment with sphinganine and 1-deoxysphingolipids reduces neurite outgrowth in sensory neurons in-vitro

(A) Primary DRG cultures were treated 3-4 hours after plating for 12 hours with 1μM Sphinganine (SA), 1-DeoxySA and 1-DeoxymethylSA or vehicle control. The cells were stained for neuronal marker β-III Tubulin (red) and co-stained with nuclear maker, DAPI (blue). Scale bar=100μm. **(B)** The longest neurite growth was determined as illustrated. The longest course for individual neurites were traced and an average neurite length per sensory neuron was recorded. **(C)** Sphingolipid treatment led to a reduction in neurite length. **(D)** Sensory neuron arborisation area was measured by tracing around the ends of individual neurites. **(E)** Sphingolipid treatment reduced sensory neuron arborisation area. Neurite arborisation data are represented as medians. Error bars= SEM (Figure C) and 95% confidence interval (Figure E). ***p<0.001, ****p < 0.0001. n=135-173 cells per condition from 5 independent experiments.

2.4.6 Effects of 1-deoxySLs on mitochondrial membrane potential in sensory neurons

Since treatment with 1-deoxySLs induced significant neuronal death and altered neurite development, I next examined whether there were any early functional deficits. Tetramethylrhodamine methyl ester (TMRM, a potentiometric dye which accumulates in mitochondria relative to the mitochondrial membrane potential) fluorescence was used as a readout for mitochondrial membrane potential. Mitochondrial membrane potentials were measured following 2hour treatment with sphingolipids to determine if there was early mitochondrial dysfunction in 1-deoxySL induced neurotoxicity. DRGs were cultured for 2-3 days prior to treatment with the sphingolipids.

DRG neurons in the vehicle treatment group displayed an average intensity of 3862 ± 48au. 1-DeoxySL treatment led to a small but significant reduction in TMRM intensity with a greater reduction observed following 1-deoxySA treatment (3627 ± 59au, p=0.0065) compared to 1-deoxymethylSA treatment (3687 ± 43au, *p*=0.045) (Figures 2.6A and B). Since the survival data for this treatment group revealed a differential vulnerability to 1-deoxySA induced toxicity between the large myelinated and small peptidergic neurons, the DRG neurons in the current experiment were sub-divided into large and small diameter neurons to determine if smaller sensory neurons exhibited a larger decline in mitochondrial membrane potential. Neurons with diameters less than 27μm were classified as 'small' and neurons with diameters ≥27μm were classified as 'large' (Scroggs *et al.*, 1994; Barabas *et al.*, 2014; Aboualizadeh *et al.*, 2015).1-DeoxySA treatment led to a reduction in TMRM intensity in both small (mean intensity of 3515 ± 38au, p=0.0002) and large neurons (mean intensity of 3582 ±59au, p=0.012) compared to control cultures, with mean TMRM intensities of 3843 ±42au and 3900 ±54au respectively (Figure 2.6C). 1-DeoxymethylSA treatment however, only induced a significant reduction in TMRM intensity (3596 ± 38au, *p*=0.003) in small neurons. 1-DeoxySA led to similar reductions in mean TMRM intensities in both the small and large DRG neurons. A significant difference in the mean TMRM intensities between the two DRG sub-populations was only seen with 1-deoxymethylSA treatment (p=0.0095).

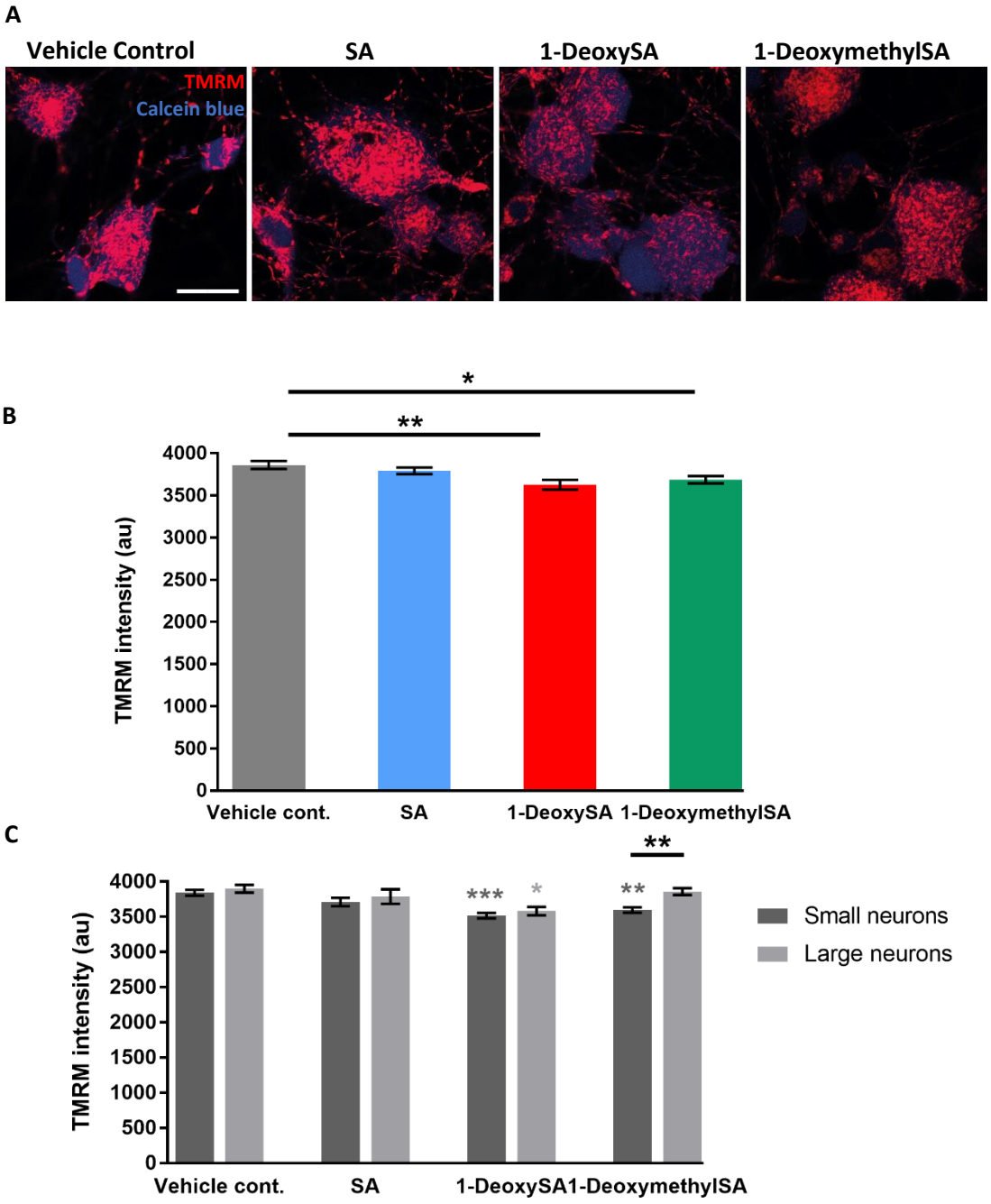

Figure 2.6 The effects of 2-hour sphingolipid treatment on mitochondrial membrane potential in sensory neurons in-vitro.

(A) Representative images of DRG cultures at 3DIV loaded with TMRM following 2 hours of treatment with 1µM sphingolipids. Scale bar=20µm. **(B)** 1-DeoxySA and 1-DeoxmethylSA treatments cause a reduction in mitochondrial membrane potential (TMRM intensity) compared to the vehicle control. **(C) 1**-DeoxySA treatment causes a reduction in mitochondrial membrane potential in both small diameter (<27µm) and large diameter (≥ 27µm) DRG neurons however 1-DeoxymethylSA treatment only reduced the membrane potential in the small diameter DRG neurons. n= 6 independent experiments representing 61-67 neurons per condition. Error bars= SEM. *p=<0.05, **p=<0.01, ***p=<0.001.

2.4.7 Effects of 1-deoxySL treatment on ER and Golgi structure

The structure of the ER and golgi were next assessed in DRG neurons treated for 24 hours with 1µM SA, 1-deoxySA and 1-deoxymethylSA and the findings were compared with that of the vehicle treated DRG neurons. The golgi marker, Giantin and the ER marker, protein disulphide isomerase (PDI) were used to visualise the organelles.

As can be seen in Figure 2.7, there was no difference in giantin immunoreactivity between the vehicle control and sphingolipid treated DRG neurons, suggesting an absence of any gross alteration in the structure of the golgi following sphingolipid treatment. Decreased PDI staining intensity was consistently observed in DRG neurons treated with SA and 1-deoxySA compared to the control cultures. An increased staining intensity was seen following 1-deoxymethylSA treatment (Figure 2.8A) which was seen maximally in the periphery of the neuronal cell bodies. These differences were quantified by Western blot analysis (Figures 2.8 B-C) using thapsigargin (TG) treatment as a positive control for ER stress. There was a significant reduction in PDI protein levels following SA and 1-deoxySA treatment (52 ± 12% and 59 ± 9% respectively, p=0.043) and a significant increase in levels following 1-deoxymethylSA and thapsigargin treatments (157 ± 16% and 139 ± 12% respectively, p=0.043).

2.4.8 Sphingolipid treatment and the activation of the Unfolded protein response (UPR).

PDI has two main functions. Firstly, it catalyses the oxidation, reduction and isomerisation of protein disulphide bonds via disulphide interchange activity (Perri *et al.*, 2016). Secondly, it acts as a chaperone which is dependent on its redox status and is involved in the UPR (Ali Khan and Mutus, 2014; Perri *et al.*, 2016). Due to its involvement in the UPR, protein levels of the three main ER stress sensors of the UPR (PERK, IRE1α and ATF6) and another ER chaperone, BiP were evaluated in the same lysates of DRG cultures treated with 1-deoxySLs. PERK, IRE1α and ATF6 are bound to BiP under basal conditions and are therefore inactive. When ER stress arises, there is accumulation of misfolded proteins in the ER lumen. BiP dissociates from the three mediators and binds to the misfolded proteins which results in the activation of the three ER stress sensors.

There was no significant change in these three ER stress sensors or BiP following treatment

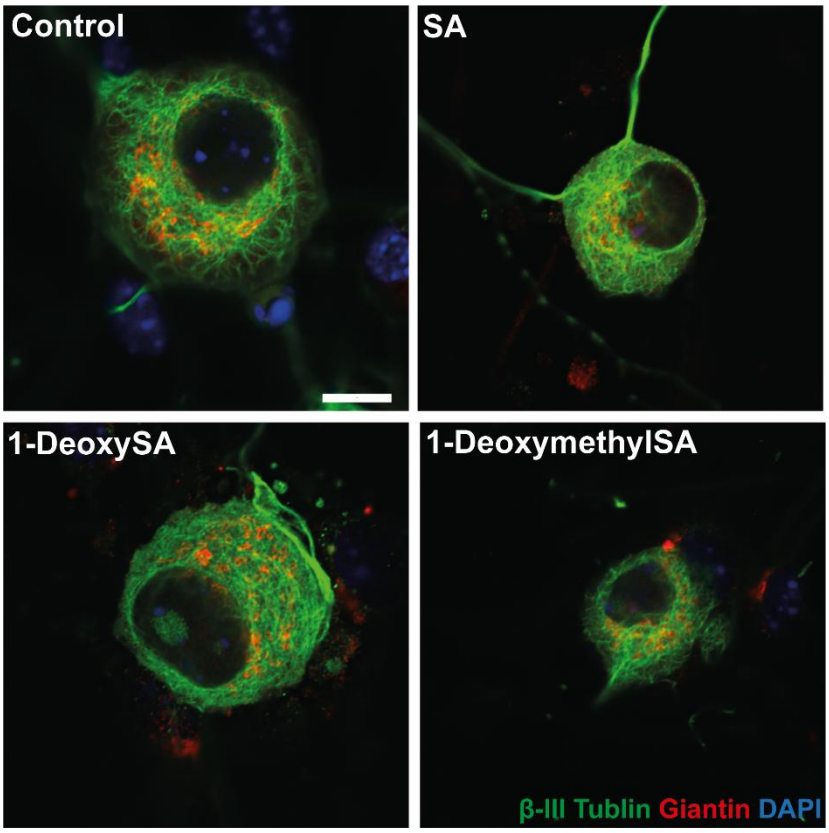

Figure 2.7 The effects of sphingolipid treatment on the Golgi structure of sensory neurons in-vitro.

DRG neurons were treated for 24 hours with 1μM Sphinganine (SA), 1-DeoxySA and 1-DeoxymethylSA or vehicle control and then fixed and immunostained with the neuronal marker β-III Tubulin (green), the Golgi marker Giantin (red) and co-stained with the nuclear marker, DAPI (blue). There is no difference in the Golgi structure between the vehicle treated and sphingolipid treated DRG neurons. Scale bar=10μm

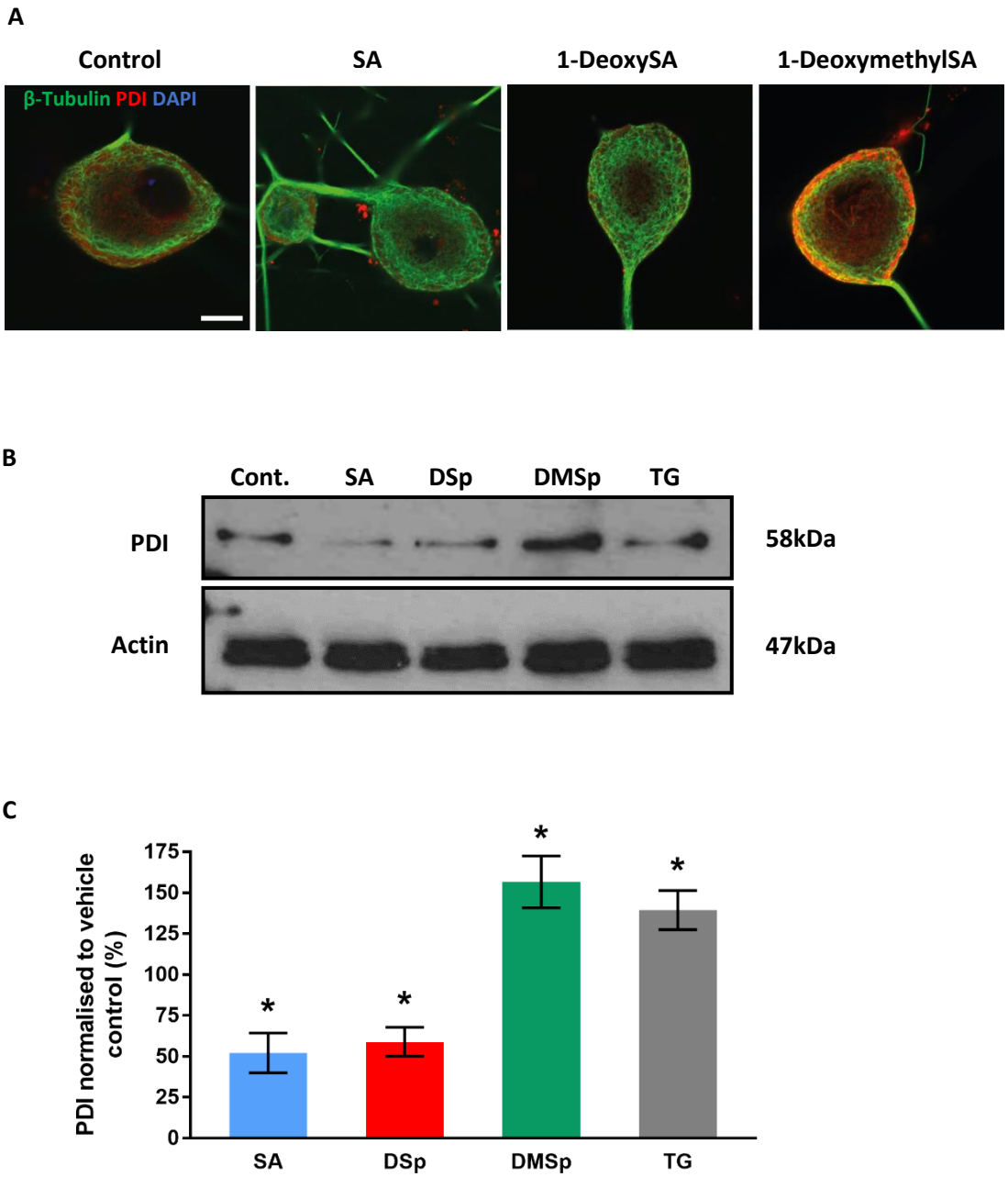

Figure 2.8 The effects of sphingolipid treatment on Protein Disulphide Isomerase (PDI) expression in sensory neurons in-vitro.

(A) DRG neurons treated for 24 hours with 1μM Sphinganine (SA), 1-DeoxySA (DSp), 1-DeoxymethylSA (DMSp) or vehicle control, then fixed and stained with the neuronal marker β-III Tubulin (green), the ER marker PDI and the nuclear marker DAPI (blue). Scale bar=10μm **(B)** Representative Western blot for PDI following 24 hour treatment with 1μM sphingolipids. 1μM thapsigargin (TG) was used as a positive control for ER stress. **(C)** PDI levels were normalised to β-actin and then normalised to vehicle control. There was a reduction in PDI expression with SA and 1-deoxySA treatments and an increase in expression with 1-deoxymethylSA and TG treatments. n=5 independent experiments. Error bars=SEM, *p<0.05

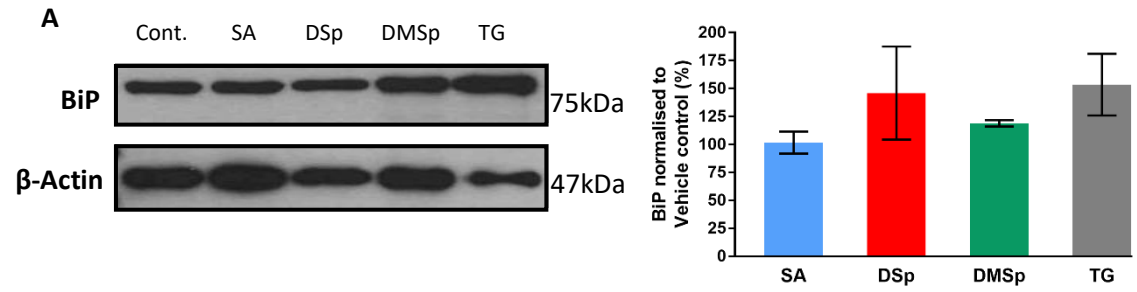
A
Cont.
SA
DSp
DMSp
TG
BiP
75kDa
β-Actin
47kDa
BiP normalised to Vehicle control (%)
200
175
150
125
100
75
50
25
0
SA
DSp
DMSp
TG

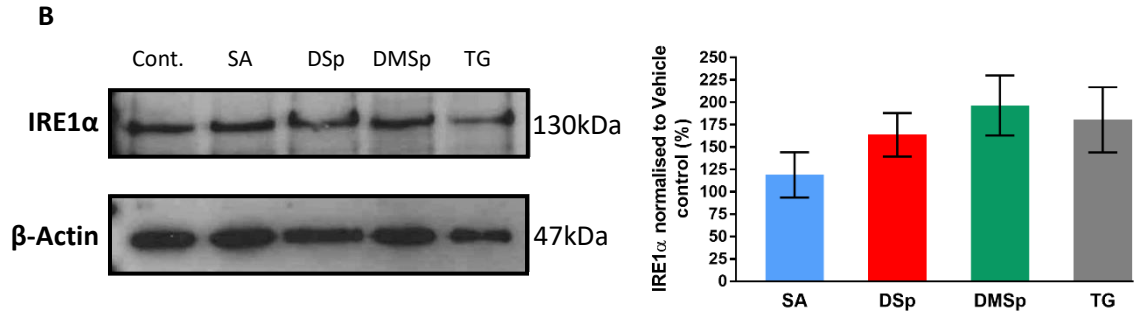
B
Cont.
SA
DSp
DMSp
TG
IRE1α
130kDa
β-Actin
47kDa
IRE1α normalised to Vehicle control (%)
250
225
200
175
150
125
100
75
50
25
0
SA
DSp
DMSp
TG

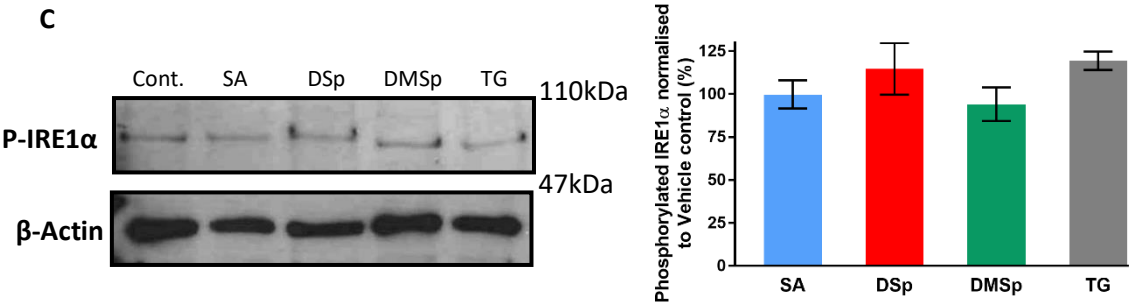
C
Cont.
SA
DSp
DMSp
TG
P-IRE1α
110kDa
47kDa
β-Actin
Phosphorylated IRE1α normalised to Vehicle control (%)
125
100
75
50
25
0
SA
DSp
DMSp
TG

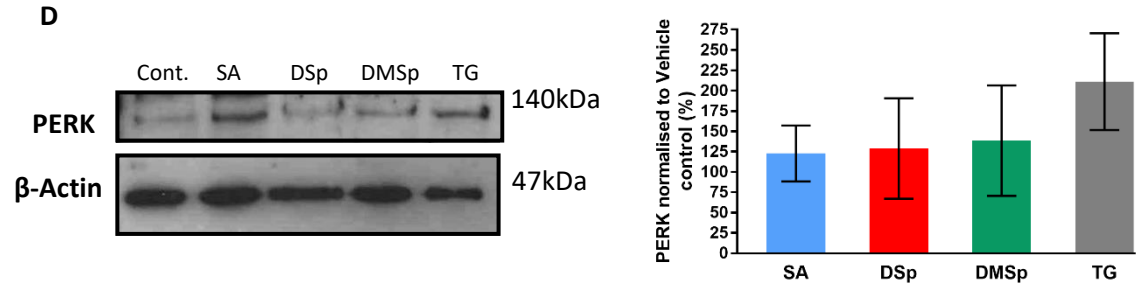
D
Cont.
SA
DSp
DMSp
TG
PERK
140kDa
β-Actin
47kDa
PERK normalised to Vehicle control (%)
275
250
225
200
175
150
125
100
75
50
25
0
SA
DSp
DMSp
TG

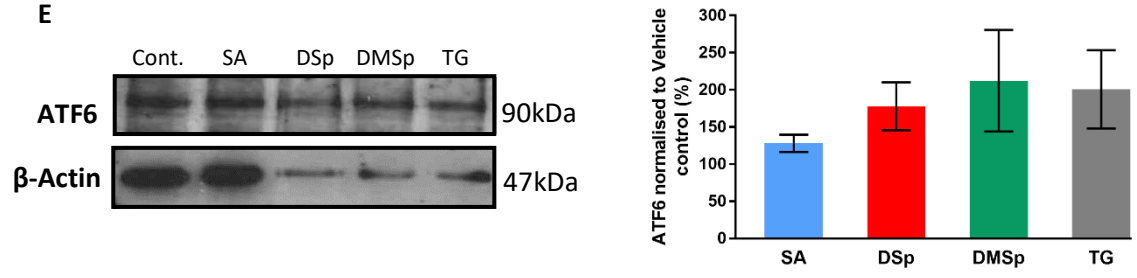
E
Cont.
SA
DSp
DMSp
TG
ATF6
90kDa
β-Actin
47kDa
ATF6 normalised to Vehicle control (%)
300
250
200
150
100
50
0
SA
DSp
DMSp
TG

Figure 2.9 The effects of Sphingolipid treatment on markers of the Unfolded Protein Response (UPR) in sensory neurons in-vitro.

DRG neurons were treated for 24 hours with 1µM Sphinganine (SA), 1-Deoxysphinganine (DSp), 1-Deoxymethylsphinanine (DMSp), thapsigargin (TG), a positive control for ER stress or vehicle control. Representative Western blots and quantification of protein levels were performed for **(A)** BiP, **(B)** IRE1α, **(C)** phosphorylated IRE1α **(D)** PERK and **(E)** ATF6**.** Protein levels were normalised to β-actin followed by normalisation to vehicle control. There were no significant changes in expression of UPR markers with sphingolipid treatment. n=4 independent experiments. Error bars=SEM

with sphingolipids when compared to the vehicle control (Figure 2.9). There was a slight increase in the levels of IRE1α (164 ± 24% for 1-deoxySA and 197 ± 37% for 1-deoxymethylSA) (Figure 2.9B) and ATF6 (178 ± 32 for 1-deoxySA and 201 ± 53% for 1-deoxymethylSA) (Figure 2.9E) following 1-deoxySL treatment compared to vehicle control. Since significant cell death was observed following 24 hours of treatment with 1-deoxySA, it is possible that a time point of 24 hours might be too late to capture early activation of the UPR. To determine if there is early activation of the UPR following sphingolipid treatment, SH-SY5Y cultures were treated for 2,6 and 24 hours with sphingolipids and the lysates analysed for levels of PDI, BiP and the UPR ER stress sensors, PERK and IRE1α. Analysis of ATF6 was attempted however the bands on the western blots were indistinct when using SH-SY5Y cultures. SH-SY5Y cultures were used instead of DRG cultures as it was difficult to obtain sufficient protein concentrations required for the Western blot technique using DRG cultures.

Following 24 hour treatment with sphingolipids, the SH-SY5Y cultures show a similar pattern of reduction in PDI levels following 1-deoxySA treatment (69 ± 6.3% versus vehicle control of 85 ± 20%) and an increase following 1-deoxmethylSA treatment (145 ± 11%) (Figures 2.10 C and D). However, these changes were not significant (p=0.10). Unlike DRG cultures, there was no reduction in PDI levels in SH-SY5Y cells following SA treatment (96 ± 23%). With a shorter treatment duration of 2hours, there was an increase in PDI levels in all treatment groups including the vehicle control relative to the untreated control (vehicle control=234 ± 59%, SA=281 ±76% and 1-deoxymethylSA=305 ± 107%) with the largest increase with 1-deoxySA treatment (481± 159%) (Figure 2.10 A and D). There was no significant difference at 2hours of treatment between the sphingolipid treatment groups and the vehicle control (p=0.70). The PDI levels peak at 2 hours, with a rapid decline seen thereafter with 1-deoxySA treatment (Figure 2.10D).

Levels of BiP, another chaperone protein involved in the UPR, increased initially at 2 hours with SA and 1-deoxySA treatments relative to the untreated control (239 ± 69% and 302 ± 132% respectively), however there is marked variability between the cultures, especially with 1-deoxySA treatment (Figures 2.11A and D). Unlike with PDI, a biphasic increase in BiP levels was seen following SA and 1-deoxySA treatments, with a second peak occurring

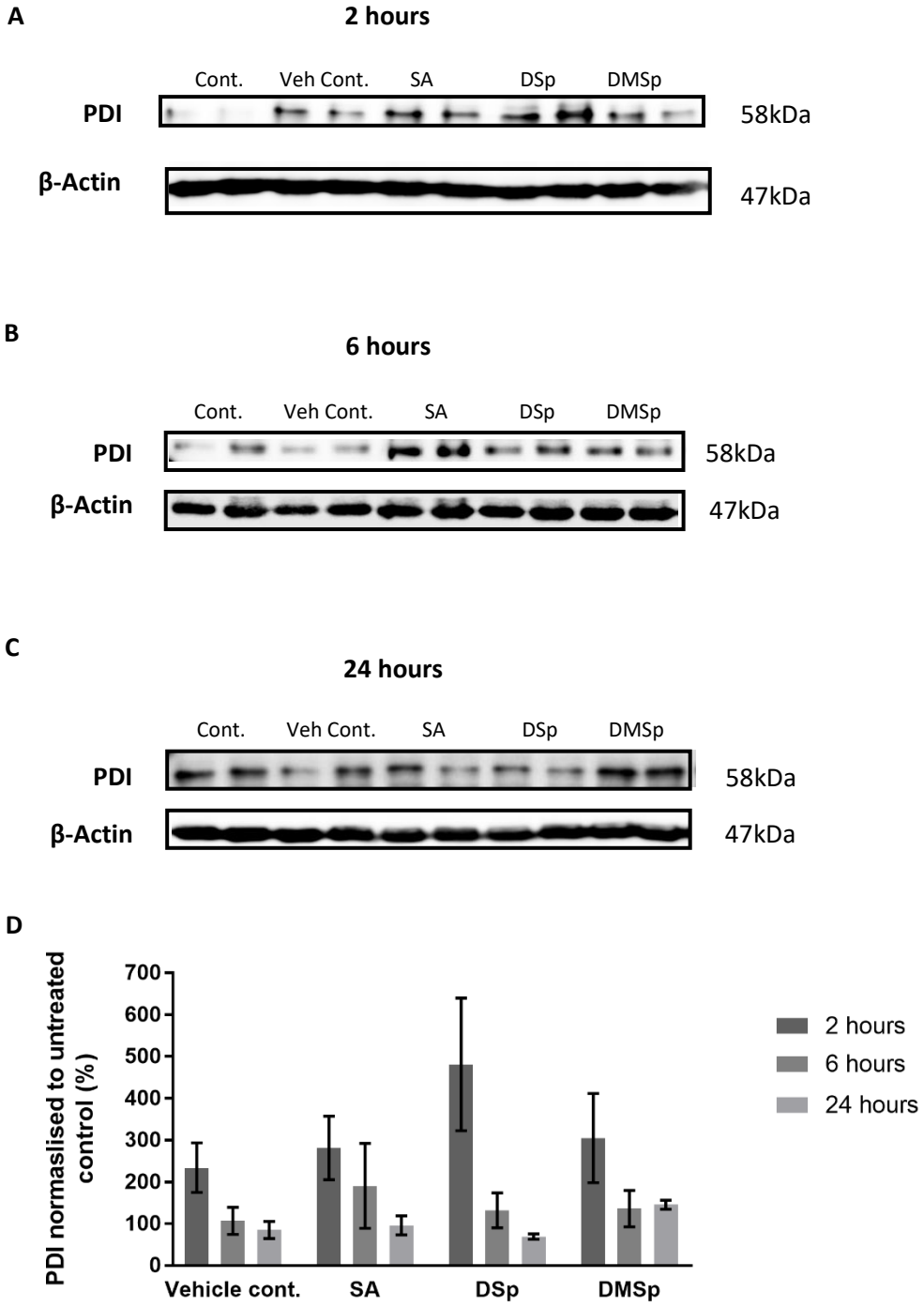

Figure 2.10 Variation in PDI levels following treatment of SH-SY5Y cells with sphingolipids.

SH-SY5Y cultures were treated for 2, 6 and 24 hours with 1µM Sphinganine (SA), 1-deoxysphinganine (DSp), 1- deoxymethylsphinganine (DMSp) or vehicle (ethanol). Representative western blots for 2 hours **(A)**, 6 hours **(B)** and 24 hours **(C)** are shown. There was an initial increase in PDI levels in all treatment groups with 1-deoxySA treatment causing the greatest increase **(D)**. Cont.=untreated control, Veh Cont./Vehicle cont.= vehicle control, n=3 cultures. Error bars=SEM

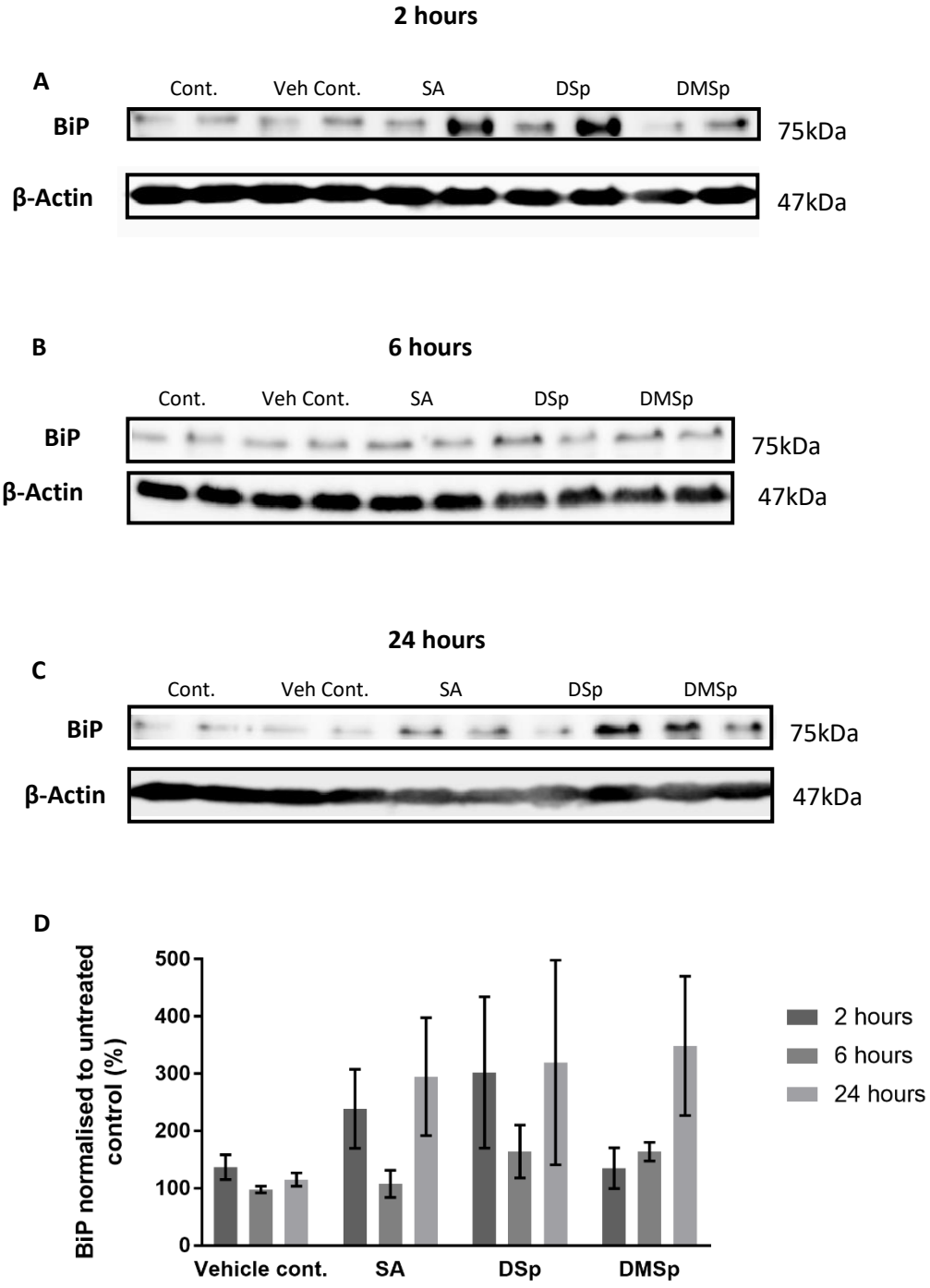

Figure 2.11 Variation in BiP levels in SH-SY5Y cells following treatment with sphingolipids.

SH-SY5Y cultures were treated for 2, 6 and 24 hours with 1μM Sphinganine (SA), 1-deoxysphinganine (DSp), 1- deoxymethylsphinganine (DMSp) or vehicle (ethanol). Representative western blots for 2 hours **(A)**, 6 hours **(B)** and 24 hours **(C)** are shown. There was a trend towards a biphasic increase at 2 and 24 hours with SA and DSp treatments **(D).** Cont.= untreated control, Veh Cont./Vehicle cont.= vehicle control, n=3 cultures. Error bars=SEM

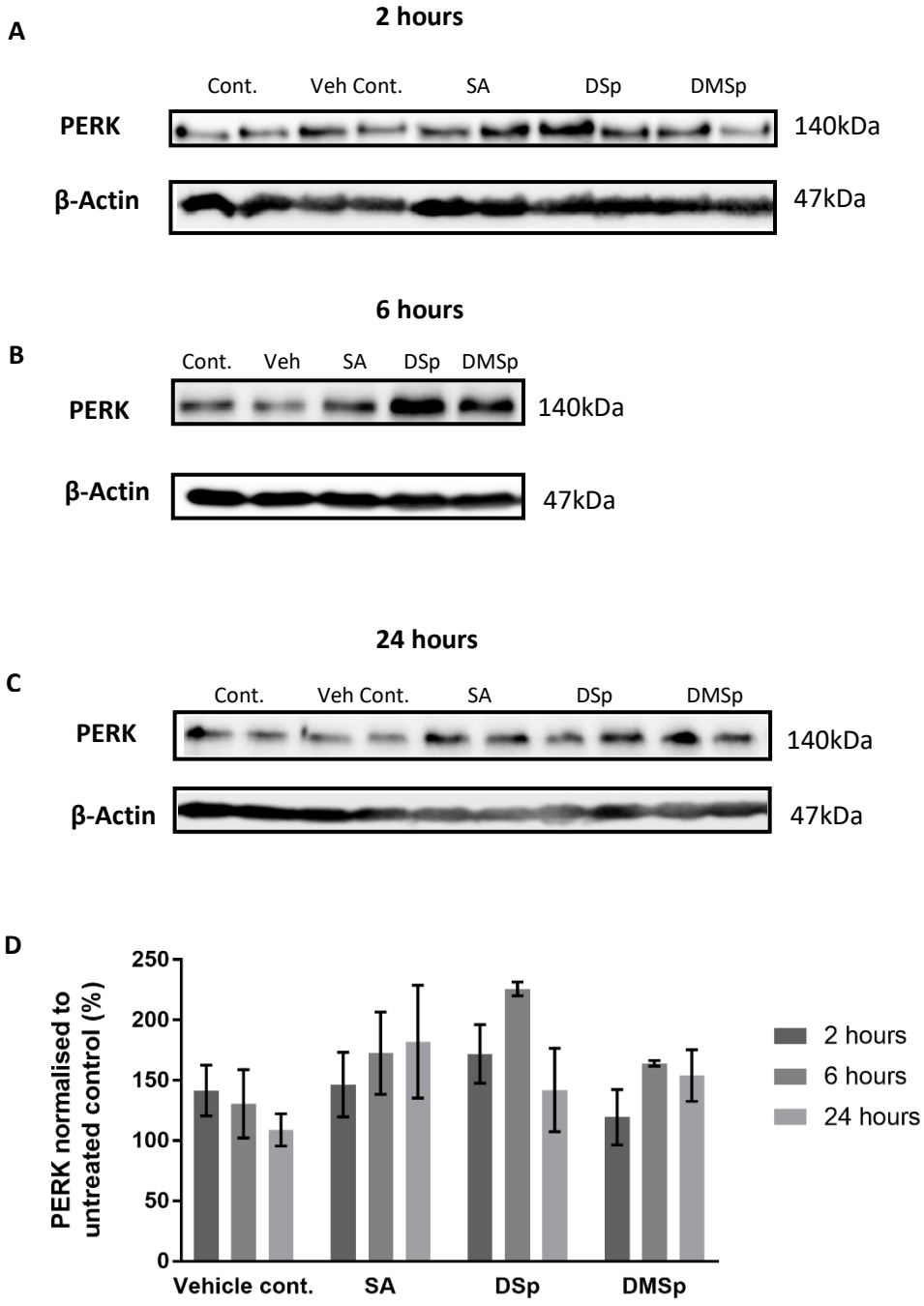

Figure 2.12 Variation in PERK levels in SH-SY5Y cells following treatment with sphingolipids

SH-SY5Y cultures were treated for 2, 6 and 24 hours with 1µM Sphinganine (SA), 1-deoxysphinganine (DSp), 1- deoxymethylsphinganine (DMSp) or vehicle (ethanol). Representative western blots for 2 hours **(A)**, 6 hours **(B)** and 24 hours **(C)** are shown. There are no significant differences (p=0.07) in the PERK levels between the different treatment groups at the three time points **(D)**. The highest PERK levels were seen with 1-deoxySA treatment which peaks at 6 hours of treatment. Similar PERK levels were seen with DMSp and the sphingolipid control, SA, treatments. Cont.= untreated control, Vehicle cont./Veh= vehicle control, n=3 cultures. Error bars=SEM

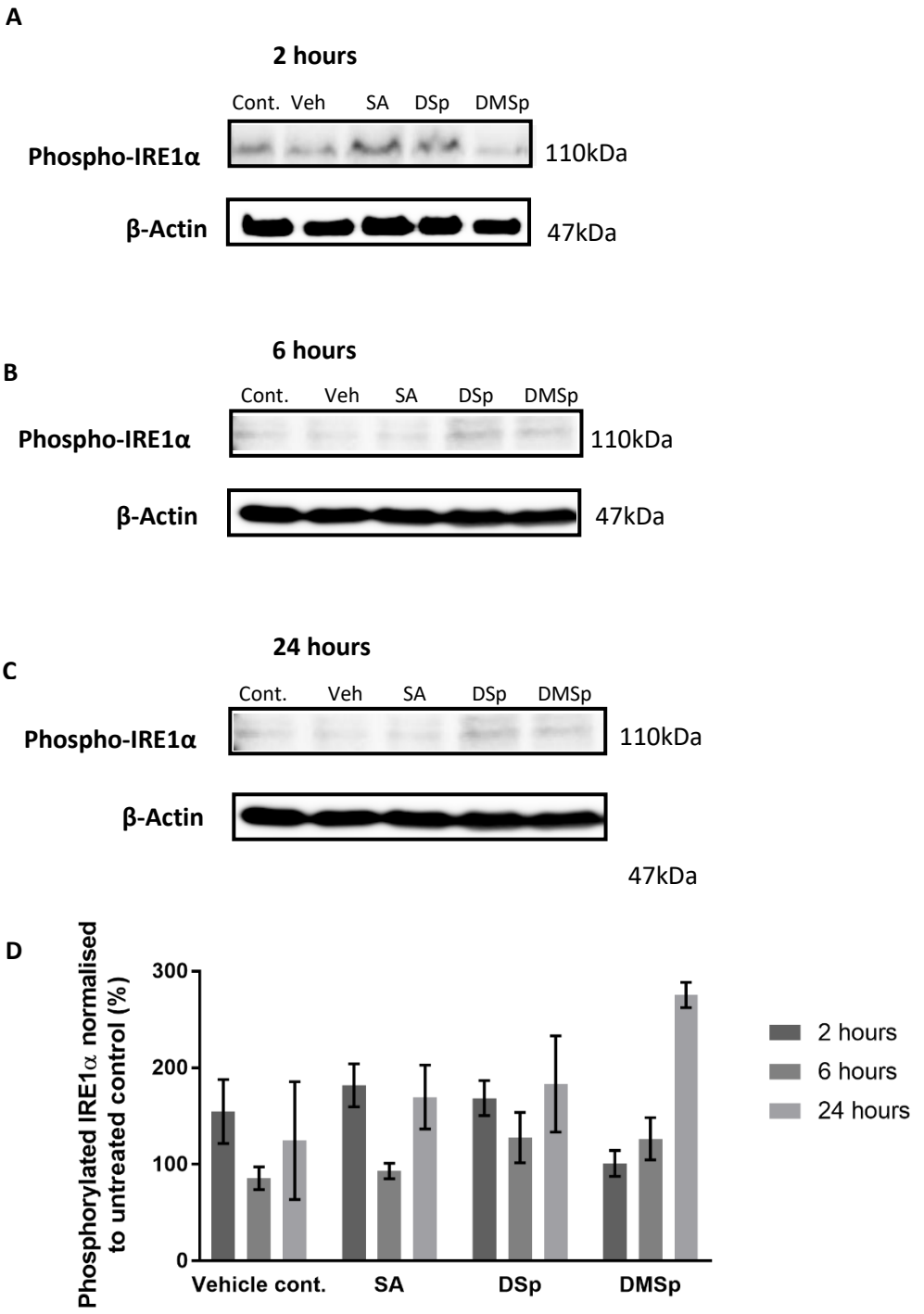

Figure 2.13 Variation in Phosphorylated IRE1α (P-IRE1α) levels in SH-SY5Y cells treated with sphingolipids.

SH-SY5Y cultures were treated for 2, 6 and 24 hours with 1µM Sphinganine (SA), 1-deoxysphinganine (DSp), 1- deoxymethylsphinganine (DMSp) or vehicle (ethanol). Representative western blots for 2 hours **(A)**, 6 hours **(B)** and 24 hours **(C)** are shown. Following an initial increase after 2 hours of treatment seen with vehicle control, SA and 1-deoxySA treatments, there was second peak in P-IRE1α levels with SA and DSp treatments. DMSp treatment, led to the highest elevation in P-IRE1α levels which was seen after 24 hours of treatment **(D)**. Cont.= untreated control, Vehicle cont./Veh= vehicle control, n=3 cultures. Error bars=SEM

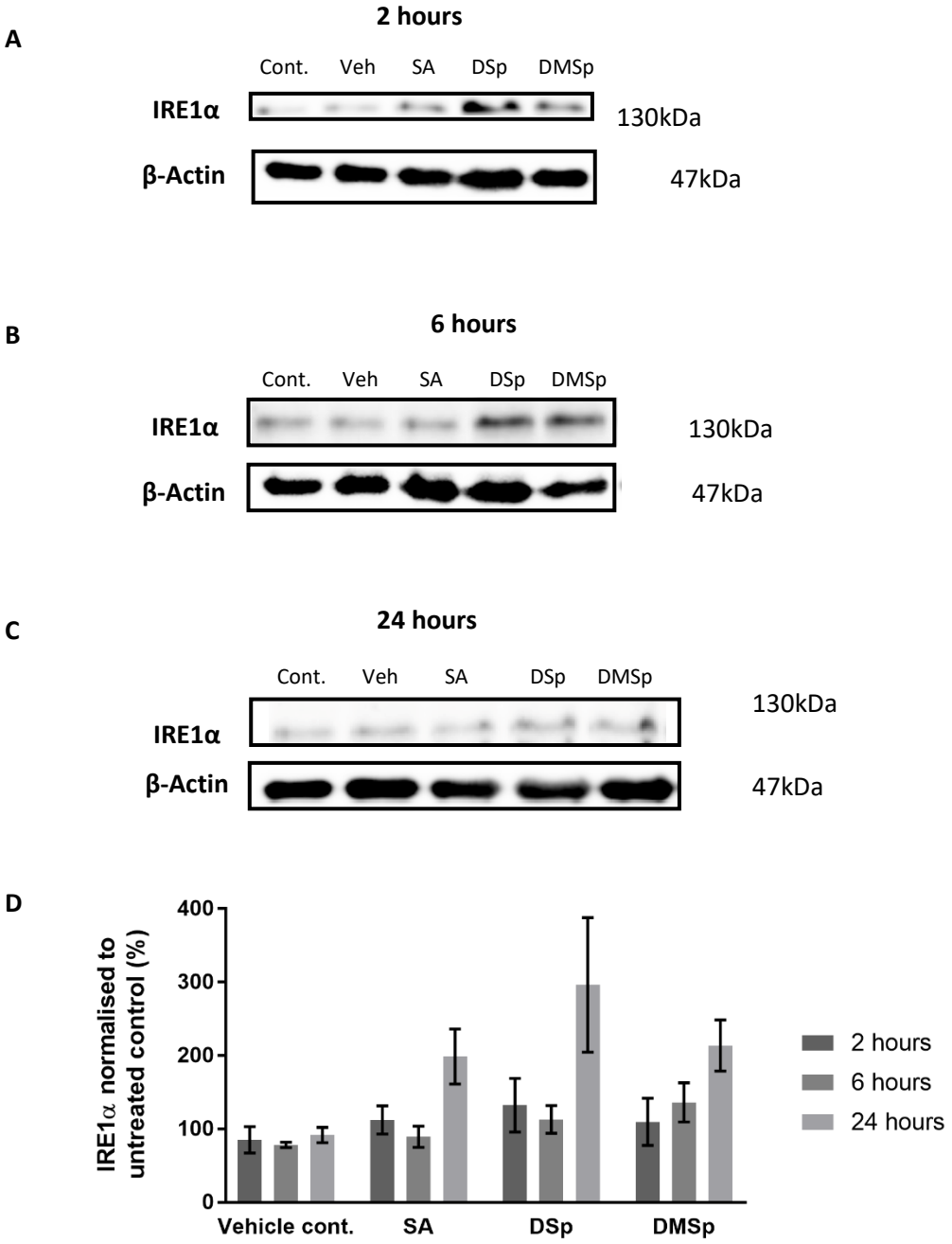

Figure 2.14 Variation in IRE1α levels in SH-SY5Y cells treated with sphingolipids.

SH-SY5Y cultures were treated for 2, 6 and 24 hours with 1µM Sphinganine (SA), 1-deoxysphinganine (DSp), 1- deoxymethylsphinganine (DMSp) or vehicle (ethanol). Representative western blots for 2 hours **(A)**, 6 hours **(B)** and 24 hours **(C)** are shown. There is a trend towards increased IRE1α levels following 24 hours of treatment with all sphingolipids **(D)**. Cont.= untreated control, Veh/Vehicle cont.= vehicle control, n=3 cultures. Error bars=SEM

at 24hours (BiP levels of 295 ± 103% with SA and 320 ± 179% with 1-deoxySA treatments) (Figure 2.11D). With 1-deoxymethylSA treatment, the increase in BiP levels was delayed and a peak (329 ± 61%) was only seen after 24 hours of treatment.

A progressive increase in PERK levels was observed in SH-SY5Y cells following all sphingolipid treatments, when compared to the untreated control cultures, whereas a progressive decline in PERK levels was observed following vehicle treatment (Figure 2.12D). The highest levels were observed following 6 hours of treatment with 1-deoxySA (226 ± 6% versus 173 ± 34% with SA, 164 ± 2% with 1-deoxymethylSA and 131 ± 28% with vehicle control treatments) however the increase was not significant (p=0.07).

The pattern of increased expression of phosphorylated IRE1α (P-IRE1α, activated form of IRE1α) was similar to that observed with BiP. There was an initial increase in P-IRE1α levels following all treatments except 1-deoxymethylSA, compared to the untreated control (vehicle control=155 ± 33%, SA=182 ± 22% and 1-deoxySA=169 ± 18%) (Figure 2.13D). A biphasic elevation in P-IRE1α levels was observed following SA and 1-deoxySA treatments, with the second peak occurring after 24 hours of treatment (170 ± 33% and 183 ± 50% respectively). A delayed elevation in P-IRE1α levels was observed following 1-deoxymethylSA treatment, with the peak (275 ± 13%) detected only after 24hours of treatment. There were no significant differences in P-IRE1α levels between the different treatment groups at the 3 time points. Levels of IRE1α were also elevated following all sphingolipid treatments compared to the untreated control and vehicle control, but only after 24hours of treatment (Figure 2.14D). There was no significant difference between the treatment groups (p=0.06). At this treatment duration of 24 hours, IRE1α was comparably elevated amongst the sphingolipids (SA=199 ± 37%, 1-deoxySA=221 ± 32% and 1-deoxymethylSA=214 ± 35%). The differences in the pattern of elevation between IRE1α and P-IRE1α might be because IRE1α reflects the summation of IRE1 and previously phosphorylated IRE1α.

In summary, these results suggest that sphingolipid treatment leads to ER stress and activation of the UPR. Initially, there is upregulation of the early players in the UPR, PDI and BiP. The largest increase in PDI levels is observed following 1-deoxySA treatment. This is followed by the increase in the ER stress sensors: PERK and IRE1α/P- IRE1α. 1-DeoxySA

and SA treatments have a similar pattern of upregulation of BiP and the ER stress sensors.1-DeoxymethylSA treatment leads to a slower upregulation of BiP and P-IRE1α.

2.5 Discussion

The aims of the experiments presented in this chapter were to determine if 1-deoxySLs were toxic to primary mammalian motor and DRG neurons and to investigate underlying pathomechanisms of 1-deoxySL induced neurotoxicity using this in-vitro model.

2.5.1 Exogenous 1-deoxySLs are toxic to mammalian neurons

The results presented in this chapter clearly demonstrate that exogenously applied 1-deoxySLs are toxic to mammalian primary motor and DRG neurons. At 1µM concentrations, 1-deoxySLs (1-deoxySA and 1-deoxymethylSA) cause a treatment duration-dependent reduction in motor and DRG neuron survival. 1-deoxySA was more toxic than 1-deoxymethylSA and this difference was more pronounced in DRG cultures. With prolonged treatment, motor neurons were equally vulnerable to 1-deoxySA and 1-deoxymethylSA induced toxicity. Penno *et al.* (2010) previously reported that they did not observe any reduction in DRG and motor neuron survival after 24 hours of treatment with 1µM 1-deoxySLs but they did observe a dose dependent effect on the number of neurites per sensory/motor neuron. However, there is a discrepancy in the data presented in this paper so that the analysis of neurite outgrowth also suggests a reduction in the number of surviving neurons.

DRG neurons appear more vulnerable to 1-deoxySLs than motor neurons, with respect to the onset and degree of toxicity so that 69%DRG neurons and 36% motor neurons died after 48 hours of treatment with 1-deoxySA. However, a direct comparison between the two neuronal cultures cannot be made as motor neuron cultures were derived from mouse embryos (E13-14) whereas DRG cultures were derived from mouse pups (P5-8). At the embryonic stage, neurons might be less susceptible to 1-deoxySL toxicity. Motor neuron and DRG cultures could also have different vulnerability to the culturing process which could influence their ability to withstand subsequent 1-deoxySL treatment. Embryonic motor neurons were used in this study because it is not possible to culture primary motor neurons from older embryos or pups. Similarly, embryonic DRG cultures could not be used due to technical limitations with the dissection procedure.

Clearly, the toxicity of 1-deoxySLs to developing neurons in culture does not reflect the phenotype of HSN patients who exhibit a very slowly progressive neuropathy. The

sphingolipid concentration of 1µM used in these experiments was chosen as this was at the higher end of the 1-deoxySA concentrations detected in plasma of HSN1 patients (Penno *et al.*, 2010) and therefore more likely to produce discernible differences in the relatively crude measure of cell survival. The concentrations of these 1-deoxySLs in the cerebrospinal fluid (CSF) of HSN1 patients remains unknown. In plasma, 1-deoxySLs are bound to low density lipoproteins (LDL) and very low density lipoproteins (VLDL), which indicates that plasma 1-deoxySLs are of hepatic origin (Bertea *et al.*, 2010). The blood brain barrier (BBB) restricts plasma lipoproteins (LDL, VLDL) from entering the central nervous system (Mahley, 2016). Based on mammalian in-vivo studies, the blood nerve barrier is only second to the BBB in terms of restrictive barrier properties (Ubogu, 2013) therefore it is possible that peripheral nerves would not be exposed to the high levels of 1-deoxySLs used in this study. This in combination with having undergone the stressful procedure of culturing, might explain the enhanced vulnerability of cells in this in-vitro model compared to peripheral nerves in HSN1 patients.

With longer treatment durations, 1-deoxySL treatment resulted in a loss of non-neuronal cells in both motor neuron and DRG cultures. This toxicity was greater with 1-deoxySA treatment. This is difficult to explain given the HSN1 phenotype (Houlden *et al.*, 2006). One possible explanation is that 1-deoxySLs may be endogenously produced. In culture, many cell lines can produce high levels of 1-deoxySLs due to the tendency to deplete L-serine and accumulate L-alanine in the medium (Zitomer *et al.*, 2009; Duan and Merrill, 2015). Rapidly multiplying non-neuronal cells, which form a dense basal layer in culture wells, could easily deplete L-serine in the surrounding media resulting in the usage of L-alanine and the production of the toxic 1-deoxySLs.

The effects of 1-deoxySLs on neurite outgrowth were analysed in DRG cultures 12 hours following treatment with 1-deoxySLs. At 1µM concentrations, SA, in addition to the 1-deoxySLs caused a reduction in neurite outgrowth including neurite length and arborization area. All three sphingolipids (SPT enzyme products) led to similar reductions in neurite outgrowth. With the same concentration, Penno *et al.* (2010) did not observe a reduction in neurite outgrowth with SA treatment and 1-deoxySA had a more toxic effect on neurite outgrowth than 1-deoxymethylSA. In this study, sphingolipid treatment was initiated 3-4 hours after plating and the neurite length assessed after 12 hours of treatment. Penno *et al.*

(2010) grew the sensory neurons for 12 hours in control medium before adding sphingolipids and the neurite lengths were analysed after 24 hours of treatment. During the very early phase of growth, the neurons might be more vulnerable to any perturbations and this could explain why SA and 1-deoxymethylSA had greater effect in this study.

2.5.2 Differential 1-deoxySL induced neurotoxicity within sensory sub-populations

HSN1 patients have dissociated sensory loss whereby pain and temperature sensation are affected earlier and more severely than joint position sense and vibration. This part of the study looked at whether there is differential toxicity between the different sub-populations of sensory neurons responsible for these modalities.

There are three principle sensory neuron subtypes: nociceptive, mechanoreceptive and proprioceptive neurons. Mechanoreceptive and proprioceptive neurons are large/medium sized neurons, myelinated, fast conducting (Aα and Aβ fibres) and can be identified based on expression of heavy chain neurofilament (NF200+ve) (Lawson and Waddell, 1991; Tucker *et al.*, 2006). These constitute about 40% of lumbar DRGs (Priestley *et al.*, 2002). This subclass of neurons also expresses the p75 neurotrophic receptor and tropomycin related kinase C (TrkC). These cells are therefore able to respond to nerve growth factor (NGF), neurotrophin 3 (NT3) and brain derived neurotrophic factor (BDNF). Some nociceptive neurons are myelinated (Aδ fibres) but most are unmyelinated (C fibres, slowly conducting) and this subtype represents the majority of the sensory neurons in the peripheral nervous system (Woolf and Ma, 2007). Aδ fibres convey cold and nociceptive input. C fibres are responsible for conveying information about innocuous warm sensations and noxious inputs from several different high threshold mechanical, chemical and thermal stimuli (Themistocleous *et al.*, 2014). Nociceptors can be separated into peptidergic and non-peptidergic neurons which differ in their expression of receptors, ion channels and innervate distinct peripheral and central targets.

Peptidergic neurons express CGRP and substance P and cannot bind isolectin B4 (IB4). These neurons also retain the expression of nerve growth factor (NGF) receptor, tropomycin related kinase A (TrKA) (Woolf and Ma, 2007) and also express high levels of p75 but preferentially respond to NGF. There is an overlap between NF200 +ve and CGRP +ve populations which corresponds to Aδ nociceptors (Priestley *et al.*, 2002). Non- peptidergic

neurons switch off TrK expression early on in development and instead express Ret tyrosine kinase receptor and growth factor receptor α and hence these neurons are responsive to glial derived neurotrophic factor (GDNF) and are unresponsive to NGF, NT3 and BDNF (Priestley *et al.*, 2002; Tucker *et al.*, 2006). These neurons can be identified by their binding of IB4. The functional difference between CGRP+ve peptidergic neurons and non-peptidergic neurons is not fully understood. There is growing evidence that CGRP positive neurons are responsible for noxious heat sensation (Ye *et al.*, 2012; McCoy *et al.*, 2014). As loss of thermal sensation occurs early in the disease process, CGRP +ve neurons were quantified in this study.

1-DeoxySA was found to be toxic to both NF200+ve (large, myelinated neurons) and the CGRP+ve, small peptidergic neurons. However, the CGRP+ve neurons appear more susceptible to 1-deoxySL toxicity with earlier onset of toxicity and a greater reduction in cell survival when compared to NF200+ve neurons. In both sensory sub-types, 1-deoxymethylSA appears to be less toxic. This is especially the case with the large NF200+ve neurons where there is no progressive loss of neurons with increasing 1-deoxymethylSA treatment time. Embryonically, small neurons are preferentially lost in NGF and TrkA mutant mice indicating these neurons rely more on the trophic support of NGF than large neurons (Ernsberger, 2009). However, the requirement of NGF for survival of CGRP+ve neurons is rapidly reduced postnatally and lost in adult (Lewin *et al.*, 1992; Ernsberger, 2009). Whether this differential requirement for NGF postnatally, despite NGF supplementation in the growth media, contributes to the intrinsic vulnerability of CGRP+ve neurons is uncertain. This intrinsic vulnerability might exaggerate the effects of 1-deoxySL induced toxicity.

The preferential loss of CGRP+ve neurons would be expected given the clinical phenotype of HSN1. However, this clear preferential loss is not seen in the sural nerve biopsies reported by Houlden *et al.* (2006).In the biopsies of six male HSN1 patients (27-65 years old), there were very few myelinated fibres, but electron microscopy revealed a reasonable number of unmyelinated fibres. Lindahl *et al*. (2006) noted similar findings in an autopsy of 93 year HSN1 female patient. Examination of the cutaneous branches of the radial and sural nerves showed almost complete depletion of myelinated fibres but less severe loss of unmyelinated fibres. This discrepancy is difficult to explain. One possible explanation is that

the non-peptidergic IB4 +ve neurons are relatively well-preserved resulting in improved unmyelinated fibre counts. Another possible explanation is that there is a phenotypic switch via alteration in transcription which changes the molecular identity of the neurons whereby they no longer express CGRP thereby mimicking the loss of CGRP+ve neurons. Phenotypic switches have been found to occur in instances of axonal injury (Woolf and Ma, 2007).

2.5.3 Potential pathomechanisms of 1-deoxySL induced toxicity

In sensory neurons both 1-deoxySA and 1-deoxymethylSA caused a small but significant reduction in mitochondrial membrane potential following just 2 hours of treatment. This could indicate that mitochondrial dysfunction is an early event in the pathological process or it could reflect the fact that exogenously applied 1-deoxySLs are first taken up by the mitochondria. In large neurons, 1-DeoxymethylSA treatment does not cause a reduction in the mitochondrial membrane potential. This finding, as with the cell survival data, supports the proposal that mitochondrial dysfunction plays a role in 1-deoxySL toxicity. Wilson *et al.* (2018) demonstrated a significant reduction in mitochondrial membrane potential in mouse primary motor neuron cultures following 2hour 1-deoxySL treatment.

Studies have suggested that it is the N-acyl downstream products of 1-deoxySA,1-deoxydihydroceramide (1-doxDHCer) and1-deoxyceramide (1-doxCer) which are the toxic agents, not 1-deoxySA itself (Güntert *et al.*, 2016; Alecu *et al.*, 2017b). The enzyme responsible for the N-acylation, ceramide synthase, resides in the ER. These N-acyl products are highly hydrophobic, especially 1-deoxymethyldihydroceramide (unable for form lipid bilayers), and are transported to the golgi (Jiménez-Rojo *et al.*, 2014). 1-Deoxyceramide cannot be converted to more complex sphingolipids or be degraded via the conventional sphingolipid degradation pathway (Penno *et al.*, 2010) and therefore is likely to accumulate in the golgi. The hydrophobic nature of these N-acyl downstream metabolites could alter the structure of the ER or the golgi.

I found no gross alterations in the morphology of the golgi in DRG cultures following 1-deoxySL treatment. However, there was a significant reduction in PDI expression, which was used to localise the ER, following 24 hours of SA and 1-deoxySA treatment and a significant elevation following 1-deoxymethylSA treatment which was most prominent in the periphery of the neuronal cell bodies. The hydrophobicity of 1-deoxymethylSA and its N-acyl

downstream metabolites could restrict their cellular localisation to the periphery following intracellular uptake and hence explain the peripheral localisation of the PDI. PDI, an ER protein, has multiple functions but two of the most well-known are as a chaperone and a catalyst of protein disulphide bond formation. Using SH-SY5Y cell cultures, it was possible to track the changes in the two ER chaperones, PDI, BiP and the ER stress sensors, PERK and IRE1α, over the course of 2-24 hours of sphingolipid treatment. Although the changes in these proteins with sphingolipid treatment are not significant when compared to the vehicle control, the changes are complementary and suggest that 1-deoxySL treatment induces early ER stress followed by the initiation of the UPR. Within 2 hours of treatment there is upregulation of PDI and BiP expression followed later by upregulation of PERK which peaks at 6 hours and IRE1α which peaks at 24 hours. This sequence of activation matches the physiological sequence of events in the UPR.

The UPR is essentially an adaptive program which combines the early inhibition of protein synthesis (via PERK mediated pathway) with later upregulation of genes that promote protein folding or disposal (IRE1α and ATF6 mediated pathways). Both the changes in translation and transcription aim to protect the cell from being overwhelmed by unfolded proteins and allow ER homeostasis to be restored. However, under conditions of chronic or unmitigated ER stress, there is a shift in the paradigm from the UPR being protective to pro-apoptotic. PERK activation, in addition to global translational suppression, induces the translation of several mRNAs including ATF4 (activation transcription factor 4) (Cao and Kaufman, 2013). One of the downstream targets of ATF4 is the transcription factor CHOP (C/EBP homologous protein), which is an important mediator of ER stress induced apoptosis. IRE1α activation can induce apoptosis by the recruitment of the apoptosis signalling kinase (ASK1) (Cao and Kaufman, 2013).

A key point to note is that both 1-deoxySLs and the canonical SPT enzyme product, SA, appear to cause ER stress and activation of the UPR. The pattern of upregulation is very similar following both SA and 1-deoxySA treatments, however the degree of PDI and PERK upregulation is greater with 1-deoxySA treatment. Since there is no significant cell death following SA treatment, this suggests either that ER homeostasis is sufficiently restored following the UPR with SA treatment but not with 1-deoxySA treatment, leading to UPR mediated apoptosis or that ER stress is not the only mechanism of 1-deoxySL induced

toxicity. Canonical dihydroceramides are converted to ceramides by the addition of a Δ4,5 *trans* double bond whereas a Δ14,15 cis double bond is most commonly added in 1-deoxydihydroceramides (Alecu *et al.*, 2017a). This suggests that 1-deoxySL metabolism may follow a different route to the canonical sphingolipids. Dihydroceramides produced by metabolism of SA are rapidly converted to sphingosine and more complex sphingolipids whereas 1-deoxydihydrosphinganine produced by metabolism of 1-deoxySA is metabolised more slowly to 1-deoxysphingosine, resulting in the accumulation of 1-deoxydihydroceramides and sustained ER stress (Alecu *et al.*, 2017b). Dihydroceramides have been shown to induce ER stress (Gagliostro *et al.*, 2012). Fuminosin B_1 is a mycotoxin which inhibits ceramide synthase (catalyses conversion of SA to dihydroceramide). Inhibition of ceramide synthase by Fuminosin B_1 mainly results in elevated levels of SA which is normally present in cells at very low concentrations (0.5-3nml/g wet weight) (Stockmann-Juvala and Savolainen, 2008). It appears to be the accumulation of SA which is responsible for most of the adverse effects of Fuminosin B_1 with some studies proposing oxidative stress as a possible pathomechanism (Linn *et al.*, 2001; Stockmann-Juvala and Savolainen, 2008). It is therefore not surprising that SA treatment led to ER stress.

Other studies using models of exogenous 1-deoxySL application have suggested ER stress as a possible mechanism of 1-deoxySL induced toxicity (Gable *et al.*, 2010; Alecu *et al.*, 2017b). During my PhD I collaborated closely with Emma Wilson, a fellow PhD student, who focused on assessing ER and mitochondrial dysfunction following 1-deoxySL treatment in mouse motor and DRG neurons using in-vivo calcium imaging. We published our combined results in Wilson *et al*. (2018). We showed a marked reduction in ER calcium concentration in mouse DRG neurons treated for just two hours with 1-deoxySLs. Of note, there was no change in the ER calcium concentration following SA treatment. In keeping with the clinical phenotype, 1-deoxySL induced calcium dysregulation was seen later (following 24 hours of treatment) in primary motor neurons. These findings support the role of ER dysfunction in 1-deoxySL induced toxicity. Our combined findings suggest that 1-deoxySLs cause severe ER stress which leads to ER dysfunction and disruption of calcium homeostasis. Following SA treatment, the UPR is able to restore ER homeostasis and mitigate disruption of calcium regulation. Loss of calcium ions during ER stress is mediated through activation of calcium handling proteins in the ER and through calcium release into the cytosol via Inositol 1,4,5-

trisphosphate receptor (IP^3R) (Görlach *et al.*, 2015). The process of protein folding is highly regulated and monitored but also very sensitive to changes in ER homeostasis such as calcium depletion, hypoxia, redox stress, oxidative stress as well as increases in protein synthesis or expression of misfolded proteins (Cao and Kaufman, 2013; Smith and Wilkinson, 2017). Calcium dysregulation following treatment with 1-deoxySLs would itself result in further ER stress creating a positive feed-back loop that leads to apoptosis.

After the initial two hours following exposure to 1-deoxySLs, the pattern of activation of the two chaperones, PDI and BiP, differ. PDI levels progressively decline beyond two hours of treatment with SA and 1-deoxySA treatment, with the greatest decline observed with 1-deoxySA treatment. BiP, however, appears to have a biphasic pattern of upregulation, initially increasing within two hours and later after 24 hours of treatment. ATF6, one of the three ER stress sensors activated by ER stress, induces translation of BiP and PDI (Walter and Ron, 2011). This could explain the second peak of BiP upregulation after 24 hours of treatment but raises the question of why PDI is downregulated. PDIs are a family of oxidoreductases. The prototype of this family is PDIA1 (referred to as PDI). PDIA5 is needed for the cleavage of the intramolecular disulphide bridges of ATF6 which is necessary for the transport of ATF6 from the ER to its target, the golgi (Higa *et al.*, 2014). Another PDI family member, PDIA6, directly interacts with the activated form of IRE1α and inactivates it by converting the disulphide linked oligomers (active form) of IRE1α to its monomers (inactive form) (Okumura *et al.*, 2015). PDIA6 can also inactivate PERK (Kranz *et al.*, 2017). Downregulation of PDI could therefore lead to persistent activation of PERK and IRE1α, the two mediators of UPR led apoptosis. PDI also facilitates the degradation of misfolded proteins via the ER associated degradation pathway (ERAD) which involves translocating misfolded proteins to the cytoplasm for subsequent proteosomal degradation (Parakh and Atkin, 2015). Decreased PDI levels would result in further accumulation of misfolded proteins in the ER, compounding existing ER stress.

A protective role of PDI has been demonstrated in several neurodegenerative diseases, in particular amyotrophic lateral sclerosis (ALS). PDI is upregulated in the SOD1 mouse models of ALS and overexpression of PDI in these mice results in a decrease in mutant SOD1 aggregation in neuronal cells and a decrease in markers of ER stress (Perri *et al.*, 2016). More recently, PDI variants have been identified as a risk factor for ALS (Perri *et al.*,

2016). However, depending on the cellular environment, high levels of PDI can have detrimental effects. In the mammalian ER, the network for the catalysis of protein disulphide formation comprises of PDIs and PDI-oxidising enzymes such as ER oxidoreductin-1α (Ero1α), oxidised glutathione and glutathione peroxidases (Parakh and Atkin, 2015). Protein disulphide formation is an oxidative process. When PDI has oxidised substrate proteins, it needs to be oxidised itself to complete the catalytic cycle. When Ero1α oxidises PDI, reactive oxygen species (ROS-hydrogen peroxide) are formed (Kanemura *et al.*, 2016). High PDI levels can lead to excess production of ROS, reducing the levels of glutathione (main redox buffer) available for reduction and increasing Ero1α. During ER stress, high levels of Ero1α have been observed which accelerates protein oxidation (oxidative stress) (Parakh and Atkin, 2015). PDI also interacts with NADPH oxidase complex (Nox) which is a major contributor of ROS (Ali Khan and Mutus, 2014). Increased PDI levels can lead to increased activation of NADPH oxidase which results in increased levels of ROS (Ali Khan and Mutus, 2014). Hence the protective/apoptotic inducing role of PDI is finely poised. In early remedial instances of ER stress, it appears to play a protective role. In unmitigating ER stress, its role is switched to promoting apoptosis. This might be the case in this study.

The functional roles thought to be played by PDIs have greatly expanded in recent years. PDIs are predominantly located in the ER but there is growing evidence that some members of the family can be found in the cytoplasm and on the cell surface (Moretti and Laurindo, 2017). Several studies have shown a novel, emerging role for PDI in cytoskeleton organisation (Moretti and Laurindo, 2017). Oestrogen can bind to PDI and non-competitively inhibit it (Tsibris *et al.*, 1989; Fu *et al.*, 2011). This might be one of the factors contributing to the milder phenotype seen in female HSN patients compared to male patients.

The ER and mitochondria are tightly linked physically via the contact sites, defined as mitochondria-associated membranes (MAM). Under normal conditions, there is a continuous ebb and flow of calcium between the ER and mitochondria (Simmen *et al.*, 2010). This exchange serves three functions (Kornmann, 2013). Firstly, it regulates cellular bioenergetics as some citric acid cycle enzymes are calcium dependent. Secondly, it is cytoprotective as the mitochondria buffers ER calcium efflux preventing cytotoxic cytosolic calcium accumulation. Thirdly, it can induce cell death as cytotoxic accumulation of calcium in the mitochondria triggers the opening of mitochondrial permeabilization pore (MPP) which

leads to the leakage of cytochrome c and other proapoptotic proteins into the cytosol. The MAM contains complexes of IP^3R on the ER membrane with mitochondrial voltage dependent anion channel (VDAC) which are linked by cytosolic BiP (Kornmann, 2013). Frequently, ER stress leads to the release of calcium from the ER lumen via the IP^3R (Deniaud *et al.*, 2008). Mitochondria take up these high levels of calcium in the microdomains of the MAM via the VDAC. Sustained ER stress leads to accumulation of calcium in the mitochondria and loss of mitochondrial membrane potential (Scorrano *et al.*, 2003). This might be the case in this study where a significant reduction in mitochondrial membrane potential was seen two hours after treatment with 1-deoxySLs. High levels of calcium in the mitochondria results in the translocation of cytochrome c from the mitochondria to the ER where it binds IP^3R (Simmen *et al.*, 2010). This binding releases the calcium mediated inhibition of IP^3R and results in a feed-forward amplification of ER calcium release.

The SPT enzyme is ubiquitously expressed, however mutations in SPT causing HSN1 result in a length dependent sensory motor neuropathy. Many cells are relatively well protected from accumulation of misfolded proteins by the continued dilution of the ER by cell replication (Roussel *et al.*, 2013). This process is unavailable to neurons which are post-mitotic and hence neurons depend exclusively on UPR for survival during insults to ER. Neurons are particularly vulnerable to redox dysregulation due to their large size, lower ability to maintain the balance between antioxidants and reactive oxygen species (ROS) and high oxygen demand which results in the formation of ROS (Parakh *et al.*, 2013; Perri *et al.*, 2016).

In summary, this study clearly shows that sphingolipids are toxic to mammalian primary motor and DRG neurons, causing adverse effects on cell survival and neurite outgrowth. Within the DRG neuronal sub-populations, the small peptidergic neurons appear to be more susceptible to this toxicity than the large, NF200 positive neurons. This mirrors the clinical phenotype observed in HSN1 patients. 1-deoxySL treatment causes early mitochondrial dysfunction and ER stress resulting in the activation of the UPR.

The in-vitro neuronal model used in this Chapter involved exogenous application of 1deoxySLs. In the next Chapter, I examined an induced pluripotent stem cell (iPSC) derived sensory neuron model of HSN1 in which the 1deoxySLs are endogenously produced by the human neurons.

3. Human induced Pluripotent Stem Cell derived sensory neuron model of HSN1

3.1 Introduction

Animal models have played a longstanding key role in medical research. As noted in earlier chapters, there is an HSN1 mouse model (McCampbell *et al.*, 2005; Eichler *et al.*, 2009) with the transgenic mice over-expressing *SPTLC1* (C133W) mutation. This same model was used in the HSN1 pre-clinical trial with L-serine (Garofalo *et al.*, 2011). The transgene expression in the mutant lines ranged between 0.4-3.9 times the endogenous levels. There are several morphological and behavioural differences between the transgenic mouse model and HSN1 patients (Houlden *et al.*, 2006). In 10month old mice, histological examination showed no difference in the unmyelinated fibres in the dorsal roots and myelin thinning (increase in g-ratio) in the ventral roots. Behavioural studies demonstrated a difference only in thermal sensitivity (hyperpathic) (McCampbell *et al.*, 2005). At 14-15 months of age, histological studies showed loss of small unmyelinated axons in the sciatic nerve and in the behavioural studies, mouse were hypopathic with deficits evident in both mechanical and thermal sensitivity (Eichler *et al.*, 2009). Overall, the mice appear to have a considerably milder phenotype compared to HSN1 patients with the same mutation.

There have been several other pre-clinical trials using murine models in inherited neuropathies e.g. curcumin in CMT1B (Patzkó *et al.*, 2012), progesterone antagonists in CMT1A (Sereda *et al.*, 2003) and vitamin C in CMT1A (Passage *et al.*, 2004). Only vitamin C progressed to the next stage in the translational process whereby there have been several double-blind randomised placebo controlled trials using vitamin C in CMT1A (Gess *et al.*, 2015). However, none of the trials demonstrated an improvement in the impairment with vitamin C intake. The high failure rate for animal models to translate to humans has pushed researchers to find alternative models to check the validity of pathogenic mechanisms and therapeutic agents identified in animal models. One of the many reasons attributed to this failure rate in transgenic animal models is the substantial species differences.

Human iPSC derived cells provide an attractive alternative model. In 2006, it was discovered that induced pluripotent stem cells (cells with a gene expression profile and developmental potential similar to embryonic stem cells) can be created from mouse somatic cells using four transcription factors, now called the Yamanaka factors: Oct4, Sox2, Klf4 and c-Myc (Takahashi and Yamanaka, 2006). A year later, two different research groups published methods to generate iPSCs from human fibroblasts using either the original four transcription factors or a different combination consisting of Oct4, Sox2, Nanog and Lin28 (Takahashi *et al.*, 2007). Since then, there continues to be advances in the reprogramming technique to simplify the process and decrease potentially detrimental side effects of the reprogramming process, such as the elimination of c-Myc which is known to promote tumour growth in some cases (Takahashi and Yamanaka, 2016). The generated iPSCs are then tested to ensure they meet the defining criteria for pluripotent stem cells: expression of stem cell markers, forming tumours containing cell types from all three primitive embryonic layers (teratoma assay) and displaying the capacity to contribute to many different tissues when injected into mouse embryos at very early stage of development. The iPSCs are also karyotyped as culturing iPSC is associated with adaptive amplification which results in the increased incidence of chromosomal trisomies and copy number gains (Lund *et al.*, 2012). Finally, the established iPSCs are also tested to ensure they are free of reprogramming transgenes or plasmids.

In-vitro iPSC differentiation protocols have been developed for many cell types. There are many human iPSC derived disease models for neurological diseases, including inherited neuropathies: Familial dysautonomia (Hereditary Sensory Neuropathy Type 3)(Lee *et al.*, 2009), axonal CMT secondary to mitofusin 2 (CMT2A) and Neurofilament light chain polypeptide (CMT2E) mutations (Saporta *et al.*, 2015). Large scale screening using familial dysautonomia iPSCs has identified compounds that rescue the expression of the gene responsible for the disease (*IKBKAP*) (Lee *et al.*, 2012). Initially neuronal differentiation protocols used the presence or absence of canonical markers on immunocytochemistry to confirm the cell lineage (for example $Brn3a^{+}$/$Peripherin^{+}$ for peripheral sensory neurons, $Tyrosine\ hydroxylase^{+}$/$Peripherin^{+}$ for peripheral sympathetic neurons and HB9 and ISLET1/2 for motor neurons) (Lee *et al.*, 2007; Dimos *et al.*, 2008). Later these neurons were also shown to be electrically active upon maturation (Burkhardt *et al.*, 2013) and in the

case of sensory neurons, to respond to specific stimuli such as capsaicin and ATP (Chambers *et al.*, 2012). Advances in reprogramming techniques and neuronal differentiation protocols have allowed the production of neurons from a large number of donors thereby reducing the possibility of results being driven by aberrant cell lines

Initially hailed as being able to model human disease in a culture dish, the iPSC field has rapidly evolved with greater understanding of the model's limitations. There are considerable clonal variations and the reasons for this variation can be grouped into three categories: cellular changes as a result of the reprogramming process; in-vitro differentiation induced heterogeneity; and differences in genetic background (Soldner and Jaenisch, 2012). Various non-integrating methods have now been developed to circumvent the risk of insertional mutagenesis and genetic alterations associated with retroviral and lentiviral transduction-mediated introduction of reprogramming factors. To reduce the effects of in-vitro induced heterogeneity, there is now a trend to increase the number of patient lines studied as well as multiple clones per patient line. Variation in clinical phenotype (age of onset/ disease progression) in monogenetic disorders have been attributed to epistatic effects from genetic background differences. These differences can make it more difficult to ascertain a distinct phenotype in the iPSC derived cells. This may be particularly problematic in later onset, slowly progressive diseases where subtle changes are expected in-vitro. Recent advances in gene editing techniques (CRISPR-Cas9 system, transcription activator-like effector nucleases-TALENs and zinc-finger nucleases) have markedly improved gene editing efficiency and provide a possible solution (Shi *et al.*, 2017). These gene editing techniques enable researchers to eliminate disease causing mutations in patient iPSCs to create isogenic controls whereby the disease causing genetic variation is the sole experimental variable.

Despite the tremendous advances in the field of iPSCs over the past decade, there is ongoing intensive debate as to the value of iPSCs as a disease model. One of the concerns is based on the genetic and epigenetic stability of human iPSCs. Somatic mosaicism is amplified during clonal generation and expansion of iPSCs. Most of the genomic variation in iPSCs have either been inherited from the cell of origin or induced during long-term culture (Tapia and Schöler, 2016). During maintenance in culture with increasing passage number,

iPSCs are prone to epigenetic alterations: X-chromosome inactivation, imprinting and DNA methylation status can vary and can be unstable (Lund *et al.*, 2012). Repeated freezing-thawing cycles or changes in the oxygen or nutrient levels can affect the epigenome of the iPSCs (Lund *et al.*, 2012). These differences will be maintained despite the use of isogenic controls.

The extent to which iPSC derived neurons recapitulate the functional features exhibited by their native counterparts remains uncertain. The reversal of cellular age during reprogramming results in embryonic-like state of iPSCs and their differentiated lineages (Studer *et al.*, 2015). Many differentiation protocols for iPSCs discuss how mature the differentiated neurons are however, the maturity of these neurons or whether they will ever reach the maturity of their in-vivo counterparts are not definitely known (Sandoe and Eggan, 2013). This poses additional challenges to modelling later onset neurodegenerative diseases such as HSN1.

Despite these difficulties, human iPSC derived sensory neurons provide a unique opportunity to study the effects of endogenously produced 1-deoxySLs, rather than just exogenous and in a human cellular context. The model also provides opportunities to identify genetic modifiers. Genetic modifiers discovered in other iPSC derived disease models have been shown to be potential therapeutic targets in monogenic diseases (Chai *et al.*, 2018) . In this model, there is a normal level of expression of mutant SPTLC1, unlike primary DRG and motor neuron cultures transfected with the mutant *SPTLC1* gene. These iPSC derived neurons can be maintained in culture for months, which is not possible with primary motor neuron and DRG cultures, and thus it would be possible to detect a subtle, slowly evolving phenotype.

3.2 Aims

1) To determine if 1-deoxySLs are neurotoxic to iPSC derived sensory neurons.

2) To determine if there is elevated autonomous production of 1-deoxySLs in HSN1 iPSC derived sensory neurons compared to controls.

3) To determine if there is a disease specific phenotype in the HSN1 iPSC derived sensory neurons when looking at:

a) Neuronal survival and neurite outgrowth

b) In vivo endoplasmic reticulum and mitochondrial function

c) Mitochondrial ultrastructure

Altered ultrastructural mitochondrial morphology has been reported in HSN1 patient lymphoblasts (Myers *et al.*, 2014) and mouse embryonal fibroblasts (MEF) treated with 1-deoxySA (Alecu *et al.*, 2017b). In HSN patient lymphoblasts (C133W and V144D mutations), mitochondria had discontinuous outer membrane with sections where there was complete breakage of the membrane and electron dense grossly swollen cristae (V144D). MEF cells treated with 1-deoxySA had spherical mitochondria with most showing loss of internal cristae structures.

d) Analysis of cell surface morphology using scanning electron microscopy

The downstream metabolites of 1-deoxySA (1deoxy-(dihydro) ceramides and 1-deoxyceramides) and 1-deoxymethylSA (1-deoxymethyl(dihydro)ceramides and 1-deoxymethylceramides) are highly hydrophobic. Jimenez-Rojo *et al.* (2014) studied the behaviour of these 1-deoxySLs and their interaction with sphingomyelin, a major constituent of neuronal membranes. Ceramides are known to be among the least polar and most hydrophobic lipids in membranes. This study showed that their 1-deoxy counterparts were even more hydrophobic and less miscible in sphingomyelin bilayers. The authors proposed that the presence of these metabolites might impact the structure and integrity of cellular membranes. Pharmacological treatments which increase the dihydroceramide/ceramide ratio result in increased rigidity of plasma membrane (Rodriguez-Cuenca *et al.*, 2015).

4) To determine if L-serine supplementation can ameliorate disease specific phenotype. In cultures of HEK cells transfected with *SPTLC1* mutants, increasing the L-serine medium concentration suppressed endogenous 1-deoxySL production, even with elevated L-alanine levels (Garofalo *et al.*, 2011). Long-term L-serine supplementation in the HSN1 mouse model resulted in reduced plasma 1-deoxySL levels and improved motor performance (Garofalo *et al.*, 2011).

3.3 Materials and Methods

3.3.1 Induced Pluripotent stem cell (iPSC) generation

3.3.1.1 Control lines

iPSC-AH017-7 (from 67 year old female) were reprogrammed using the SeVdp(KOSM)302L Sendai virus system containing genes for KLF4, OCT3/4, SOX2 and c-MYC and has been described previously (Handel *et al.*, 2016).The iPSCs were karyotyped and pleuripotency checked using PleuriTest which is an open access bioinformatic assay of pleuripotency based on gene expression profile (Muller *et al.*, 2011). Clearance of the Sendai virus from the iPSCs was confirmed by RT-qPCR.

iPSC- AD2-1 (from 51 year old male) was derived from commercial fibroblasts (Lonza, CC-2511) and reprogrammed using the CytoTune® iPSC Reprogramming kit (ThermoFisher Scientific). This is a commercially available kit and uses Sendai virus based reprogramming vectors each capable of expressing one of the four Yamanaka factors (KLF4, OCT3/4, SOX2 and c-MYC). Quality control checks performed include tests for Sendai virus clearance via RT-qPCR, fluorescence- activated cell sorting (FACS) and immunocytochemistry analysis for pleuripotency markers, genomic integrity checks and embryoid body tri-lineage differentiation experiments (van de Bunt *et al.*, 2016).

iPSC-NHDF1 (from 44 year old female) was derived from commercial fibroblasts (Lonza, CC-2511) reprogrammed with retroviruses SOX2, KLF4, OCT3/4, c-MYC and NANOG. Quality checks undertaken were assessment of genomic integrity, PluriTest, generation of embryoid bodies and differentiated into three germ layers (Hartfield *et al.*, 2014).

iPSC-AD4-01 (from 68 year old male) fibroblasts were obtained from a commercial source (Lonza, CC-2511) and reprogrammed using the CytoTune® iPSC Reprogramming Kit (ThermoFisher). Quality control checks performed were Sendai virus clearance, FACS for pleuripotency markers, genomic integrity checks and embryoid body tri-lineage differentiation experiments. This line was obtained through the IMI/EU sponsored StemBANCC consortium via the Human Biomaterials Resource Centre, University of Birmingham, UK.

3.3.1.2 Patient lines

Three male patients with similar age and disease severity were chosen from the natural history study to provide the fibroblasts for the generation of the patient iPSC lines. The fibroblasts were obtained from upper thigh skin biopsies. All the patient derived iPSC lines were obtained through the StemBANCC consortium. The fibroblasts were reprogrammed using the CytoTune®-iPSC Reprogramming Kit (ThermoFisher). During the bulking up process, the passage number was kept to a minimum. The following quality control checks were performed on the lines: Sendai virus clearance, FACS for pleuripotency markers, genomic integrity checks including cytoSNP and embryoid body tri-lineage differentiation assays.

3.3.1.3 Ethics

Skin biopsies for the fibroblasts were obtained following signed informed consent. AH017-7 and NHDF1 were reprogrammed with the approval from research ethics committee: Health Research Authority, NRES Committee South Central, Berkshire (REC 10/H0505/71). The reprogramming of the patient lines was approved by the Health Research Authority, NRES Committee London-Queen Square (REC 09/H0716/61).

3.3.2 Expansion and maintenance of iPSCs

iPSCs were thawed in 10ml of PBS and centrifuged at 400 x g for 4 minutes. The iPSC pellet was re-suspended in mTeSR®1 (STEMCELL Technologies) medium containing 1% Antibiotic-antimycotic (100x, ThermoFisher) and Rho-associated coiled-coil containing protein kinase (ROCK) inhibitor (ScienCell) (10μM). The cells were plated onto Matrigel® coated 6 well plate. The media was changed daily (maintained in mTeSR®1 medium containing 1% penicillin/streptomycin/amphotericin B). iPSCs were split when 90% confluent usually at a ratio of 1:3. The spent medium was removed and the cells were washed with 1ml of phosphate-buffered saline (PBS, Gibco) and then incubated in warmed 0.02% EDTA (ethylenediaminetetraacetic acid) at 37^0C for 4-5 minutes. The EDTA was removed and the wells were flushed with mTeSR®1 medium containing 1% penicillin/streptomycin/amphotericin B and ROCK inhibitor (10μM) to remove the adhered cells. The cells were plated onto Matrigel® coated 6 well plates. ROCK inhibitor was included in the medium for 24 hours after each passage.

Each line was expanded until four T75 (75cm^3) culture flasks were 90% confluent. The flasks were washed with PBS and the cells incubated in 5ml of warmed TrypLE express (Gibco) at 37^{0}C for 5 minutes. The flasks were gently shaken to dissociate the cells and cell suspension was aspirated and diluted in PBS (1:6). The cells were counted using a haemocytometer and then centrifuged at 400 x g for 5 minutes. The cells were re-suspended in 1ml chilled freezing media containing 20% Dimethyl sulfoxide (DMSO, Sigma), 60% embryonic stem cell qualified Foetal Bovine Serum (FBS, Gibco) and 20% KnockOut® DMEM (DMEM, ThermoFisher). The cells were gently titurated to evenly mix the suspension. Further freezing media was added to reach the desired freezing density of 2million/ml. Cryovials containing 1ml of freezing media were quickly placed into isopropanol containing freezing container and placed in a -80 freezer overnight. The vials were transferred to liquid nitrogen for storage the following day.

3.3.3 Differentiation of iPSCs into sensory neurons

The differentiation protocol by Chambers *et al.* (2012) was used for the differentiation of iPSCs into sensory neurons (Table 3.1). For each experiment, all the iPSC lines used had the same passage number. Prior to the start of differentiation, the iPSCs were plated onto Matrigel® coated 6-well plates. When the cells were about 30% confluent, the medium was exchanged from mTeSR®1 to mouse embryonic fibroblast conditioned medium (MEF, (ScienCell) supplemented with 10ng/ml human recombinant Fibroblast Growth Factor 2 (FGF2) and maintained in this medium for 24 hours.

At the start of the protocol, the medium was exchanged to knockout serum replacement (KSR) medium (KnockOut® DMEM, 15% knockout-serum replacement (ThermoFisher), 1% Glutamax (100x, Thermofisher), 1% nonessential amino acids (100x, ThermoFisher), 100μM β-mercaptoethanol (ThermoFisher), 1% penicillin/streptomycin/amphotericin B) containing SMAD inhibitors: SB431542 (10μM, Sigma) and LDN-193189 (100nM, Stratech). The medium was gradually transitioned from KSR medium to N2 medium (Neurobasal medium without phenol red (ThermoFisher), 1 % Glutamax (ThermoFisher) and 1% penicillin/streptomycin/amphotericin B) over a 11day period as shown on Table 3.1. From day 2, SMAD inhibitors were combined with the three small molecules: CHIR99021 (3 μM, Apollo Scientific), SU5402 (10μM, R&D Systems) and DAPT (10μM, Sigma). Densely

covered wells on day 2/3 were passaged at this stage to provide more growing area for the neurons to develop into. On day six, the SMAD inhibitors were removed leaving only the three small molecules. From day 8 onwards, depending on the cell line, immature neurons can be seen.

On day 11, the immature neurons were re-plated onto 24 well plates. Glass coverslips were coated with 150µl of Matrigel® droplets and incubated at 37^0C for at least one hour. The immature neurons were washed with PBS and then incubated with warmed TrypLE express at 37^0C for 5 minutes. The TrypLE was aspirated with a 1ml pipette and used to gently flush the cells. The cells were gently titurated to break up any clumps. If significant clumps were still visible, a cell strainer (100µM) was used to remove the clumps. The suspension was diluted in 10ml PBS and 10µl sample removed for cell counting with a haemocytometer. The remaining suspension was centrifuged at 400 x g for 5 minutes and the pellet resuspended in N2 containing human recombinant Nerve Growth Factor (NGF), Glial Derived Neurotrophic Factor (GDNF), Brain Derived Neurotrophic Factor (BDNF) and Neurotrophin3 (NT3) (all at 25ng/ml, Peprotech). The medium was also supplemented with ROCK inhibitor (10µM) and CHIR99021 (3µM). The Matrigel® was partially removed from the coverslips and 150µl of the cell suspension was pipetted on to the coverslip, again to form droplets. The cells were plated at a density of approximately 3000 cells per well and placed in an incubator. The next day, the wells were flooded with 250µl of N2 medium as above but without the ROCK inhibitor. If needed, Cytosine β-D-arabinofuranoside (araC, 2µM, Sigma) was added to this N2 medium to eliminate any non-neuronal dividing cells present in the culture.

Medium changes were performed twice weekly. CHIR99021 was only included in the medium until day 14. AraC was withdrawn from the medium once a pure neuronal culture was established as judged by the absence of morphologically non-neuronal cells on phase contrast light microscopy. Laminin (1µg/ml, ThermoFisher) was added to the media from day 20 onwards.

Day	Medium	Inhibitors/small molecules
0	KSR medium	2 SMAD inhibitors: SB431542 (10μM) and LDN-193189 (100nM)
1		
2	KSR medium	2 SMAD inhibitors: SB431542 (10μM) and LDN-193189 (100nM) 3 small molecules: CHIR99021 (3μM), SU5402 (10μM) and DAPT (10μM)
3		
4	75% KSR medium 25% N2 medium	2 SMAD inhibitors: SB431542 (10μM) and LDN-193189 (100nM) 3 small molecules: CHIR99021 (3μM), SU5402 (10μM) and DAPT (10μM)
5		
6	50% KSR medium 50% N2 medium	3 small molecules: CHIR99021 (3μM), SU5402 (10μM) and DAPT (10μM)
7		
8	25% KSR medium 75% N2 medium	3 small molecules: CHIR99021 (3μM), SU5402 (10μM) and DAPT (10μM)
9		
10	N2 medium	3 small molecules: CHIR99021 (3μM), SU5402 (10μM) and DAPT (10μM)

Table 3.1 iPSC sensory neuron differentiation protocol

3.3.4 L-Alanine Supplementation and L-Serine supplementation

To enhance any 1-deoxySL induced phenotype, the media was supplemented with varying concentrations of L-Alanine one week after the end of the differentiation. Selection of the concentrations used was guided by the findings of Garofalo *et al.* (2011) who looked at endogenous 1-deoxySL production in HEK cells at various concentrations of L-alanine and L-serine supplementation. The concentrations of the alanine supplementation, 0.4mM, 0.8mM and 1.6mM were chosen to represent serine: alanine ratios of 1.1, 1:2 and 1:4 respectively. Stock concentrations of L-alanine (Sigma) were made by dissolving it in PBS.

A trial of L-serine supplementation on long-term cell survival was performed and treatment was initiated three weeks after the end of the differentiation protocol. Concentrations of 2.5mM and 5.0mM were selected. Higher concentrations resulted in very little further reduction in 1-deoxySA formation in the HEK cells (Garofalo *et al.*, 2011). Stock concentrations of L-serine (Sigma) were made by dissolving it in PBS.

3.3.5 Neuronal collection for 1-deoxySL analysis

For 1-deoxySL analysis, the immature neurons at the end of the differentiation protocol were re-plated onto six well plates (3 wells per line). The cells were collected 28 days later.

The cells were washed with PBS and 1ml of TrypLE express added to each well and then incubated at 37ºC for 10 minutes. The adhered cells were removed by forceful flushing with the TrypLE using a 1ml pipette. The suspension was made up to 10 ml with PBS and centrifuged at 500 x g for 5 minutes. The pellet was re-suspended in 1ml of PBS and the suspension titurated several times to disperse any clumps. 50µl was removed and stored separately for protein quantification. All the samples were stored in a -80ºC freezer.

Protein quantification was performed using Nanodrop 1000 spectrophotometer (A280 method) (ThermoFisher). Initially, a blank measurement was made by loading a 2µl PBS sample. This was followed by loading 2µl samples of cell lysates after tituration of the sample to homogenise the solution. For each sample, an average protein value was taken from triplicate measurements. The detection limit of the Nanodrop 1000 A280 method is 0.10mg/ml.

3.3.6 1-DeoxySL analysis of neuronal lysates

Sphingolipid analysis were performed by Thorsten Hornemann's lab at the University Hospital Zurich, Switzerland as previously described (Suriyanarayanan *et al.*, 2016). In summary, the 0.95ml samples of cell suspension were centrifuged at 4ºC and at 1.2rcf for 5 minutes. The cell pellet was re-suspended in 100µl of PBS. 500µl of methanol (Honeywell, Germany) and 200pmol of deuterated internal standards (d7-sphinganine and d7-sphingosine, Avanti Polar Lipids) were added to the cell suspension. The lipids were extracted for one hour at 37ºC with constant agitation and the precipitated protein centrifuged at 16000 x g for 5 minutes. 75µl of hydrochloric acid (32%) was added to hydrolyse the lipids and the lipids were incubated at 65ºC for 16 hours. Hydrochloric acid was neutralised with 100µl of 10M potassium hydroxide. Free sphingoids were extracted by adding 125µl of chloroform, 100µl of 2M ammonium hydroxide and 500µl of alkaline water. These bases were separated on a C18 column (Uptispere 120 Å, 5µm, 125 x 2 mm,

Interchim, France) and analysed using a TSQ Quantum Ultra Mass Spectrometer (Thermo Scientific).

The following sphingolipids were measured: Sphinganine (SA), sphingosine (SO), 1-deoxysphinganine (1-deoxySA), 1-deoxysphingosine (1-deoxySO), 1-deoxymethylsphinganine (1-deoxymethylSA) and 1-deoxymethylsphingosine (1-deoxymethylSO).

3.3.7 1-DeoxySL treatment of control lines

1mM sphingolipid stock solutions were prepared for SA, 1-deoxySA and 1-deoxymethylSA as described earlier (section 2.3.4).

Control (AH017-7, AD2-1 and NHDF-1) iPSC derived sensory neurons were treated with the sphingolipids 3 weeks after the end of differentiation protocol (day 11). 1mM Stock solutions were diluted in culture medium to the desired concentrations of 1µM, 3µM and 6µM. An ethanol vehicle control was included for each concentration. The sensory neurons were treated with the sphingolipids for 48 hours.

3.3.8 Immunocytochemistry

The coverslips were transferred to PBS and fixed in ice cold 1% paraformaldehyde for 20 minutes. The coverslips were then washed 2/3 times in PBS followed by incubation with the primary antibody mixed in blocking solution (5% donkey serum, 0.5% milk powder, 0.05% sodium azide, 0.3% Triton x100, 0.1% dimethylsulphoxide and 0.1% bovine serum albumin) at 4^{0}C overnight. Next, the coverslips were washed with PBS three times (middle wash consisting of incubation with DAPI at 1:300 dilution for 5 minutes) and then incubated with the secondary mixed in PBS for 2 hours at room temperature. The secondary antibody was washed off with three PBS washes and the coverslips were mounted onto Superfrost Plus microscope slides (Thermo Scientific) using Vectashield mounting medium (Vector laboratories). The primary antibodies used and their dilutions are shown in table 3.2. The secondary antibodies used were Alexa Fluor 488 and 546 at 1:1000 dilutions.

Confocal images (Zeiss LSM-710 confocal microscope) were acquired using Zen Black Software (Zeiss, Germany). Ten images were taken at random per coverslip, systematically covering the area of the coverslip to ensure objective sampling.

Antigen	Host species	Dilution	Manufacturer
Neurofilament 200 (NF200)	Mouse	1: 1000	Sigma
ATF3	Rabbit	1:900	Santa Cruz (C-19, SC188)
β III Tubulin	Mouse	1:100	R&D Systems
Cleaved Caspase III	Rabbit	1:400	Cell Signaling
BRN3A	Rabbit	1:200	Millipore
CGRP	Sheep	1:500	Enzo
IB4	Streptavidin conjugated	1:100	Sigma Aldrich

Table 3.2 Primary antibodies used in the iPSC study

3.3.9 Analysis of cell survival, axonal injury and caspase 3 activation.

Cell survival and axonal injury were assessed in the control iPSC derived sensory neurons following treatment with sphingolipids. Cells positive for Neurofilament 200 (NF200) and DAPI counter-stain were counted as neurons. Axonal injury was assessed by determining the percentage of these neurons that also co-stained for ATF3, a marker of axonal injury.

Activated caspase III (cleaved) is a key mediator of apoptosis in neuronal cells (D'Amelio *et al.*, 2010). At four weeks after the end of differentiation protocol, control and patient iPSC derived sensory neurons were fixed and stained for cleaved caspase 3 and βIII tubulin. Images were randomised and analysed blind to cell line and treatment. Cells positive for βIII tubulin and DAPI were counted as neurons. Percentage of these neurons that co-stained for cleaved caspase 3 was determined. Later, at 3 months, axonal injury was also assessed in these neurons.

3.3.10 Assessment of neurite outgrowth

Neurite outgrowth was assessed at 3 months in NF200 stained neurons. Images were processed and analysed using Fiji (Fiji Is Just ImageJ) (NIH) software. Binary images were created using a thresholding technique (Otsu's thresholding method) by a purpose written macro program (written by Steve West, Nuffield Department of Clinical Neurosciences, University of Oxford). Percentage of each image area covered by neurites was normalised to the number of neurons (NF200 and DAPI co-staining) within that area.

3.3.11 Assessment of long-term neuronal survival

Long-term neuronal survival was assessed at 5 months. At this stage, the coverslips are covered with a dense network of neurites which are prone to peeling off with media changes and the fixation process. Due to this, live imaging was performed to assess cell viability using Neurite Outgrowth Staining Kit (Life Technologies). The kit consists of a cell permeable viability indicator dye that is converted by live cells to emit green fluorescence and fluorescent outer cell membrane surface stain (orange-red). The two agents were combined (1:1000) in Dulbecco's Phosphate Buffered Saline containing calcium and magnesium (DPBS, Gibco). The cells were washed with PBS and then incubated in the DPBS containing the two dyes at room temperature for 15 minutes. After the incubation, the staining solution was removed and replaced with DPBS containing the background suppression dye (1:200). The cells were imaged with a Zeiss LSM-710 confocal microscope (x10 magnification) and analysed using Zen Black Software (Zeiss, Germany).

3.3.12 Transmission Electron Microscopy (TEM) and Scanning Electron Microscopy (SEM)

Fixation, processing and imaging were performed by the Dunn School Electron Microscopy Facility, University of Oxford.

For TEM, cells adhered to coverslips were fixed in pre-warmed fixative (4% PFA [Agar Scientific] +2.5% glutaraldehyde in 0.1M PIPES buffer [Sigma] at pH of 7.2) for 1 hour at room temperature and then incubated at 4^0C overnight. Cells were then thoroughly washed 5 times in 0.1M PIPES buffer, each wash lasting 15 minutes. 50mM Glycine was included in the fourth wash to quench free aldehydes. Cells then underwent secondary fixation in 0.1M PEPES containing 1% osmium tetroxide (TAB Laboratories) at 4ºC for one hour followed by five washes with milliQ water, each 10minutes each. Tertiary fixation involved incubation in 0.5%uranyl acetate (agar Scientific) overnight at 4ºC, in the dark followed by a wash with milliQ water for 10minutes.The cells were dehydrated in 30%, 50%, 70%, 80%, 90% and 95% ethanol (Sigma), each for ten minutes followed by incubation in 100% ethanol for 90 minutes with three solution changes during this time. To infiltrate with the epoxy resin, the cells were incubated in 3:1 100% dry ethanol: Agar100 resin (Agar Scientific) for 1 hour, then 1:1 100% dry ethanol:Agar100 resin for 2 hours, and 1:3 100% dry ethanol:Agar100

resin for 1 hour. This was followed by incubation in 100% Agar100 overnight at room temperature and 2 resin changes the following day. For embedding process, the coverslips were inverted onto Beem capsules filled with fresh 100%Agar 100 resin. The blocks were polymerized for 24 hours at 60ºC then submerged in liquid nitrogen. The cover slip was snapped, leaving the cells embedded as a monolayer on the surface of the block. Ultrathin sections (90nm) were cut using a Diatome diamond knife (Leica UC7 ultramicrotome) and mounted onto 200 mesh copper grids. Sections were post-stained with Reynold's lead citrate for 5 minutes, washed with degassed water and dried. Sections were imaged with FEI Tecnai 12 transmission electron microscope at 120kV. Images were acquired using Gatan OneView CMOS camera with Digital Micrograph 3.0 software.

For SEM, the culture was fixed in fixative containing 2.5% glutaraldehyde and 2-4%PFA in 0.1M sodium cacodylate buffer and incubated at room temperature for at least one hour. The cells were rinsed three times with 0.1M phosphate buffer with each wash lasting 5 minutes. Secondary fixation involved incubating the samples in 0.1M phosphate buffer with 1% osmium tetroxide at 4ºC for one hour. This was followed by three washes with MilliQ water, each lasting 5 minutes. The ethanol dehydration series was the same as that used with TEM. The coverslip was then dried for 3 minutes using hexamethyldisilazane (HMDS, Sigma) and mounted on carbon adhesive tape and placed onto an SEM stub and sputter coated with 10-15nm thickness of gold.

TEMs were analyzed qualitatively to determine if there were any abnormalities in mitochondrial and ER ultrastructure. Mitochondria were screened for structural abnormalities such as swollen or whirling cristae, discontinuous outer membranes, inclusions, compartmentalization, linearization of the cristae, nanotunneling and hyperbranching (Sisková *et al.*, 2010; Vincent *et al.*, 2016). ER images were compared to published descriptions of ER (Wu *et al.*, 2017).

3.3.13 ER and mitochondrial calcium imaging

ER calcium concentration can be indirectly determined by measuring cytosolic calcium concentration following the administration of drugs that selectively deplete ER calcium such as Thapsigargin. Thapsigargin is a non-competitive inhibitor of sarcoplasmic reticulum calcium-ATPases (SERCA) which are calcium re-uptake pumps. Mitochondrial calcium

levels were determined by measuring cytosolic calcium following the application of ionomycin, an ionophore. After my initial optimisation, the experiments were carried out by Alex Clark (Nuffield Department of Clinical Neurosciences, University of Oxford).

Calcium imaging experiments were performed on 3.5 month old neurons. Cultures were incubated with media containing 5μM Fluo4AM (non-ratiometric, single wave dye) and 80μM pleuronic acid (ThermoFisher Scientific) for one hour at 37ºC. The cells were then washed twice with calcium free extracellular fluid (145mM NaCl, 5MM KCl, 10mM HEPES, 10mM D-glucose, 1mM $MgCl_2$ and 0.5mM EGTA, pH 7.4). ER and mitochondrial calcium concentrations were measured in this calcium free extracellular fluid. Confocal images were taken using a Zeiss LSM 710 confocal microscope using x40 oil objective lens. Within a single field of view, sensory neuron cell bodies stained for Fluo4-AM were marked as 'region of interest'. A time lapse image was taken at 1 second intervals for 10 minutes. Fluo4-AM was excited at a wavelength of 488nm and emission fluorescence was measured at 518nm.

Baseline fluorescence was measured for 2 minutes. At 2 minutes, thapsigargin (Sigma) was added to the extracellular fluid at a final concentration of 4μM (stock solution 40μM). At 7 minutes ionomycin (Sigma) was added to the extracellular fluid at a final concentration of 2μM (stock solution 20μM).

ER calcium concentration was estimated by subtracting average baseline fluorescence from the peak fluorescence following the addition of thapsigargin. Mitochondrial ER calcium was estimated by subtracting the stable post-thapsigargin fluorescence from the peak fluorescence following the administration of ionomycin. Both estimates were normalised to baseline fluorescence to minimise differences in Fluo4 due to differences in cell density between the cell lines.

3.3.14 Statistical analysis

Statistical analysis was performed using IBM SPSS Statistics (version 22) and GraphPad Prism Version 7.02. Following review of normality by plotting frequency plots, statistical significance was determined in non-normally distributed data by using Kruskall Wallis test followed by Mann Whitney U-test with post-hoc Dunn's multiple comparisons test as appropriate. In normally distributed data, One-way ANOVA was used with post-hoc

correction for multiple comparisons using Dunnett's/Bonferroni's test as appropriate. Statistical significance for cell survival relative to control was determined using Wilcoxon Signed rank test.

Results are reported as mean ± standard error of the mean (SEM).

3.4 Results

3.4.1 Characterisation of human iPSC derived sensory neurons

The ages of all neurons will be quoted from the end of the differentiation protocol. Figures 3.1 and 3.2 show representative images for mature (5 months old) iPSC derived neurons for 2 of the control lines (AD2-1 and AHO17-7) and all the patient lines (S997, S998 and S999). All the differentiated neurons in both the control and patient lines were immunoreactive for Neurofilament heavy chain (NF200) and BRN3A, a sensory neuron transcription factor (Figure 3.1). None of the mature neurons (5 months post re-plating) in both the control and patient lines expressed nociceptor markers: CGRP or IB4 (Figure 3.2). At this stage, there were none or only very few non-neuronal cells.

3.4.2 Effects of 1-deoxysphingolipid induced neurotoxicity in human iPSC derived sensory neurons

Both 1-deoxySA and 1-deoxymethylSA were toxic to 3 week old iPSC derived sensory neurons (Figure 3.3). There was a decrease in sensory neuron survival following 48 hour 1-deoxySA treatment with 78.2 ± 3.9% ($p=0.028$) and 71.4 ± 9.7% ($p=0.028$) of the neurons surviving relative to vehicle control at 3µM and 6µM concentrations respectively (Figure 3.3B). A smaller loss in sensory neurons was seen with 3µM 1-deoxymethylSA treatment (81.9 ± 6.0% relative to vehicle control, $p=0.028$). Small loss of neurons was also seen with 3µM SA treatment (87.6 ± 6.8% relative to control vehicle) however this was not significant.

There was a clear dose-dependent increase in the expression of ATF3 (used as a marker of axonal injury/stress) with both 1-deoxySA and 1-deoxymethylSA treatment (Figure 3.3C). Following treatment with 1µM, 3µM and 6µM 1-deoxySA, 15.9 ± 6.4%, 48.8 ± 2.9% and 62.7 ± 6.9% of cells were ATF3 positive respectively. 1-DeoxySA treatment led to significant increase in the percentage of ATF3 positive neurons at all doses tested ($p=0.006$ at 1µM, $p<0.0001$ at 3 and 6µM). 1-deoxymethylSA treatment led to significant increase in the percentage of ATF3 positive neurons only at the higher doses of 3µM (18.1 ± 3.6%, $p=0.001$) and 6µM (29.4 ± 3.3%, $p<0.0001$). Appreciable increase in ATF3 positive neurons following 48 hour SA treatment was only seen at the highest dose of 6µM (2.5 ± 1.6%) and this was not significant.

There was variability in the susceptibility of the individual control lines to the 1-deoxySL induced toxicity (Figure 3.4). In terms of neuronal survival, AHO17-7 control line is the least susceptible with 87.1 ± 6.3% of the sensory neurons surviving compared to vehicle control at the highest treatment dose of 1-deoxySA (6µM). AD2-1 (only one experiment) and NHDF-1 lines are similarly vulnerable with 57.7% and 55.1 ± 23.7% of the neurons surviving compared to the vehicle control.

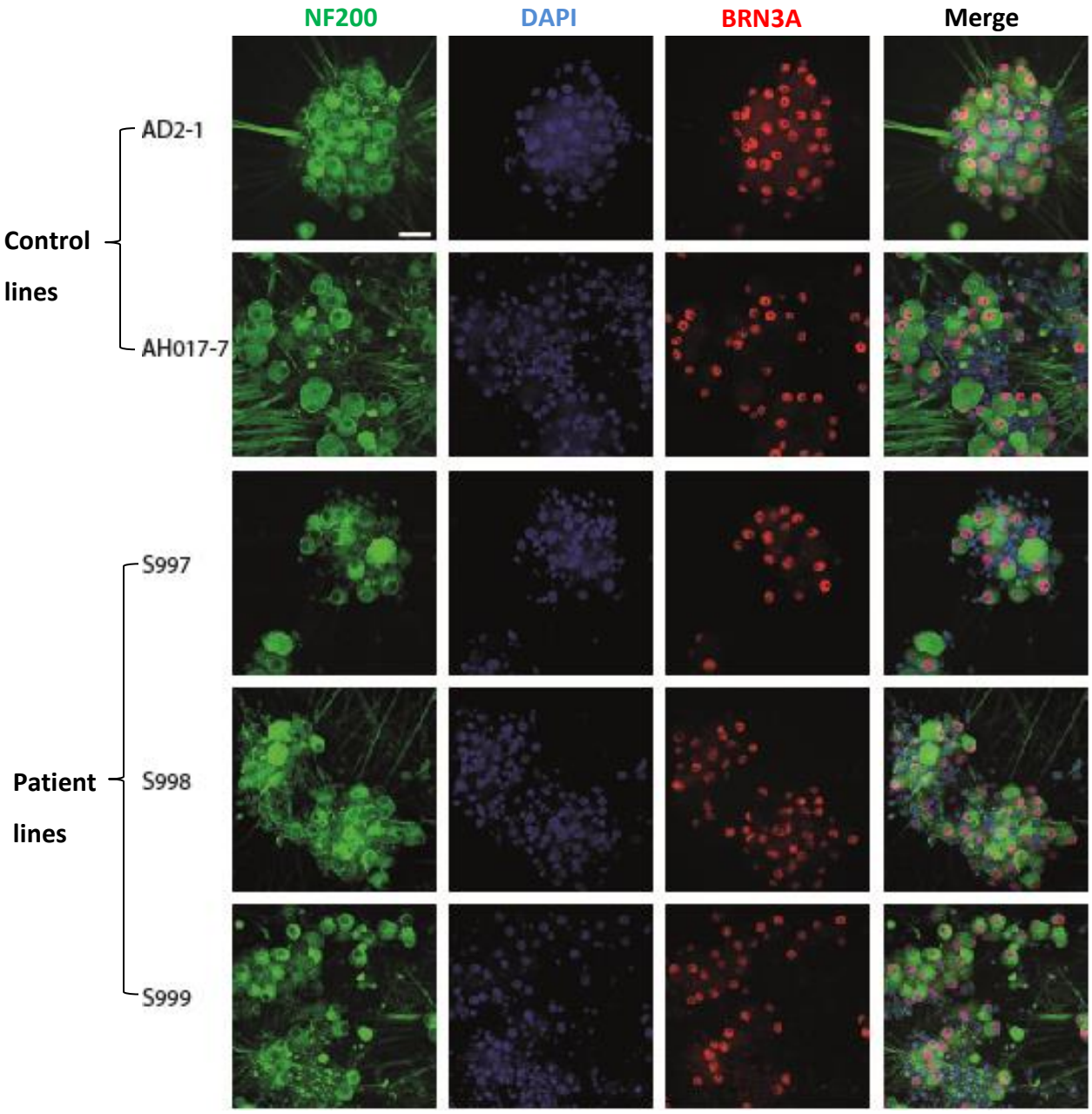

Figure 3.1 Characterisation of 3month old iPSC derived neurons

Representative split channel images of iPSC sensory neurons following differentiation (three months old) from two control lines and all three patient lines. All the differentiated neurons were positive for Neurofilament heavy chain (NF200) and BRN3A, a sensory neuron marker. DAPI=nuclear stain. Scale bar=50μm

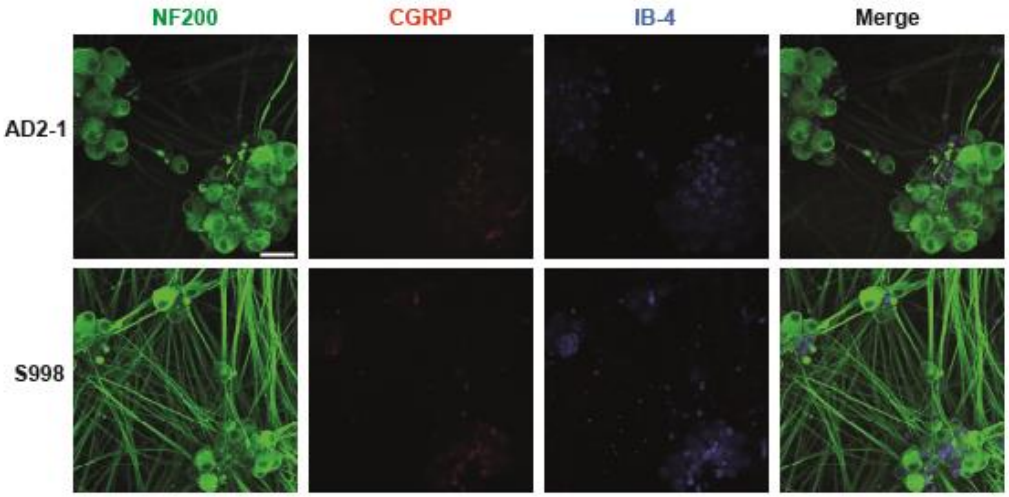

Figure 3.2 Expression of nociceptor markers in 5 month old iPSC derived sensory neurons

Representative images of control (AD2-1) and patient (S998) derived neurons at 5 months. No CGRP (Calcitonin Gene Related Peptide) or IB-4 (Isolectin-B4) immunoreactive neurons were seen in either the control or patient lines. Scale bar=50μm

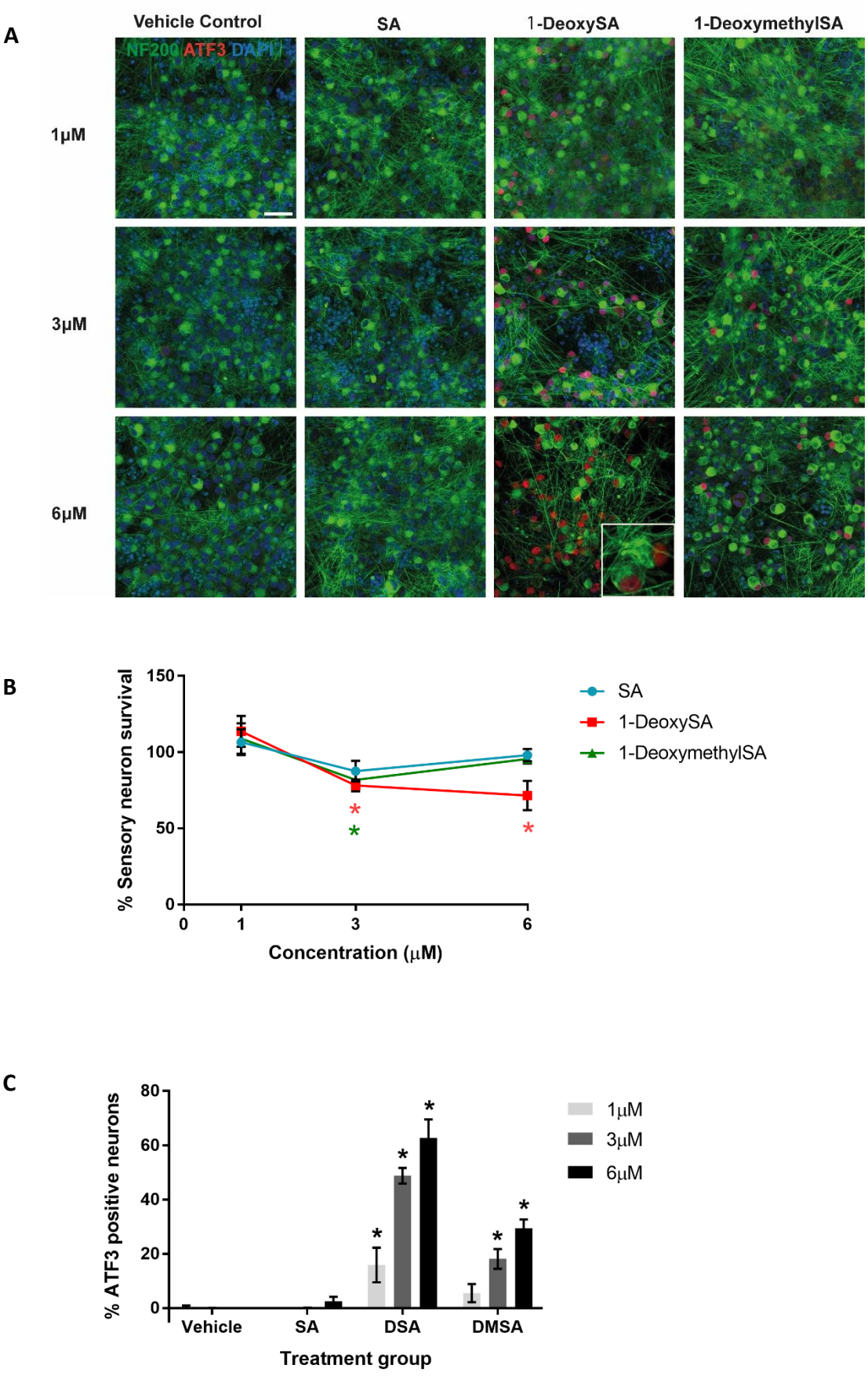
A
Vehicle Control
SA
1-DeoxySA
1-DeoxymethylSA
NF200 ATF3 DAPI
1μM
3μM
6μM
B
% Sensory neuron survival
150
100
50
0
0
1
3
6
Concentration (μM)
SA
1-DeoxySA
1-DeoxymethylSA
C
% ATF3 positive neurons
80
60
40
20
0
Vehicle
SA
DSA
DMSA
Treatment group
1μM
3μM
6μM

Figure 3.3 1-Deoxysphingolipids are toxic to iPSC derived sensory neurons

(A)Three week old human iPSC-derived sensory neurons were treated with sphinganine (SA), 1-deoxySA and 1-deoxymethylSA and vehicle control at 1, 3 and 6µM concentrations for 48 hours and immunostained for NF200 (green), ATF3 (red) and DAPI (blue). High power inset shows the ATF3 expression in a neuronal nucleus. **(B)** Sensory neuron survival is quoted as a percentage of the neurons in the ethanol vehicle treatment group. There is a reduction in neuron survival with 3µM and 6 µM 1-deoxySA and 3µM 1-deoxmethylSA treatment. **(C)** 1-DeoxySL treatment also resulted in a dose dependent increase in the number of neurons with ATF3 expression (marker of axonal injury/stress). n= 5 separate experiments, *p<0.05. Error bars=S.E.M Scale bar= 50µm

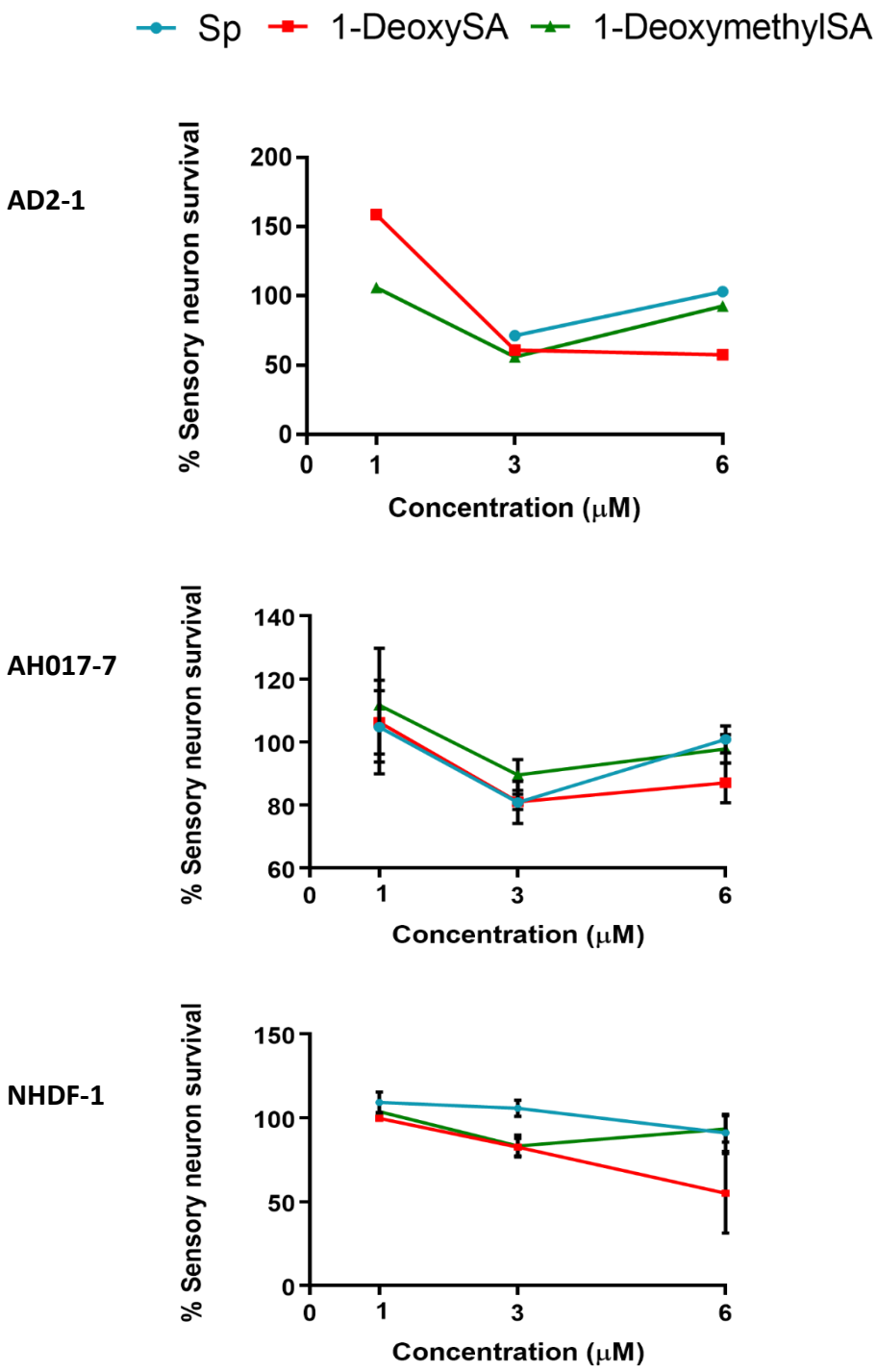

Figure 3.4 Variability in the susceptibility of the control lines to 1-deoxysphingolipid induced toxicity

Effects of 1-deoxySLs on sensory neuron survival in 3 weeks old differentiated sensory neurons from individual control cell lines are displayed. Sensory neuron survival is quoted as a percentage of the neurons in the ethanol vehicle treatment group. n=1 for the AD2-1 line and for this line, data for the 1μM sphinganine treatment is not available. Error bars=SEM

3.4.3 Phenotype of patients

Patient iPSCs (lines S997, S998 and S999) were derived from three male HSN1 patients (aged 27-43 years) with moderately severe neuropathy (CMTNS 10-20). The phenotypic characteristics are summarised in Tables 3.3 and 3.4. Patient 13 (cell line S997) had the most severe phenotype followed by patient 7.3 (cell line S998) and patient 9.4 (cell line S999) had the mildest phenotype. All three patients reported painless ulcers

The distribution of the reported pain profile is also similar with S997 having the highest NPSI total score and S999 having the lowest score (Table 3.4). All three patients had the characteristic lancinating pain. The two patients who were taking neuropathic pain medication felt that pregabalin was the most effective medication at dampening this pain.

3.4.5 Autonomous 1-deoxysphingolipid production by patient iPSC derived sensory neurons.

Levels of endogenous sphingolipids were analysed in 4 week old iPSC derived sensory neurons (Figure 3.5). SA is the typical product of the enzyme SPT when its canonical substrates, L-serine and palmitoyl-co enzyme A are condensed together (Figure 1.2). There was no significant difference in the C18-sphinganine (SA) levels between the control and patient lines (1.87 ± 0.44μM/mg protein versus 2.28 ± 0.82μM/mg protein respectively). However, C-18 Sphingosine (SO) which is a downstream metabolite of SA was significantly lower in patient lines (30.79 ± 4.03μM/mg protein in the controls versus 19.43± 4.33μM/mg protein in the patient lines, p=0.01).

Measurable levels of the atypical product of SPT enzyme, 1-deoxySA (condensation of L-Alanine and palmitoyl-co enzyme A)

were seen in both control and patient lines. The levels were significantly higher in the patient lines (0.077 ± 0.015μM/mg protein in the controls versus 0.952 ± 0.327 μM/mg protein in the patient lines, p<0.0001). In all patient lines, 1-deoxySA levels were clearly above those of the control lines. 1-deoxysphingosine (1-deoxySO), the downstream metabolite of 1-deoxySA, was also significantly elevated in the patient lines (0.152 ± 0.014 μM/mg protein in the control lines versus 2.569 ± 1.083μM/mg protein in the patient lines, p<0.0001).

Levels of 1-DeoxymethylSA (condensation of L-glycine with palmitoyl-coenzyme A) in the patient lines was not significantly elevated compared to the control lines (0.02 ± 0.005μM/mg protein versus 0.01 ± 0.002μM/mg protein respectively, p=0.08). Its downstream metabolite, 1-deoxymethylsphingosine (1-deoxymethylSO) was also not significantly different between the patient and control lines (0.06 ± 0.03μM/mg protein versus 0.03 ± 0.01μM/mg protein respectively, p=0.19).

Patient lines S999 and S998 had similar levels of 1-deoxySLs: 1-deoxySA (0.49 ± 0.02μM/mg protein and 0.48 ± 0.08μM/mg protein respectively), 1-deoxySO (0.79 ± 0.09μM/mg protein and 1.01 ± 0.09μM/mg protein respectively), 1-deoxymethylSA (0.010 ± 0.001μM/mg protein and 0.012 ± 0.003μM/mg protein respectively) and 1-deoxymethylSO (0.019 ± 0.002 and 0.028 ± 0.005μM/mg protein respectively). However, there was a consistent trend towards higher sphingolipid levels in S997 patient line compared to the other two patient lines: SA (4.80 ± 1.82μM/mg protein versus 0.98 ±0.05μM/mg and 1.06 ± 0.09μM/mg protein in S999 and S998 respectively),1-deoxySA (1.88 ± 0.80μM/mg protein), 1-deoxySO (5.91 ± 2.38μM/mg protein), 1-deoxymethylSA (1.88 ± 0.80μM/mg protein) and 1-deoxymethylSO (0.13 ±0.07μM/mg protein). 1-DeoxymethylSA level was significantly higher in S997 when compared to S999 (p=0.025) and S998 (p=0.033). This global increase in sphingolipids in the S997 line could partially be explained by the inaccuracies in quantifying very small protein levels (S997 cell density was much less than that of S999 and S998) but not completely as NHDF-1 control line had similar cell density (total protein of 0.095-0.190mg/ml for NHDF-1 versus 0.085-0.365mg/ml for S997).

Cell line	S997	S998	S999
Patient ID	13	7.3	9.4
Age (yrs)	27	37	43
Onset age (yrs)	13	15	27
CMTNSv2	21	21	16
Cold detection threshold: hand (ºC)	6.7	18.3	24.4
Warm detection threshold: Hand (ºC)	Undetectable	48.9	49.8
Mechanical detection threshold: Hand (mN)	157.6	Undetectable	24.3
Plasma 1-deoxySA (µM)	1.056	0.417	0.574
Plasma 1-deoxySO (µM)	1.751	0.715	1.228

Table 3.3 Patient characteristics of iPSC lines

Phenotypic summary of the HSN1 patients who provided the patient iPSC lines. CMTNSv2=Charcot Marie-Tooth Neuropathy Score version 2, 1-deoxySA=1-deoxysphinganine, 1-deoxySO=1-deoxysphingosine (downstream metabolite of 1-deoxySA), undetectable = beyond the safety limit used (50ºC).

Cell line	S997	S998	S999
Age at pain onset	22	15	35
NPSI TOTAL (0-100)	48	40	30
NPSI Burning (0-10)	6	3	6
NPSI Pressing (0-10)	4.5	7.5	0
NPSI Paroxysmal (0-10)	5	8.5	6
NPSI Evoked (0-10)	3	1	0
NPSI Paraesthesia/ dysaesthesia (0-10)	7	1	6
Pain description	Lasts 10-15s. Highly variable frequency Pain worsening	Difficulty sleeping because of pain Lancinating pain, decreasing with worsening sensory deficit	Few episodes a day lasting <5sec Not worsening Worse in cold

Table 3.4 Patient pain phenotype of iPSC lines

Pain characteristics of the HSN1 patients who contributed to the patient iPSC lines. Neuropathic Pain Symptom Inventory (NPSI) was used to characterise the pain. NPSI total scores and scores of some of the components of the inventory are shown.

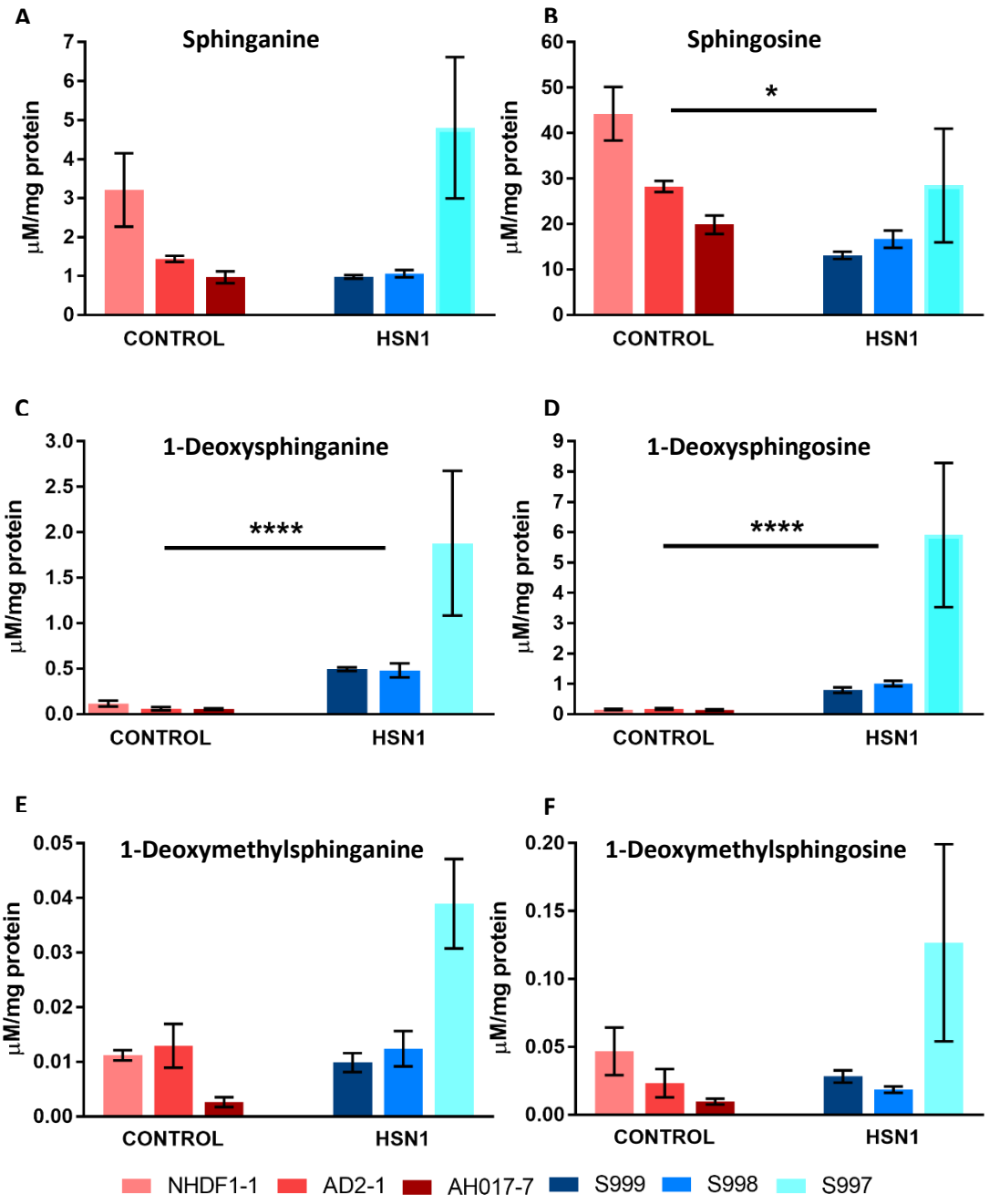

Figure 3.5 Levels of endogenous sphingolipids in control and patient iPSC derived sensory neurons (4 weeks old)

Sphingolipid levels were normalised to internal lipid standard, d7-sphingosine. (A) Sphinganine (canonical product of SPT enzyme). (B) Sphingosine (downstream product of sphinganine) was significantly lower in the patient lines compared to the control ($p=0.011$). (C) 1-Deoxysphinganine levels were significantly higher in the patient lines compared to the control ($p<0.0001$). (D) Elevated levels of 1-deoxysphingosine (downstream metabolite of 1-deoxysphinganine) were seen in the patient lines compared to the control. (E) 1-deoxymethylsphinganine and 1-deoxymethylsphingosine (F) (downstream metabolite of 1-deoxymethylsphinganine) levels were not significantly different between the patient and control lines. n=3 independent differentiations. Statistics performed on pooled group data. *$p<0.05$, ****$p<0.0001$, Error bars=SEM

3.4.6 Early loss of HSN1 iPSC derived sensory neurons

Early neuronal loss was determined by assessing the percentage of neurons that were immunoreactive for cleaved Caspase 3. Cleaved caspase 3 is the activated form of caspase 3, which is one of the key executioners of apoptosis. The cultures were fixed at three weeks after the end of the differentiation. Cultures were supplemented with L-alanine to augment 1-deoxySL production in the patient lines with the aim to amplify the phenotype. Supplementation started 1 week after the end of the differentiation.

Significantly higher percentage of caspase 3 immunoreactivity was seen in patient lines compared to the control lines at all L-alanine supplementation concentrations (Figure 3.6). In the untreated group, 3.9 ± 0.6% of the control versus 29.7 ± 5.0% in the patient lines were immunoreactive for caspase 3 ($p=0.0002$). Similar differences between control and patient lines were seen at 0.4mM (4.9 ± 1.5% versus 31.7± 5.37%, $p=0.003$), 0.8mM (5.3 ± 1.2% versus 34.6 ± 3.5%, $p<0.0001$) and 1.6mM (7.4 ± 1.4% versus 29.1 ± 3.6%, $p=0.008$) L-alanine supplementations. In the control lines there was a suggestion that L-alanine treatment led to a dose dependent increase in the percentage of caspase 3 positive neurons but this was not statistically significant. However, in the patient lines, there was no dose dependent increase in caspase 3 immunoreactivity with L-alanine treatment.

S999 and S998 patient lines had similar percentages of caspase 3 positivity with all concentrations of L-alanine supplementation but S997 line appears to have higher caspase 3 positivity. In the untreated group, 23.4 ± 2.8% and 21.8 ±3.6% of S999 and S998 lines respectively were caspase 3 positive but 43.9 ±11.2% were positive in the S997 line. With 0.4mM supplementation, 19.9 ±2.5% and 22.9 ± 6.8% of S999 and S998 neurons respectively were positive compared to 52.2 ± 4.1% of S997 neurons. With 0.8mM supplementation, 30.1 ± 1.1% and 25.8 ± 2.2% of S999 and S998 neurons respectively were positive for caspase versus 47.8 ± 1.4% of S997 neurons. The smallest difference was seen at the highest L-alanine supplementation dose of 1.6Mm where 28.6 ± 1.1% and 21.6 ±2.5% of S999 and S998 neurons were caspase 3 positive compared to 39.0 ± 8.4% of S997 neurons. Only at 0.4mM supplementation, there was a significant difference in caspase 3 positivity between S997 and S999 neurons ($p=0.01$) and between S997 and S998 neurons ($p=0.03$).

3.6A

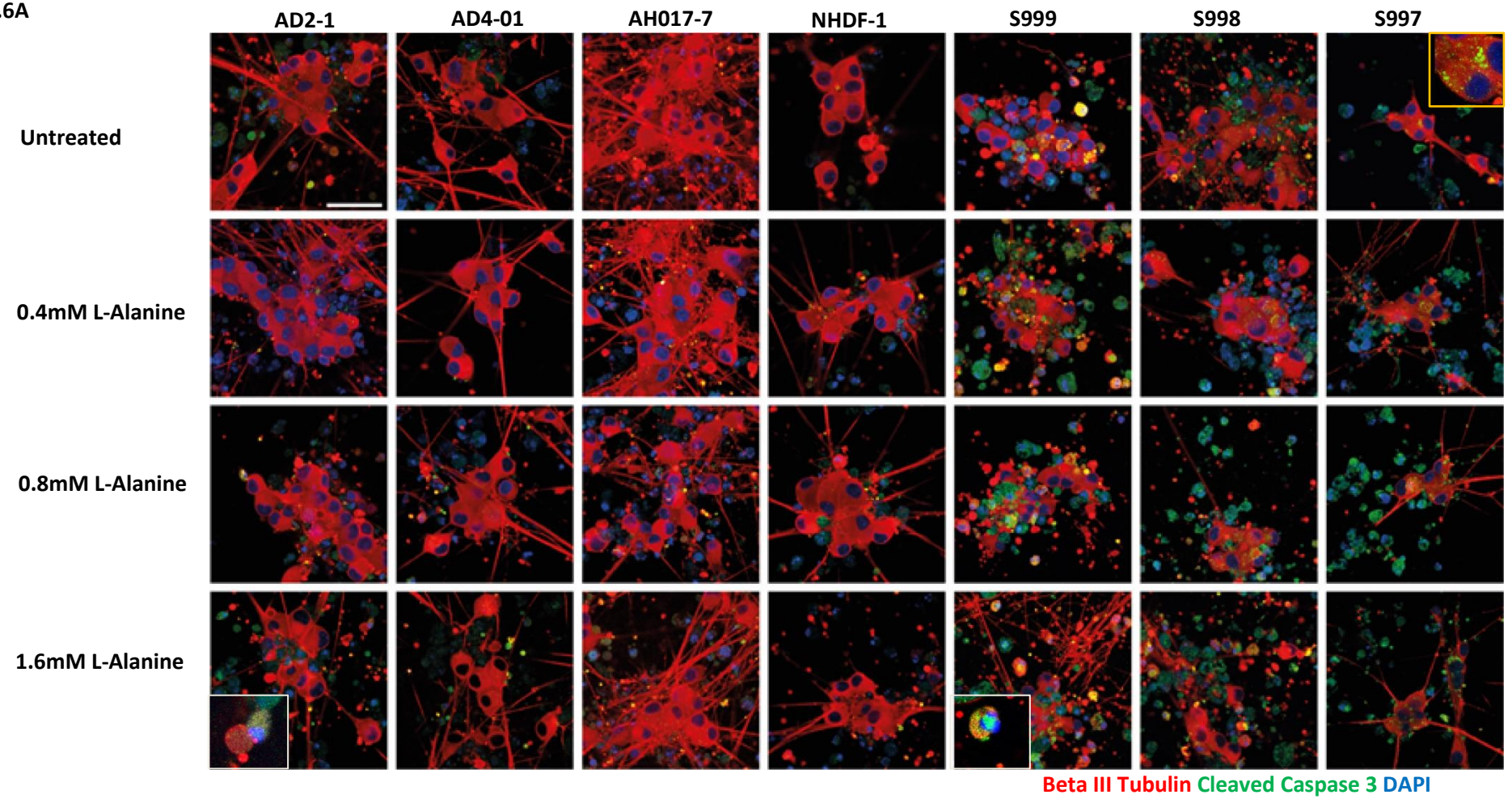
AD2-1
AD4-01
AH017-7
NHDF-1
S999
S998
S997
Untreated
0.4mM L-Alanine
0.8mM L-Alanine
1.6mM L-Alanine
Beta III Tubulin Cleaved Caspase 3 DAPI

B

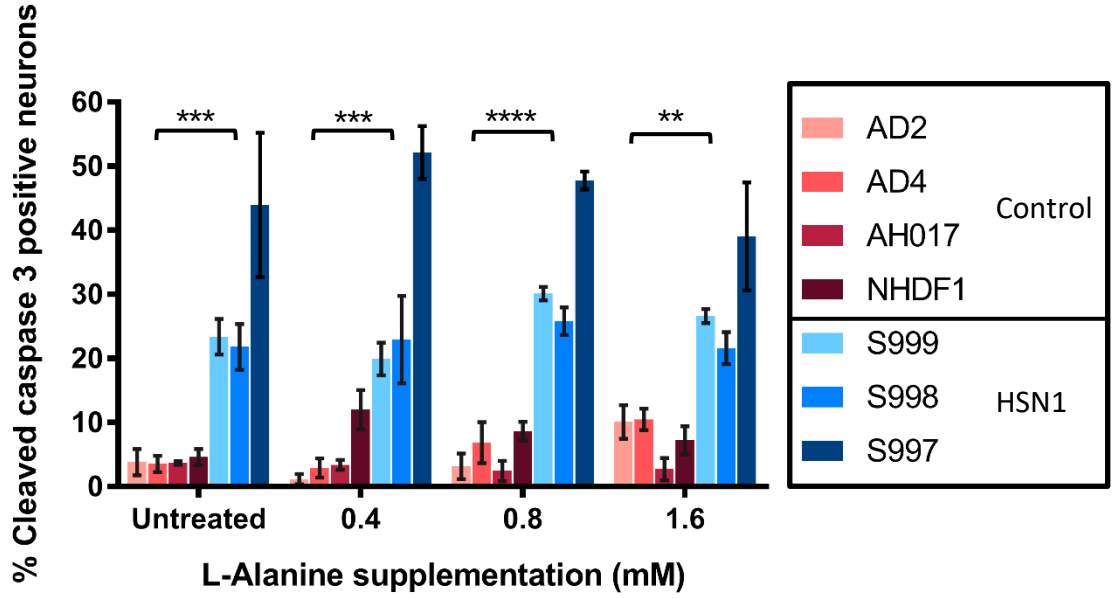

Figure 3.6 Early sensory neuron loss in HSN1 patient lines

(A) Early cell loss in 3 week old iPSC derived sensory neurons was evaluated using cleaved caspase III staining (pro-apoptotic marker). Yellow box high power insert shows the cytoplasmic cleaved caspase III staining. L -alanine supplementation was initiated when the neurons were one week old. There were increased cell debris (fragments of cell co-staining positive for beta III tubulin and cleaved caspase 3 with hyperdense DAPI staining) in the patient lines (S999, S998 and S997), especially with the highest dose (1.6mM) of L-alanine. Cell debris were also seen in the control lines (AD2-1, AD4-01, AH017-7 and NHDF-1) at the highest dose of L-alanine supplementation, but to a lesser extent. Examples of these cell debris are shown in the high power inserts in white boxes. **(B)** At three weeks, HSN1 patient lines had increased cleaved caspase 3 immunoreactivity compared to the 4 control lines in the untreated and L-alanine supplemented groups. n= 3 independent differentiations. Statistics were performed on pooled group data from three independent differentiations. **P<0.01, ***P<0.001 and ****P<0.0001. Error bars=SEM Scale bar=50µm

3.4.7 Neurite outgrowth in mature sensory neurons

Neurite arborisations in the control and patient lines were compared in 3 month old neurons. Extensively arborized neurites were seen in both the control and patient lines (Figure 3.7A). There was no significant difference in the neurite coverage area per neuron between the control lines (3.35 ± 0.60%) and the patient lines (3.88 ± 0.61%) (Figure 3.7B). A major determinant of neurite coverage per neuron was the cell density. In the denser cultures, there were thick layers of neurites which were difficult to capture with the threshold technique used in this analysis. Also, with higher cell densities, the area available for growth was more limited, therefore reduced neurite area per neuron. Consequently, the relationship between total neurite coverage area and total neuron number is not linear (Figure 3.7C). NHDF-1, AD4-01, S999 and S997 lines had similar low cell densities. Cultures with similar density in both the control and patient lines had similar percentage neurite coverage. The only exception is with S997 patient line which despite having similar low density, has neurite coverage area per neuron similar to lines with much higher cell densities suggesting that there might be a reduction in neurite outgrowth in this patient line.

After three months in culture, features of axonal degeneration (blebbing, fragmentation of the neurite) were clearly visible in the S997 and to a lesser degree in the S999 patient lines (Figure 3.7A-insets).

3.4.8 Axonal integrity in mature sensory neurons

As noted above, features of axonal degeneration were seen in few of the neurons in 3 month old neurons from S997 and S999 patient lines. To quantify this, ATF3 expression was examined in 3 month old neurons (Figure 3.8).

There were no significant differences in ATF3 expression between the control and patient lines in the untreated (1.6 ± 0.9% in the control lines versus 2.2 ±0.9% in the HSN1 lines) or 1.6mM L-Alanine supplemented (2.2 ±0.6% in the control lines versus 6.7 ± 3.2% in the HSN1 counterparts) treatment groups (Figure 3.8B).

There was a trend towards increased ATF3 immunoreactivity with 1.6mM L-alanine treatment in the S997 line when compared to the 1.6mM L-Alanine control group (2.2 ±

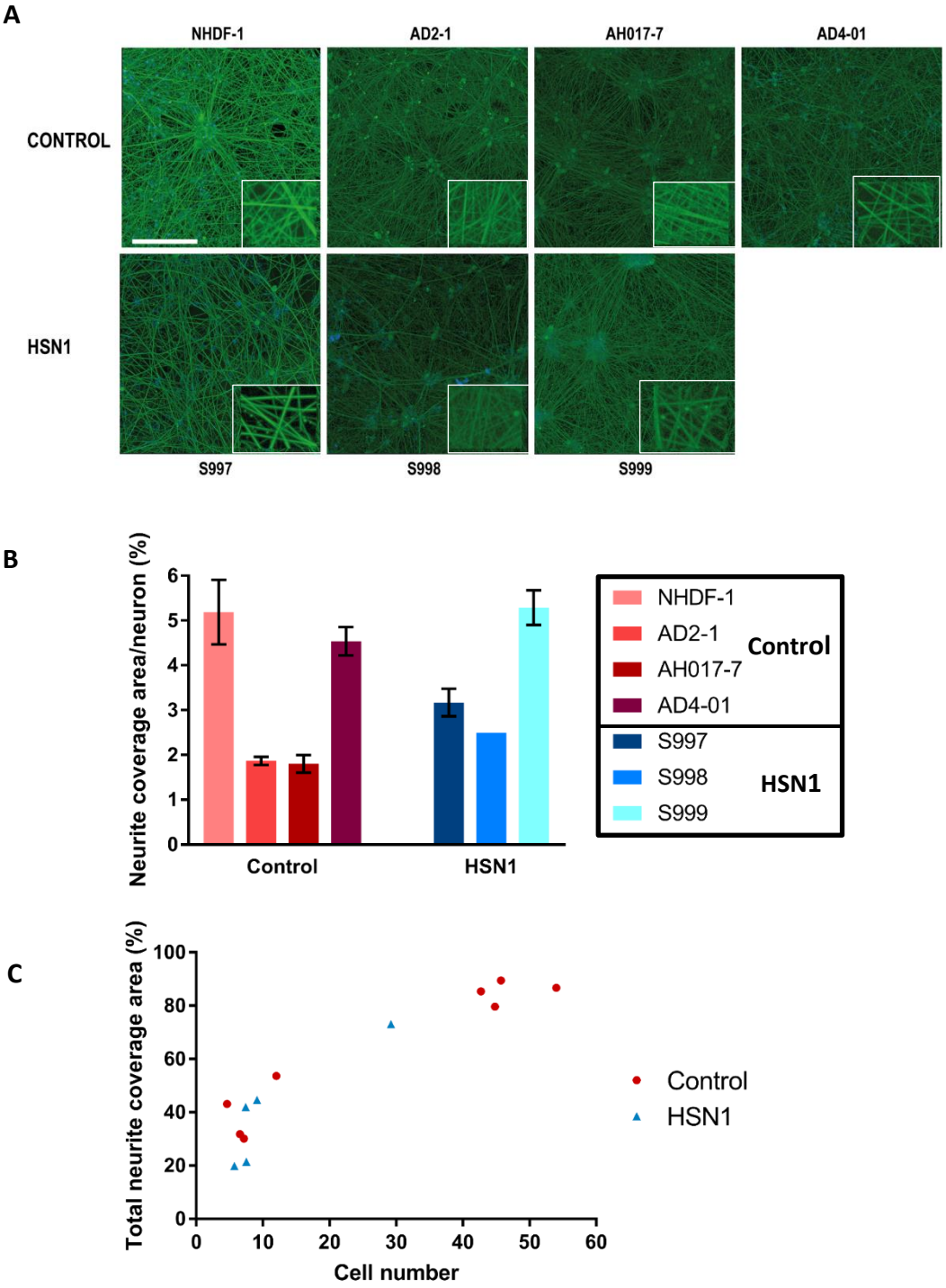

Figure 3.7 Neurite outgrowth in mature sensory neurons (3 months old)

(A) Extensive neurite arborizations were seen in both control and patient lines. In the S997 and S999 patient lines, some of the neurons had features of axonal damage such as blebbing (insets). **(B)** There is no significant difference in the percentage neurite outgrowth between the control and HSN1 patient lines. **(C)** The relationship between neuron number and total percentage neurite coverage area is not linear. n= two independent differentiations (n=1 for S998). Error bars=SEM, scale bar= 200µm

3.8A

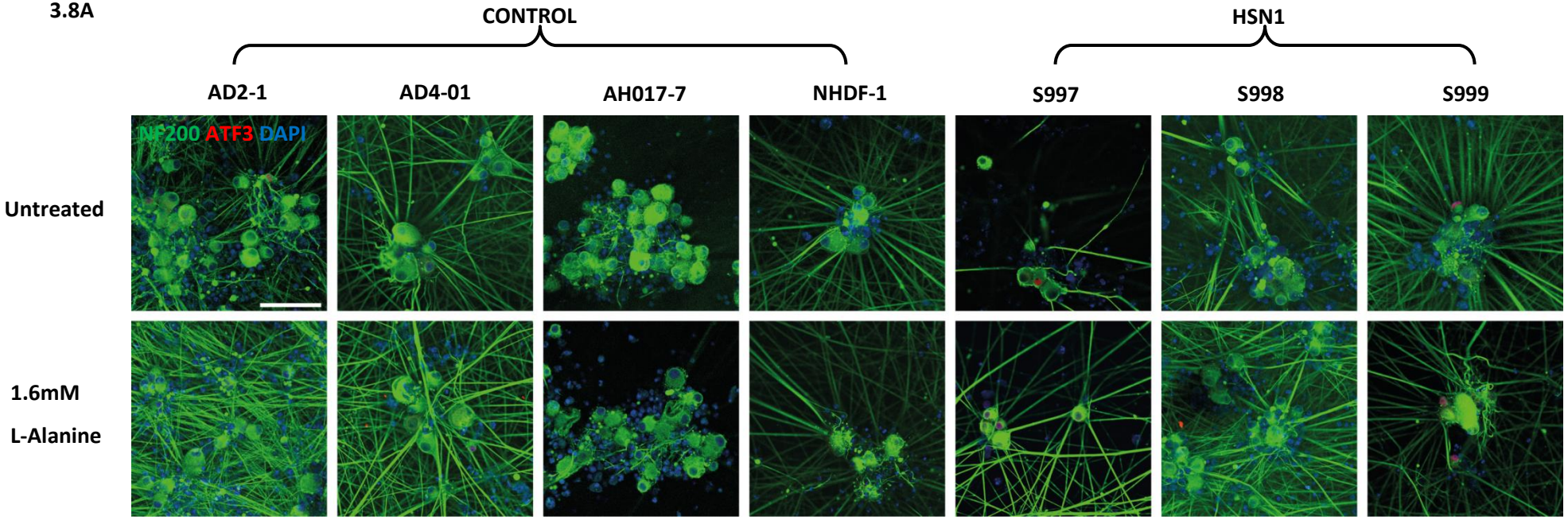
CONTROL
HSN1
AD2-1
AD4-01
AH017-7
NHDF-1
S997
S998
S999
NF200 ATF3 DAPI
Untreated
1.6mM
L-Alanine

B

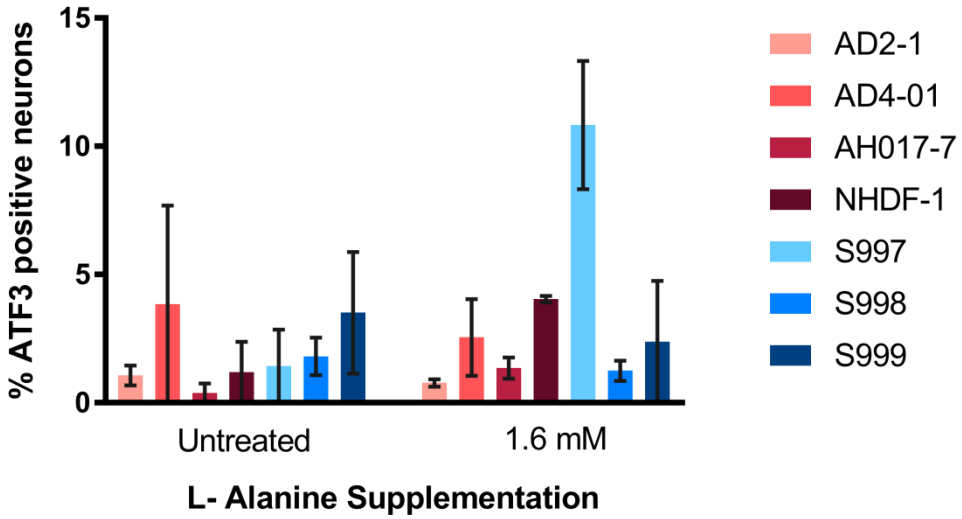

Figure 3.8 ATF3 expression in 3 month old iPSC derived sensory neurons

(A) Three month old control and patient iPSC derived sensory neurons have been immunostained for ATF3 (red) which is a marker of axonal injury. **(B)** There is no significant difference in the percentage of ATF3+ve neurons between the control and patient lines in the untreated and 1.6mM L-alanine treatment groups. n= two independent differentiations. Error bars=SEM, scale bar= 100µm

0.6% in the control group versus 10.8 ± 2.5% in the S997 line).

3.4.9 Effects of long-term L-alanine and L-serine treatment on cell survival

Effects of long term L-alanine and L-serine treatment were assessed in 5 month old neurons (n=1 differentiation). L-alanine and L -serine supplementations were initiated at one and three weeks after the end of the differentiation, respectively. This later time point was chosen for L-serine supplementation in-order to assess the effects of L-serine when treatment is initiated in more mature neurons as would be the case in a clinical setting.

Live imaging was performed to assess cell survival (Figure 3.9). With long-term L-Alanine treatment, there appeared to be no dose dependent reduction in cell survival in the patient lines (91.8 ± 10.1% with 0.4mM, 94.0 ± 5.0% with 0.8mM and 97.5 ± 9.2% with 1.6mM L-alanine treatment compared to the untreated group) (Figure 3.9B). In this one differentiation, L-serine supplementation appears to improve cell survival in both control (131.2 ± 40.3% with 2.5mM serine and 122.7 ± 34.0% with 5.0mM serine treatments) and patient lines (115.6 ± 21.1% with 2.5mM serine and 144.7 ± 29.7% with 5.0mM serine treatments) however these differences were not significant. The improvement in cell survival with L-serine treatment appears to be dose dependent in the patient lines.

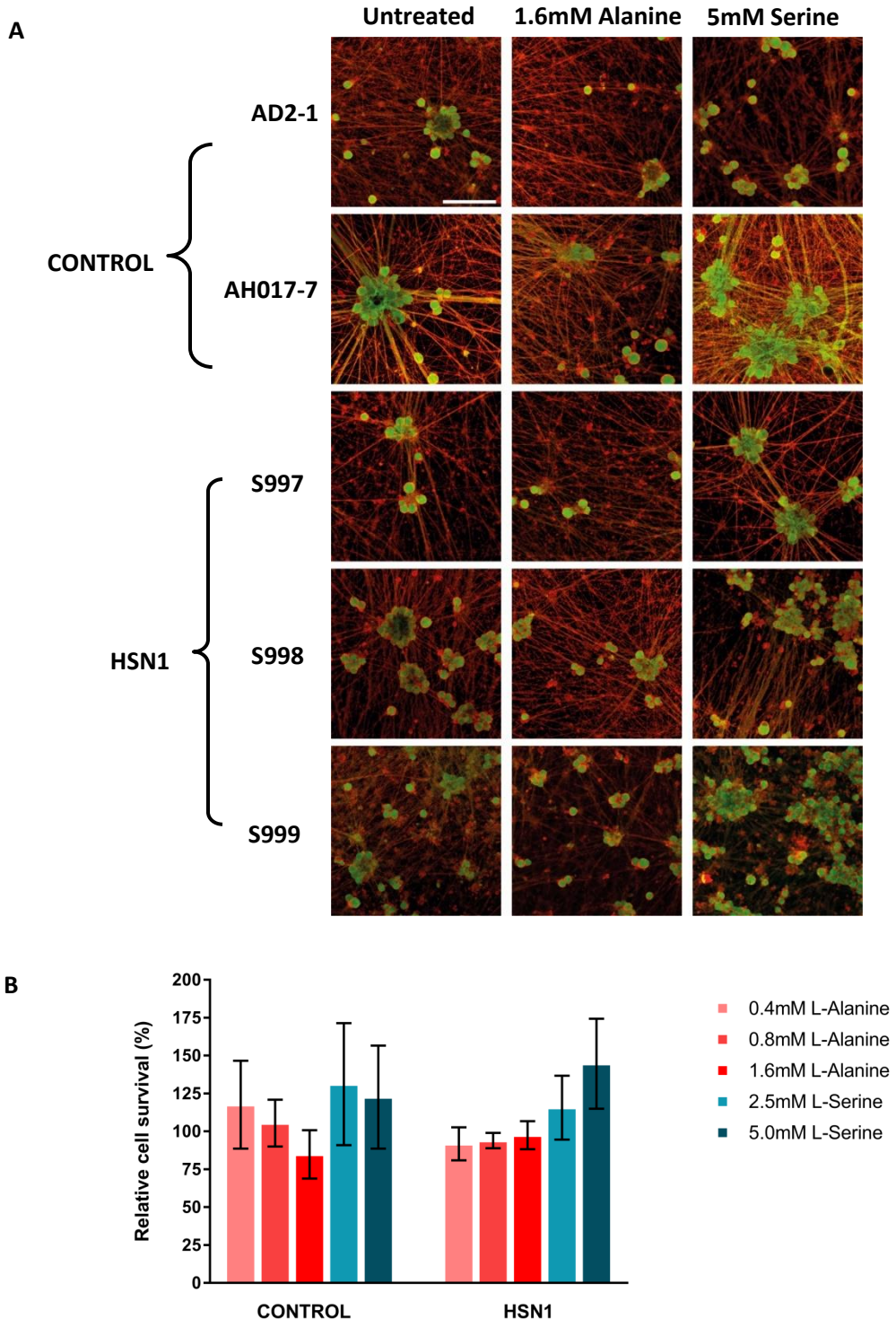

Figure 3.9 Long-term L-alanine and L-serine supplementation.

(A) Representative live cell images of the control and patient lines at 5 months are shown for the untreated and highest used concentrations of L-Alanine and L-Serine treatment. Viable cell bodies are marked green and outer cell membrane surfaces are marked red. **(B)** There is a suggestion that L-Serine supplementation improves cell survival in both control and patient lines. n= one differentiation. Error bars=SEM, scale bar=200µm

3.4.10 Electron Microscopy (EM)

EM images were taken of 5-month-old neurons by the Dunn School Electron Microscopy Facility, University of Oxford. Images were taken from two representative control lines (AD2-1 and AH017-7) and all three patient lines.

3.4.10.1 Transmission Electron Microscopy (TEM)

TEM was performed to determine if there were any gross alterations in the mitochondrial or ER ultrastructure between control and patient lines. Qualitatively, there were no prominent differences in mitochondrial ultrastructure between the control and patient lines (Figure 3.10). In all three patient lines, there were occasional mitochondria which contained whirling (concentric) cristae which was not seen in the control lines. There were no swollen cristae, discontinuous outer membranes, inclusions, compartmentalization, linearization of the cristae, nanotunneling or hyperbranching (Sisková *et al.*, 2010; Vincent *et al.*, 2016) in either the patient or control lines.

There were no clear differences in the ER morphology between the control and patient lines (Figure 3.11). There were also no overt differences in the ER- mitochondria contacts (Figure 3.16).

3.4.10.2 Scanning Electron Microscopy (SEM)

Both in the control and patient lines, the iPSC derived sensory neurons aggregated into clumps (Figure 3.12). The healthier neurons had a smoother cell surface with extensive perikaryal projections (Matsuda *et al.*, 2000). There was no clear difference in the extent of the perikaryal projections between the control and patient lines. There were no distinctive surface morphological features which were common to all three patient lines.

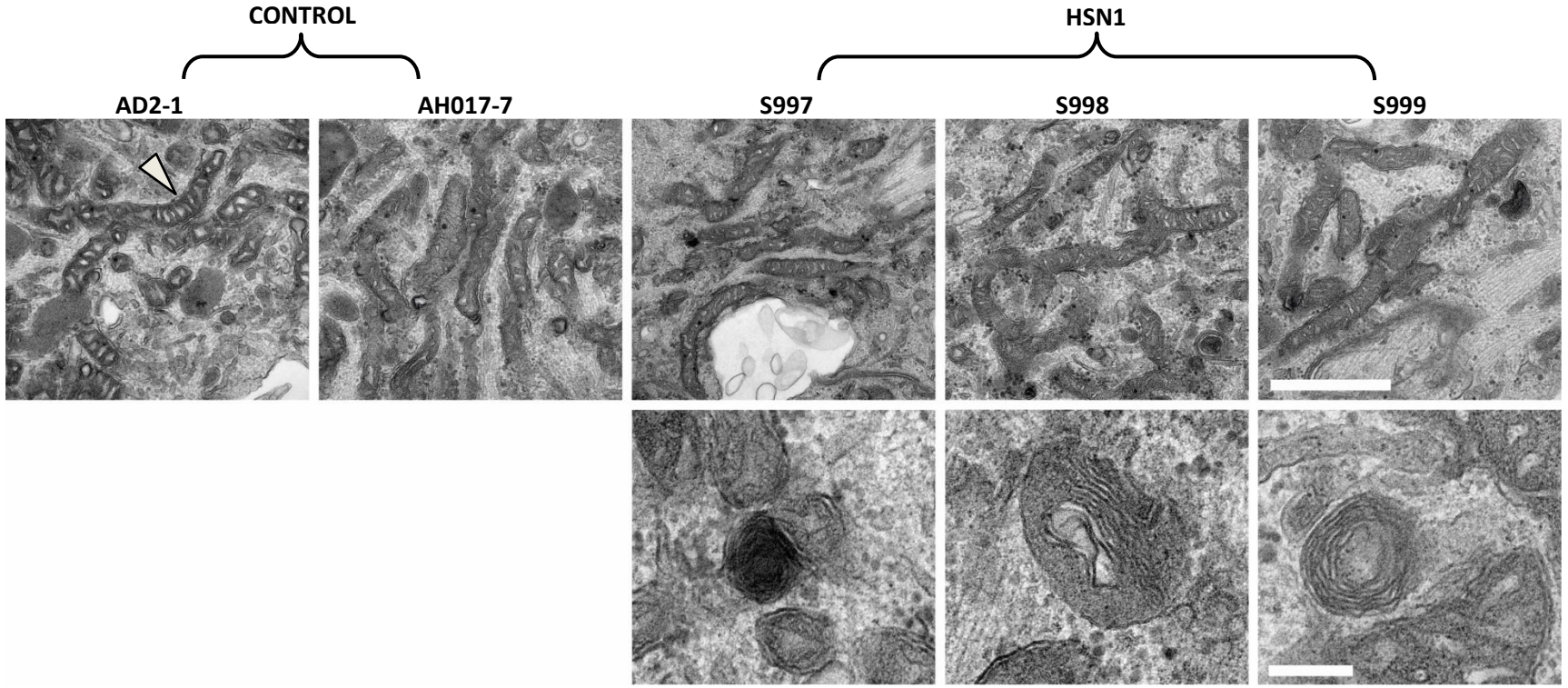

Figure 3.10 Electron micrographs of mitochondria in iPSC derived sensory neurons (5 months old).

Representative Transmission Electron Microscope images of mitochondria (illustrative example shown with white arrow) in the patient and control iPSC derived sensory neurons at 5 months (upper panel). In the patient lines, occasional mitochondria were seen with whirling/concentric cristae (onion-like mitochondria) (bottom panel). Scale bar= 1000nm (upper panel), 200nm (bottom panel).

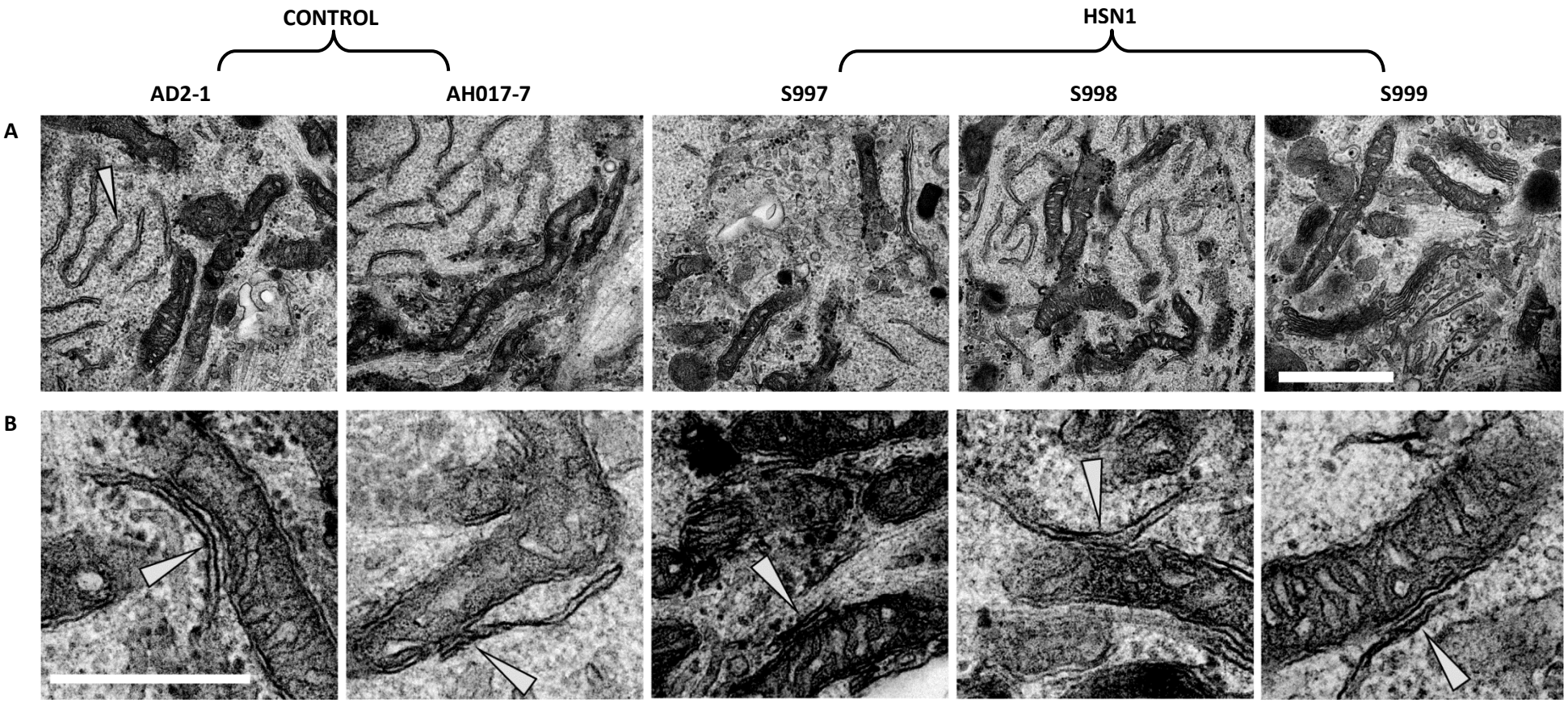

Figure 3.11 Electron micrographs demonstrating ER and ER-mitochondria contacts in iPSC derived sensory neurons (5 months old).

(A) Representative Transmission Electron Microscope images of smooth ER (illustrative example shown with white arrow) in the patient and control human iPSC derived sensory neurons. (B) Images highlighting the ER-mitochondria contacts (arrows) in control and patient iPSC derived sensory neurons. Scale bar= 1000nm (A) and 200nm (B).

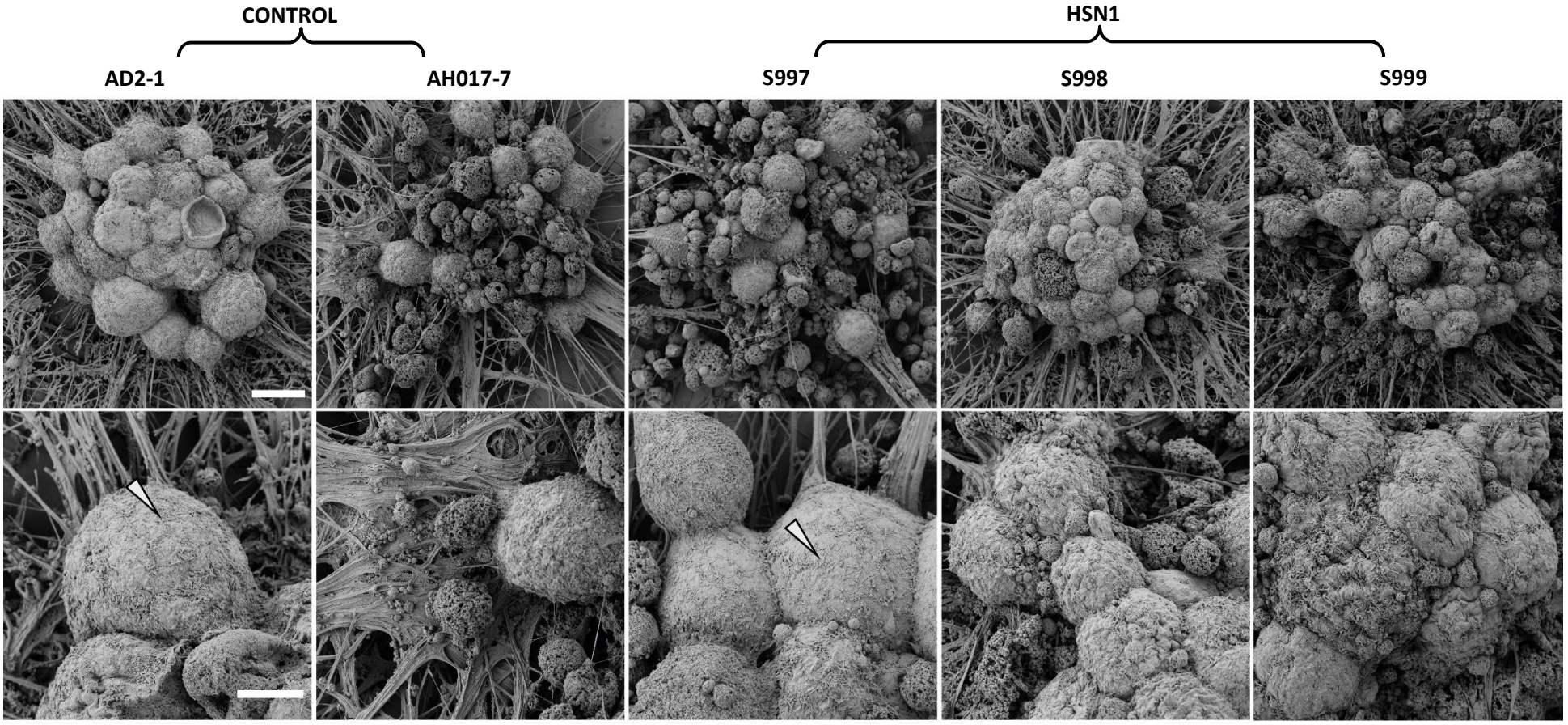

Figure 3.12 Scanning Electron micrographs demonstrating surface morphology of iPSC derived sensory neurons (5 months old).

Representative images of control and patient iPSC derived sensory neurons at 5 months of age. Extensive perikaryal projections (illustrative examples shown with white arrows) can be seen covering the surfaces of both control and patient lines. Scale bar = 20µm (top panel) and 10µm (bottom panel).

3.4.12 ER and mitochondrial calcium imaging

The ER is the most important intracellular calcium store and depletion of ER calcium can trigger ER stress and vice versa (Deniaud *et al.*, 2008; Carreras-Sureda *et al.*, 2018). To determine if there is ER dysfunction/dysregulation of calcium homeostasis in the patient iPSC derived sensory neurons, ER calcium levels were estimated using a SERCA pump (ER calcium re-uptake pump) inhibitor, thapsigargin. The rise in cytosolic calcium following the addition of thapsigargin can be assumed to correlate with ER calcium concentration in the presence of calcium free media. ER and mitochondrial calcium homeostasis are tightly interconnected. Depletion of ER calcium content is followed by rapid accumulation inside the mitochondrial matrix through the mitochondrial uniporter (MCU) complex (Marchi *et al.*, 2017). Mitochondrial calcium was estimated by using ionomycin which is an ionophore and results in the release of all intracellular calcium stores into the cytoplasm of which the largest contribution is from the mitochondria. Calcium imaging experiments were carried out by Dr Alex Clark (Nuffield Department of Clinical Neurosciences, University of Oxford).

In 4-5 month old neurons, there was no difference in the ER calcium concentrations between control and patient lines (mean calcium concentration of 1.17 ± 0.03au in control lines versus 1.11 ± 0.02au in patient lines) (Figure 3.13A). There is a suggestion of decreased ER calcium in the two patient lines S997 and S998. However, there was no significant difference when individual patient lines are compared to the control lines (mean calcium concentrations of 1.09 ± 0.02 for S997, 1.09 ±0.03au for S998 and 1.15 ± 0.06au for S999).

There was no difference in the mitochondrial calcium concentrations between the control and patient lines (mean mitochondrial calcium concentration of 1.45 ± 0.13au in the controls versus 1.36 ± 0.12au in the patient lines) (Figure 3.13B). Greater variations within and between lines were seen with mitochondrial calcium concentrations compared to ER calcium concentrations.

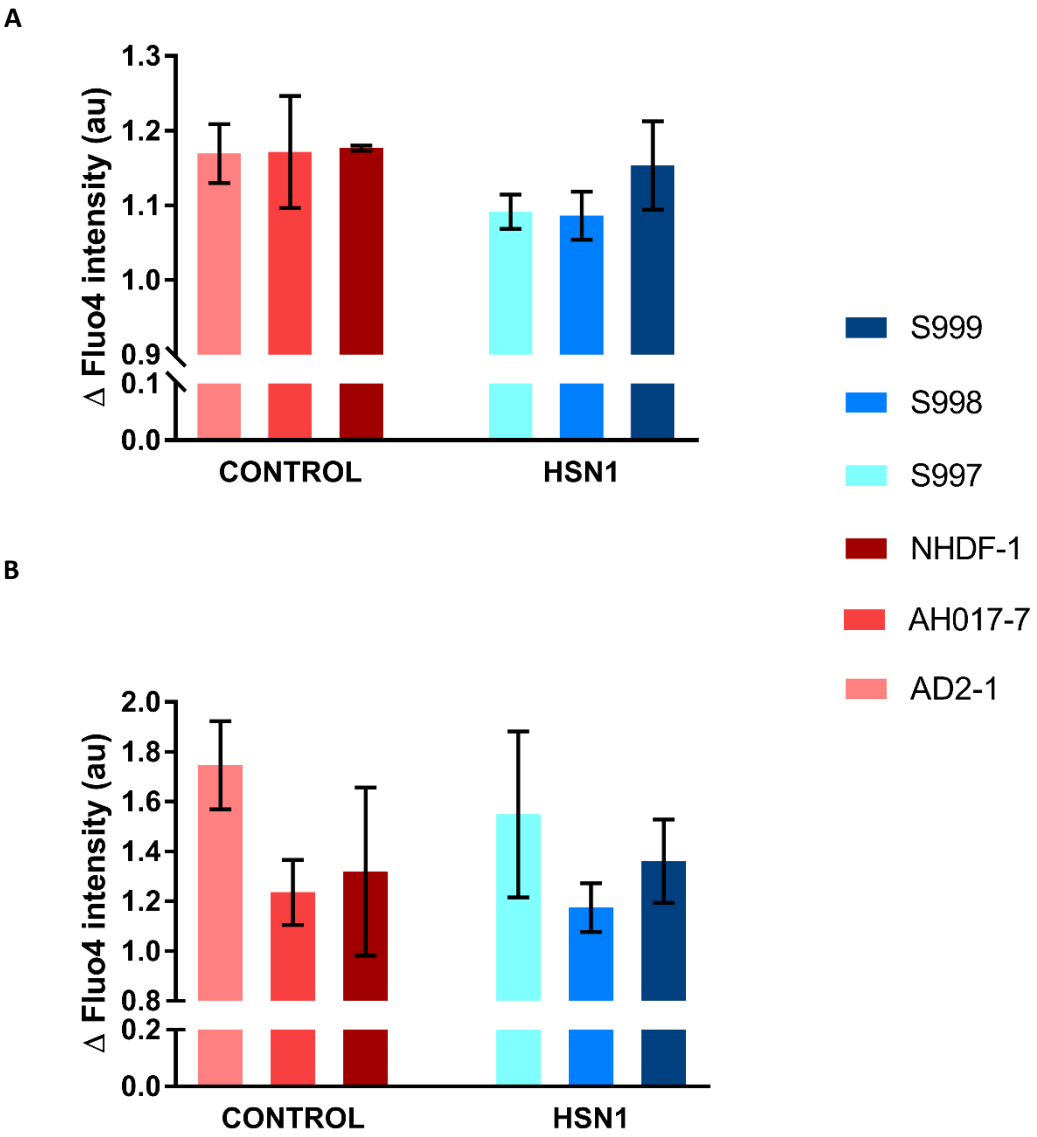

Figure 3.13 Estimates of ER and mitochondrial calcium concentrations in 4-5month old iPSC derived sensory neurons

(A) There is no significant difference in the ER calcium concentrations between the control and patient lines **(B)** There is no difference in the mitochondrial calcium concentrations between the control and patient lines. n=3 independent differentiations (20-30 neurons per cell line). Error bars=SEM

3.5 Discussion

Characterisation of human iPSC derived sensory neurons

The differentiated neurons expressed BRN3A, a canonical marker of sensory neurons. The sensory neuron differentiation protocol by Chambers *et al.* (2012) was used in this study which has been shown to be a valuable model of human pain disorders (Cao *et al.*, 2016). The protocol was reported to produce nociceptive neurons based on expression profiles and electrophysiological characteristics. A subset of these neurons was shown to express CGRP and substance P one month after the start of differentiation. In this study, all the neurons expressed NF200. NF200 is a marker for myelinated A-fibre neurons such as mechanoreceptors and proprioceptors in rodent DRGs. However, in human DRGs, it has been shown that NF200 co-localises with TRPV1, a marker for C-fibre neurons in rodent DRG (Chang *et al.*, 2018). There was no CGRP or IB4 expression, which are markers of nociceptors, in mature neurons (5 months old). The differences in the expression profiles of the sensory neurons between the two studies could be due to differences in the generation of the pluripotent stem cells, variations in protocol implementation and batch effects in the materials used (Schwartzentruber *et al.*, 2018).

It is likely that this differentiation protocol produces mixed neuronal types consisting of nociceptors and non-nociceptors. In voltage-clamp experiments, both Chambers *et al.* (2012) and our lab have demonstrated tetrodotoxin resistant currents in neurons derived from this protocol, which is a characteristic feature of SCN10A sodium channels (selectively expressed in nociceptive neurons) (Han *et al.*, 2016). These differentiated neurons have also been shown to express SCN9A which is a marker for nociceptors and respond to algogens like low pH and ATP (Chambers *et al.*, 2012; Young *et al.*, 2014; Cao *et al.*, 2016; McDermott *et al.*, 2019). However, a sizeable proportion of neurons generated using this protocol had action potential characteristics of non-nociceptive afferents and it was possible to myelinate some of these neurons by co-culturing with rat Schwann cells (Clark *et al.*, 2017).

1-Deoxysphingolipids are toxic to human iPSC derived sensory neurons

In 3 week old neurons, both 1-deoxySA and 1-deoxymethylSA caused a reduction in cell survival and dose dependent increase in the expression of ATF3, a marker of axonal injury. As in the mouse in-vitro model, 1-deoxySA was more toxic than 1-deoxymethylSA. There was variability in the susceptibility of the control lines to the 1-deoxySLs but there was no correlation with the gender of the subjects who donated the fibroblasts. The lines that were the least and most vulnerable to the 1-deoxySL toxicity were from female subjects. 1-DeoxySL cytotoxicity was seen at higher concentrations (3 and 6µM concentrations of 1-deoxySLs) in this iPSC derived sensory neuron model compared to the mouse in-vitro model (1µM concentration of 1-deoxySLs). In addition, the toxicity was more rapid and profound in the mouse in-vitro model where a significant reduction in sensory neuron survival was seen after 12 hours of 1-deoxySA treatment. 48 hours of 1-deoxySA treatment in the mouse model, same duration of treatment as that used with iPSC derived sensory neurons, resulted in only 31% of sensory neurons surviving. This likely reflects differences in neuronal subtypes, neuronal maturation and culture protocols.

Autonomous 1-deoxysphingolipid production by patient iPSC derived sensory neurons

Patient iPSC derived sensory neurons (all lines) produced significantly higher levels of 1-deoxySA compared to their control counterparts. The downstream metabolite, 1-deoxySO (see figure 1.2) was also elevated in all patient lines. However, 1-deoxymethylSA levels were not significantly different between the two groups which contrasts with the findings in plasma from HSN1 patients (all C133W carriers) and EBV transformed lymphoblasts of HSN patients (all C133W carriers) where patients/patient lines had significantly higher levels of 1-deoxymethylSA compared to controls (Penno *et al.*, 2010). This difference could be due the inherent errors associated with quantifying the very small levels of 1-deoxymethylSA present in iPSC derived sensory neurons which might mask any differences between patient and control lines.

The ratio of Sphinganine: Sphingosine is smaller than the ratio of 1-deoxySA:1-deoxySO suggesting that the conversion of 1-deoxySA to 1-deoxySO is less efficient than the conversion of SA to SO. Penno *et al.* (2010) noted similar findings in HSN1 patient

lymphoblasts. This could result in the build-up of intermediates such as 1-deoxydihydroceramide and 1-deoxyceramide. In keeping with this, Alecu *et al.* (2017a) showed that labelled dihydroceramide species were undetectable after 24 hours of incubation with labelled SA but constituted approximately 70% of the total 1-deoxySL species detected following incubation with labelled 1-deoxySA. These downstream metabolites of 1-deoxySA have been proposed to mediate 1-deoxySL induced toxicity rather than 1-deoxySA (Güntert *et al.*, 2016; Alecu *et al.*, 2017b).

Early studies into HSN1 pathogenesis noted a reduction mutant SPT activity (Bejaoui *et al.*, 2002; Gable *et al.*, 2002; Dedov *et al.*, 2004). However, in this study, similar to Dedov *et al.* (2004) who used HSN1 lymphoblasts, there was no reduction in Sphinganine levels when compared to controls. Dedov *et al.* also reported no significant difference in sphingosine which is not the case with this study. HSN1 iPSC derived sensory neurons had significantly lower levels of SO compared to controls. This might reflect cell specific differences in sphingolipid metabolism. Garafalo *et al.* (2011) noted that total Sphingosine levels were about 50% lower in sciatic nerves of transgenic C133W mice than wild-type mouse but not in other tissues such as liver and brain.

There is some correlation between HSN1 iPSC derived neuronal 1-deoxySL production and clinical phenotype of the patients. Patient line (S997) derived from the HSN1 patient with the most severe phenotype in this cohort produced the highest levels of 1-deoxySA and 1-deoxySO. Patient lines S998 and S999 (S999 derived from the patient with the mildest phenotype) produced comparable levels of 1deoxySLs. There was no clear correlation between the sensory neuron and plasma 1-deoxySL levels for these three patients. Sciatic nerves of transgenic C133W mice (12-15 months old) had elevated levels of 1-deoxySA compared to wild-type (Eichler *et al.*, 2009; Garofalo *et al.*, 2011). It was not possible to compare neuronal 1-deoxySLs in this study with published levels in transgenic C133W mice sciatic nerves and patient lymphoblasts due to differences in quantification methods.

Phenotype of HSN1 patient iPSC derived sensory neurons

There was early loss of HSN1 iPSC derived sensory neurons demonstrated by the increased expression of cleaved caspase 3 (key mediator of apoptosis) at 3weeks after the end of differentiation protocol. Highest percentages of caspase 3 positive neurons were

seen in the S997 patient line and correlates with the clinical phenotype (patient with most severe neuropathy). This early phase of cell loss could represent selective loss of cells which have closer resemblance to nociceptor lineages. Following this early neuronal loss, the remaining neurons remain relatively stable over the next 2-3 months. At three months, there was no significant difference in the percentage of ATF3 positive neurons between the control and patient lines, even with L-alanine supplementation. At this time point, subtle features of axonal degeneration (blebbing, fragmentation of the neurite) were seen in some of the patient lines. Evaluation of axonal integrity at a later time point, for example after six months, might be needed to detect quantifiable changes in these neurons modelling a slowly progressive neuropathy.

L-alanine supplementation, which should theoretically exacerbate the phenotype did not have any clear effect on patient lines with regards to the percentage of neurons that are cleaved caspase 3 positive. The culture media was supplemented with glutaMAX as a source of L-glutamine. However, in-order to improve stability by preventing the spontaneous breakdown of L-glutamine into ammonia, glutaMAX is made up of L-alanyl-L-glutamine dipeptide. Cells cleave the dipeptide bond as required to release L-glutamine and L-alanine. Therefore, the exact L-Alanine concentration in the media is not certain and the additional L-alanine provided by Glutamax may have a ceiling effect on the HSN1 iPSC cell lines. In contrast, L -alanine supplementation appeared to cause a dose dependent increase in the percentage of caspase 3 positive neurons and reduction in cell survival in the control lines. The consumption of the L-serine in the media by the neurons and the resultant alteration in the L-serine: L-alanine ratio might lead to increased L-alanine utilization by the control lines.

Neurite outgrowth was assessed in 3 month old neurons. Extensively arborized neurites were seen in both control and patient lines with no difference in the percentage neurite coverage area per neuron between the two groups. This finding is different to the reduced neurite outgrowth observed following 1-deoxySL treatment in the in-vitro mammalian model described in chapter 2 and the published in-vitro models of HSN1 (Penno *et al.*, 2010; Alecu *et al.*, 2017b). This could be due to differences in neuronal maturation and 1-deoxySL concentrations. It was not possible to trace individual neurites in these dense, overlapping neurite arborizations and hence coverage area per neuron was quantified using a threshold technique. This a relatively crude technique. Cell density was a major determinant of the

variation in the measurements of neurite outgrowth because of the technical limitations of the technique and the dependence on density for the area available per neuron for growth. It might be possible to obtain more accurate measures of neurite outgrowth by re-plating the neurons at a lower density.

Altered mitochondrial ultrastructure have been reported in HSN1 lymphoblasts and Mouse Embryonic Fibroblasts (MEF) treated with 1-deoxySA (Myers *et al.*, 2014; Alecu *et al.*, 2017b). There were no prominent qualitative differences in the mitochondrial ultrastructure between 5 month old control and HSN1 iPSC derived sensory neurons. Importantly, there were no disruptions to the outer membrane or loss of internal cristae structures as previously reported (Myers *et al.*, 2014; Alecu, *et al.*, 2017b). However, in all three patient lines, the occasional mitochondria were noted to have whirling (concentric) cristae which was not seen in the control lines. Whirling/concentric cristae have been seen in patients with mitochondrial myopathy (Vincent *et al.*, 2016). The lack of prominent mitochondrial structural defects in this study could be secondary to differences in preparation techniques. Preparation of samples for TEM involved chemical fixation, staining, dehydration and embedding in a resin. All of these steps introduce considerable artefacts (Vanhecke *et al.*, 2008). Contact with too much saline can cause swollen mitochondria and delay in fixation can cause alteration in mitochondrial matrix (Stirling *et al.*, 2013). Mitochondria are susceptible to hypoxia therefore even short delays in fixation can lead to morphological change (Stirling *et al.*, 2013).

There were no gross morphological differences in the ER ultrastructure or ER-mitochondria contacts between the patient and control lines. Scanning electron microscopy did not reveal any distinctive surface morphological feature which was present in all patient lines. Increase in the dihydroceramide /ceramide ratio results in increased rigidity of the plasma membrane (Rodriguez-Cuenca *et al.*, 2015). The lack of any clear differences in surface morphology between the S998 and S999 lines and the control lines might be because of the limited incorporation of these highly hydrophobic downstream metabolites of 1-deoxySA (Jiménez-Rojo *et al.*, 2014) into plasma membranes. Dihydroceramides derived from the canonical SPT product, SA, are found in the plasma membrane (Rodriguez-Cuenca *et al.*, 2015). Alecu *et al.* (Alecu *et al.*, 2017b) using alkyne-deoxySA probe were able to trace the fate of the exogenously applied 1-deoxySA. After 24 hours of treatment, there was little to no

labelling of the plasma membrane indicating that most of the downstream metabolites of 1-deoxySA do not reach the plasma membrane.

The next part of the study focused on functional characterisation of the HSN1 iPSC derived sensory neurons. The mouse in-vitro model described in the previous chapter suggested ER stress as a possible pathomechanism of 1-deoxySL induced toxicity. Wilson *et al.* (2017) noted reduced ER calcium levels in DRG neurons following 2 hours of treatment with 1-deoxySLs. In this study, we examined ER and mitochondrial calcium levels in 4-5 month old iPSC derived sensory neurons. At this age, there were no significant differences in ER or mitochondrial calcium levels between the patient and control lines. However, there was a suggestion that ER calcium levels were reduced in two of the patient lines: S997 and S998, belonging to the 2 patients with the more severe phenotype. This reduction may become significant with increased n numbers or if the study was performed in older neurons. In the in-vitro models in the previous chapter, ER stress was assessed following application of toxic concentrations of 1-deoxySLs. In the current study, the toxicity is from the gradual build-up of endogenous 1-deoxySLs which are likely to become significant in more mature neurons. As sphingolipid metabolism is highly compartmentalised within cells, the differences between the models could also reflect differences in how cells handle endogenous versus exogeneous 1-deoxySLs.

On continuing this project, Clark *et al*. (2019) have shown using electrophysiological studies that HSN1 iPSC derived sensory neurons were hyperexcitable which could explain the distinctive lancinating pain frequently reported by HSN1 patients. S998 and S997 patient lines had significantly increased repetitive firing (number of action potentials following an input current stimulus) compared to the controls however S999 patient line had a firing rate comparable to that of the controls. This correlates with the clinical phenotype: S999 line was derived from the patient who had the lowest total Neuropathic Pain Symptom Inventory Score (NPSI=30). S997 and S998 lines were derived from patients who had NPSI total scores of 48 and 40, respectively. The latter patient had the highest paroxysmal NPSI sub-score and their iPSC derived sensory neurons had the most hyperexcitable profile electrophysiologically.

It is possible that 1-deoxySLs can interact with ion channels, altering their function and resulting in increased excitability. Guntert *et al*. (2016) investigated rapid (5 second exposure) current responses following 1-deoxySA treatment in cortical neurons. They found that ≥2μM 1-deoxySA led to irreversible depolarisation of the membrane potential and that lower concentrations of 1-deoxySA resulted in current responses only in neurons that had functional N-methyl-D-aspartate receptors (NMDAR). Using cortical neurons to model a peripheral neuropathy is a critical caveat of this study however it does suggest that for 1-deoxySA to have such a fast effect, it must interact directly with receptors. Ceramide has been shown to inhibit store operated calcium channels (SOCs- calcium influx channels on the plasma membrane) (Leanza *et al.*, 2016). Sphingosine can also inhibit SOCs and increase membrane capacitance (Leanza *et al.*, 2016). Hydrophobic ceramide molecules spontaneously associate with each other to form rigid, gel-like ceramide enriched membrane domains. These domains fuse together to create highly hydrophobic ceramide enriched domains/platforms which can trap and cluster receptors, ion channels and intracellular signalling molecules to optimise signal transduction. It is possible that 1-deoxyceramide could have similar effects on ion channels. 1-deoxyceramide levels will be elevated in cells since 1-deoxySLs cannot be degraded via the sphingosine-1 lyase pathway or be converted to more complex sphingolipids (Alecu *et al.*, 2017b). Multitude of endogenous lipids have been described to modulate Transient Receptor Potential (TRP) channels (Taberner *et al.*, 2015). In primary sensory neurons, TRP channels act as sensors for innocuous and noxious physical stimuli such as heat and cold (Sousa-Valente *et al.*, 2014). The vulnerability of peripheral neurons to 1-deoxySL induced toxicity, especially subtypes of sensory neurons, might be due to their expression profiles of specific ion channels/receptors.

The final aim of this study was to determine if L-serine supplementation could ameliorate disease specific phenotype. Effects of long-term L-alanine (initiated one week after the end of differentiation) and L-serine (initiated 3 weeks after the end of differentiation) supplementation on cell survival were analysed in one differentiation. There were no significant differences in cell survival between control and patient lines with both treatments. L- alanine supplementation had no dose dependent reduction in cell survival in the patient lines. Long-term L-serine supplementation appears to improve neuronal survival in both

control and patient lines with a dose dependent increase in patient lines. It is possible that with higher doses of L-serine supplementation, there might be further improvement in cell survival. In a HSN1 mouse model, L-serine supplementation led to a 2 fold increase in the number of unmyelinated fibres (Garofalo *et al.*, 2011). Due to insufficient time, it was not possible to look at the effects of L-serine supplementation on cell survival in additional differentiations.

In summary, HSN1 iPSCs can be differentiated into sensory neurons which produce increased levels of 1deoxySLs compared to their control counterparts. There is early loss of these neurons followed by relative stability of the surviving neurons. These neurons exhibit increased excitability and there is suggestion of decreased ER calcium in two of the patient lines. However, even after 5 months in culture, there is no clear progressive loss of these neurons compared to the control lines.

HSN1 is a slowly progressive neuropathy with onset typically in the mid-late teens (Table 2.1). Human iPSC derived cells generally resemble foetal rather than adult cells (Brennand, 2013; Eberhardt *et al.*, 2015; Cornacchia and Studer, 2017). There is mixed opinion on the maturity of iPSC derived sensory neurons created with the protocol used in this study. Eberhardt *et al.* (2015) showed that human pluripotent stem cell derived neurons exhibited an embryonic like expression pattern of tetrodotoxin resistant sodium channels. Young *et al.* (2014) reported, based on transcriptome data and ion channel function assessed electrophysiologically and pharmacologically, that iPSC derived sensory neurons within six weeks of directed differentiation were comparable to adult human DRGs. However, they differentiated neurons from human embryonic stem cells and used a slightly modified protocol (neuronal media supplemented with ascorbic acid in addition to growth factors used in this study). Modelling late onset disease like HSN1 using iPSC derived sensory neurons therefore poses a challenge.

There is now evidence for a cell autonomous clock like mechanism that dictates the dynamics of cell fate acquisition in these differentiated neurons which mirrors in-vivo developmental timing (Brennand, 2013; Studer *et al.*, 2015). In addition to the functional immaturity of iPSC derived cells, reprogramming fibroblasts to induced pluripotent stem cells, resets their identity back to an embryonic stage (Miller *et al.*, 2013; Studer *et al.*,

2015). Miller *et al*. (2013) reprogrammed fibroblasts from old donors into iPSCs then re-differentiated them back into fibroblasts. They noted that the re-differentiated fibroblasts were different from their older derivatives and were indistinguishable from young donor derived iPSCs. This raises the question whether iPSC derived cells model predisposition to disease rather than disease itself (Brennand, 2013).

Various strategies are being used to promote in-vitro maturation of iPSC derived cells. One strategy is to use chemical compounds or expression of transcription factors to accelerate cell maturation in-vitro (Cornacchia and Studer, 2017). Another is to mimic in-vivo development, for example using co-cultures. Clark *et al*. (2017) have established co-cultures of iPSC derived sensory neurons and rat Schwann cells which reproduced the molecular organization of myelinated axons. These co-cultures could be maintained for >9 months without showing any signs of axonal or myelin deterioration. These co-cultures would be useful for studying in-vitro HSN1 phenotype in more mature neurons and for studying effects on myelination. Both clinical (conduction slowing in motor nerve conduction studies, see Figure 4.6) and animal model (increase in g-ratio of axons in transgenic HSN1 mice, indicating thinning of myelin (Eichler *et al.*, 2009; Garofalo *et al.*, 2011)) data suggest nodal/myelin dysfunction.

Several techniques have been used to mimic aging in-vitro: using molecules involved in signalling pathways associated with aging and progerin (a truncated form of lamin A which is associated with premature aging) expression induced aging (Miller *et al.*, 2013; Cornacchia and Studer, 2017). Since cellular immaturity and age erasure of iPSC progeny is believed to stem from the transition through the pluripotent state, several studies have used methods to circumvent the pluripotent intermediate by direct conversion (transdifferentiation) of mature lineages into different cell types (Cornacchia and Studer, 2017). Several studies have demonstrated that directly reprogrammed human neurons (induced neurons, iNs) from fibroblasts retained ageing associated transcriptomic signatures and aging hallmarks such as DNA damage unlike iPSC derived neurons (Mertens *et al.*, 2015; Tang *et al.*, 2017). Liu *et al.* (2016) have shown that motor neurons from directly converted fibroblasts of ALS patients exhibit cytological and electrophysiological profiles of spinal motor neurons and form functional neuromuscular junctions. In addition, these neurons show disease specific degeneration. Protocols are now available for directly

converting fibroblasts into peripheral sensory neurons (Blanchard *et al.*, 2015; Wainger *et al.*, 2015). HSN1 induced neurons which are directly reprogrammed from patient fibroblasts might exhibit clear phenotypic features, including progressive cell loss, at an earlier time point. This will make it easier to test the efficacy of potential therapeutic agents such as L-serine.

The elevated production of 1-deoxySLs by HSN1 iPSC derived sensory neurons and the correlation of their phenotypic features with disease severity of the HSN1 patients they originated from suggest that this is a potential in-vitro model of HSN1.

4. HSN1 Natural history study: In-depth cross sectional baseline phenotyping

4.1 Introduction

As noted in the introduction chapter, HSN1 is a rare neuropathy and hence phenotypic descriptions in most of the literature are based on a handful of cases. The largest study by Houlden *et al*. (2006) looked at 6 HSN1 families and one sporadic case (37 patients), all of whom carried the C133W mutation. They noted considerable intra and inter-familial variability and differences in disease severity between males and females. The also noted slowing of motor conduction velocities in the electrophysiological studies of some patients.

Friedman *et al.* (2015) further explored the phenotype of HSN1 by quantifying small fibre (intra-epidermal nerve fibre density measurements) and autonomic involvement. The study demonstrated universal epidermal denervation at the distal leg site and scarce autonomic symptoms with only mild objective dysfunction. Variable autonomic involvement has been reported in HSN1 with some studies reporting no involvement (Geraldes *et al.*, 2004; Houlden *et al.*, 2006) and others reporting frequent involvement, consisting mainly of altered sweating (Auer-Grumbach *et al.*, 2003; Davidson *et al.*, 2012; Rotthier *et al.*, 2012).

To date, there have been no studies specifically looking at the gender differences in the phenotype or using quantitative sensory testing (QST) in HSN1 patients to profile the sensory involvement. Also, there have been no studies in HSN1 using MRI determined fat fraction measurements to quantify muscle atrophy.

4.2 Aims

1) In-depth characterisation of the HSN1 phenotype using a variety of assessments to capture the spectrum of clinical features with specific focus on:
    I. Phenotypic differences between males and females
    II. Electrophysiological profile of HSN1
    III. QST profile of HSN1

IV. Correlation of plasma 1-deoxySL levels with clinical phenotype

V. Quantification of muscle atrophy in HSN1 using MRI determined calf muscle fat fraction.

4.3 Methods

4.3.1 Ethics

This study was approved by The National Hospital for Neurology and Neurosurgery Research Ethics Committee (REC reference: 09/H0716/61). Written informed consent was obtained from all subjects prior to enrolment into the study.

4.3.2 Study design and patient selection

This is a prospective longitudinal observational study. HSN1 patients over the age of 18 with genetically confirmed HSN1 due to *SPTLC1* and *SPTLC2* mutations were identified from the two centres providing genetic testing for HSN1: Neurogenetics Laboratory at the National Hospital for Neurology and Neurosurgery and Bristol Genetics Laboratory.

Exclusion criteria:

1) Concomitant neuromuscular disease
2) Significant co-morbidities including medication dependent diabetes
3) Very advanced disease state that precludes travelling
4) Safety related MRI contraindications

Age matched control subjects were enrolled for the MRI part of the study to ensure any changes noted in the patients were disease related rather than MRI/technical related.

4.3.3 Study design

At the baseline visit, demographic and clinical information were collected in a standardised form. The following features were systematically collected: age of onset, age of onset of sensory and motor symptoms (upper and lower limb), first ulcer/painless injury, neuropathic pain and any complications secondary to the neuropathy (e.g. osteomyelitis, amputations). A general medical history, including drug history was taken along with a neurological examination. The following procedures were performed by a single researcher (UK): Charcot-Marie-Tooth Neuropathy Score version 2 (CMTNSv2), neurophysiological studies, quantitative sensory testing, computerised myometry and skin biopsies. The researcher was blinded to the results of baseline assessments when performing follow-up assessments. MRI data was analysed by Dr Matt Evans, MRC Centre for Neuromuscular Diseases,

London.

4.3.4 Assessments

Charcot -Marie-Tooth Neuropathy Score version 2 (CMTNSv2)

Clinical impairment was assessed using the CMTNSv2 (Murphy *et al.*, 2011). CMTNS is a composite score (0-36 points) consisting of patient symptoms, examination findings and neurophysiological assessment. A score of ≤10 is considered to indicate mild impairment, 11-20, moderate impairment and >20 severe impairment (Murphy *et al.*, 2011). The more recent Rasch modified version of the CMTNSv2 (CMTNSv2-R) (Sadjadi *et al.*, 2014) was also used and the results compared with the conventional CMTNSv2.

Neurophysiological studies.

Nerve conduction studies were performed using standard techniques using Nicolet Viasys Select EMG system (Preston and Shapiro, 2005). Hand temperature was maintained above 30°C. Conventional bipolar stimulating electrodes (bar electrodes) and standard surface silver chloride pre-gelled electrodes were used. Sural and radial sensory responses were recorded antidromically. For the ulnar sensory studies, orthodromic recording technique was used. Motor studies were performed for the posterior tibial (recording from abductor hallucis brevis, stimulating at ankle and popliteal fossa), common peroneal (recording from extensor degitorum brevis, stimulating at the ankle, fibular head and above popliteal fossa), median (recording from abductor pollicis brevis, stimulating at wrist and antecubital fossa) and ulnar (recording from adductor digiti minimi, stimulating at wrist, elbow and axilla). In the upper limbs, the distal stimulation distances (distance from recording electrodes to stimulation point) were kept at 6cm. F waves were also recorded for the ulnar and median nerves when the compound muscle action potentials (CMAPs) were ≥1mV. Assessments were performed bilaterally and averaged to give overall sensory nerve action potential (SNAP) and CMAP values per nerve.

Sympathetic skin responses (SSR) were also tested in the hands (palms) and feet (soles). SSR is a somato-sympathetic reflex with spinal, bulbar and suprabulbar components (Vetrugno *et al.*, 2003) and can be used in the assessment of small fibre neuropathies (Themistocleous *et al.*, 2014). Electrical stimulation was used to trigger the response and

the site of the stimulation was tested beforehand to ensure the sensation was normal. Three trials were done on each site, using increasing intensities and random stimulation intervals to avoid habituation. Presence or absence of the response was noted. Amplitudes were not recorded as these have high intra-individual variability (Vetrugno *et al.*, 2003).

Quantitative Sensory Testing (QST)

The German Research Network on Neuropathic Pain (DFNS) protocol was used (Rolke *et al.*, 2006). The protocol included: warm detection threshold (WDT), cold detection threshold (CDT), heat pain threshold (HPT), cold pain threshold (CPT), mechanical detection threshold (MDT), mechanical pain threshold (MPT), mechanical pain sensitivity (MPS), dynamic mechanical allodynia (DMA), wind-up ratio (WUR), vibration detection threshold (VDT) and pressure pain threshold (PPT). To cater for different severities of this length dependent neuropathy, the test sites chosen were the left dorsum of the foot, dorsum of the hand and cheek. In patients with undetectable thresholds in the feet and hands, QST was also performed on the left trunk area (between thoracic T10 and lumbar L3, posterior axillary line).

Thermal testing was performed using TSA 2001-II (MEDOC, Israel) thermal testing machine. Safety cut-off temperatures of 0 and 50ºC were used. Vibration thresholds (VDT) were tested over the medial malleolus (foot), ulnar styloid process (hand), 10th rib- posterior axillary line (trunk) and maxillary process (face). Pressure pain thresholds (PPT) were examined over the following muscle groups: abductor hallucis (foot), thenar eminence (hand), gluteal muscle (trunk) and masseter (face). Pressures greater than 10kg/cm^2 were not applied due to concerns over tissue damage and the inability of the examiner to increase the pressure in a smooth graded manner when exerting pressures above this range.

For the baseline measures, Z-scores were calculated [Z-score= (value of patient-mean value of controls)/standard deviation of controls] (Pfau *et al.*, 2014).

Computerised myometry

Lower limb myometry was performed using HUMAC NORM dynamometer (CSMi, MA, USA). The comprehensive protocol (Morrow *et al.*, 2015) included: knee extension and

flexion, ankle dorsiflexion and plantarflexion and ankle inversion and eversion. Both isometric and isokinetic exercises were used. For each measurement, the maximum torque in Nm was recorded. Isometric testing consisted of four trials, each 3 seconds in duration and separated by 10s intervals. The best trial was selected. For the isokinetic assessments, there was a practice run and a 10s rest period followed by three successive movements through the full range where the highest force obtained was measured. At baseline assessment, the machine was set up for each individual subject and the setting was kept the same for the follow up visit. In cases where the myometry was performed before the MRI, at least a 45 minute gap was left between the two tests to minimise any potential secondary effects of the exercise on the MRI. Right and left measurements were averaged to give an overall value for each test.

Intra-epidermal nerve fibre density (IENFD) measurements

A 3mm diameter skin biopsy punch was taken on the lateral side of the thigh, 20 cm below the anterior superior iliac spine. This site rather than the conventional site of distal leg was chosen in accordance with ethical advice due to concerns over poor healing and floor effects in patients with this length dependent neuropathy. The biopsies were performed under sterile technique using local anaesthesia (2% lidocaine). The specimens were immediately fixed by transferring to 2% paraformaldehyde-lysine-periodate solution for 24 hours. They were then cryoprotected overnight and then stored at -80°C. The processing of the specimens and quantification of the IENFDs were performed in the “Carlo Besta” Neurological Institute, Milan, Italy according to established guidelines (Lauria, 2005). IENFD was expressed as fibres per mm of dermis.

Plasma 1-deoxySL levels

For plasma 1-deoxySL levels, blood samples were taken 1-2 hours after lunch. The plasma samples were analysed at the Institute of Clinical Chemistry, University Hospital, Zurich, Switzerland. 1-deoxySLs (1-deoxySA, 1-deoxySO, 1-deoxymethylSA and 1-deoxymethylSO) levels were measured as already described (Mwinyi *et al.*, 2017). In summary, this involved lipid extraction and hydrolysis followed by liquid chromatography and mass spectroscopy. Both the baseline and follow-up samples were analysed together to eliminate inter-assay variability and were calibrated using internal standards.

Patient based questionnaires

The Neuropathic Pain Symptom Inventory (NPSI) (Bouhassira *et al.*, 2004) and SF-36 (version 2) (Brazier *et al.*, 1992) were used to assess pain and quality of life respectively. Norm based scoring was used for SF36 (Ware *et al.*, 2007). In the SF-36v2 norm-based scoring system, each domain was scored to have the same average (50) and the same standard deviation (10) with lower scores reflecting poorer health status. Group mean scale scores below 47 are considered indicative of impaired functioning within that health domain (Ware *et al.*, 2007).

Lower limb MRI

Participants were examined lying feet-first and supine in a 3T MRI scanner (TIM Trio, Siemens, Erlangen, Germany), using a multi-channel peripheral angiography coil (Siemens 'PA Matrix') and 'spine matrix' coil elements. As part of a wider protocol with a total acquisition time of 40 minutes, the three-point Dixon technique (Glover and Schneider, 1991) was used for fat quantification of the proximal calf muscles. The imaging block encompassed both calves and was centred 130mm distal to the right lateral tibial plateau (Fischmann *et al.*, 2014). Three 3D gradient-echo acquisitions were performed with echo-times (TE1/TE2/TE3)=3.45/4.60/5.75ms, time to repetition (TR)=100ms, flip angle=10º, bandwidth 420Hz/pixel, number of excitations averaged (NEX) =4, 82 x 5mm contiguous slices, 512x240matrix, parallel imaging acceleration factor (iPat) =2. Phase unwrapping was performed using PRELUDE (FSL, FMRIB, Oxford). Images were post-processed offline with a Python programming language pipeline according to Glover and Schneider's algorithm (Glover and Schneider, 1991) assuming a single-peak fat component and separated fat (f) and water (w) images were used to calculate pixel-wise fat fraction maps. After fat (F) and water (W) image decomposition, Fat fraction (FF) was calculated as FF = 100% x F/(F+W).

A single observer (Dr Matt Evans) blinded to diagnosis, manually defined individual muscle-group regions of interest (ROI) on the TE=3.45ms Dixon image using the ITK Snap software. For each participant, a single baseline proximal calf slice was chosen for analysis on each lower limb. The slice was defined separately for each leg on the coronal scout image, as that slice lying 130mm below the lateral tibial plateau. In the two patients with total knee replacement, the slice was chosen visually. For longitudinal data from the same

participant, the slice was selected by the same measurement on the coronal scout image, and then visually verified against the baseline image to maintain longitudinal anatomical consistency. Bilateral ROI were defined for seven lower limb muscles at this level: tibialis anterior (TA), extensor hallucis longus (EHL), Peroneus longus (PL), medial gastrocnemius (MG), lateral gastrocnemius (LG), soleus (SO) and the deep posterior group (DP) (Figure 4.1). The observer defined ROI for baseline and follow up scans from the same participant with direct reference to each image-set to maximise inter-scan reproducibility, whilst blinded to the acquisition in order to prevent bias.

The segmented ROI were transferred to the co-registered fat fraction maps, and visually inspected for placement errors or the presence of gross artefact, and minor adjustments were made, as necessary. For all individual ROIs, custom-written software extracted individual muscle-group ROI mean fat fraction (%) and cross-sectional area (CSA) in mm^2. The total acquisition time per participant per visit was about 40 minutes.

The MRI images were analysed altogether at the end of the study and were randomised prior to analysis. Right and left leg MRI fat fraction values for each muscle were averaged to give an overall mean value per patient. A summary measure ('combined overall fat fraction') was calculated for each participant, representing the combined fat fraction across both lower limbs weighted to cross sectional surface area.

4.3.5 Statistical analysis

SPSS statistics Version 22 (IBM) and GraphPad Prism version 6/7 (GraphPad Software, La Jolla California, USA) were used for statistical analysis. All data were tested for normality by Shapiro Wilk test in conjunction with visual inspection of frequency distribution plots. In order to make it easier to compare different subsets, all cross sectional baseline data are quoted as medians with interquartile ranges (IQR). Mann Whitney test was used for comparison between controls and patients for the plasma 1-deoxySL levels and MRI fat fraction measurements. Linear regression was performed to assess the dependence of CMTNSv2 on gender and disease duration. Spearman Rank correlation analysis was used to assess correlation between plasma 1-deoxySA and 1-deoxySO and other measures used

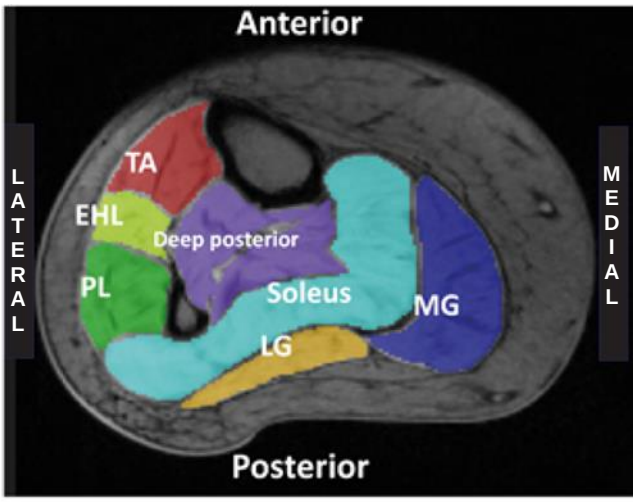

Figure 4.1 Individual muscle regions of interest (ROI)

Whole muscle regions of interest drawn manually on a single right proximal axial calf slice situated 130mm distal to the lateral tibial plateau. TA=tibialis anterior, EHL=extensor hallucis longus/extensor digitorum longus, PL=peroneus longus, Deep posterior=tibialis posterior +flexor hallucis longus + flexor digitorum longus + popliteus, MG=medial gastrocnemius and LG=lateral gastrocnemius

in the study. Correlations with plasma 1-deoxySLs were performed following normalisation of plasma 1-deoxySA and 1-deoxySO by log transformation.

4.4 Results

4.4.1 Patient demographics and clinical profile

Between September 2013 and July 2014, 35 patients were recruited (Figure 4.2). The demographics and summary of clinical baseline profiles are presented in Table 4.1. Individual patient profiles are illustrated in Table 4.2. There was no significant difference in the age at baseline between males and females (Table 4.1). Thirty-one patients had *SPTLC1* (C133W) and 4 had *SPTLC2* mutations (S384F and A182P). Age and sex matched control subjects (50% males, mean age of males=44.4yrs [SD:7.7, range 36-51], mean age of females=41.6yrs [SD:12.6, range 24-57]) were enrolled for the MRI (previously validated (Morrow *et al.*, 2015)) part of the study to ensure any changes noted in the patients were related to disease rather than to MRI/technical factors. The healthy controls (no history of neuromuscular disorders) were recruited from departmental staff and their families.

Loss of sensation (43% of patients) followed by painless foot injury (31% of patients) were the commonest initial symptoms (Figure 4.3). A small subset of patients reported hypersensitivity (9%) and positive sensory symptoms (9%) as initial symptoms. One of the patients, who reported hypersensitivity in the feet as the initial symptom, reported hypersensitivity particularly to heat sensations. Only two patients with the mildest phenotypes (Patient 3.2, male with CMTNSv2=5 and Patient 5.1, female with CMTNSv2=3) had no history of painless ulcers. Complications such as osteomyelitis and amputations appeared to be more frequent in *SPTLC1* males than females (33% in males versus 0% and 6% in males versus 0%, respectively). None of the patients reported any autonomic symptoms. There was a suggestion of diaphragmatic involvement in two of the most severely affected patients (Patient 7.2 with CMTNS of 34 and Patient 8 with CMTNS of 35).

A greater heterogeneity was seen within the *SPTLC1* female subgroup compared to the *SPTLC1* males with a larger variation in age of onset (range 10-50 years versus 12-37 years in males, p=0.003 [Levene's test]) (Figure 4.4A) and disease severity (CMTNSv2 range = 3-34 versus 16-35 in males) (Figure 4.4B). There was also a variation in disease progression within *SPTLC1* females (Figure 4.4C). Some have a similar rate of progression to males whereas others have a later onset and a slower rate of progression (lower

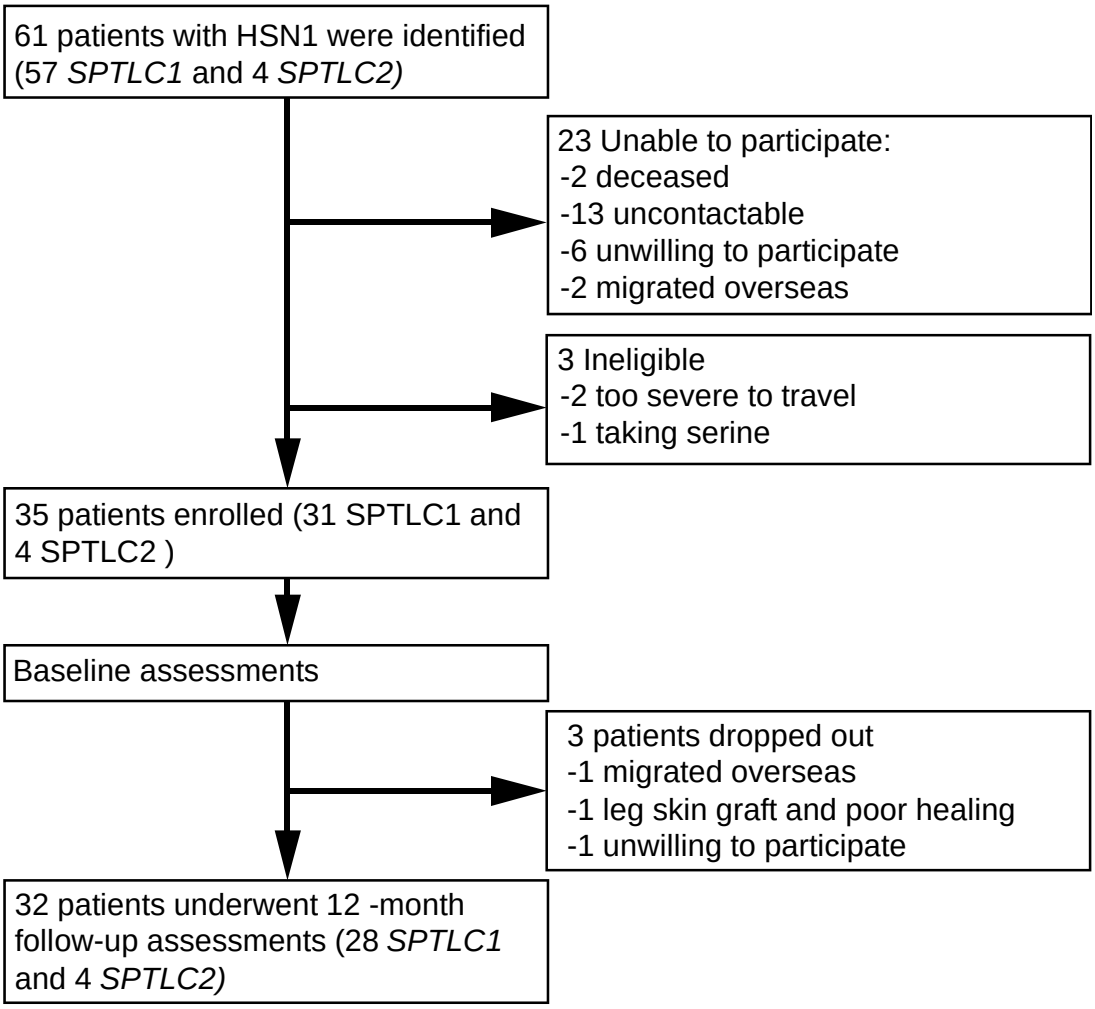

Figure 4.2: Flow chart of patient selection

CMTNSv2 for similar disease durations). There was a significant difference in disease severity as determined by the CMTNSv2 between the *SPTLC1* males and females with males being more severely affected than females (Median CMTNSv2=28, IQR16-35 in males versus median=10, IQR 5-24 in females, p=0.0009) (Figure 4.4B). In patients with *SPTLC1* (C133W) mutations, gender was a significant predictor of CMTNSv2 (R2= 0.38, ß =-0.63, p<0.001) accounting for 40% of the variation seen in CMTNSv2. Duration of disease accounted for 46% of the variation in CMTNSv2 (R2= 0.44, ß=0.68, p<0.001).

A similar heterogeneity in the age of onset was seen in the *SPTLC2* females (range of disease onset=13-47 years) (Figure 4.4A). However, a similar difference in disease severity was not seen between *SPTLC2* males and females (median CMTNSv2=15.0, IQR 6-24 in males versus median=24, IQR 19-29 in females, p=0.66) (Figure 4.4B).There was a suggestion that the *SPTLC2* male subgroup consisting of 2 patients had a milder phenotype than their *SPTLC1* counterparts (median CMTNSv2=13.5, IQR 5-22 in *SPTLC2* males versus median=28, IQR 23-29 in *SPTLC1* males)

There was variation in disease severity within families, both for those with *SPTLC1* and *SPTLC2* mutations, that cannot be attributed to gender alone. For example, in family 5 with *SPTLC1* mutation (Table 4.2), patient 5.1, who is the mother of patient 5.2, has a considerably milder phenotype than her daughter. In family 3 with *SPTLC2* mutation, patient 3.2 has a considerably milder phenotype than other members in the pedigree.

	SPTLC1		*SPTLC2*	
	Males	Females	Males	Females
Patients	18	13	2	2
Mutation	C133W	C133W	S384F	S384F A182P
Mean age, yrs (SD; range)	48.9 (13.1; 23-71)	43.9 (17.3; 20-73)	52.5 (49-56)	66.5 (65-68)
Mean disease duration, yrs (SD; range)	27.2 (14.1; 7-54)	18.8 (15.6; 3-63)	16 (16-16)	36.5 (21-52)
Mean age at onset, yrs (SD; range)	21.7 (7.2; 12-37)	25.1 (14.3; 10-50)	36.5 (33-40)	30.0 (13-47)
Mean age of onset of LL sensory symptoms (SD; range)	22.8 (11.2; 13-42)	25.5 (14.9; 10-50)	36.5 (33-40)	30.0 (13-47)
Mean age of onset of LL motor symptoms (SD; range)	34.4 (11.2; 14-53)	35.3 (17.5; 18-64)	42.0 (N=1)	50.0 (N=1)
Mean duration from disease onset to upper limb sensory (SD; range)	10.6 (7.1;0-23) (N=17)	8.8 (8.1; 1-26) (N=9)	10.0 (N=1)	29.0 (N=1)
Mean age at first ulcer, yrs (SD; range)	28.0 (10.9; 16-63)	28.6 (15.8; 10-65) (N=12)	41 (N=1)	31.5 (13-50)
Mean age at onset of neuropathic pain, yrs (SD; range)	30.6 (12.9; 14-61) (N=16)	30.8 (13.4; 15-52) (N=12)	40.5 (40-41)	54.0 (53-55)
Complication: osteomyelitis	33% (6/18)	0%	50% (1/2)	0%
Complication: amputation	6% (1/18)	0%	50% (1/2)	50%
Median CMTNSv2 (IQR; range)	28 (23-29; 16-35) (N=17)	10 (5-24; 3-24)	13.5 (5-22)	20.0 (15-25)
Median CMTNSv2-R (IQR; range)	33 (28-35; 17-39)	11 (6-28; 4-39)	15.0 (6-24)	24.0 (19-29)

Table 4.1 Baseline characteristics- Patient demographics and clinical profile

LL= Lower limb, N= number of patients reporting the specified symptom when different from that quoted at the top of the table. CMTNSv2= Charcot-Marie-Tooth Neuropathy Score version 2 CMTNSv2-R = CMTNSv2-Rasch modified.

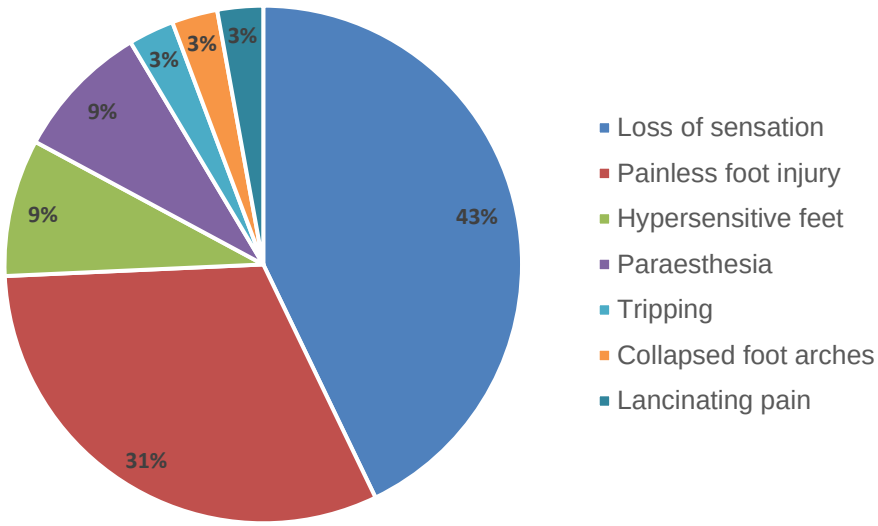

Figure 4.3 First symptoms

Family/ Patient I.D	Gender	Gene *SPTLC1/2*	Age	Onset age	Onset of sensory symptoms LL	Onset of motor symptoms LL	Onset of sensory symptoms UL	Onset of motor symptoms UL	Onset of pain	Age of first ulcer	Complications: osteomyelitis	Complications: amputations	Autonomic symptoms	CMTNS
1	M	1	67	18	18	37	41	45	30	30	Y	Y	N	29
2.1	F	1	47	15	15	20	20	30	28	15	N	N	N	28
2.2	F	1	40	18	18	26	25	30	32	28	N	N	N	27
3.1	F	2 (S384F)	68	47	47	Absent	63	Absent	53	50	N	N	N	15
3.2	M	2 (S384F)	40	40	40	Absent	Absent	Absent	41	None	N	N	N	5
3.3	M	2 (S384F)	49	33	33	42	43	48	40	41	Y	Y	N	23
4.1	F	1	64	45	50	54	62	Absent	50	45	N	N	N	9
4.2	M	1	47	33	37	44	40	43	40	33	N	N	N	24
4.3	M	1	45	20	20	35	34	37	30	24	N	N	N	27
5.1	F	1	55	50	50	Absent	Absent	Absent	52	None	N	N	N	3
5.2	F	1	21	15	16	Absent	Absent	Absent	15	18	N	N	N	8
6.1	F	1	67	49	49	64	50	Absent	49	65	N	N	N	21
6.2	M	1	57	37	42	53	55	55	51	37	Y	N	N	19 (CMTES)
6.3	M	1	50	29	30	29	30	30	35	33	N	N	N	28
6.4	M	1	41	28	28	33	30	34	33	34	N	N	N	29
6.5	M	1	23	16	16	18	19	20	17	16	N	N	N	25

Family/ Patient I.D	Gender	Gene *SPTLC1/2*	Age	Onset age	Onset of sensory symptoms LL	Onset of motor symptoms LL	Onset of sensory symptoms UL	Onset of motor symptoms UL	Onset of pain	Age of first ulcer	Complications: osteomyelitis	Complications: amputations	Autonomic symptoms	CMTNS
6.6	F	1	20	17	17	19	19	Absent	18	19	N	N	N	10
7.1	M	1	71	17	17	49	Absent	57	61	63	N	N	N	29
7.2	M	1	53	18	18	31	35	43	33	21	Y	N	N	34
7.3	M	1	37	12	17	25	23	36	15	23	N	N	N	21
8	M	1	63	18	18	47	37	53	20	20	N	N	N	35
9.1	M	1	68	20	23	48	36	53	20	26	Y	N	N	29
9.2	M	1	51	14	14	14	18	18	14	18	N	N	N	34
9.3	M	1	46	25	25	39	40	41	Absent	25	N	N	N	22
9.4	M	1	43	27	27	Absent	32	Absent	35	35	Y	N	N	16
10	F	1	47	35	35	45	40	42	35	43	N	N	N	19
11	F	2 (A182P)	65	13	13	50	55	55	55	13	N	N	N	25
12.1	F	1	73	10	10	36	36	39	30	10	N	N	N	34
12.2	F	1	30	17	17	Absent	Absent	Absent	20	25	N	N	N	4
12.3	F	1	30	16	16	Absent	29	Absent	20	18	N	N	N	4
13	M	1	27	13	13	24	25	25	22	20	N	N	N	21
14	M	1	44	18	18	30	31	32	33	18	N	N	N	25
15	F	1	46	22	22	Absent	Absent	Absent	30	35	N	N	N	9
16	F	1	30	17	17	18	20	Absent	18	22	N	N	N	13
17	M	1	48	28	29	28	28	30	30	28	Y	N	N	28

Table 4.2 Phenotype within HSN1 families.

CMTNS=Charcot-Marie-Tooth Neuropathy Score, CMTES=CMTNSv2 examination score, LL=lower limb, UL=upper limb

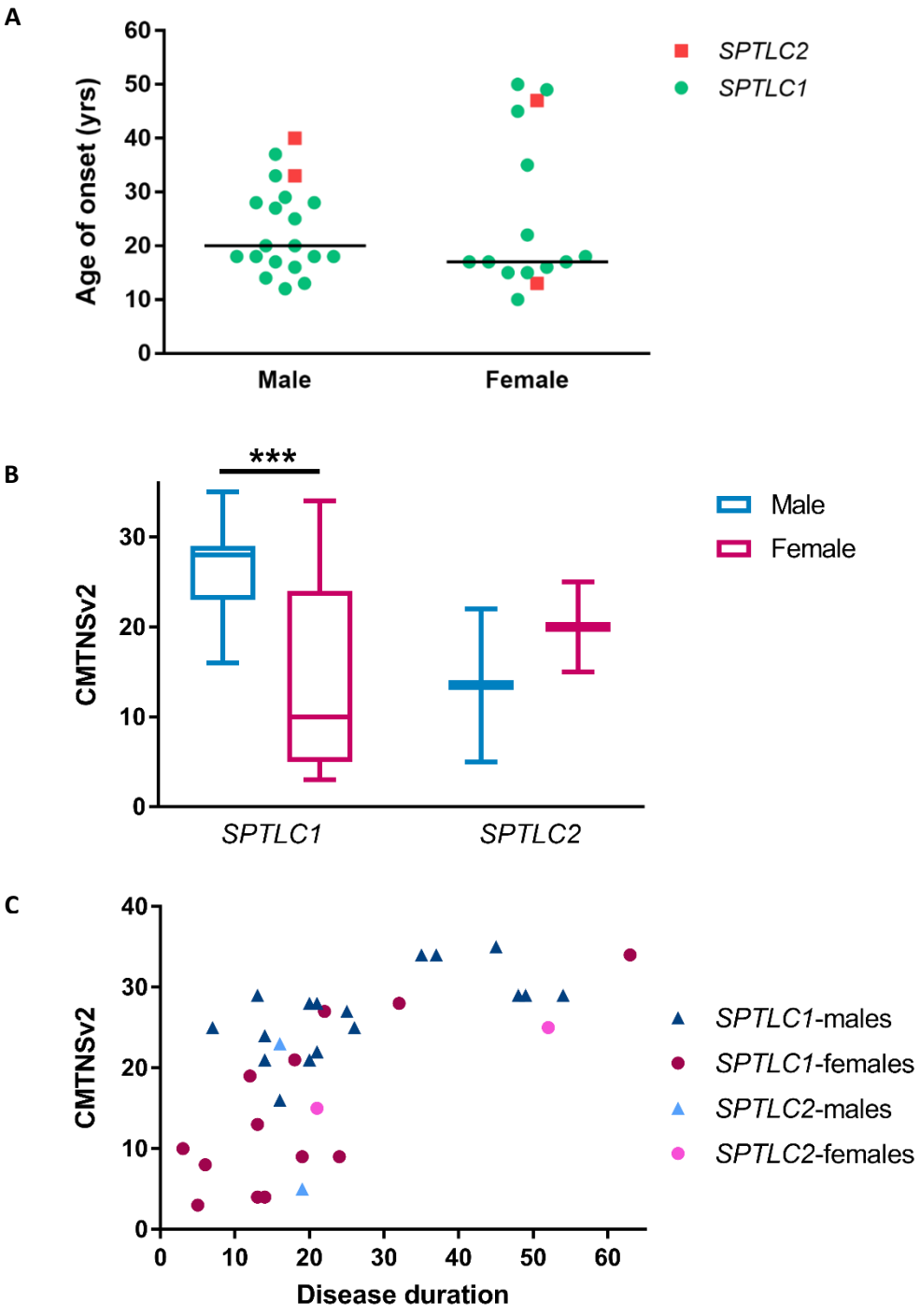

Figure 4.4 Phenotypic variation between male and female HSN1 patients

(A) Variation in age of onset between male and female patients with *SPTLC1* and *SPTLC2* mutations. (B) Tukey Box plot showing the distribution of CMTNSv2 in males and females with *SPTLC1* and *SPTLC2* mutations. There is a significant difference in disease severity between *SPTLC1* males and females (***p=0009, Mann-Whitney test). Box (lower to upper quartile) = Inter quartile range (IQR), horizontal line =median, whiskers= Upper quartile +1.5 IQR/ lower quartile - 1.5IQR. (C) Disease progression in male and female *SPTLC1* and *SPTLC2* patients

4.4.2 Nerve conduction studies

Results of baseline nerve conduction studies are summarised in Table 4.3 and Figures 4.5 and 4.6. One patient declined neurophysiology assessment. 94% of patients (32/34) had absent lower limb sensory responses. Tibial motor responses were absent in 71% (24/34) and common peroneal motor responses were absent in 79% (27/34) of patients. In the upper limbs, 95% (18/19) and 40% (6/15) of the male/female patients had absent sensory responses respectively and 47% (9/19) and 20% (3/15) male/female patients had absent motor responses respectively. There was a large variation in the sensory (radial SNAP IQR = 0.0-40.0µV and ulnar SNAP IQR = 0.0-7.5 µV) and motor responses (median CMAP IQR = 2.8-8.1mV and ulnar CMAP IQR = 2.4-9.6mV) in the upper limbs for female patients (Figure 4.5).

In 24% (8/34) of patients (50% males), 2 of whom had *SPTLC2* mutations, conduction slowing (conduction velocity less than 75% of the lower limit of normal (Preston and Shapiro, 2005)) was seen in the upper limbs which could not be attributed to axonal loss (range of CMAP=1.6-11.3mV) (Figure 4.6A). All these patients had CMTNSv2 greater than 12. 73% of patients with CMTNS>10 and CMAPS>1mV had conduction slowing. 50% of the patients with conduction slowing had dispersion of proximal waveforms (Figure 4.6B). Conduction slowing was also seen in the lower limbs in one patient (conduction velocity of 20m/s in tibial motor study with CMAP of 2.0mV). Terminal latency index (TLI=distal distance/[proximal conduction velocity x distal latency]) (Simovic and Weinberg, 1997) was used to determine if there was distal accentuation of the slowing. TLI of less than 0.34 is considered to indicate distal accentuation of the conduction slowing (Simovic and Weinberg, 1997; American Association of Electrodiagnostic Medicine, 2002). Only one ulnar nerve recording with conduction slowing had TLI less than 0.34.

Proximal (above elbow-axilla) ulnar motor conduction velocities appeared more homogenous compared to the distal forearm segment (Figure 4.6C). Apart from one nerve (3%, 1/35), all ulnar nerves had conduction velocities greater than 38m/s. Minimal F-wave latencies were measured to determine the extent of proximal motor conduction slowing. F-waves result from the antidromic travel of the electrical stimulation signal to the anterior horn, backfiring of some anterior horn cells and orthodromic travel back down the nerve to

Nerve	ALL	Males	Females
Ulnar SNAP, μV (IQR)	0.0 (0.0-1.3)	0.0 (0.0-0.0)	1.0 (0.0-7.5)
Radial SNAP, μV (IQR)	0.0 (0.0-6.5)	0.0 (0.0-0.0)	6.0 (0.0-40.0)
Median CMAP, mV (IQR)	3.4 (0.0-6.9)	0.2 (0.0-3.9)	6.9 (2.8-8.1)
Ulnar CMAP, mV (IQR)	2.0 (0.0-7.5)	0.1 (0.0-2.4)	7.2 ((2.4-9.6)
Posterior Tibial CMAP , mV (IQR)	0.0 (0.0-0.1)	0.0 (0.0-0.0)	0.02 (0.0-0.5)
Common Peroneal CMAP, mV (IQR)	0.0 (0.0-0.0)	0.0 (0.0-0.0)	0.0 (0.0-1.0)
Presence of Sympathetic skin response in the feet (%)	53	39	71
Presence of sympathetic skin response in the hands (%)	85	83	87

Table 4.3 Baseline electrophysiology

Electrophysiological data are presented as median (IQR). Measurements from the right and left were averaged to give overall value for each nerve.

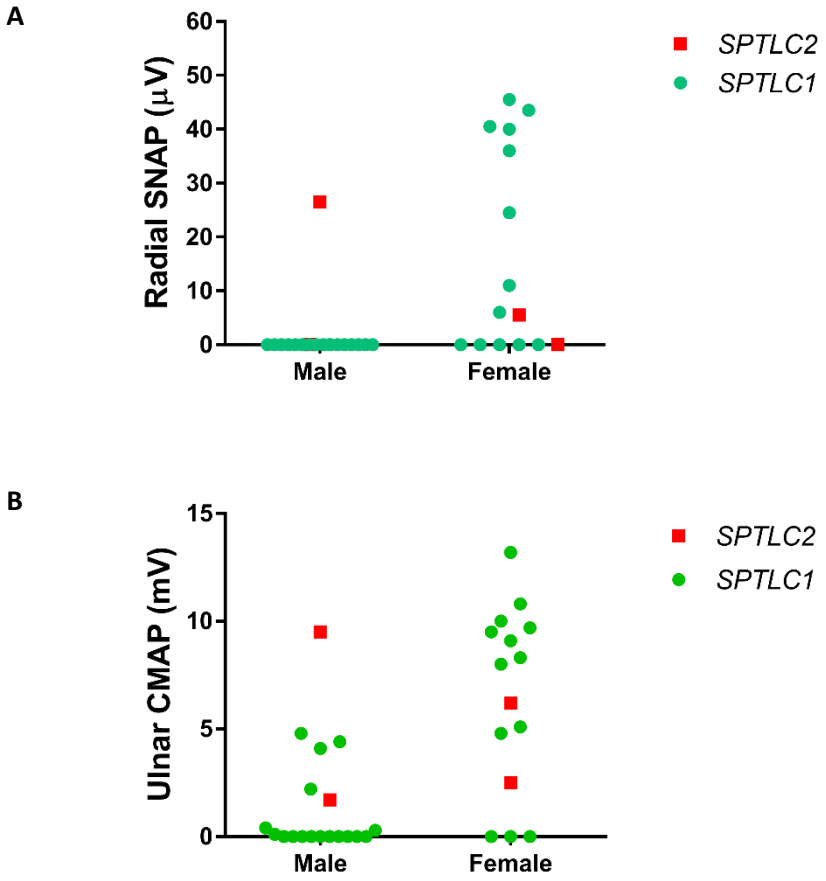

Figure 4.5 Distribution of upper limb sensory (A) and motor responses (B) in males and females

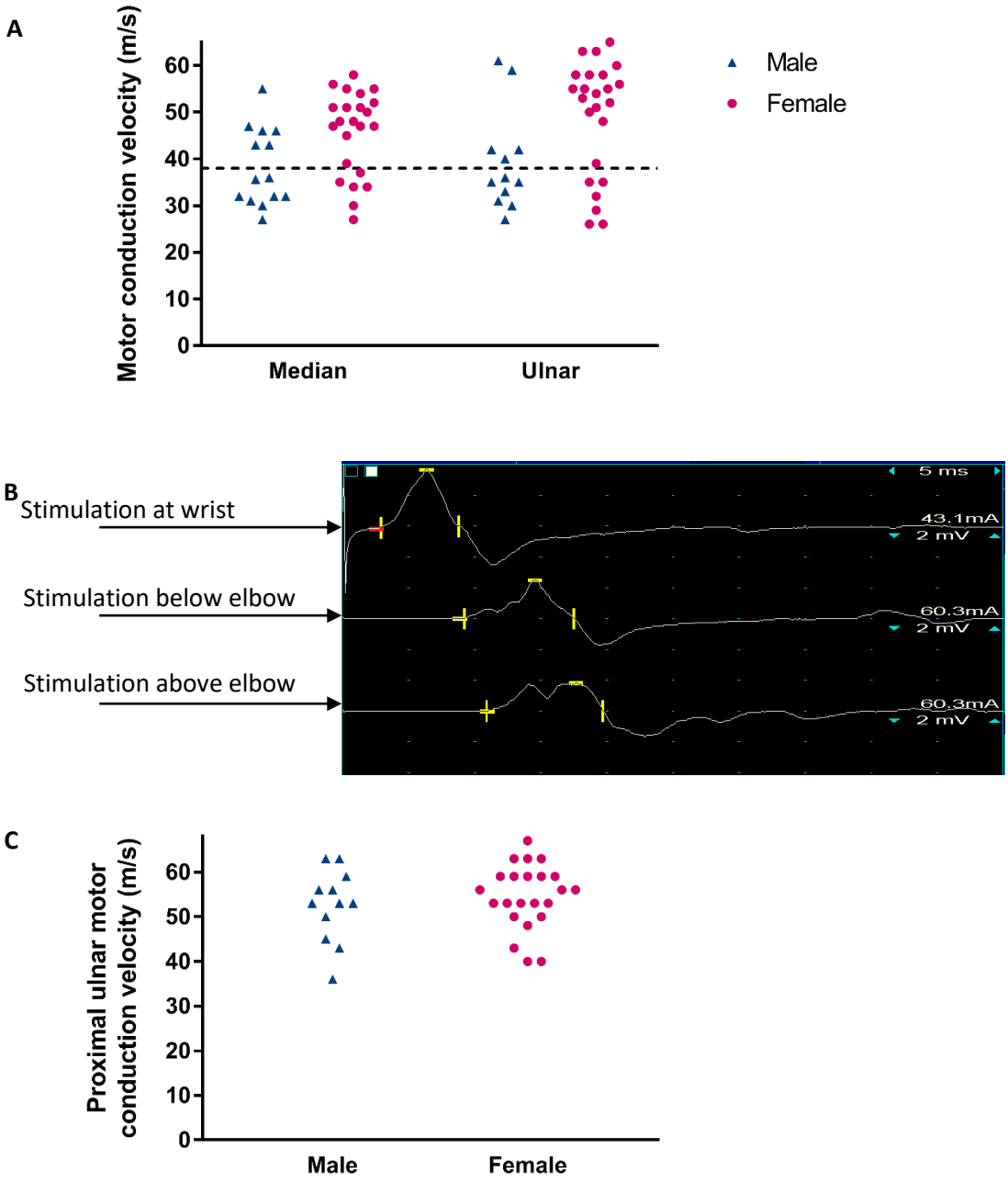

Figure 4.6 Upper limb motor conduction slowing

(A) Distribution of median and ulnar motor conduction velocities (right and left hand values shown separately) in the forearm segment (wrist-below elbow) when CMAP amplitudes are >1mV. Conduction velocities less than 38m/s (dashed line, <75% lower limit of normal conduction velocity) were considered to demonstrate conduction slowing. **(B)** Representative nerve conduction study recording of ulnar motor study showing progressive dispersion of proximal waveforms when recording from adductor digiti minimi (distal CMAP=3.9mV). **(C)** Distribution of proximal (above elbow-axilla) ulnar motor conduction velocities (right and left hand values shown separately).

the muscle (Preston and Shapiro, 2005). The mean median F-wave latency was 37.8ms (SD=3.2ms) (normal ≤31ms) and mean ulnar F- wave latency was 38.4ms (SD=3.2ms) (normal ≤32ms). If there was fixed slowing at 38m/s throughout the length of the nerve, the predicted F-wave latencies would be greater than 50ms. This and the proximal ulnar studies suggest that the conduction slowing is not homogenous throughout the course of the nerve.

The sympathetic skin responses were better preserved than the sensory and motor responses (Table 4.3) with 53% and 85% of patients having responses in the feet and hands, respectively.

4.4.3 Quantitative Sensory Testing (QST)

Results of the QST are shown in Table 4.4 and Figures 4.7 and 4.8. QST showed a clear length dependent pattern of sensory loss (Figure 4.7). In QST testing on the feet, 90-95% of male patients and 60-93% of female patients had unrecordable (beyond the detection limit) responses for each QST parameter apart from VDT. On the hands, 55-95% of male patients and 20-53% of female patients had unrecordable responses for each QST component apart from VDT. All patients had detectable responses when tested on the face and trunk.

QST profiles when tested on the hands, face and trunk are shown in Figure 4.8. These profiles illustrate early small (WDT and CDT) and large fibre (MDT and VDT) involvement in HSN1. On the face and trunk, none of the QST parameters had abnormal median Z scores apart from PPT when tested on the face (median Z score of 2.60 in males and 3.45 in females indicating gain of function). Individually, in the more severely affected patients, abnormal QST parameters were seen on the face and trunk regions, trunk more so than face.

All the QST parameters showed predominantly a loss of function (negative Z-scores); however, PPT was reduced (gain of function) in a subset of patients when tested on the hand, trunk and face. The distribution of the abnormal PPTs (face>trunk>hands) suggests

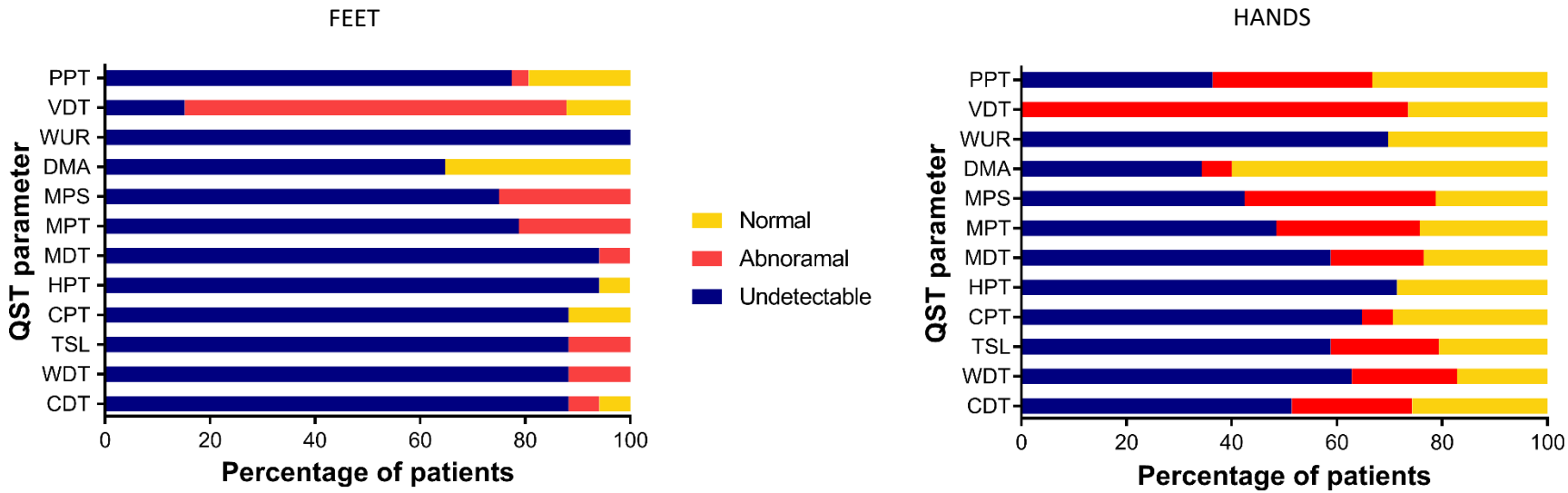

Figure 4.7 Quantitative Sensory Testing (QST) in feet and hands

Most of the responses are undetectable/beyond recordable range (feet>hands). CDT=Cold Detection Threshold, WDT=Warm Detection Threshold, TSL=Thermal Sensory Limen, CPT=Cold Pain Threshold, HPT=Heat Pain Threshold, MDT=Mechanical Detection Threshold, MPT=Mechanical Pain Threshold, MPS=Mechanical Pain Sensitivity, DMA=Dynamic Mechanical Allodynia, WUR= Wind-Up Ratio, VDT=Vibration Detection Threshold and PPT=Pressure Pain Threshold.

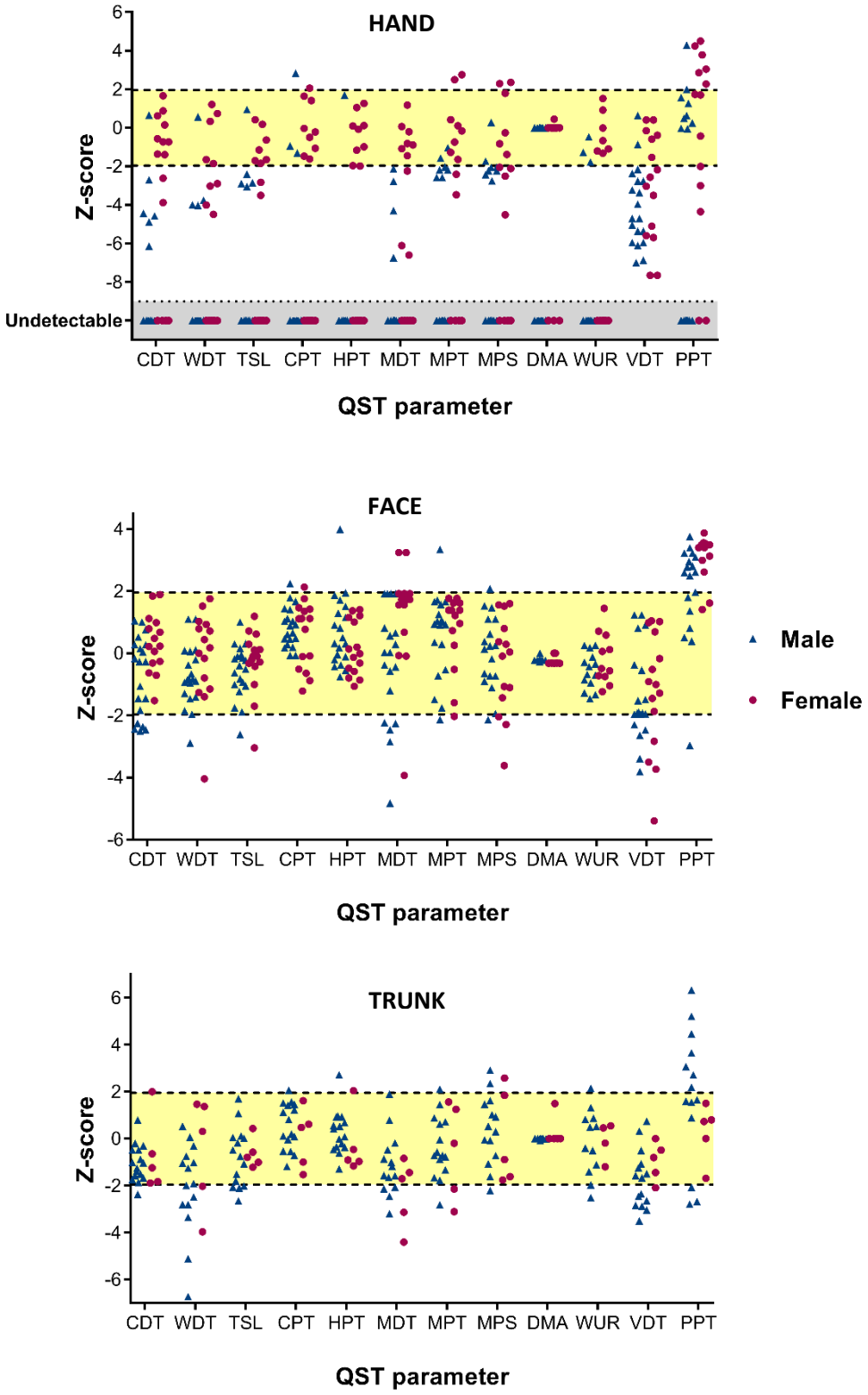

Figure 4.8 Somatosensory profiles of the hand, face and trunk

Somatosensory profiles determined with QST in the hands, face and trunk. Data are expressed as Z-scores with standard deviations. Yellow area indicates normal range (95% confidence interval). Z values below “0” indicate loss of function and above “0” indicate gain of function.

	FOOT			HAND			TRUNK					FACE		
	ALL	Male	Female	ALL	Male	Female	ALL	Male		Female		ALL	Male	Female
	Median (IQR)	Median (IQR)	Median (IQR)	Median (IQR)	Median (IQR)	Median (IQR)	Median (IQR)	N	Median (IQR)	N	Median (IQR)	Median (IQR)	Median (IQR)	Median (IQR)
CDT	UR (UR to UR)	UR (UR to UR)	UR (UR to -8.38)	UR (UR to -1.36)	UR (UR to -5.20)	-1.36 (UR-0.15)	-1.24 (-1.71 to -0.49)	16	-1.15 (-1.65 to -0.49)	5	-1.24 (-1.86 to 0.68)	0.04 (-1.45 to 0.68)	-0.27 (-2.15 to 0.27)	0.23 (-0.31 to 0.99)
WDT	UR (UR to UR)	UR (UR to UR)	UR (UR to UR)	UR (UR to -3.76)	UR (UR to UR)	-4.01 (UR to -1.65)	-1.59 (-2.81 to -0.03)	15	-1.91 (-2.81 to -0.75)	5	0.31 (-3 to 1.42)	-0.66 (-1.26 to 0.44)	-0.85 (-1.38 to -0.01)	0.18 (-1.15 to 0.93)
TSL	UR (UR to UR)	UR (UR to UR)	UR (-8.12 to UR)	UR (UR to -2.26)	UR (UR to -3.04)	-2.83 (UR to –1.14)	-0.78 (-1.73 to 0.04)	15	-0.76 (-2.02 to 0.05)	5	-0.8 (-1.11 to -0.07)	-0.23 (-1 to 0.12)	-0.46 (-1.04 to -0.06)	-0.09 (-0.42 to 0.29)
CPT	UR (UR to UR)	UR (UR to UR)	UR (UR to -7.97)	UR (UR to -1.3)	UR (UR to UR)	-1.62 (UR to -0.21)	0.48 (-0.54 to 1.45)	16	0.51 (-0.41 to 1.46)	5	0.48 (-1.26 to 1.12)	0.88 (0.17 to 1.4)	0.77 (0.32 to 1.33)	1.11 (-0.51 to 1.42)
HPT	UR (UR to UR)	UR (UR to UR)	UR (UR to -1.96)	UR (UR to UR)	-1.69 (UR to 0.1)	-1.96 (UR to 0.1)	-0.02 (-0.54 to 0.81)	16	0.25 (-0.36 to 0.87)	5	-0.91 (-1.07 to 0.80)	0.2 (-0.38 to 1.21)	0.41 (-0.19 to 1.46)	-0.01 (-0.58 to 1.15)
MDT	UR (UR to UR)	UR (UR to UR)	UR (UR to UR)	UR (UR to -2.21)	UR (UR to UR)	-2.24 (UR to -0.81)	-1.56 (-2.13 to -0.84)	14	-1.37 (-2.08 to -0.41)	5	-1.70 (-3.77 to -1.14)	0.65 (-0.51 to 1.92)	0.02 (-2.23 to 0.82)	1.73 (0.50 to 1.92)
MPT	UR (UR to UR)	UR (UR to UR)	UR (UR to -3.52)	-3.47 (UR to -1.42)	UR (UR to -2.18)	-1.46 (UR to 0.19)	-0.64 (-1.58 to 0.84)	15	-0.71 (-1.33 to 0.71)	5	-0.20 (-2.63 to 1.41)	1.01 (-0.13 to 1.60)	0.94 (-0.53 to 1.57)	1.31 (0.07 to 1.62)
MPS	UR (UR to UR)	UR (UR-to UR)	UR (UR to -2.45)	-2.63 (UR to -1.81)	UR (UR to -2.23)	-2.08 (UR to 0.26)	0.30 (-1.07 to 1.62)	14	0.12 (-0.81 to 1.51)	5	-0.89 (-1.69 to 2.21)	0.09 (-1.09 to 1.03)	0.19 (-0.77 to 1.1)	-0.03 (-1.58 to 0.98)

	FOOT			HAND			TRUNK					FACE		
	ALL	Male	Female	ALL	Male	Female	ALL	Male		Female		ALL	Male	Female
	Median (IQR)	Median (IQR)	Median (IQR)	Median (IQR)	Median (IQR)	Median (IQR)	Median (IQR)	N	Median (IQR)	N	Median (IQR)	Median (IQR)	Median (IQR)	Median (IQR)
DMA	UR (UR to 0)	UR (UR to UR)	0 (0 to 0)	0 (UR to 0)	0 (UR to 0)	0 (-2.5 to 0)	0 (0 to 0)	14	0 (0 to 0)	5	0 (0 to 0.75)	0 (-0.23 to 0)	0 (-0.23 to 0)	0 (-0.31 to 0)
WUR	UR (UR to UR)	UR (UR to UR)	UR (UR to UR)	UR (UR to -1.30)	UR (UR to UR)	-5.66 (UR to -0.50)	0.14 (-1.18 to 0.75)	12	0.05 (-1.34 to 0.86)	4	0.14 (-0.95 to 0.53)	-0.49 (-0.31 to 0.15)	-0.56 (-1.03 to -0.05)	-0.49 (-0.75 to 0.59)
VDT	-3.56 (-4.83 to -2.73)	-4.12 (-6.06 to -3.12)	-3.02 (-3.81 to -2.16)	-3.43 (-5.62 to -2.00)	-4.70 (-6.00 to -2.76)	-2.56 (-5.59 to -0.38)	-1.53 (-2.6 to -0.58)	15	--1.67 (-2.84 to -1.07)	5	-0.8 0 (-1.77 to -0.25)	-1.51 (-2.34 to 0.05)	-1.92 (-2.3 to -0.37)	-1.00 (-2.83-0.69)
PPT	UR (UR to -0.34)	UR (UR to UR)	UR (UR to 0.73)	-0.04 (UR to 1.94)	UR (UR to 0.64)	1.74 (-2.5 to 3.42)	1.55 (0 to 3.07)	14	1.92 (0.15 to 3.85)	5	0.73 (-0.85 to 1.15)	2.97 (1.84 to 3.47)	2.60 (1.22 to 3.12)	3.45 (2.90 to 3.52)

Table 4.4 Baseline Quantitative sensory testing

QST data are expressed as Z scores (Inter-quartile range, IQR) where values above 2 represent abnormal gain of function and values below -2 represent abnormal loss of function. In the trunk, N= number of patients tested. UR=unrecordable, CDT=Cold Detection Threshold, WDT=Warm Detection Threshold, TSL=Thermal Sensory Limen, CPT=Cold Pain Threshold, HPT=Heat Pain Threshold, MDT=Mechanical Detection Threshold, MPT=Mechanical Pain Threshold, MPS=Mechanical Pain Sensitivity, DMA=Dynamic Mechanical Allodynia, WUR=Wind-Up Ratio, VDT=Vibration Detection Threshold and PPT=Pressure Pain Threshold

there might be early hypersensitivity followed by decreased sensitivity as the neuropathy progresses. A small number of patients were hyperalgesic (static mechanical hyperalgesia as measured by MPS) with increased MPS in the hands (6% [2/35]) and trunk (15% [3/20]). The range of CMTNSv2 of patients with increased MPS in the hands and trunk (CMTNSv2 range of 3-6 and 21-27respectively) also suggests that hyperalgesia precedes sensory loss in HSN1. None of the patients had allodynia (determined by DMA) or increased temporal summation of pain (determined by WUR).

4.4.4 Computerised myometry

Results of the baseline computerised myometry are summarised in Table 4.5. Ankle dorsiflexion was the worst affected with zero power detected in 68% (13/19) of male patients and 20% (3/15) of female patients with isometric testing. For ankle plantar flexion, zero power was detected in 37% (7/20) of males and 7% (1/15) of females with isometric testing. Ankle inversion and eversion were better preserved when compared to ankle dorsiflexion (for both, zero power was detected in 42% (8/19) of males and 13% (2/15) of females with isometric testing at 0°). Lower quartile values were similar or lower in males for knee extension and flexion, suggesting there is more prominent proximal involvement in males.

4.4.5 Intra-epidermal Nerve Fibre Density (IENFD)

IENFD assessment was not performed on one female patient as she was on warfarin. The upper thigh skin biopsies were completely denervated in 60% (12/20) of male patients and 21% (3/14) of female patients (Figure 4.9 and Table 4.6). All the patients had severely reduced IENFD measurements (median 0.1 (IQR=0.0-1.8) compared to published normative data (mean=21.1, SD=10.4, 5th centile=5.2 fibres/mm) (McArthur *et al.*, 1998) apart from the two patients with the mildest phenotype (one *SPTLC2* male with CMTNSv2 of 5 and one *SPTLC1* female with CMTNSv2 of 3) who had normal fibre densities of 5.5 and 5.2 fibres/mm respectively.

Movement	Type	Angle	ALL	Males	Females
Ankle Dorsiflexion	Isometric	10°	0 (0-18)	0 (0-3)	10 (0-23)
	Isometric	30°	1 (0-17)	0 (0-5)	4(0-23)
	Isokinetic	60°/s	3 (0-17)	0 (0-10)	14 (1-18)
Ankle Plantarflexion	Isometric	10°	7 (0-25)	2 (0-18)	20 (1-27)
	Isokinetic	60°/s	6 (0-18)	3 (0-14)	12 (1-30)
Ankle Inversion	Isometric	0°	5 (0-14)	4 (0-14)	5 (2-14)
	Isokinetic	60°/s	4 (0-9)	3 (0-9)	5 (2-19)
Ankle Eversion	Isometric	0°	4 (0-12)	2 (0-9)	6 (1-14)
	Isometric	20°	7 (01-14)	6 (0-13)	8 (2-18)
	Isokinetic	60°/s	4 (0-10)	4 (0-10)	4 (1-12)
Knee Extension	Isometric	45°	100 (63-137)	132 (66-152)	86 (63-100)
		90°	92 (68-159)	129 (48-163)	76 (71-110)
	Isokinetic	60°/s	79 (48-112)	93 (39-121)	76 (48-95)
		120°/s	52 (26-72)	53 (26-96)	51 (26-57)
Knee Flexion	Isometric	45°	51 (32-71)	64 (31-76)	45 (32-55)
		90°	38 (16-50)	43 (13-50)	33 (22-40)
	Isokinetic	60°/s	38 (20-55)	41 (20-55)	36 (19-48)
		120°/s	22 (7-35)	22 (9-40)	21 (6-29)

Table 4.5 Baseline myometry

Data are median (IQR) in units of Nm. Isometric values are the peak torque at the fixed angle listed. Isokinetic values are the peak torque at the fixed speed listed.

4.4.6 Plasma 1-deoxySL levels

Plasma 1-deoxySL levels were elevated in all the patients compared to laboratory controls (p=0.01-0.003) (Table 4.7). There were no significant differences in plasma 1-deoxySA (p=0.17), 1-deoxySO (p=0.11), 1-deoxymethylSA (p=0.91) or 1-deoxymethylSO (p=0.34) levels between males and females (Table 4.6 and Figure 4.10). 1-deoxySA and 1-deoxySO levels correlated moderately with CMTNSv2, ulnar CMAP, IENFD and overall calf muscle fat fraction (Table 4.7). There was no correlation between NPSI scores and plasma 1-deoxySL levels. Plasma 1-deoxymethylSA and 1-deoxymethylSO did not correlate with CMTNSv2 (r_s=0.341, p=0.52 and r_s=0.180, p=0.31 respectively). In males, plasma 1-deoxySA level correlated moderately (r_s=0.549, p=0.01) and 1-deoxySO level correlated strongly (r_s=0.712, p=0.0006) with CMTNSv2. However, in females, there was no correlation between either plasma 1-deoxySA (r_s= 0.274, p=0.32) or 1-deoxySO levels (r_s= 0.273, p=0.33) and CMTNSv2. There was one major outlier (*SPTLC1* female who had CMTNSv2 of 34 and a history of diet controlled type II diabetes) with plasma 1-deoxySA level of 2.88µM (Figure 4.10A).

4.4.7 Neuropathic pain and the Neuropathic Pain Symptom Inventory (NPSI)

All but one patient (Patient 9.3, CMTNSv2=22) had the typical lancinating pain (Table 4.2). In most cases the pain occurred at random with the interval between attacks ranging from a day to months. They often only lasted seconds but tended to occur in clusters which can last the whole day. In one of the patients, the pain only occurred with infections and in another, it was triggered by stress.

54% (19/35) of the patients took regular analgesia. Pregabalin was the most commonly used neuropathic pain medication (58%, 11/19). 11% (4/35) of patients used paracetamol/ co-dydramol combinations as needed during the attacks of pain. 14% (5/35) of patients required combination therapy with 9% (3/35) taking opiate based medications such as buprenorphine and fentanyl.

	ALL Median (IQR)	Males Median (IQR)	Females Median (IQR)
Intra-Epidermal Nerve Fibre Density (IENFD)			
IENFD (fibres/mm)	0.1 (0.0-1.8)	0.0 (0.0-1.3)	1.2 (0.1-2.7)
Neuropathic Pain Symptom Inventory (NPSI)			
Total NPSI score (0-100)	25.0 (14.0-37.0)	25.5 (14.5-39.5)	22.0 (13.0-36.0)
Paroxysmal sub-score (0-10)	5.0 (3.0-8.0)	6.3 (3.3-8.4)	5.0 (2.0-7.0)
SF-36v2			
Physical component score	37.5 (33.5-49.8)	34.8 (31.9-40.2)	51.4 (36.6-55.9)
Mental component score	53.6 (44.8-59.3)	51.4 (43.9-58.6)	54.3 (46.4-59.9)
Physical functioning	34.6 (26.9-53.7)	30.8 (54.0-41.3)	44.2 (32.7-57.5)
Role-physical	47.1 (34.1-57.2)	39.2 (32.5-51.5)	57.2 (45.9-57.2)
Bodily pain	42.2 (38.2-50.7)	43.0 (8.1)	45.0 (12.3)

Table 4.6: Baseline measures for intra-epidermal nerve fibre density, Neuropathic Pain Symptom Inventory and SF-36v2.

Measures are given as medians (IQR). SF-36v2=Short Form Health Survey version 2 (1998).

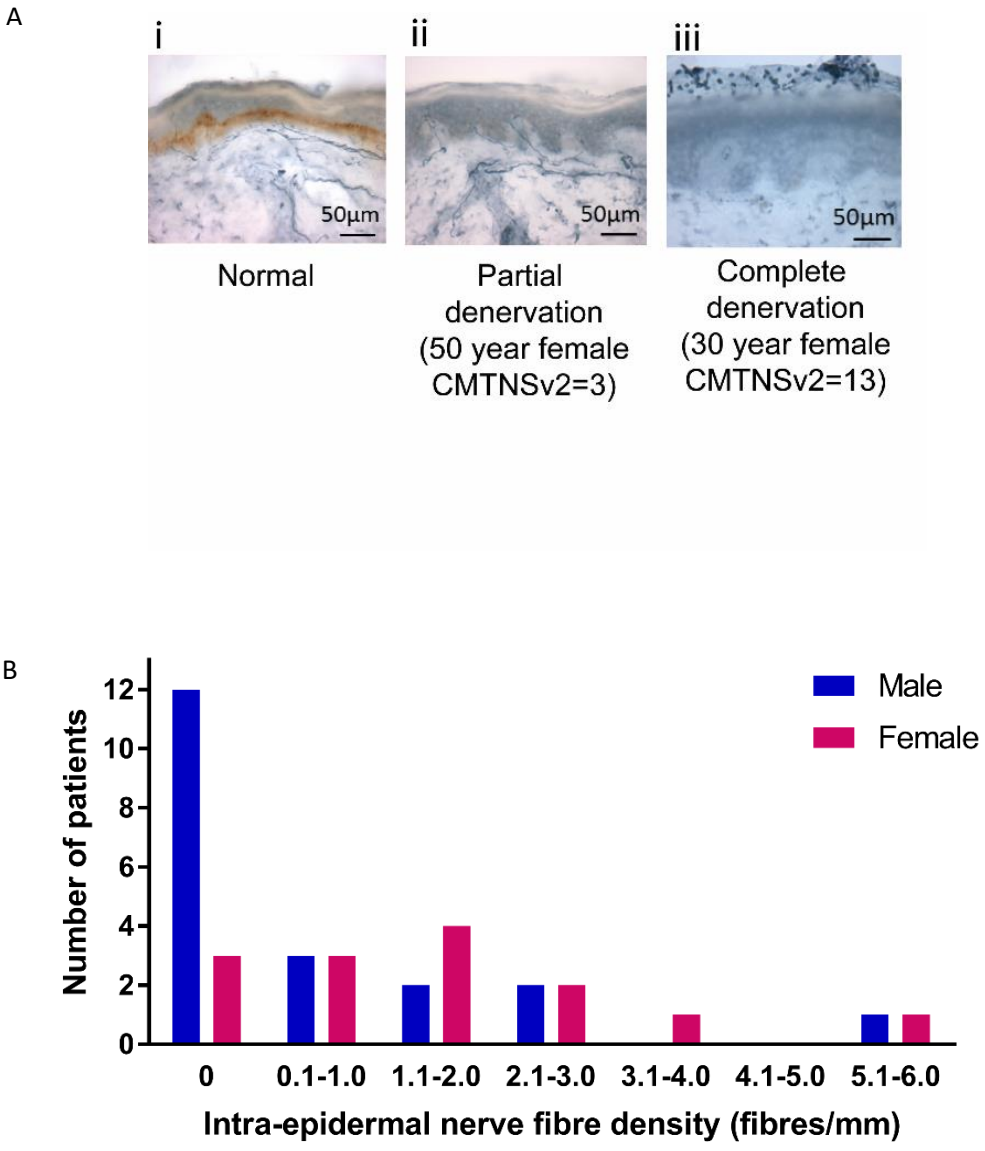

Figure 4.9 Baseline Intra-epidermal nerve fibre density (IENFD)

(A) Proximal thigh skin innervation (nerve fibres immunostained with anti-PDP905) in a control subject (i), 50 year old female (ii) and 30 year old female (iii) HSN1 (C133W) patients illustrating the complete denervation that is seen in moderately affected patients and the heterogeneity in *SPTLC1* females. (B) Distribution of IENFDs in males and females

	Lab control Median (IQR)	ALL Median (IQR)	Males Median (IQR)	Females Median (IQR)
1-deoxysphinganine (µM)	0.07 (0.06-0.08)	0.79 (0.49-1.03)	0.94 (0.50-1.23)	0.54 (0.32-0.99)
1-deoxysphingosine (µM)	0.25 (0.23-0.27)	1.50 (0.96-2.40)	1.68 (1.18-2.48)	1.13 (0.80-2.18)
1-deoxymethylsphinganine (µM)	0 (0-0)	0.02 (0.02-0.03)	0.03 (0.02-0.03)	0.02 (0.02-0.03)
1-deoxymethylsphingosine (µM)	0.03 (0.03-0.03)	0.06 (0.05-0.07)	0.06 (0.05-0.07)	0.06 (0.05-0.06)
Correlation of plasma 1-deoxysphingolipids with other assessments				
Assessment	Log 1-deoxysphinanine		Log 1-deoxysphingosine	
	r_s	p	r_s	p
CMTNSv2	0.490	0.003	0.544	0.0009
Radial SNAP	-0.333	0.06	-0.375	0.03
Ulnar CMAP	-0.453	0.007	-0.500	0.003
Hand WDT	0.330	0.06	0.407	0.02
Hand MDT	0.242	0.17	0.290	0.10
Ankle dorsiflexion	-0.357	0.04	-0.373	0.04
Intra-epidermal nerve fibre density (IENFD)	-0.487	0.004	-0.500	0.003
Neuropathic Pain Symptom Inventory (NPSI)	-0.013	0.94	-0.084	0.64
Overall calf muscle fat fraction	0.609	0.0002	0.645	<0.0001

Table 4.7: Plasma 1-deoxysphingolipid levels and their correlation with other assessments

1-deoxySL levels are given as median (IQR). CMTNSv2=Charcot-Marie-Tooth Neuropathy Score version 2, SNAP=Sensory Nerve Action Potential, CMAP=Compound Muscle Action Potential, WDT=Warm Detection Threshold, MDT=Mechanical Detection Threshold.

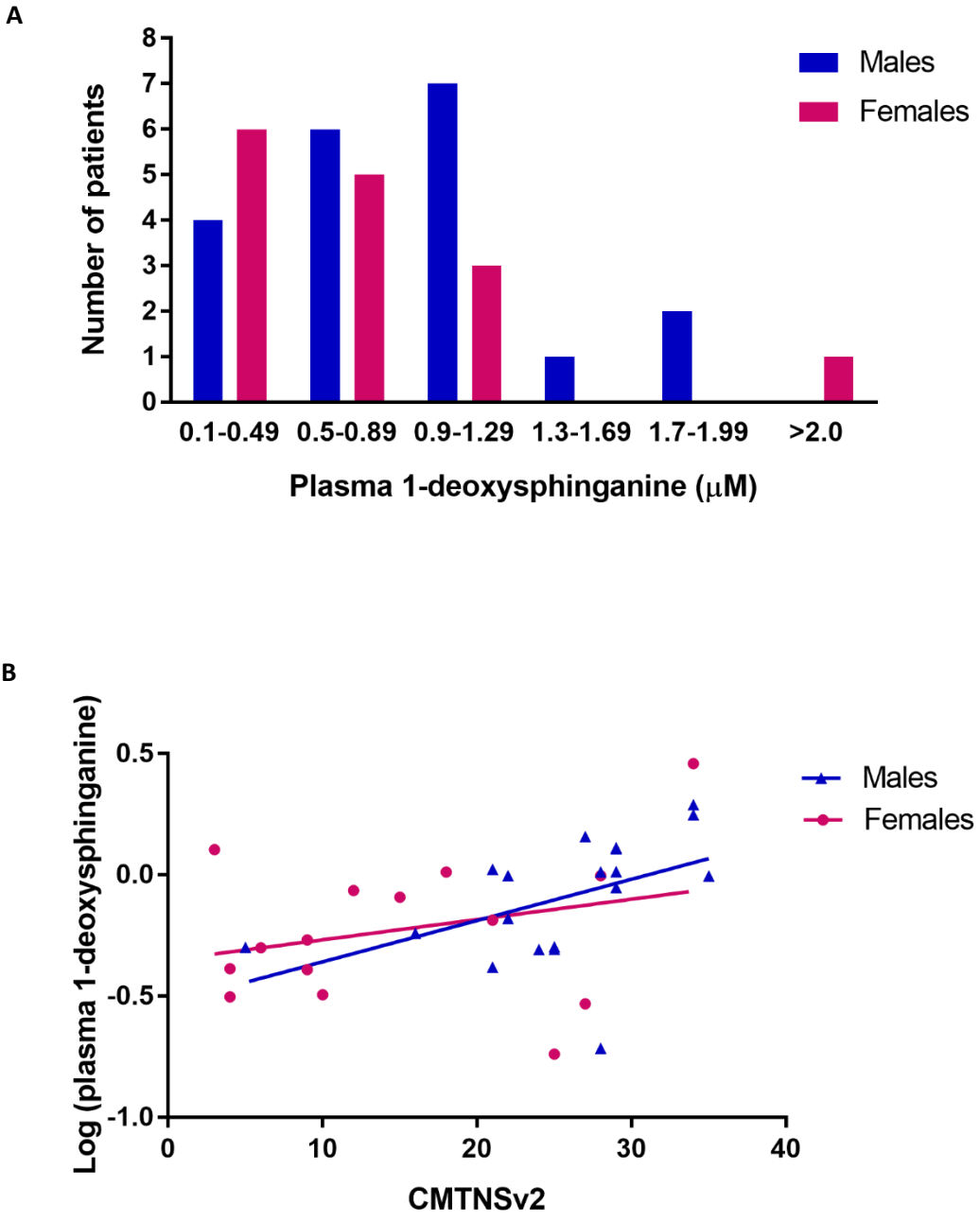

Figure 4.10 Plasma 1-deoxysphinganine levels in males and females and its correlation with CMTNSv2

A) Distribution of plasma 1-deoxySA levels in males and females. B) Correlation between CMTNSv2 and plasma 1-deoxySA in males and females.

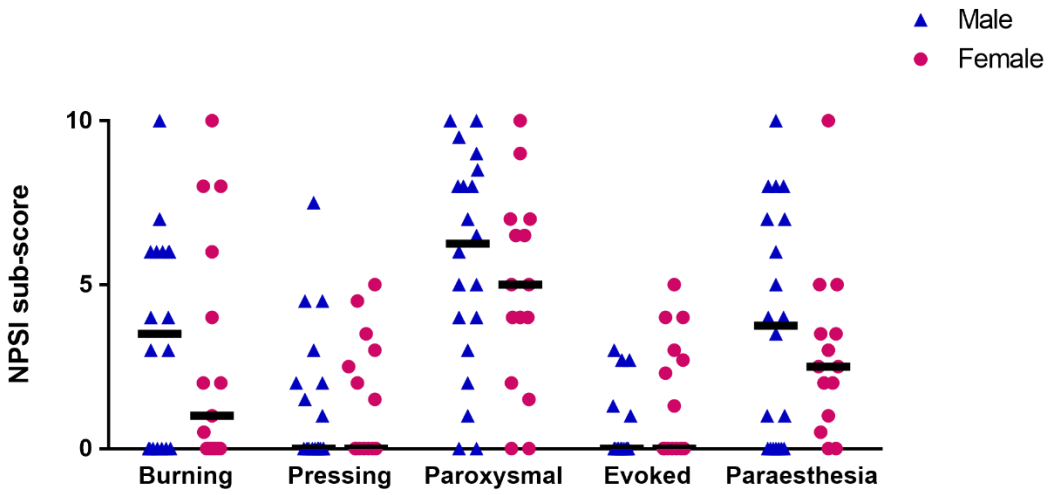

Figure 4.11 Neuropathic Pain Symptom Inventory (NPSI) profiles in males and females.

The neuropathic pain profile was similar between males and females (Figure 4.11) and there was no significant difference in the total NPSI score between the sexes (median 25.5 [IQR 14.5-39.5] in males versus median 22.0 [13.0-36.0] in females, p=0.65) (Table 4.6). The most common description of the pain was paroxysmal followed by painful paraesthesia.

4.4.8 SF-36v2

In the SF-36v2 for the whole cohort, physical domains (Physical component score, physical functioning and Bodily pain) had lower scores compared to age matched control subjects indicating impaired function in these domains (Table 4.6). In the physical domains, males consistently reported greater impairment with significant difference between males and females seen for Physical component (p=0.007), Physical function (p=0.01) and Role physical (p=0.01). In both sexes, lowest scores were seen for Physical functioning.

4.4.9 MRI determined calf-level intramuscular fat accumulation

For the MRI assessments, 34 patients with HSN and 11 controls were analysed at baseline and the results are summarised in Table 4.8 and representative images for a male control subject and HSN1 male patients with different disease severities are shown in Figure 4.12A. The combined overall muscle and each individual muscle mean fat fractions were significantly higher in HSN patients than healthy controls for the whole cohort (p values range = <0.001) and when subdivided into gender (p values range = 0.001 - <0.001 in males, 0.02- <0.001 in females). The muscles were differentially affected with lateral gastrocnemius showing the highest fat fraction in HSN1 patients.

The greatest difference in fat fraction between HSN1 males and females was seen for the medial gastrocnemius (median of 33.9% versus 3.0% respectively). Males (both HSN1 patients and controls) generally had higher fat fraction values than their female counterparts. HSN1 males had 10-91% higher fat fraction values than their female counterparts. Despite low fat fraction values in control subjects (0.8%-1.6%), control males had 11-45% higher fat fraction values than control females. The only exception is the fat

fraction values for lateral gastrocnemius whereby females had higher fat fraction values than males with fat fraction values of 49.7%/1.3% in female patients/controls versus 32.4%/1.2% in male patients/controls. Overall calf muscle fat fraction correlated strongly with CMTNSv2 in both males (r_s=0.850, p<0.0001) and females (r_s=0.859, p<0.0001) (Figure 4.12B). Once there is motor involvement, intramuscular fat accumulation progresses similarly between males and females (Figure 4.12C).

	ALL HSN1 group Median FF% (IQR)	ALL Control group Median FF% (IQR)	p value	HSN1 MALES Median FF% (IQR)	Control MALES Median FF% (IQR)	p value	HSN1 FEMALES Median FF% (IQR)	Control FEMALES Median FF% (IQR)	p value
Tibialis Anterior	13.1 (2.9-41.9)	0.8 (0.7-1.8)	<0.0001	14.3 (4.9-41.1)	0.9 (0.7-2.1)	0.0002	12.0 (1.4-44.3)	0.8 (0.7-1.3)	0.02
Extensor Hallucis Longus	16.8 (3.3-57.3)	1.3 (1.0-1.9)	<0.0001	17.8 (10.6-59.8)	1.9 (1.1-3.4)	0.0009	16.0 (1.6-54.7)	1.2 (1.0-1.4)	0.0003
Peroneus Longus	26.2 (4.8-64.3)	1.6 (1.2-2.2)	<0.0001	37.0 (18.3-69.3)	2.2 (1.7-4.4)	0.0002	9.9 (2.6-60.5)	1.2 (1.1-1.7)	0.0004
Soleus	24.4 (4.8-63.2)	1.6 (1.1-2.6)	<0.0001	28.0 (11.4-75.6)	2.0 (1.4-6.9)	0.001	5.7 (2.0-56.6)	1.3 (1.1-1.8)	0.003
Lateral Gastrocnemius	37.1 (4.5-79.8)	1.2 (1.2-2.4)	<0.0001	32.4 (11.5-78.1)	1.2 (1.1-4.0)	0.0006	49.7 (2.0-82.5)	1.3 (1.1-2.1)	0.005
Medial Gastrocnemius	33.9 (4.2-71.8)	1.4 (1.0-2.8)	<0.0001	34.3 (14.0-79.1)	1.7 (1.3-6.4)	0.0003	3.0 (1.3-52.5)	1.0 (0.9-1.7)	0.02
Deep Posterior group	13.6 (2.5-52.4)	1.3 (1.1-1.6)	<0.0001	15.7 (9.2-54.0)	1.6 (1.1-3.1)	0.0002	1.8 (1.6-36.3)	1.2 (1.1-1.3)	0.0005
Combined overall	22.3 (5.9-59.6)	1.3 (1.1-1.9)	<0.0001	22.7 (9.6-66.6)	1.5 (1.3-5.3)	0.0002	14.7 (1.6-58.7)	1.1 (1.1-1.5)	0.001

Table 4.8 Baseline measures for proximal calf muscle fat fraction

Measures are given as medians (IQR). FF%=Fat Fraction percentage

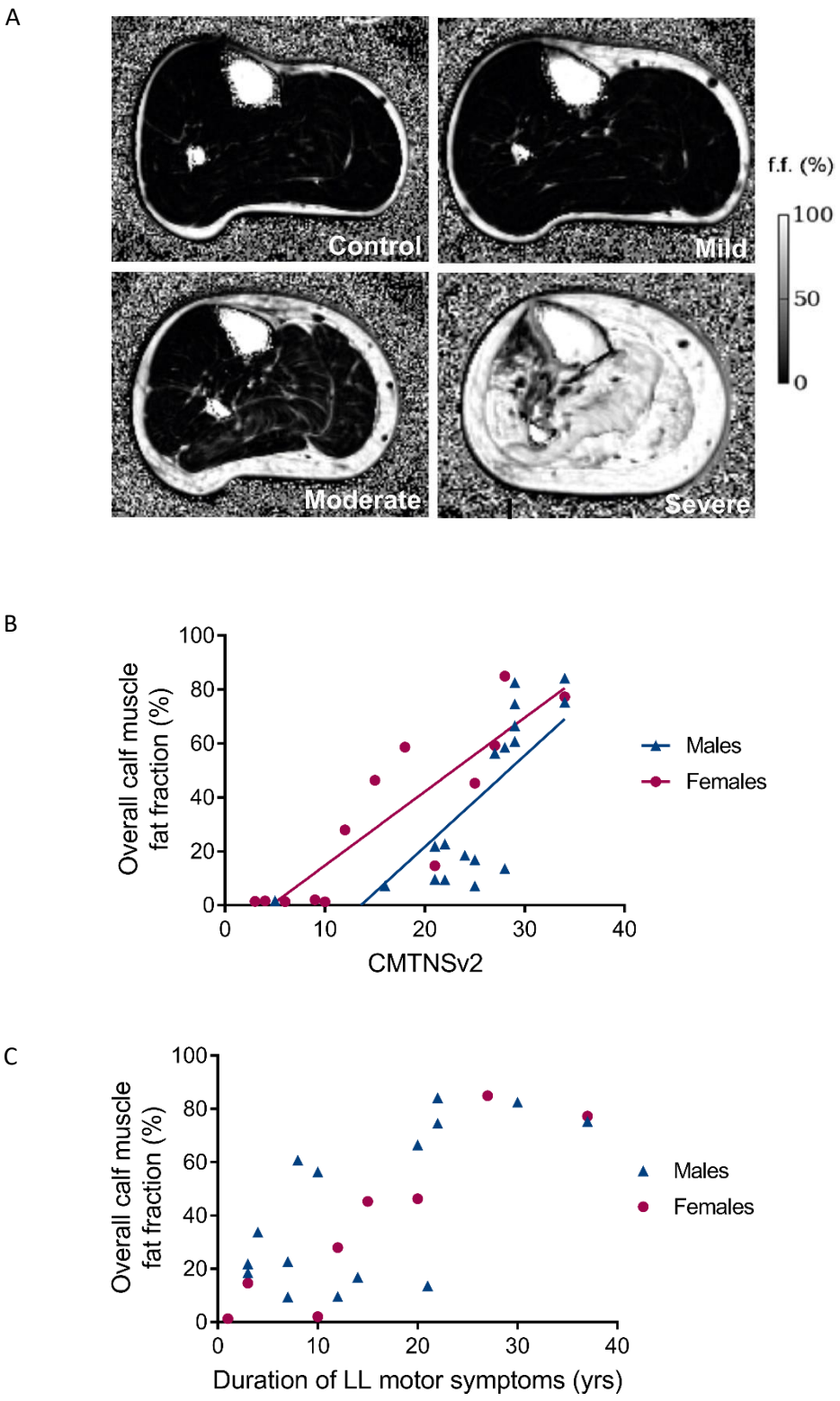

Figure 4.12 Baseline MRI calf-level overall fat fraction characteristics

(A) Fat fraction map of a control male subject, mildly affected (CMTNSv2=5), moderately affected (CMTNSv2=16) and severely affected (CMTNSv2=34) HSN1 male patients. **(B)** Correlation between overall calf muscle fat fraction and CMTNSv2. **(C)** Change in overall calf-level muscle fat fraction with duration of lower limb (LL) motor symptoms in males.

4.5 Discussion

This study highlights the large phenotypical heterogeneity in *SPTLC1* HSN1 patients in the UK harbouring the same mutation (C133W). We have previously shown that this mutation has a common UK founder (Houlden *et al.*, 2006). This heterogeneity was largely due to the differences in severity seen between males and females where males were generally more severely affected.

Within the *SPTLC1* female sub-group, there appeared to be phenotypic spectrum. On the one end, there are females that have age of onset and disease progression similar to males and on the other end there are females with late onset and much slower rate of progression. A difference between the genders was also noted by Fridman *et al.* (2015) in a cohort of *SPTLC1* patients (20 patients with C133Y and 3 patients with C133W mutations) where males had a significantly earlier age of onset compared to females and like in this study, greater variation in the phenotype was seen within the female group. Such clear gender difference in clinical severity has not been reported in autosomal CMT. Two studies looking at gender-dependent differences in a cohort of CMT patients (Wozniak *et al.*, 2015), one focused on CMT1A (Colomban *et al.*, 2014), have not found significant differences in CMTNS between the sexes.

Phenotypical heterogeneity was also seen within families for the same sex. A similar finding was noted by Houlden *et al.* (2006) and suggests that acquired as well as genetic factors could contribute to the clinical variability. The highest plasma 1-deoxySL levels were seen in the most severely affected female patient (CMTNSv2=34) who also had Type II diabetes (diet controlled). Plasma1-deoxySLs have been shown to be elevated in patients with Type II diabetes and metabolic syndrome and are predictive biomarkers of type II diabetes (Othman *et al.*, 2015c). It is possible that the elevated 1-deoxySL levels could have contributed to the increased severity of the neuropathy in this patient.

The *SPTLC2* male patients in this study had a milder phenotype compared to their *SPTLC1* counterparts. However, as this is based on only 2 patients, caution is needed when interpreting this.

Dissociated sensory loss where nociception and temperature sensation (small fibre involvement) are affected early and more severely compared to vibration and proprioception (large fibre involvement) is well documented in HSN1 (Auer-Grumbach *et al.*, 2003; Houlden *et al.*, 2006) . QST profiles in this study demonstrate that there is also early large fibre involvement with deficits in mechanical perception mirroring that of temperature perception. We noted, as has been previously reported (Rotthier *et al.*, 2012), an initial period of hypersensitivity to noxious pressure (lowered PPTs) and hyperalgesia (increased MPS). Interestingly, in the mouse model of HSN1 (over-expression of mutant SPTLC1-C133W), where the mice have a milder phenotype than that seen in HSN1 patients, the 8-10 months old mice exhibited thermal hyperalgesia. At this stage, there was no difference in mechanical detection thresholds determined using Von Frey.

In this study, upper thigh skin biopsies were completely denervated in 60% of male patients and 21% of female patients. This is in contrast to the cross-sectional study by Fridman *et al* (2015) where none of their HSN1 patients were completely denervated at the thigh level. In that study, the CMTES of the six patients who had skin biopsies ranged from 7-23. In our study, the patients' CMTES ranged from 10-27. The disparity in the findings between the two studies could be due to differences in sample sizes or the techniques used for analysis.

Despite the name, prominent motor involvement was seen in both male and female HSN1 patients. The same computerised myometry protocol that was used in this study was used to assess plantarflexion and dorsiflexion strengths in CMT1A patients with ages similar to that of our cohort of HSN1 patients (Morrow *et al.*, 2015). On comparing the two groups, the HSN1 patients had much greater motor impairment: mean isometric plantarflexion was 26.0Nm (SD=14.3) and dorsiflexion was 10.8Nm (SD=7.5) in CMT1A patients versus median isometric plantarflexion of 7Nm (IQR=0-25) and dorsiflexion of 0Nm (IQR=0-18) in HSN1 patients. Two of the most severely affected (CMTNSv2 of 34 and 35) male patients from two different families with *SPTCL1* mutation had diaphragmatic weakness. Diaphragmatic weakness was also noted by Houlden *et al.* (2006) in two family members with the weakness becoming evident in their early 50's.

MRI determined fat fraction quantification revealed differential involvement of lower leg muscles. At the proximal calf level examined in the study, highest fat fraction values were

seen in the lateral gastrocnemius and considerably lower fraction values were seen in the tibialis anterior and the deep posterior group. Some of this could possibly relate to the different distribution of motor end plates in the different muscles. For example, the motor end points are concentrated in the upper third of the gastrocnemius muscle (Van Campenhout and Molenaers, 2011) whereas they are located along the entire length of the tibialis anterior muscle (Aquilonius *et al.*, 1984) which will lead to differential involvement in a length dependent neuropathy like HSN1. This however cannot explain the gender difference in the involvement of the lateral gastrocnemius whereby females have a higher fat fraction. Different activation patterns of the lateral gastrocnemius between the sexes could contribute to the gender difference in fat fractions of this muscle (Flaxman *et al.*, 2014).

In this study, we found motor conduction slowing in the intermediate range (25-45m/s,(Fridman and Reilly, 2015)) in the majority of patients who were moderately affected. Motor conduction slowing has been described previously in HSN1 (Houlden *et al.*, 2006; Auer-Grumbach, 2008) however there is little evidence of demyelination on nerve biopsies (Houlden *et al.*, 2006). Teased nerve fibre examination of myelinated fibres in the sural nerve from one HSN1 patient with conduction velocities in the demyelinating range showed only two fibres possibly undergoing primary (segmental) demyelination.(Houlden *et al.*, 2006). It is possible, that the conduction slowing could reflect abnormalities of ion channels and resultant alterations in nerve excitability or changes in Schwann cell-axon interactions rather than be a marker of myelin dysfunction (Pareyson *et al.*, 2006). The lack of motor conduction slowing in the initial stages with emergence only in moderately affected patients suggests there might be a threshold effect, possibly related to the accumulation of 1-deoxySLs. Nodal architecture in terms of constituent ion channels and ion channel dysfunction can affect motor conduction (Hashimoto *et al.*, 2015; Uncini and Vallat, 2018). The plasma membrane consists of distinct cholesterol and sphingolipid enriched regions known as lipid rafts. Ion channels from almost every class have been reported to associate with lipid rafts (Dart, 2010). Alteration in the lipid rafts as a result of disruption in the de-novo sphingolipid biosynthetic pathway could result in ion channel dysfunction and motor conduction slowing. Also, recent studies have suggested that oestrogen could provide a

neuroprotective effect by playing a role in lipid homeostatic balance of lipid rafts (Marin and Diaz, 2018) and hence could explain some of the gender differences in clinical severity.

None of the patients in this study reported any autonomic symptoms. Sympathetic skin responses were also better preserved than sensory and motor responses in the upper and lower limbs. Autonomic involvement has occasionally been noted in HSN1 due to *SPTLC1/2* mutations however these have only been mild, subjective symptoms (Geraldes *et al.*, 2004; Houlden *et al.*, 2006; Auer-Grumbach, 2008) and possibly related to severity (Houlden *et al.*, 2006; Fridman *et al.*, 2015).

All but one patient in this study reported the characteristic lancinating pain. The frequency of the pain was highly variable between patients and there was no significant difference in the NPSI scores between males and females. The variability may partially reflect the limitation of the NPSI in assessing episodic pain. Similar pain profile has already been well documented in HSN1 secondary to *SPTLC1/2* mutations (Houlden *et al.*, 2006; Auer-Grumbach, 2008). Pain is frequently reported by patients with CMT (Carter *et al.*, 1998; Jeong *et al.*, 2013) however a study evaluating the nature of pain in CMT1A patients found that the pain is likely to be multifactorial and that only a small percentage of patients had features of neuropathic pain (Laurà *et al.*, 2014). Similar neuropathic pain has not been reported in other hereditary sensory neuropathies.

Plasma 1-deoxySL levels were raised in all patients compared to laboratory controls with no significant difference in the levels between males and females. Therefore, the significant difference in clinical severity, determined with CMTNSv2, between males and females cannot be attributed to differences in plasma 1-deoxySL levels. MRI determined calf muscle fat fraction correlated strongest with plasma 1-deoxySA followed by CMTNSv2 and IENFD. In males, 1-deoxySA levels appeared to correlate with CMTNSv2 but this was not the case in females, suggesting that possible additional factors are modulating the neuropathy in females. Plasma 1-deoxySLs have been reported to be elevated in patients with diabetes (1-deoxySO of 0.19 ±0.15µM [SD] versus 1.50 µM [IQR=0.96-2.40] in HSN1 patients in this study) (Bertea *et al.*, 2010). However, elevated plasma 1-deoxySL levels in patients with diabetic distal sensorimotor polyneuropathy did not correlate with clinical severity and there was no significant difference in the deoxysphingolipid profiles in sural nerve biopsies

between patients with diabetic distal sensorimotor polyneuropathy and CIDP (Dohrn *et al.*, 2015). Similarly elevated plasma 1- deoxySL levels are also seen in patients with metabolic syndrome and in patients with Glycogen Storage Disease Type I, a condition not known to be associated with a peripheral neuropathy (Othman *et al.*, 2012; Hornemann *et al.*, 2018). The plasma 1-deoxySLs evaluated in this study are therefore not the main components determining the extent of deoxysphingolipid induced neurotoxicity.

In summary, there was marked heterogeneity in the phenotype mainly due to differences between the sexes with males generally more severely affected than females. In females, there was a phenotypic spectrum ranging from a similar phenotype as seen in males to one of late onset with slower disease progression. The differences between the sexes cannot be accounted for by differences in plasma 1-deoxySL levels. Although HSN1 is sensory predominant, there is significant motor involvement.

5. HSN1 Natural history study: Identifying responsive outcome measures

5.1 Introduction

A study by Garafalo *et al.* (2011) has raised the possibility of a clinical trial of L-serine in the UK HSN1 population. They demonstrated a mild treatment effect with L-serine oral supplementation using transgenic mice expressing mutant *SPTLC1*. In the same study, a 10 week pilot trial of L-serine oral supplementation in HSN1 patients showed that L-serine was well tolerated by the patients and led to a reduction in plasma 1-deoxySL levels. Oral supplementation with L-serine for one year in a HSN1 patient with *SPTLC2* mutation (R183W) produced no side effects and led to persistent reduction in plasma 1-deoxySL levels throughout the treatment course (Auranen *et al.*, 2017).

A small (18 patients) randomised placebo-controlled trial in HSN1 which has just been published has shown that oral L-serine treatment potentially slows disease progression although there were too few patients in the study to be definitive (Fridman *et al.*, 2019). After one year, the L-serine treatment group showed a mild improvement in CMTNSv2 relative to the placebo group (-1.5units, 95% CI-2.8 to -0.1, p=0.03). However, the primary outcome, the proportion of patients progressing more than one point on the CMTNSv2 at one year, did not differ between the L-serine and placebo groups. A larger definitive efficacy trial of serine in the HSN1 population is warranted, however the major barrier is the lack of natural history data and responsive outcome measures.

Outcome measures were traditionally classified into measures of impairment, disability and handicap (Molenaar *et al.*, 1995). Since the modification of this classification by the World Health Organisation, the terms now used are body functions and structures, activities and participation, respectively (World Health Organisation, 2013) . An outcome measure should be simple, valid, reliable and responsive to change over time and should represent one of the WHO outcome domains listed above (Merkies and Lauria, 2006). Responsiveness has been defined as the ability of an outcome variable to accurately detect change when it has occurred (Roach, 2006).

Many challenges confront the development of outcome measures in inherited neuropathies. The disease progression is slow. Axonal loss in peripheral nerves is unlikely to be reversed therefore treatments are expected to slow or halt progression. This limits the magnitude of difference that can be observed between treatment and placebo groups of a therapeutic clinical trial. Inherited neuropathies are rare which limits recruitment. International trials may be needed which has implications for outcome measure reliability as a result of inter-site variability. Responsiveness is often where outcome measures in inherited neuropathies are weakest due to their slowly progressive nature.

Version one of the CMT Neuropathy Score (CMTNS) was published in 2005 (Shy *et al.*, 2005). It is a composite measure based on patient's symptoms, neurologic examination and neurophysiological testing. The CMTNS was used in multicentre international trials of ascorbic acid in Charcot-Marie-Tooth disease 1A (CMT1A) (Micallef *et al.*, 2009; Verhamme *et al.*, 2009; Pareyson *et al.*, 2011; Lewis *et al.*, 2013). These studies highlight the difficulties in conducting clinical trials due to the lack of responsive outcome measures in slowly progressive inherited neuropathies. In addition to failing to detect any benefit with ascorbic acid, the studies demonstrated no significant changes in their primary outcome measures over 2 years, and negligible to small responsiveness of the secondary outcome measures. These difficulties are compounded in a rarer condition like HSN1 where limited patient numbers and marked phenotypic heterogeneity require the outcome measures to be even more responsive.

Following on from these trials, the CMTNS was modified (CMTNS version 2, CMTNSv2) to reduce floor and ceiling effects and standardise patient assessments and thus increase the sensitivity of the scale to change (Murphy *et al.*, 2011). The revised CMTNSv2 still has poor discriminatory power in the moderately affected CMT patients which is the most common group (Mannil *et al.*, 2014). Rasch analysis of CMTNSv2 demonstrated that it tended to clump impairment scores from many patients in the middle range of severity (Sadjadi *et al.*, 2014). The Rasch modified version of CMTNSv2 (CMTNS-R), where the responses are weighted, was created in order to make the scoring more linear thereby making it easier to detect smaller differences in clinical change (Sadjadi *et al.*, 2014).

Several secondary outcome measures have been validated in CMT1A patients. These include quantitative motor strength assessment using dynamometers, 10 minute timed walk, 9-hole peg test, work stimulation tasks, hand function/dexterity tests and Overall Neuropathy Limitations Scale (Solari *et al.*, 2008; Reilly *et al.*, 2010). Some of these secondary outcome measures; the 10minute walk test, nine hole peg test, Overall neuropathy limitations scale and quantitative motor strength assessment (distal maximal voluntary isometric contraction), have been assessed longitudinally over a two year period in a clinical trial setting (Pareyson *et al.*, 2011). However, changes from baseline to 24 months were negligible in both treatment and placebo groups for all these measures. Mannil *et al.* (2014) combined CMTNS with six secondary outcome measures (9 hole peg test, 10 minute timed walk, distal arm and leg maximal voluntary isometric contraction, Overall Neuropathy Limitations Scale and pain and fatigue visual analogue scale). They found the combination of five components from the CMTNS (Compound Muscle Action Potential, motor symptoms legs, motor symptoms arms, leg strength and sensory symptoms) and three of the secondary outcome measures (10 minute walk test, 9 hole peg test and foot dorsal flexion dynamometry) had the strongest power to discriminate between different severities.

In children, the CMT Paediatric Scale (CMTPedS) has been developed and used (Burns *et al.*, 2012). This validated scale predominantly assess functional disability and has demonstrated responsiveness to change over 2 years in children with different CMT types. The CMT Functional Outcome Measure (CMT-FOM) for adults has recently been developed (Eichinger *et al.*, 2018) and is modelled on CMTPedS. CMT-FOM assesses strength, upper limb function (functional dexterity test, 9-hole peg test), lower limb function (10m walk/run, stair climb and sit to stand), balance and mobility (timed up and go, 6min walk test). This has however not been tested longitudinally.

Morrow *et al.* (2015) demonstrated that MRI quantified intramuscular fat accumulation at the calf level was a responsive outcome measure in CMT1A and correlated with strength and disease severity (determined with CMTNS). The responsiveness also greatly exceeded that of the CMTNSv2. A recent study has shown that plasma neurofilament light chain concentrations are significantly raised in patients with CMT, including HSN1 (*SPTLC1*) and correlated with disease severity (Sandelius *et al.*, 2018). However, in a small subset of CMT

patients where the levels were measured longitudinally, there was no significant change over one year.

In HSN1, the natural history study by Fridman *et al.* (2015) evaluated autonomic function longitudinally in six patients and reported no significant change in the scores after 1 year. Cross-sectionally, the study also looked at the feasibility of using the CMTES (subset of the CMTNS without the electrophysiological assessment), intra-epidermal nerve fibre density assessments in distal leg and thigh and composite nerve conduction studies. Due to floor and ceiling effects, only intra-epidermal nerve fibre density assessments at the thigh was suggested as a potential measure of disease severity in HSN1.

It is unlikely that a single outcome measure will be sufficient to measure disease progression in all patients because of the variability between patients (often pure sensory neuropathy early in the disease and severe motor and sensory neuropathy in late disease). Hence, a variety of assessment methods to cover the spectrum of deficits noted in this condition were used in this natural history study.

5.2 Aim

To identify responsive markers of disease progression over one year that can be used in a therapeutic clinical trial in HSN1 patients.

5.3 Methods

Description of patient selection (Figure 4.2) and assessments used in the study are described in the Methods section of Chapter 4.

5.3.1 Statistical analysis

SPSS statistics Version 22 (IBM) and GraphPad Prism version 6/7 (GraphPad Software, La Jolla California, USA) were used for statistical analysis. All data were tested for normality by Shapiro Wilk test in conjunction with visual inspection of frequency distribution plots.

Cross sectional baseline data are provided for patients who had both baseline and follow-up measures. These are shown as means with standard deviations (SD) for normally distributed data and as medians with interquartile ranges (IQR) for non-normally distributed data. Change over one year (follow-up minus baseline) is represented as a mean with 95% confidence interval when normally distributed and as median change with IQR when not normally distributed. Missing data were excluded from the analysis and change was only calculated in patients who had both baseline and 12 month follow-up data. The significance of mean change was evaluated using one sample two tailed t-test for normally distributed data and one sample Wilcoxon-signed rank test for non-normally distributed data. Statistical significance was set at 5%.

Spearman Rank correlation analysis was used to assess correlation between CMTNSv2, SF-36v2-Physical component, disease duration and the outcome measures used in the study. Correlations with plasma 1-deoxySLs were performed following normalisation of plasma 1-deoxySA and 1-deoxySO by log transformation. Statistical significance was set at 0.1% ($p<0.001$) following Bonferroni correction for multiple comparisons.

The Standardised Response Mean (SRM) (García de Yébenes Prous *et al.*, 2008), also known as Cohen's d, was used to measure effect size. SRM is an established term in this field as a measure of outcome responsiveness and will enable comparison between different outcome measures within and between studies (Morrow *et al.*, 2015; Piscosquito *et al.*, 2015). It was calculated by dividing the mean change (follow up-baseline) by the standard deviation. SRMs of 0.20-0.49, 0.50-0.79 and ≥0.80 reflect small, moderate and large responsiveness respectively (Husted *et al.*, 2000; Piscosquito *et al.*, 2015).

5.4 Results

5.4.1 Validity of outcome measures

Validity is defined as the degree to which an outcome variable measures what we intend to measure (Roach, 2006). Criterion validity is the most straightforward and can be demonstrated through correlation of the outcome measure to relevant patient function. The outcome measures at baseline were correlated with CMTNSv2 (only validated impairment scale for inherited neuropathies), disease duration and the physical component of the SF-36v2 (SF-36v2PC) (Table 5.1). Due to multiple comparisons, the statistical significance was set at p<0.001 (Bonferroni correction). CMTNSv2 itself correlated strongly with SF-36v2PC (r_s=-0.824, p<0.0001) and disease duration (r_s=-0.718, p<0.0001).

Both upper limb sensory and motor nerve amplitudes correlated strongly with CMTNSv2 (r_s >0.768, p<0.0001), SF-36v2PC (r_s >0.673, p<0.0001) and moderately with disease duration (r_s >0.484, p=0.003-0.0004). In QST, only measurements from the hand correlated strongly with all three CMTNSv2 (r_s > 0.645, p<0.0001), SF-36v2PC (r_s>0.499, p=0.003-<0.0001) and disease duration (r_s >0.464, p=0.02-0.0002). There were too few recordable values for most QST parameters when tested on the feet for correlations to be meaningful apart from for VDT which correlated strongly with CMTNSv2 (r_s =-0.622, p=0.0001) and moderately with disease duration (r_s =-0.568, p=0.0007). Values from the face and trunk (face<trunk) did not correlate significantly with CMTNSv2, SF-36v2PC or disease duration.

Isometric ankle dorsiflexion, ankle plantarflexion, ankle inversion and ankle eversion also correlated strongly with CMTNSv2 (r_s >-0.810, p<0.0001), SF-36v2PC (r_s >0.539, p=0.002-<0.0001) and duration of disease (r_s >-0.570, p<0.0004). Moderate-strong correlations only with CMTNSv2 were seen with IENFD (r_s =-0.748, p=<0.0001) and plasma 1-deoxySO level (r_s =0.544, p=0.0009). Plasma 1-deoxySA level also correlated moderately with CMTNSv2 (r_s =0.490) however it was not significant following multiple comparisons (p=0.003). NPSI scores were the only assessment not to correlate with any of the three correlation variables. Calf muscle fat fraction (Overall calf muscle fat fraction) correlated strongly with CMTNSv2 (r_s =0.851, p<0.0001), SF-36v2PC (r_s =-0.673, p<0.0001) and disease duration (r_s =0.685, p<0.0001).

Assessment		CMTNSv2		SF-36v2 : Physical component		Disease duration	
		r_s	*p*	r_s	*p*	r_s	*p*
CMTNSv2							
CMTNSv2				-0.824	<0.0001	0.718	<0.0001
Nerve conduction studies							
Radial SNAP		-0.802	<0.0001	0.705	<0.0001	*-0.494*	*0.003*
Ulnar SNAP		-0.768	<0.0001	0.673	<0.0001	-0.484	0.004
Ulnar CMAP		-0.934	<0.0001	0.758	<0.0001	-0.555	0.0007
Median CMAP		-0.888	<0.0001	0.752	<0.0001	-0.572	0.0004
Quantitative Sensory Testing							
FOOT	VDT	-0.622	0.0001	*0.254*	*0.17*	-0.587	0.0004
HAND	CDT	-0.790	<0.0001	*0.499*	*0.003*	-0.542	0.0009
	WDT	0.775	<0.0001	-0.650	<0.0001	0.566	0.0005
	TSL	0.758	<0.0001	-0.602	0.0003	*0.512*	*0.002*
	CPT	-0.749	<0.0001	0.656	<0.0001	*-0.394*	*0.02*
	HPT	0.793	<0.0001	-0.733	<0.0001	*0.532*	*0.001*
	MDT	0.803	<0.0001	-0.636	<0.0001	0.598	0.0002
	MPT	0.660	<0.0001	-0.753	<0.0001	*0.466*	*0.007*
	VDT	-0.645	<0.0001	0.727	<0.0001	-0.561	0.0007
	PPT	0.821	<0.0001	-0.702	<0.0001	0.620	0.0002
TRUNK	CDT	*-0.455*	*0.04*	*0.514*	*0.02*	*-0.429*	*0.05*
	WDT	0.727	0.0002	*-0.499*	*0.03*	*0.526*	*0.01*
	TSL	*0.372*	*0.12*	*-0.618*	*0.006*	*0.263*	*0.28*
	CPT	*-0.030*	*0.90*	*0.475*	*0.046*	*-0.004*	*0.99*
	HPT	*0.295*	*0.21*	*-0.405*	*0.09*	*0.123*	*0.61*
	MDT	*0.203*	*0.42*	*-0.263*	*0.31*	*0.078*	*0.66*
	MPT	*0.485*	*0.04*	-0.750	0.0003	*-0.060*	*0.74*
	VDT	*-0.526*	*0.02*	*0.309*	*0.21*	*-0.262*	*0.14*
	PPT	*0.049*	*0.85*	*-0.272*	*0.29*	*0.057*	*0.82*
FACE	CDT	*-0.263*	*0.13*	*0.273*	*0.12*	*-0.375*	*0.03*
	WDT	*0.287*	*0.10*	*-0.314*	*0.07*	*0.267*	*0.13*
	TSL	*0.085*	*0.632*	*-0.397*	*0.02*	*0.128*	*0.47*
	CPT	*0.075*	*0.67*	*-0.009*	*0.96*	*0.144*	*0.42*
	HPT	*0.163*	*0.36*	*-0.163*	*0.37*	*-0.008*	*0.96*
	MDT	*0.096*	*0.60*	*-0.062*	*0.74*	*0.064*	*0.73*
	MPT	*0.066*	*0.72*	*-0.115*	*0.54*	*-0.068*	*0.71*
	VDT	*-0.402*	*0.02*	*0.325*	*0.07*	*-0.262*	*0.14*
	PPT	*-0.083*	*0.66*	*0.018*	*0.92*	*-0.039*	*0.84*
Myometry							
Isometric ankle dorsiflexion		-0.867	<0.0001	0.684	<0.0001	-0.590	0.0004
Isometric ankle plantarflexion		-0.863	<0.0001	0.539	0.002	-0.727	<0.0001
Isometric ankle inversion		-0.810	<0.0001	0.658	<0.0001	-0.604	0.0002
Isometric ankle eversion		-0.819	<0.0001	0.664	<0.0001	-0.668	<0.0001
IM knee extension		*-0.292*	*0.09*	*0.297*	*0.09*	*-0.531*	*0.001*
IM knee flexion		*-0.429*	*0.01*	*0.404*	*0.02*	*-0.565*	0.0005
Intra-epidermal nerve fibre density (IENFD)							
IENFD		-0.748	<0.0001	*0.517*	*0.003*	*-0.382*	*0.03*
Plasma deoxysphingolipids							
Log 1-deoxysphinganine		*0.490*	*0.003*	*-0.456*	*0.008*	*0.301*	*0.08*
Log 1-deoxysphingosine		0.544	0.0009	*-0.426*	*0.01*	*0.332*	*0.06*

Assessment	CMTNSv2		SF-36v2 : Physical component		Disease duration	
	r_s	*p*	r_s	*p*	r_s	*p*
Neuropathic Pain Symptom Inventory (NPSI)						
NPSI	*0.091*	*0.61*	*-0.384*	*0.03*	*-0.109*	*0.54*
SF36v2						
Physical component	-0.792	<0.0001			*-0.53*	*0.002*
Mental component	*0.227*	*0.21*	*-0.011*	*0.95*	*0.312*	*0.08*
Physical function	-0.830	<0.0001	0.813	<0.0001	-0.601	0.0002
Role physical	*-0.547*	*0.001*	0.813	<0.0001	*-0.341*	*0.05*
Bodily pain	*-0.303*	*0.08*	0.700	<0.0001	*-0.129*	*0.47*
Calf muscle fat fraction						
Overall calf muscle	0.851	<0.0001	-0.673	<0.0001	0.680	<0.0001

Table 5.1 Correlation of CMTNSv2, SF-36v2-Physical component and disease duration with assessments used in the study.

CMTNSv2=Charcot-Marie-Tooth (CMT) Neuropathy score second version, SNAP=Sensory Nerve Action Potential and CMAP=Compound Muscle Action Potential, CDT= Cold detection threshold, WDT= Warm detection threshold, TSL= Thermal sensory limen, CPT= Cold pain threshold, HPT= Heat pain threshold, MDT= Mechanical detection threshold, MPT= Mechanical pain threshold, VDT= Vibration detection threshold, PPT= Pressure pain threshold and SF-36v2= 36- Short Form Health Survey version 2 (1998).

5.4.2 Change over 12 months

Follow-up assessments were done after 1 year (mean = 364 days +/- 7days). Detailed results are summarised in Tables 5.2-5.5. Three patients were lost to follow-up (Figure 4.1)

There was no significant change in the CMTNSv2 (p=0.33) over 12 months (Table 5.2). There was also no significant change using the Rasch modified version of CMTNSv2, CMTNSv2-R (p=0.41). In both CMTNSv2 and CMTNSv2-R, the CMT symptom score (CMTSS) showed the least change and CMT signs comprising of only the examination component contributed most to the change in CMTNSv2. There was minimal, non-significant change in the nerve conduction studies over 12 months (Table 5.2) with deterioration over one year seen only in radial SNAP (mean change=-0.26μV, 95% CI=-0.86-0.34).

In QST testing of the feet, only 1 to 6 patients had recordable responses at baseline and follow-up for the different parameters except VDT where 24 patients had recordable results (Table 5.3). Change in VDT on the feet was not significant (p=0.07) over 12 months. For most of the QST parameters when tested on the hands, just fewer than half the patients (10-12 patients) had recordable results and hence quantifiable change. Larger number of patients had recordable change for VDT (31/35) and PPT (19/35). In the hands, significant mean/median change was only seen in HPT (p=0.02) and PPT (p=0.04) however the change in HPT was in the direction of clinical improvement. On the face, significant change was noted for VDT (p=0.04) and PPT (p<0.0001). Serial QST measurements on the trunk were only available for a limited number of patients (7-9 patients). None of the trunk QST parameters showed significant change (p values range = 0.10-0.99).

In myometric measurements, significant changes over 1 year were noted in ankle plantar flexion (p=0.0007), ankle inversion (p=0.03) and ankle eversion (p=0.006) (Table 5.4). Although the median follow-up ankle inversion and eversion measurements were stronger than at baseline, there was a mean deterioration in both over 1 year. There was a significant change in IENFD measurements however it was an increase in nerve fibre density (mean change=0.47fibres/mm, 95% CI=0.01-0.93, p=0.04). Plasma 1-deoxySA levels significantly decreased over 1 year (mean change=-0.13μM, 95% CI=-0.24 to-0.02, p=0.02). There was also a decrease in plasma 1-deoxySO levels over 1 year but this was not significant. There

was no significant change in the reported pain as measured by the NPSI (p=0.29). SF-36v2 questionnaire did not detect any significant deterioration over one year but detected an improvement in the bodily pain component.

For the MRI, 25 HSN patients and 10 controls were analysed at 12 months (Table 5.5). Other than the three patients lost to follow-up, other data are 'missing completely at random' due to technical reasons with the MRI or data transfer. In HSN1 patients, there were significant increases in all the individual calf muscle fat fractions and the overall calf muscle fat fraction (p values range= 0.03-<0.0001). There were no significant changes in the control group (p values range = 0.16-0.79). All the muscles had a relatively similar degree of change in fat fraction (fat fraction mean/median change range = 1.7-2.9%).

In summary, calf muscle fat fraction, hand PPT and isometric ankle plantarflexion, inversion and eversion significantly changed over 12 months and correlated with CMTNSv2, SF36-v2PC and disease duration. Their relative responsiveness (SRMs) are shown in Table 5.6. Calf muscle fat fraction had the best responsiveness both in individual muscles and as overall calf muscle fat fraction (Overall calf muscle fat fraction SRM 0.81 versus SRM of 0.49 for Hand-PPT and SRM<0.40 for myometry). Overall calf muscle fat fraction changes were smaller in patients with baseline fat fraction less than 5% or greater than 70% (Figure 5.1). All patients with overall calf muscle fat fraction less than 5% had CMTNSv2 of 10 or less. Patients with fat fraction greater than 70% had CMTNSv2 ranging from 28-34. Focusing on the patients with baseline overall calf muscle fat fraction of 5-70% (20 patients, 59% of MRI cohort) markedly improved the responsiveness with peroneus longus and overall calf muscle fat fractions having the greatest responsiveness (SRMs of 2.07 and 1.60 respectively).

CMTNSv2				
	Median baseline (IQR)	**Median follow-up (IQR)**	**Mean change (95% CI)**	**p value**
CMTNSv2	22.0 (10-28)	21.0 (11-29)	0.23 (-0.24-0.68)	0.33
CMTESv2	*15.6 (6.9)	*15.8(6.8)	0.19 (-0.19-0.57)	0.33
CMTSS	7.0 (3.5-8)	7.0 (4.3-8)	-0.03 (-0.31-0.25)	0.82
CMT- signs	*9.3 (4.0)	*9.5 (4.1)	0.22 (-0.04-0.47)	0.09
CMTNSv2-R				
CMTNSv2-R	26.0 (11-33)	24.0 (12-34)	0.19 (-0.27-0.66)	0.41
CMTESv2-R	*18.3 (8.2)	*18.6 (7.9)	0.25 (-0.16-0.67)	0.23
CMTSS	8.0 (3.3-9)	8.0 (4-9.8)	0.06 (-0.21-0.34)	0.65
CMT-signs	*11.1 (4.3)	*11.3 (4.2)	0.19 (-0.17-0.55)	0.30
Neurophysiology				
	Median baseline (IQR)	**Median follow-up (IQR)**	**Mean change (95%CI)**	**p value**
Ulnar SNAP (μV)	0.0 (0.0-2.0)	0.0 (0.0-3.0)	0.32 (-0.01-0.66)	0.06
Radial SNAP, (μV)	0.0 (0.0-11.0)	0.0 (0.0-10.0)	-0.26 (-0.86-0.34)	0.39
Median CMAP (mV)	2.5 (0.0-7.0)	3.4 (0.0-7.0)	0.06 (-0.-0.21-0.33)	0.66
Ulnar CMAP (mV)	2.2 (0.0-8.3)	1.5 (0.0-8.1)	0.02 (-0.35-0.38)	0.93

Table 5.2: Change in CMTNSv2, CMTNSv2-R and Nerve conduction studies

Baseline (BL) and follow-up (F/U) data are quoted as median (IQR) unless marked with an asterisk (*) in which case mean (SD) is quoted. The change over one year is represented as mean change (95% CI mean). CMTNSv2=Charcot-Marie-Tooth (CMT) Neuropathy score second version, CMTES=CMT Examination score of CMTNS comprising of CMT symptom and examination scores, CMTSS= CMT symptom score of CMTNS, CMT signs= only the clinical examination component of CMTNS, CMTNSv2-R= CMTNSv2 Rasch modified. P value=p value for the change. SNAP=Sensory Nerve Action Potential and CMAP=Compound Muscle Action Potential.

		CDT (ºC)	WDT (ºC)	TSL (ºC)	CPT (ºC)	HPT (ºC)	MDT (mN)	MPT (mN)	VDT (0-8)	PPT (kPa)
FOOT	**N**	3	3	3	2	2	1	5	24	6
	Median BL (IQR)	10.7 (7.6-28.8)	48.1 (46.9-49.2)	21.2 (16.0-49.4)	7.3 (0-14.6)	49.9 (49.8-49.9)	na	1024 (1024-1024)	4.0 (2.8-5.0)	339 (263-435)
	Median F/U (IQR)	2.6 (1.3-21.2)	48.4 (47.3-49.7)	47.2 (28.8-49.9)	2.2 (0-4.3)	49.9 (49.9-49.93)	na	1024 (1024-1024)	3.3 (2.4-4.3)	398 (283-430)
	Mean Change (95% CI)	-7.6 (8.1- to -6.3)	0.4 (0.2-0.6)	12.8 (-2.2-28.7)	-5.2 (-10.3-0)	0.07 (0-0.13)	na	0 (0-0)	†-0.39 (-0.8-0.03)	8 (-36-71)
HAND	**N**	12	11	11	11	10	12	17	31	19
	Median BL (IQR)	30.3 (28.4-31.1)	36.0 (33.8-42.0)	6.2 (2.9-16.2)	15.4 (0-25.3)	*44.3 (3.8)	1.6 (1.3-52.0)	256 (77-716)	*6.1 (1.3)	*276 (123)
	Median F/U (IQR)	30.6 (27.4-30.9)	35.1 (33.8-41.3)	5.9 (3.1-11.3)	21 (0-26.2)	*42.6 (3.7)	4.2 (1.8-32.7)	338 (119-1024)	*5.9 (1.4)	*316 (139)
	Mean Change (95% CI)	-0.02 (-1.0-0.1.0)	-0.3 (-2.7-2.1)	0.5 (-2.2-3.3)	-0.06 (-3.2-3.1)	†-0.75 (-2.6- -0.05)‡	†2.1 (-0.4-16.1)	41 (-120-202)	-0.19 (-0.5-0.2)	40 (0.7-80)‡
FACE	**N**	32	32	32	32	32	31	31	31	30
	Median BL (IQR)	30.9 (30.0-31.2)	33.7 (33.0-34.7)	2.2 (1.9-3.8)	20.0 (13.2-24.4)	*42.6 (3.7)	0.18(0.1-0.3)	16.5 (8-49)	6.0 (5.7-7.0)	101 (98-121)
	Median F/U (IQR)	30.9 (30.1-31.2)	33.7 (33.2-35.1)	2.5 (1.7-4.0)	24.7 (11.4-27.6)	*42.0 (4.0)	0.15 (0.1-0.3)	16.0 (8-42)	6.0 (5.0-6.3)	140 (113-182)
	Mean Change (95% CI)	0.05 (-0.2-0.3)	0.12 (-0.5-0.7)	-0.36 (-1.5-0.7)	0.94 (-2.5-4.4)	-0.60 (-2.2-1.0)	-0.17 (-0.5-0.2)	-14.6 (-37-7)	-0.50 (-1.0 to -0.02)‡	33 (21-45)‡
TRUNK	**N**	9	9	8	8	9	8	8	8	7
	Median BL (IQR)	29.3 (28.1-30.3)	36.2 (35.1-42.2)	8.6 (4.1-14.8)	20.3 (13.3-25.8)	46.0 (39.7-47.5)	4.2 (1.0-30.4)	112 (27-398)	*5.3 (1.0)	*194 (90)
	Median F/U (IQR)	28.6 (26.0-30.5)	37.4 (35.2-44.2)	7.0 (4.2-11.5)	23.4 (4.9-25.2)	45.2 (42.7-47.9)	13.2 (3.8-32.7)	54 (36-796)	4.9 (0.8)	*243 (70)
	Mean Change (95% CI)	†-0.4 (-0.8-0.9)	0.89 (-1.2-2.9)	-0.33 (-5.1-4.5)	†1.1 (-3.0-5.6)	†0.1 (-1.0-1.5)	6.6 (-14.5-27.7)	†10.2 (-76.1-232.2)	-0.4 (-1.0-0.2)	49.6 (-12.2-111.4)

Table 5.3: Change in Quantitative sensory testing

Baseline (BL) and follow-up (F/U) data are quoted as median (IQR) unless marked with an asterisk (*) in which case mean (SD) is quoted. The change over one year is represented as mean change (95% CI mean) unless marked with † in which case median (IQR) are noted. N= number of patients with recordable BL and F/U responses. CDT: Cold detection threshold, WDT: Warm detection threshold, TSL: Thermal sensory limen, CPT: Cold pain threshold, HPT: Heat pain threshold, MDT: Mechanical detection threshold, MPT: Mechanical pain threshold, VDT: Vibration detection threshold, PPT: Pressure pain threshold, na: not applicable and ‡: Significant difference ($p<0.05$) in mean change from zero.

	Median baseline (IQR)	Median follow-up (IQR)	Mean change (95% CI)	p value
Myometric measurements				
Isometric ankle dorsiflexion (Nm)	0 (0-17)	0 (0-18)	-0.07 (-0.81-0.66)	0.84
Isometric ankle plantar flexion (Nm)	7 (0-23)	4 (0-15)	†-0.5 (-9.5-0)	0.0007
Isometric ankle inversion (Nm)	3 (0-13)	3.8 (0-11)	-0.89 (-1.66 to-0.12)	0.03
Isometric ankle eversion (Nm)	2 (0-12)	2.8 (0-8)	-1.61 (-2.72 to -0.51)	0.006
Isometric knee extension (Nm)	*99 (44)	*94 (47)	-0.88 (-9.66-7.91)	0.84
Isometric knee flexion (Nm)	*51 (27)	*51 (26)	-0.63 (-4.34-3.09)	0.73
Intra-Epidermal Nerve Fibre Density (IENFD)				
IENFD (fibres/mm)	0.1 (0-1.9)	1.3 (0-3.0)	0.0 (0.0-0.4)	0.04
Plasma deoxysphingolipids				
1-deoxysphinganine (µM)	0.72 (0.44-1.03)	0.63 (0.43-0.90)	-0.13 (-0.24- -0.02)	0.02
1-deoxysphingosine (µM)	1.44 (0.89-2.33)	1.43 (0.95-1.91)	†-0.11 (-0.42-0.14)	0.13
Neuropathic Pain Symptom Inventory (NPSI)				
Total NPSI score (0-100)	23.0 (13-36)	19.5 (6-30)	-2.5 (-7.2-2.2)	0.29
Paroxysmal sub-score (0-10)	5.0 (2-8)	3.2 (0-6)	-1.4 (-2.4- -0.3)	0.01
SF-36v2				
Physical component score	*41.4 (10.6)	*42.7 (11.3)	1.2 (-1.0-3.4)	0.26
Mental component score	*51.9 (9.9)	*53.3 (9.5)	1.4 (-1.8-4.6)	0.38
Physical functioning	*38.0 (12.9)	*38.7 (12.8)	0.7 (-1.2-2.7)	0.45
Role-physical	48.2 (37.0-57.2)	45.9 (34.7-57.2)	0.1 (-2.8-3.1)	0.92
Bodily pain	*40.5 (9.9)	*47.9 (10.6)	3.9 (1.0-6.8)	0.01

Table 5.4: Change in myometry, intra-epidermal nerve fibre density, plasma 1-deoxysphingolipids, Neuropathic Pain Symptom Inventory and SF36v2

Baseline and follow-up measures are given as medians (IQR) unless indicated by an asterisk (*), in which case mean (SD) is quoted. Change over one year is quoted as means (95% CI) unless marked with † in which case median change (IQR) is quoted. SF-36v2=36-Short Form Health Survey version 2 (1998).

	HSN1 patients				CONTROLS			
	Median baseline FF% (IQR)	Median Follow-up FF % (IQR)	Mean change in FF % (95% CI)	p value	Median baseline FF %(IQR)	Median Follow-up FF % (IQR)	Mean change in FF% (95% CI)	p value
Tibialis anterior	11.7 (1.5-29.2)	14.1 (2.1-34.9)	2.0 (0.7-3.3)	0.004	0.9 (0.7-1.8)	0.8 (0.6-1.7)	-0.04 (-0.15-0.07)	0.41
Extensor Hallucis Longus	16.1 (1.8-53.8)	20.1 (2.2-62.2)	†2.5 (0.3-4.4)	0.0003	1.3 (1.0-2.1)	1.3 (1.0-2.0)	†0.1 (-0.1-0.2)	0.56
Peroneus Longus	24.4 (2.7-61.6)	27.1 (3.1-65.8)	2.4 (1.2-3.5)	0.0002	1.7 (1.2-2.6)	1.8 (1.1-2.6)	0.02 (-0.16-0.2)	0.79
Soleus	21.2 (2.1-58.3)	25.9 (2.3-65.7)	1.8 (0.7-2.8)	0.003	1.7 (1.1-3.7)	1.5 (1.1-3.3)	-0.06 (-0.21-0.08	0.34
Lateral Gastrocnemius	21.9 (2.5-77.1)	39.7 (4.1-82.6)	†2.5 (-0.1-6.9)	0.03	1.3 (1.2-2.6)	1.2 (0.9-2.2)	-0.2 (-0.6-0.1)	0.16
Medial Gastrocnemius	30.1 (1.7-68.8)	36.1 (2.4-76.6)	†1.7 (0.1-5.5)	0.005	1.4 (1.0-3.5)	1.3 (0.9-3.4)	-0.05 (-0.3-0.2)	0.66
Deep posterior group	12.8 (1.8-51.1)	15.5 (2.1-58.4)	2.5 (1.0-4.0)	0.002	1.3 (1.1-1.8)	1.3 (1.0-2.1)	0.06 (-0.1-0.2)	0.43
Overall calf muscle	16.9 (2.0-57.5)	20.4 (2.5-63.3)	2.36 (1.2-3.6)	0.0004	1.4 (1.1-2.8)	1.4 (1.1-2.6)	-0.1 (-0.16-0.05)	0.26

Table 5.5: Change in calf muscle fat fraction

Baseline and follow-up measures are given as medians (IQR). Change over one year is quoted as means (95% CI) unless marked with † in which case median change (IQR) is quoted. FF%=Fat Fraction percentage.

	Mean change (95%CI)	SRM	p value
Quantitative Sensory Testing			
HAND-PPT (kPa)	40 (0.7-80)	0.49	0.046
Computerised myometry			
Isometric ankle plantar flexion (Nm)	*-0.50 (-9.5-0)	na	0.0007
Isometric ankle inversion (Nm)	-0.89 (-1.66 to-0.12)	-0.33	0.03
Isometric ankle eversion (Nm)	-1.61 (-2.72 to -0.51)	-0.40	0.006
Calf muscle fat fraction			
Tibialis Anterior (FF%)	2.03 (0.72-3.33)	0.64	0.004
Extensor Hallucis Longus (FF%)	2.93 (1.50-4.37)	0.84	0.0003
Peroneus Longus (FF%)	2.35 (1.22-3.48)	0.86	0.0002
Soleus (FF%)	1.75 (0.66-2.84)	0.66	0.003
Lateral Gastrocnemius (FF%)	*2.46 (-0.12-6.87)	na	0.003
Medial Gastrocnemius (FF%)	*1.68 (0.10-5.49)	na	<0.0001
Deep posterior group (FF%)	2.51 (0.99-4.02)	0.68	0.002
Overall calf muscle (FF%)	2.36 (1.16-3.55)	0.81	0.0004
MRI proximal calf fat fraction in subgroup with baseline overall calf FF=5-70%			
Tibialis Anterior (FF%)	3.98 (2.37-5.59)	1.49	0.0002
Extensor Hallucis Longus (FF%)	4.94 (2.70-7.19)	1.33	0.0004
Peroneus Longus (FF%)	4.25 (3.01-5.48)	2.07	<0.0001
Soleus (FF%)	3.33 (1.62-5.04)	1.18	0.001
Lateral Gastrocnemius (FF%)	4.66 (-0.56-9.89)	0.54	0.08
Medial Gastrocnemius (FF%)	6.57 (2.35-10.79)	0.94	0.005
Deep posterior group (FF%)	4.91 (3.01-6.80)	1.56	0.0001
Overall calf muscle (FF%)	4.34 (2.70-5.99)	1.60	<0.0001

5.6: Responsiveness of tests which had significant change over 12 months

Change is reported as mean change unless marked with an asterisk (*) in which median change (IQR) is reported. na=not applicable as SRM values cannot be calculated in cases where the change is not normally distributed. PPT=Pressure Pain Threshold, FF%=Fat Fraction percentage.

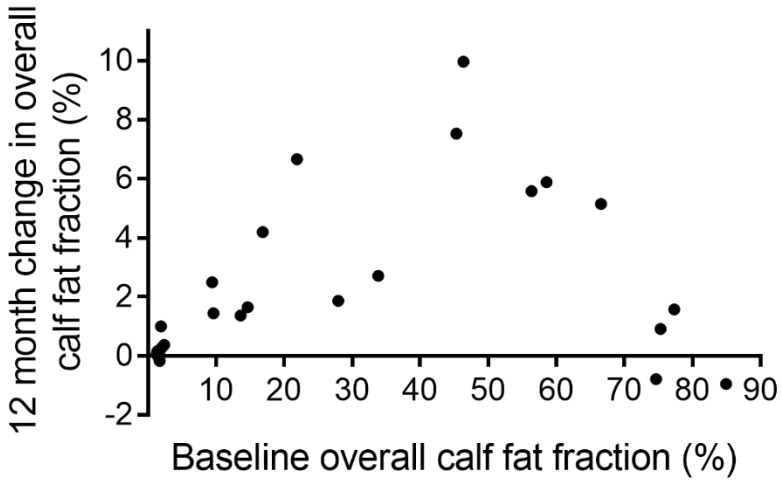

Figure 5.1: Degree of change in overall calf muscle fraction over one year with varying baseline fat fractions.

5.5 Discussion

For our longitudinal study we used a comprehensive range of measures including clinical, neurophysiological, myometric, plasma 1-deoxySL levels, intraepidermal nerve fibre density and MRI measurement of calf intramuscular fat accumulation. To determine validity of the outcome measures, the measures were correlated with a clinical composite measure of disability, CMTNSv2, patient self-assessment score, SF36-v2PC and disease duration. Calf muscle fat fraction, upper limb nerve conduction studies, QST in the hand and isometric ankle plantarflexion, dorsiflexion, inversion and eversion correlated strongly/moderately with all three validation variables.

However, due to the heterogeneity in the cohort, many of the outcome measures studied were limited by both floor and ceiling effects. No significant changes were observed for most of the measures over 12 months and hence cannot be used in a 12 month HSN1 clinical trial if the aim of the therapy, as is likely, is disease stabilisation.

The CMTNSv2, which is the only validated impairment scale in adults with CMT, an earlier version of which (CMTNS) had been used in all the ascorbic acid trials in adult CMT1A patients (Gess *et al.*, 2015), did not show any significant changes over 12 months in our current study. The limitations in the CMTNS with regards to discriminating between different degrees of clinical severity and for longitudinal use in clinical trials have previously been highlighted (Merkies *et al.*, 2012; Mannil *et al.*, 2014; Piscosquito *et al.*, 2015). The Rasch modified version of the CMTNS increased the spread of the data but did not increase responsiveness. A recent randomised, placebo controlled trial in HSN patients using oral L-serine supplementation by Fridman *et al*. (2019) did not show a significant difference in the primary outcome measure (proportion of patients progressing more than one point on the CMTNS at 1 year) between L-serine and placebo groups. However, it showed a decline in CMTNS (-1.5units, CI: -2.8-0.1, p=0.03) in L-serine participants relative to placebo whereas the placebo group experienced a mean increase in CMTNS of 1.1 point (±0.53, p=0.04). The difference in the CMTNS progression in their placebo group and our study (change in CMTNS=0.23, CI:-0.24 to 0.68), despite patients in both studies having a similar distribution of severity (mean CMTNS= 24.6 [7.0] versus median=22.0 [10-28]), could be due to differences in sample size. The annual change in CMTNS noted in CMT1A patients ranged

between -0.92 and +1.0 unit (Shy *et al.*, 2005; Micallef *et al.*, 2009; Verhamme *et al.*, 2009; Pareyson *et al.*, 2011; Lewis *et al.*, 2013). This variability highlights the limitations of using the CMTNS as a primary outcome measure in slowly progressive neuropathies. Comparable changes over one year were noted in nerve conduction studies and SF36v2 between this study and the placebo group of the HSN1 trial (Fridman *et al.*, 2019)

The motor and sensory amplitudes showed no detectable changes over 12 months demonstrating a marked floor effect. Most patients had globally absent sensory responses. Motor unit number estimation (MUNE) has been used in a study as an alternative neurophysiological method of assessing motor axonal loss in CMT(Lewis *et al.*, 2003). With chronic denervation, there is collateral sprouting and remodelling of surviving units which means the motor (Compound Muscle Action Potential, CMAP) amplitudes can be relatively well preserved early on in the disease. The study suggested that MUNE can assess motor unit loss in CMT and that it may better reflect axonal loss than CMAP. However, in HSN1 where there is a significant floor effect, this technique will have the same limitations. Of the neurophysiological measures, only Hand-PPT significantly changed over 12 months and correlated strongly with all three validation variables. However, it only has small/moderate responsiveness (SRM=0.49) and it is unlikely that QST parameters could be used singly as a primary outcome measure.

Significant change over 1 year was noted in myometric measurements of ankle plantar flexion, ankle inversion and ankle eversion however ankle inversion and eversion have small responsiveness (SRMs<0.40). SRM could not be calculated for ankle plantarflexion as the change was not normally distributed but if normal distribution were assumed, it would have moderate responsiveness with a SRM of 0.62 (mean=-4.5Nm, 95% CI=-7.2 to -1.9Nm). Isometric ankle plantarflexion could therefore be explored as a potential secondary outcome measure in HSN1. A limitation of this study is the lack of control myometric data to rule out possible systematic bias contributing to this change.

Most of the variation in the IENFD measurements between baseline and 1 year follow-up values were similar to the inter-test variability reported by Lauria *et al.* (2015). Hence, IENFD measurements would not be a suitable outcome measure in HSN1 patients. Fridman *et al.* (2015) suggested IENFD measurements from thigh skin biopsies as a potential

outcome measure for clinical trials in their cohort of HSN1 patients as none of the patients were completely denervated at this level in their cross-sectional study. However, in their recent randomized trial of L-serine in HSN1 patients, there was a large variability in the change in IENFD (thigh), which limited its responsiveness (Fridman *et al.*, 2019).

Surprisingly, a small but significant decrease in the plasma 1-deoxySA level was found after 1 year. Differences in diet (intake of serine and alanine) and technical factors (differences in number of freeze thaw cycles, transport time from UK-Switzerland) between the two time points could be possible explanations. Plasma 1-deoxySL levels have been shown to dramatically decrease with L-serine treatment and remain suppressed for the duration of treatment (Garofalo *et al.*, 2011; Fridman *et al.*, 2019). Therefore, plasma1-deoxySL levels are potentially very useful to show compliance and target engagement in an L-serine trial aiming to reduce these levels but they are unlikely to be useful as a marker of disease stabilisation. It is possible that in the context of neuropathy, 1-deoxySL levels in cerebrospinal fluid (CSF) may be more relevant however no studies have investigated this in HSN1 patients.

There was no deterioration in the total NPSI score or the paroxysmal sub-component over 1 year. Due to the infrequent episodic nature of the pain experienced by the HSN1 patients, pain questionnaires capturing relatively short periods may not be suitable for a therapeutic clinical trial. In the SF-36v2 questionnaire, there was no significant change over 1 year apart from an improvement in the bodily pain component. The results were similar to those reported in the ascorbic acid trials in CMT1A where a mixture of improvements and deteriorations in health status were noted (Gess *et al.*, 2015). It may be that a disease specific Health related quality of life (HRQoL) questionnaire is needed (Rajabally and Cavanna, 2015).

MRI determined fat quantification using the Dixon method has been shown to be reliable, sensitive and responsive as an outcome measure in recent natural history studies in various neuromuscular disorders (Willis *et al.*, 2013; Bonati *et al.*, 2015; Morrow *et al.*, 2015). Of all the tests performed, the MRI fat fraction quantification is the most promising as an outcome measure in HSN1 patients. In the present longitudinal study, despite large heterogeneity in the HSN group, the changes in both combined overall fat fraction and individual muscle fat

fraction over 12 months were significant in HSN1 patients whereas healthy controls showed no significant change (range of increased combined fat fraction of 1.4-2.5% in patients versus change of -0.2-0.1% in healthy controls) and showed greater responsiveness (overall calf muscle fat fraction SRM 0.81) when compared to the other outcome measures in the study (SRM<0.49). Morrow *et al.* reported a comparable change/responsiveness in overall calf fat fraction (SRM 0.83) in a 12 month follow-up study in a cohort of CMT1A patients (Morrow *et al.*, 2015).

A degree of caution is needed in using Cohen's well known thresholds for effect sizes, ES ('small' if ES ≥0.20< 0.50, 'moderate' if ES≥0.50<0.80 and 'large' if ES≥0.80) to interpret the SRMs. These cut-offs were calculated with pooled standard deviation (independent samples) rather than standard deviation of the change (dependent samples) therefore extrapolation of these thresholds to SRMs may lead to over or underestimates of the effects (Middel and van Sonderen, 2002).

Assessments focusing on sensory impairment (sensory nerve conduction studies, most of the QST parameters and IENFD) have been hampered by floor effects. Due to the variable episodic nature of the neuropathic pain, another element of the condition, and the use of various analgesics, assessing longitudinal change in neuropathic pain will be difficult, especially with many of the existing pain questionnaires capturing only short periods of time. However, if there was a dramatic improvement in the pain with a therapy, pain questionnaires may become responsive but this is unknown.

Despite the name HSN1, this study demonstrates that that there is significant motor involvement with a consistent pattern of disease progression: early progressive sensory involvement followed later by progressive motor involvement. The purpose of this study was to assess which of the potential outcome measures showed the largest effect size over 12 months across the whole cohort. This was MRI determined calf muscle fat fraction. To translate this into responsiveness in a clinical trial, the intervention must be able to exert an effect on the outcome measure in question, which would be expected for intramuscular fat fraction unless the intervention only affected sensory pathways. This should be borne in mind when designing clinical trials, as an intervention which does not slow the motor progression and hence the increase in intramuscular fat accumulation could not be

considered a complete treatment, and this study has shown that MRI determined fat accumulation is the most responsive measure of motor axonal loss. The change in CMTNS noted in the landmark natural history study in CMT1A (Shy *et al.*, 2008) was greater than that seen in the placebo groups in the three major ascorbic acid trials in CMT1A (Micallef *et al.*, 2009; Pareyson *et al.*, 2011; Lewis *et al.*, 2013). A possible 'trial effect' whereby trials have a positive effect on the outcome of patients was given as a possible explanation (Braunholtz *et al.*, 2001). Using a completely objective measurement like MRI determined fat fraction may reduce this effect. There is a potential caveat in using MRI fat fraction as a biomarker if functional improvement in muscle strength is not accompanied by structural changes on MRI.

The effect size can be increased further if we select patients with baseline overall calf muscle fat fraction of 5-70% (20 patients, 59% of MRI cohort), which doubles the responsiveness of overall calf muscle fat fraction (SRM of 0.81 to 1.60). With this responsiveness, using Lehr's formula [$n = \frac{16}{(E \times SRM)^2}$] (Morrow *et al.*, 2015), the number required in each study arm to detect a 50% reduction in disease progression is 25. This is a feasible number to be recruited in the UK into a clinical therapeutic trial.

A limitation with measures of responsiveness is that they do not indicate if the change is meaningful. The minimum clinically significant difference (MCID) (Copay *et al.*, 2007) in fat fraction is yet to be determined. It remains important to include overall disease severity scores such as the CMTNSv2 and patient reported outcome measures in a clinical trial to confirm the longitudinal validity of change in MRI calf muscle fat fraction. Our research group has assessed this over 4 years in CMT1A and initial analysis shows promising results (Evans *et al.*, 2018). Furthermore, the reliability, validity and responsiveness of the MRC Centre MRI calf muscle fat fraction protocol used in this study has been confirmed in an independent cohort of CMT1A patients at a different site. Further analysis of a more proximal slice than that analysed in this study in those HSN1 patients with >70% FF and a more distal slice for those with <5% FF may result in higher responsiveness of MRI muscle fat fraction over the full range of disease severity.

In conclusion, calf muscle fat fraction, Hand-PPT and computerised myometric assessments of ankle plantarflexion and ankle inversion/eversion significantly changed over 1 year and

correlated with disease severity, patient reported HRQoL and disease duration. MRI determined calf muscle fat fraction was the most responsive (highly responsive) of these tests and looks very promising as an outcome measure to be used in therapeutic trials in HSN1.

6. Conclusion

HSN1 secondary to *SPTLC1/2* mutations is a rare neuropathy which causes profound sensory loss and variable but often severe motor deficits. Mutations in *SPTLC1/2*, which encode for separate subunits of the enzyme SPT, result in altering the enzyme's substrate specificity and the formation of atypical sphingolipids, 1-deoxySA and 1-deoxymethylSA, collectively referred to as 1-deoxySLs. Although various pathomechanisms of 1-deoxySL induced neurotoxicity have been proposed, the exact mechanism of how these atypical products cause nerve damage has not been established. Recent studies have suggested L-serine supplementation as a potential therapeutic agent (Garofalo *et al.*, 2011; Fridman *et al.*, 2019). An obstacle to undertaking a definite therapeutic trial of L-serine is the lack of responsive outcome measures.

In this thesis, I have investigated the pathomechanisms of HSN1 using two different in-vitro models. I have also performed a one-year natural history study of HSN1 secondary to *SPTLC1/2* mutations with the aim of identifying responsive outcome measures.

6.1 Mouse in-vitro model of HSN1

This model involved the application of exogeneous sphingolipids to primary motor neuron and DRG cultures from wild-type mice. 1-deoxySLs were found to have time dependent neurotoxic effects on both primary motor and sensory neurons, resulting in significant reduction in cell survival. Within the sensory neurons, 1-deoxySA was toxic to both NF200+ve neurons which are typically the large, myelinated neurons and the CGRP+ve neurons, which are the small peptidergic neurons. However, the CGRP+ve neurons appear to be more vulnerable to the toxicity which would be in keeping with the dissociated sensory loss characteristically seen in HSN1 patients whereby pain and temperature sensation are affected before large fibre mediated joint position sense and vibration. Both the canonical product of SPT, sphinganine and the atypical products, 1-deoxySLs had detrimental effects on sensory neuron neurite outgrowth. 1-deoxySA appears to be more neurotoxic than 1-deoxymethylSA.

These neurotoxic effects might be mediated by mitochondrial dysfunction and ER stress. Two hour treatment with 1-deoxySLs led to a reduction in mitochondrial membrane potential. Twenty-four hour treatment with 1-deoxySA led to reduced expression of PDI, an ER protein with multiple functions one of which includes acting as an ER chaperone. 1-deeoxymethylSA treatment however led to an increased expression of PDI. I further explored the effects of 1-deoxySLs on ER stress using SH-SY5Y cells. The complementary time dependent increases in the ER chaperones, PDI and BiP, and UPR stress sensors, PERK and IRE1α , suggest that 1-deoxySLs treatment induces early ER stress and subsequent initiation of the UPR.

This model, however, is not without limitations. The toxicity of 1-deoxySLs to developing neurons in culture does not reflect the slowly progressive sensory-motor neuropathy seen in HSN1 patients. One of the key limitations is that the sphingolipids were applied exogenously. Sphingolipid biosynthesis is highly compartmentalised and the 1-deoxySLs, especially their downstream metabolites, are highly hydrophobic. It is possible that endogenously produced sphingolipids may act via different pathomechanisms. The concentrations used in the study were based on the higher end of plasma 1-deoxySA concentrations detected in HSN1 patients. The levels of 1-deoxySLs in the CSF of HSN1 patients are not known, therefore these concentrations may not be physiological. It is not possible to sustain healthy primary cultures for prolonged periods (longer than two weeks) and hence effects of long-term treatment with low dose 1-deoxySLs cannot be evaluated. It is also not possible to assess therapeutic agents, such as L-serine supplementation, using this model.

6.2: Human iPSC derived model of HSN1

This model used iPSCs derived from HSN1 patient fibroblasts which have been differentiated into sensory neurons. With this model, it is possible to assess the effects of endogenously produced sphingolipids in a human cellular context with normal levels of expression of mutant SPTLC1. The iPSC derived sensory neurons can be maintained in culture for months which enables the detection of subtle, slowly developing phenotypes. Potential therapeutic agents can also be evaluated using this model.

It was possible to differentiate HSN1 patient derived iPSCs into sensory neurons. All the differentiated neurons expressed BRN3A, a canonical marker of sensory neurons, and NF200, a marker of large myelinated neurons in rodent DRG neurons. It is likely that the differentiation protocol resulted in the formation of mixed neuronal types consisting of nociceptors and non-nociceptors.

Initially, the effects of 1-deoxySL treatment on control iPSC derived sensory neurons were assessed. 1-deoxySLs were toxic to iPSC derived human sensory neurons with 1-deoxySA again being more damaging than 1-deoxymethylSA.

There was autonomous production of 1-deoxySLs in the HSN1 iPSC derived sensory neurons with the patient lines having significantly elevated levels of 1-deoxySA and its downstream metabolite, 1-deoxySO, compared to the control lines. There was early loss of HSN1 iPSC derived sensory neurons with relative stability of the surviving neurons over the next 2-3 months. There was no demonstrable difference in neurite outgrowth between the patient and control lines. There was also no gross alteration in the ER and mitochondrial ultrastructure in the patient lines. Functionally, there was no difference in the ER and mitochondrial calcium concentrations between the patient and control iPSC derived sensory neurons at 4-5months old. Clark *et al.* (2019), who have continued with this project, have shown electrophysiologically that HSN1 iPSC derived neurons are hyperexcitable. This could explain the lancinating pain experienced by almost all HSN1 patients.

Effects of long-term L-serine supplementation on cell survival was analysed in one differentiation. There was no significant difference in cell survival between patient and control lines. However, there was a trend towards improved cell survival with L-serine treatment in both groups with a dose dependent increase seen in the patient lines.

There are limitations with this model also. Genetic and epigenetic variability of the iPSCs is a concern in using iPSC derived cells to model diseases. The other major concern is the immaturity of the differentiated neurons, especially in modelling neurodegenerative diseases like HSN1. Further work needs to be done to compare these in-vitro generated neuronal cells to their putative counterparts in-vivo.

Despite these limitations, this model provides a unique opportunity to study the effects of endogenous sphingolipids in a human cellular model and to assess potential therapeutic

agents. The increased production of 1-deoxySLs by the HSN1 iPSC derived sensory neurons and the suggestion of correlation between the phenotypic features of these sensory neurons (levels of 1-deoxySL production, extent of early cell loss and degree of hyperexcitability) and the disease severity of the HSN1 patients they originated from, suggests this is a promising in-vitro model of HSN1.

Evidently there are pros and cons for these two in-vitro models. In addition, both models lack axo-glial interactions and it remains a challenge to model length dependent neuropathies using in-vitro cultures

6.3 Ideas for future research into understanding the pathomechanisms underlying HSN1

Using different models and obtaining similar findings across the models is a strong indicator that the underlying pathomechanism is a key contributor to the disease process.

With both models, co-culturing with schwann cells might enable the neurons to be maintained in culture for much longer periods (beyond a year for iPSC derived sensory neurons) and will provide an opportunity to study the effects of neuronally produced 1-deoxySLs on myelination. Protocols for co-culturing rodent primary motor neurons and DRG neurons with schwann cells are available (Hyung *et al.*, 2015; Sakai *et al.*, 2017). Human iPSC derived sensory neurons have been co-cultured with rat schwann cells (Clark *et al.*, 2017). Clark *et al*. (2019) have co-cultured HSN1 iPSC derived sensory neurons with rat schwann cells and provisional results show that myelination is disturbed in HSN1 neurons with overall reduction in myelin formation and prominent myelin blebbing. This phenotype was rescued with L-serine treatment.

Another area to study is the assessment of ER stress in older neurons (>6 months). RNA sequencing of HSN1 iPSC derived sensory neurons at different time points, for example young and mature neurons, could provide information about ER dysfunction and other pathways involved in the pathogenesis of HSN1. The finding that the HSN1 neurons are hyperexcitable suggests a possible channel involvement. The highly hydrophobic downstream metabolites of 1-deoxySA and 1-deoxymethylSA could associate together to

form rigid platforms, lipid rafts, which can trap receptors and ion channels. Investigating the effects on lipid rafts and associated proteins could be another avenue of future research. Tracking the intracellular localisation of endogenous 1-deoxySLs by labelling L-alanine in the media could provide information about which organelles/structures are involved in the pathogenicity.

With the iPSC derived sensory neuron model, it is possible to test therapeutic agents. The effects of long-term L-serine treatment on cell survival and neuronal excitability can be assessed. Cytochrome P450 enzymes have been proposed as possible mediators of 1-deoxySL catabolism. Cytochrome P450 enzymes, located intracellularly within the ER and mitochondria, are predominantly found in hepatocytes but can also be found in many other cells, including sensory neurons. Enhancers of these enzymes are therefore potential therapeutic agents that can be tested in the iPSC model.

Although the raised 1-deoxySLs in patients with type II diabetes and metabolic syndrome are secondary to metabolic disturbances, information gathered regarding modes of pathogenicity in these diseases can be used in HSN1 in-vitro models. In both HSN1 and diabetes, there is emerging consensus that it is the downstream metabolites of 1-deoxySA that are likely to be responsible for the toxicity rather than 1-deoxySA itself.

6.4: HSN1 Natural history study

Although HSN1 is sensory predominant, there was significant motor involvement in most patients. There was marked heterogeneity in the phenotype mainly due to differences between the sexes. The HSN1 males were generally more severely affected than females. In females, I found there was a spectrum ranging from a phenotype similar to that found in males to one consisting of late onset and slower disease progression. There is moderate correlation between clinical severity and plasma 1-deoxySL levels. However, the differences between the sexes cannot be accounted for by differences in levels of 1-deoxySLs.

Various assessments were used in the natural history study to capture the spectrum of deficits noted in our HSN1 patients. These included CMTNSv2, comprehensive nerve conduction studies, quantitative sensory testing, intra-epidermal nerve fibre density (upper

thigh), computerised myometry, MRI determined proximal calf fat fraction and patient based questionnaires (Neuropathic Pain Symptom Inventory and SF-36v2).

Due to the heterogeneity in the cohort, many of the assessments used were limited by both floor and ceiling effects, especially assessment of sensory deficits (quantitative sensory testing and intra-epidermal nerve fibre density assessments). Calf muscle fat fraction, Hand-pressure pain threshold and computerised assessments of ankle plantarflexion and ankle inversion/eversion significantly changed over 1 year and correlated with disease severity, patient reported HRQoL and disease duration. As HSN1 is a rare disease thereby severely limiting the potential size of any clinical trial, outcome measures optimised for maximum responsiveness are required. MRI determined calf fat fraction, which was highly responsive, was the most responsive of these outcome measures. The responsiveness can be further increased if we select patients with baseline overall calf muscle fat fraction of 5-70% such that the number required in each study arm of a clinical trial designed to a detect a 50% reduction in disease progression is 25. This is a feasible number of HSN1 patients to be recruited into a clinical trial in the UK. MRI determined calf fraction, therefore, is a promising outcome measure that can be used in therapeutic trials in HSN1.

6.5 Potential other outcome measures to consider in HSN1

Corneal confocal microscopy is a non-invasive ophthalmology imaging technique which allows in-vivo examination of unmyelinated C-fibres of the cornea. There is an emerging body of evidence that corneal nerve fibre density (CNFD) correlates with intra-epidermal nerve fibre density and quantitative sensory testing in patients with diabetic peripheral neuropathy (Petropoulos *et al.*, 2018). Since there is early, small sensory fibre involvement in HSN1, corneal confocal microscopy could be a potential outcome measure in HSN1.

As the minimum clinically significant difference (MCID) in fat fraction is yet to determined, it is important to include patient reported outcome measures to confirm the clinical validity of change in MRI calf fat fraction. The recently published CMT specific patient reported outcome measure, CMT Health Index (CMTHI) could be useful in clinical trials in HSN1 but needs to be evaluated longitudinally (Johnson *et al.*, 2018).

6.6 Final remarks

In this thesis, I have developed a human in-vitro model of HSN1 that allows the evaluation of the effects of endogenous 1-deoxySLs.This model will also be useful in screening for therapeutic agents in HSN. In both the mouse and human neuronal in-vitro models, 1-deoxysSLs have been shown to be toxic and HSN1 iPSC derived sensory neurons have significantly elevated levels of 1-deoxySLs. These observations provide further theoretical support for the potential therapeutic use of L-serine supplementation in HSN1 patients. There is marked heterogeneity in the HSN1 phenotype, mainly due to differences between the sexes. Despite this heterogeneity, MRI determined calf fat was found to be highly responsive over one year. By selecting patients with 5-70% overall calf fat fraction, the responsiveness is sufficient to require only a small, feasible number of patients to be recruited into a clinical trial in HSN1. There is scope to include all patients in a clinical trial by using thigh and distal calf slices for very severely and mildly affected patients respectively. This thesis has brought us closer to the goal of a definitive therapeutic trial of L-serine supplementation in our UK HSN1 population.

References

Aboualizadeh, E., Mattson, E. C., O'Hara, C. L., Smith, A. K., Stucky, C. L. and Hirschmugl, C. J. (2015) 'Cold shock induces apoptosis of dorsal root ganglion neurons plated on infrared windows', *The Analyst*. Royal Society of Chemistry, 140(12), pp. 4046–4056.

Alecu, I., Othman, A., Penno, A., Saied, E. M., Arenz, C., von Eckardstein, A. and Hornemann, T. (2017) 'Cytotoxic 1-Deoxysphingolipids Are Metabolized by a Cytochrome P450-Dependent Pathway', *Journal of Lipid Research*, 58, pp. 60–71.

Alecu, I., Tedeschi, A., Behler, N., Wunderling, K., Lamberz, C., Lauterbach, M. A. R., Gaebler, A., Ernst, D., Van Veldhoven, P. P., Al-Amoudi, A., Latz, E., Othman, A., Kuerschner, L., Hornemann, T., Bradke, F., Thiele, C. and Penno, A. (2017) 'Localization of 1-deoxysphingolipids to mitochondria induces mitochondrial dysfunction', *Journal of Lipid Research*, 58(1), pp. 42–59.

Ali Khan, H. and Mutus, B. (2014) 'Protein disulfide isomerase a multifunctional protein with multiple physiological roles', *Frontiers in Chemistry*, 2(August), pp. 1–9.

American Association of Electrodiagnostic Medicine (2002) 'Practice parameter for electrodiagnostic studies in carpal tunnel syndrome: summary statement.', *Muscle & nerve*, 25(6), pp. 918–22.

Aquilonius, S., Askmark, H., Gillberg, P., Nandedkar, S., Olsson, Y. and Stalberg, E. (1984) 'Topographical localisation of motor endplates in cryosections of whole human muscles', *Muscle and Nerve*, 7(4), pp. 287–93.

Auer-Grumbach, M. (2008) 'Hereditary sensory neuropathy type I.', *Orphanet journal of rare diseases*, 3(Hsn I), p. 7.

Auer-Grumbach, M., Bode, H., Pieber, T. R., Schabhüttl, M., Fischer, D., Seidl, R., Graf, E., Wieland, T., Schuh, R., Vacariu, G., Grill, F., Timmerman, V., Strom, T. M. and Hornemann, T. (2013) 'Mutations at Ser331 in the HSN type I gene SPTLC1 are associated with a distinct syndromic phenotype', *European Journal of Medical*

Genetics, 56(5), pp. 266–269.

Auer-Grumbach, M., De Jonghe, P., Verhoeven, K., Timmerman, V., Wagner, K., Hartung, H. and Nicholson, G. (2003) 'Autosomal dominant inherited neuropathies with prominent sensory loss and mutilations: a review', *Archives of Neurology*, 60(3), pp. 329–34.

Auranen, M., Toppila, J., Suriyanarayanan, S., Lone, M. A., Paetau, A., Tyynismaa, H., Hornemann, T. and Ylikallio, E. (2017) 'Clinical and metabolic consequences of L-serine supplementation in hereditary sensory and autonomic neuropathy type 1C', *Cold Spring Harb Mol Case Stud*, 3(6), p. a002212.

Barabas, M. E., Mattson, E. C., Aboualizadeh, E., Hirschmugl, C. J. and Stucky, C. L. (2014) 'Chemical structure and morphology of dorsal root Ganglion neurons from naive and inflamed mice', *Journal of Biological Chemistry*, 289(49), pp. 34241–34249.

Bejaoui, K., Uchida, Y., Yasuda, S., Ho, M., Nishijima, M., Brown, R. H., Holleran, W. M. and Hanada, K. (2002) 'Hereditary sensory neuropathy type 1 mutations confer dominant negative effects on serine palmitoyltransferase , critical for sphingolipid synthesis', *Journal of Clinical Investigation*, 110(9), pp. 1301–1308.

Bejaoui, K., Wu, C., Scheffler, M. D., Haan, G., Ashby, P., Wu, L., De Jong, P. and Brown, R. H. (2001) 'SPTLC1 is mutated in hereditary sensory neuropathy, type 1.', *Nature Genetics*, 27(3), pp. 261–262.

Bertea, M., Rütti, M. F., Othman, A., Marti-Jaun, J., Hersberger, M., von Eckardstein, A. and Hornemann, T. (2010) 'Deoxysphingoid bases as plasma markers in diabetes mellitus.', *Lipids in health and disease*, 9, p. 84.

Blair, I. P., Dawkins, J. L. and Nicholson, G. A. (1997) 'Fine mapping of the hereditary sensory neuropathy type I locus on chromosome 9q22.1-->q22.3: exclusion of GAS1 and XPA.', *Cytogenetics and cell genetics*, 78(2), pp. 140–4.

Blanchard, J. W., Eade, K. T., Szűcs, A., Lo Sardo, V., Tsunemoto, R. K., Williams, D., Sanna, P. P. and Baldwin, K. K. (2015) 'Selective conversion of fibroblasts into peripheral sensory neurons', *Nature Neuroscience*, 18(1), pp. 25–35.

Bode, H., Bourquin, F., Suriyanarayanan, S., Wei, Y., Alecu, I., Othman, A., Von Eckardstein, A. and Hornemann, T. (2016) 'HSAN1 mutations in serine palmitoyltransferase reveal a close structure-function-phenotype relationship', *Human Molecular Genetics*, 25(5), pp. 853–865.

Bonati, U., Hafner, P., Schädelin, S., Schmid, M., Naduvilekoot Devasia, A., Schroeder, J., Zuesli, S., Pohlman, U., Neuhaus, C., Klein, A., Sinnreich, M., Haas, T., Gloor, M., Bieri, O., Fischmann, A. and Fischer, D. (2015) 'Quantitative muscle MRI: A powerful surrogate outcome measure in Duchenne muscular dystrophy', *Neuromuscular Disorders*, 25(9), pp. 679–685.

Bouhassira, D., Attal, N., Fermanian, J., Alchaar, H., Gautron, M., Masquelier, E., Rostaing, S., Lanteri-Minet, M., Collin, E., Grisart, J. and Boureau, F. (2004) 'Development and validation of the Neuropathic Pain Symptom Inventory.', *Pain*, 108(3), pp. 248–57.

Bouhouche, a, Benomar, a, Bouslam, N., Chkili, T. and Yahyaoui, M. (2006) 'Mutation in the epsilon subunit of the cytosolic chaperonin-containing t-complex peptide-1 (Cct5) gene causes autosomal recessive mutilating sensory neuropathy with spastic paraplegia.', *Journal of medical genetics*, 43(5), pp. 441–3.

Braunholtz, D. A., Edwards, S. J. L. and Lilford, R. J. (2001) 'Are randomized clinical trials good for us (in the short term)? Evidence for a "trial effect"', *Journal of Clinical Epidemiology*, 54(3), pp. 217–224.

Brazier, E., Harper, R., Jones, N. M. B., Cathain, A. O., Thomas, K. J., Usherwood, T. and Westlake, L. (1992) 'Validating the SF-36 health survey questionnaire : new outcome', *British Medical Journal*, 305(8), pp. 160–164.

Brennand, K. J. (2013) 'Inducing cellular aging: Enabling neurodegeneration-in-a-dish', *Cell Stem Cell*, 13(6), pp. 635–636.

Breslow, D. K., Collins, S. R., Bodenmiller, B., Aebersold, R., Simons, K., Shevchenko, A., Ejsing, C. S. and Weissman, J. S. (2010) 'Orm family proteins mediate sphingolipid homeostasis.', *Nature*, 463(7284), pp. 1048–53.

van de Bunt, M., Lako, M., Barrett, A., Gloyn, A. L., Hansson, M., McCarthy, M. I., Beer, N. L. and Honoré, C. (2016) 'Insights into islet development and biology through

characterization of a human iPSC-derived endocrine pancreas model', *Islets*. Taylor & Francis, 8(3), pp. 83–95.

Burkel, W. E. (1967) 'The Histological Fine Structure of Perineurium', *Anat Rec*, 158(2), pp. 177–189.

Burkhardt, M. F. *et al.* (2013) 'A cellular model for sporadic ALS using patient-derived induced pluripotent stem cells', *Molecular and Cellular Neuroscience*, 56, pp. 355–364.

Burns, J., Ouvrier, R., Estilow, T., Shy, R., Laurá, M., Pallant, J. F., Lek, M., Muntoni, F., Reilly, M. M., Pareyson, D., Acsadi, G., Shy, M. E. and Finkel, R. S. (2012) 'Validation of the Charcot-Marie-Tooth disease pediatric scale as an outcome measure of disability', *Annals of Neurology*, 71(5), pp. 642–652.

Van Campenhout, A. and Molenaers, G. (2011) 'Localization of the motor endplate zone in human skeletal muscles of the lower limb: Anatomical guidelines for injection with botulinum toxin', *Developmental Medicine and Child Neurology*, 53(2), pp. 108–119.

Camu, W. and Henderson, C. (1992) 'Purification of embryonic rat motoneurons by panning on a monoclonal antibody to the low-affinity NGF receptor', *Journal of neuroscience methods*, 44, pp. 59–70.

Cantalupo, A., Zhang, Y., Kothiya, M., Galvani, S., Obinata, H., Bucci, M., Giordano, F., Jiang, X., Hla, T. and Di Lorenzo, A. (2015) 'Nogo-B regulates endothelial sphingolipid homeostasis to control vascular function and blood pressure', *Nature Medicine*, 21(9), pp. 1028–1037.

Cao, L *et al.* (2016) 'Pharmacological reversal of a pain phenotype in iPSC-derived sensory neurons and patients with inherited erythromelalgia', *Science Translational Medicine*, 8(335), p. 335ra56.

Cao, S. S. and Kaufman, R. (2013) 'Unfolded Protein Response', *Current Biology*, 13(16), pp. 622–626.

Carreras-Sureda, A., Pihán, P. and Hetz, C. (2018) 'Calcium signaling at the endoplasmic reticulum: Fine-tuning stress responses', *Cell Calcium*, 70, pp. 24–31.

Carter, G., Jensen, M., Galer, B., Kraft, G., Crabtree, L., Beardsley, R., Abresch, R. and Bird, T. (1998) 'Neuropathic pain in Charcot-Marie-Tooth disease.', *Arch Phys Med Rehabil*, 79(12), pp. 1560–4.

Chai, S., George, A. L. and Deschênes, I. (2018) 'Physiological genomics identifies genetic modifiers of long QT syndrome type 2 severity The Journal of Clinical Investigation', *J Clin Invest*, 128(3), pp. 1043–1056.

Chambers, S. M., Qi, Y., Mica, Y., Lee, G., Zhang, X.-J., Niu, L., Bilsland, J., Cao, L., Stevens, E., Whiting, P., Shi, S.-H. and Studer, L. (2012) 'Combined small-molecule inhibition accelerates developmental timing and converts human pluripotent stem cells into nociceptors.', *Nature biotechnology*, 30(7), pp. 715–20.

Chang, W., Berta, T., Kim, Y. H., Lee, S., Lee, S. Y. and Ji, R. R. (2018) 'Expression and Role of Voltage-Gated Sodium Channels in Human Dorsal Root Ganglion Neurons with Special Focus on Nav1.7, Species Differences, and Regulation by Paclitaxel', *Neuroscience Bulletin*, 34(1), pp. 4–12.

Chen, Y.-C. *et al.* (2015) 'Transcriptional regulator PRDM12 is essential for human pain perception.', *Nature genetics*, 47(7), pp. 803–8.

Clark, A. J., Kaller, M. S., Galino, J., Willison, H. J., Rinaldi, S. and Bennett, D. L. H. (2017) 'Co-cultures with stem cell-derived human sensory neurons reveal regulators of peripheral myelination', *Brain*, 140(4), pp. 898–913.

Clark, A., Kugathasan, U., Blesneac, I., Reilly, M. and Bennett, D. (2019) 'Investigating the pathophysiology of Hereditary Sensoary Neuropathy Type 1 (HSN1) using human iPSC derived sensory neurons', in *The Challenge of Chronic Pain*

Colomban, C., Micallef, J., Lefebvre, M. N., Dubourg, O., Gonnaud, P. M., Stojkovic, T., Jouve, E., Blin, O., Pouget, J. and Attarian, S. (2014) 'Clinical spectrum and gender differences in a large cohort of Charcot-Marie-Tooth type 1A patients', *Journal of the Neurological Sciences*, 336(1–2), pp. 155–160.

Copay, A. G., Subach, B. R., Glassman, S. D., Polly, D. W. and Schuler, T. C. (2007) 'Understanding the minimum clinically important difference: a review of concepts and methods.', *The spine journal : official journal of the North American Spine Society*,

7(5), pp. 541–6.

Cornacchia, D. and Studer, L. (2017) ‘Back and forth in time: Directing age in iPSC-derived lineages’, *Brain Research*, 1656, pp. 14–26..

Cuadros, R., Montejo De Garcini, E., Wandosell, F., Faircloth, G., Fernández-Sousa, J. M. and Avila, J. (2000) ‘The marine compound spisulosine, an inhibitor of cell proliferation, promotes the disassembly of actin stress fibers’, *Cancer Letters*, 152(1), pp. 23–29.

D’Amelio, M., Cavallucci, V. and Cecconi, F. (2010) ‘Neuronal caspase-3 signaling: Not only cell death’, *Cell Death and Differentiation*, 17(7), pp. 1104–1114.

Dart, C. (2010) ‘Lipid microdomains and the regulation of ion channel function’, *Journal of Physiology*, 588(17), pp. 3169–3178.

Davidson, G. L. *et al.* (2012) ‘Frequency of mutations in the genes associated with hereditary sensory and autonomic neuropathy in a UK cohort.’, *Journal of neurology*, 259(8), pp. 1673–85.

Davis-dusenbery, B. N., Williams, L. A., Klim, J. R. and Eggan, K. (2014) ‘How to make spinal motor neurons’, *Development*, 141, pp. 491–501.

Davis, D., Kannan, M. and Wattenberg, B. (2018) ‘Orm/ORMDL proteins: Gate guardians and master regulators’, *Advances in Biological Regulation*, 70(August), pp. 3–18.

Davis, D. L., Gable, K., Suemitsu, J., Dunn, T. M. and Wattenberg, B. W. (2019) ‘The ORMDL/Orm–serine palmitoyltransferase (SPT) complex is directly regulated by ceramide: Reconstitution of SPT regulation in isolated membranes’, *Journal of Biological Chemistry*, 294(13), pp. 5146–5156.

Dawkins, J. L., Hulme, D. J., Brahmbhatt, S. B., Auer-Grumbach, M. and Nicholson, G. a (2001) ‘Mutations in SPTLC1, encoding serine palmitoyltransferase, long chain base subunit-1, cause hereditary sensory neuropathy type I.’, *Nature Genetics*, 27(3), pp. 309–312.

Dedov, V. N., Dedova, I. V, Merrill, A. H. and Nicholson, G. a (2004) ‘Activity of partially inhibited serine palmitoyltransferase is sufficient for normal sphingolipid metabolism

and viability of HSN1 patient cells.', *Biochimica et biophysica acta*, 1688(2), pp. 168–75.

Deniaud, A., Sharaf El Dein, O., Maillier, E., Poncet, D., Kroemer, G., Lemaire, C. and Brenner, C. (2008) 'Endoplasmic reticulum stress induces calcium-dependent permeability transition, mitochondrial outer membrane permeabilization and apoptosis', *Oncogene*, 27(3), pp. 285–299.

Denny-Brown, D. (1951) 'Hereditary sensory radicular neuropathy', *J NeurolNeurosurg Psychiatry*, 14, pp. 237–52.

Dickson, R. C., Lester, R. L. and Nagiec, M. M. (2000) 'Serine palmitoyltransferase.', *Methods in enzymology*, 311, pp. 3–9.

Dimos, J. T., Rodolfa, K. T., Niakan, K. K., Weisenthal, L. M., Mitsumoto, H., Chung, W., Croft, G. F., Saphier, G., Leibel, R., Goland, R., Wichterle, H., Henderson, C. E. and Eggan, K. (2008) 'Induced pluripotent stem cells generated from patients with ALS can be differentiated into motor neurons. TL - 321', *Science*, 321 VN-(5893), pp. 1218–1221.

Dohrn, M. F., Othman, A., Hirshman, S. K., Bode, H., Alecu, I., Fähndrich, E., Karges, W., Weis, J., Schulz, J. B., Hornemann, T. and Claeys, K. G. (2015) 'Elevation of plasma 1-deoxy-sphingolipids in type 2 diabetes mellitus: A susceptibility to neuropathy?', *European Journal of Neurology*, 22(5), pp. 806–814.

Duan, J. and Merrill, A. H. (2015) '1-deoxysphingolipids encountered exogenously and made de novo: Dangerous mysteries inside an enigma', *Journal of Biological Chemistry*, 290(25), pp. 15380–15389.

Dubourg, O., Barhoumi, C., Azzedine, H., Birouk, N., Brice, A., Bouche, P. and Leguern, E. (2000) 'Phenotypic and genetic study of a family with hereditary sensory neuropathy and prominent weakness', *Muscle & nerve*, 23(10), pp. 1508–1514.

Dyck, P. (1975) 'Peripheral neuropathy', in Dyck, P., Thomas, P., and Lambert, E. (eds). Philadelphia: W.B. Saunders, pp. 825–867.

Dyck, P., Thomas, P., Griffin, J., Low, P. and Poduslo, J. (1993) 'Peripheral Neuropathy', in

Dyck, P., PK, T., JW, G., PA, L., and Poduslo, J. (eds). Philadelphia: W.B. Saunders, pp. 1051–64.

Eberhardt, E., Havlicek, S., Schmidt, D., Link, A. S., Neacsu, C., Kohl, Z., Hampl, M., Kist, A. M., Klinger, A., Nau, C., Schüttler, J., Alzheimer, C., Winkler, J., Namer, B., Winner, B. and Lampert, A. (2015) 'Pattern of Functional TTX-Resistant Sodium Channels Reveals a Developmental Stage of Human iPSC- and ESC-Derived Nociceptors', *Stem Cell Reports*, 5(3), pp. 305–313.

van Echten-Deckert, G., Zschoche, a., Bar, T., Schmidt, R. R., Raths, a., Heinemann, T. and Sandhoff, K. (1997) 'cis-4-Methylsphingosine Decreases Sphingolipid Biosynthesis by Specifically Interfering with Serine Palmitoyltransferase Activity in Primary Cultured Neurons', *Journal of Biological Chemistry*, 272(25), pp. 15825–15833.

Edvardson, S., Cinnamon, Y., Jalas, C., Shaag, A., Maayan, C., Axelrod, F. B. and Elpeleg, O. (2012) 'Hereditary sensory autonomic neuropathy caused by a mutation in dystonin.', *Annals of neurology*, 71(4), pp. 569–72.

Eichinger, K., Burns, J., Cornett, K., Bacon, C., Shepherd, M. L., Mountain, J., Sowden, J., Shy, R., Shy, M. E. and Herrmann, D. N. (2018) 'The Charcot-Marie-Tooth Functional Outcome Measure (CMT-FOM)', *Neurology*, 91(15), pp. e1381–e1384.

Eichler, F. S. *et al.* (2009) 'Overexpression of the wild-type SPT1 subunit lowers desoxysphingolipid levels and rescues the phenotype of HSAN1.', *The Journal of neuroscience : the official journal of the Society for Neuroscience*, 29(46), pp. 14646–51.

Einarsdottir, E., Carlsson, A., Minde, J., Toolanen, G., Svensson, O., Solders, G., Holmgren, G., Holmberg, D. and Holmberg, M. (2004) 'A mutation in the nerve growth factor beta gene (NGFB) causes loss of pain perception.', *Human molecular genetics*, 13(8), pp. 799–805.

Ernsberger, U. (2009) 'Role of neurotrophin signalling in the differentiation of neurons from dorsal root ganglia and sympathetic ganglia.', *Cell and tissue research*, 336(3), pp. 349–84.

Ernst, D., Murphy, S. M., Sathiyanadan, K., Wei, Y., Othman, A., Laurá, M., Liu, Y.-T. T., Penno, A., Blake, J., Donaghy, M., Houlden, H., Reilly, M. M. and Hornemann, T. (2015) 'Novel HSAN1 Mutation in Serine Palmitoyltransferase Resides at a Putative Phosphorylation Site That Is Involved in Regulating Substrate Specificity.', *NeuroMolecular Medicine*, 17(1), pp. 47–57.

Esaki, K., Sayano, T., Sonoda, C., Akagi, T., Suzuki, T., Ogawa, T., Okamoto, M., Yoshikawa, T., Hirabayashi, Y. and Furuya, S. (2015) 'L-serine deficiency elicits intracellular accumulation of cytotoxic deoxysphingolipids and lipid body formation', *Journal of Biological Chemistry*, 290(23), pp. 14595–14609.

Evans, M., Morrow, J., Wastling, S., Sinclair, C., Fischmann, A., Shah, S., Emira, A., Hanna, M., Yousry, T., Thornton, J. and Reilly, M. (2018) 'MRI quantification of intramuscular fat accumulation in CMT1A: four year follow up data', in *Peripheral Nerve Society Annual Meeting*, p. 160.

Ferreira, C. R., Goorden, S. M. I., Soldatos, A., Byers, H. M., Ghauharali-van der Vlugt, J. M. M., Beers-Stet, F. S., Groden, C., van Karnebeek, C. D., Gahl, W. A., Vaz, F. M., Jiang, X. and Vernon, H. J. (2018) 'Deoxysphingolipid precursors indicate abnormal sphingolipid metabolism in individuals with primary and secondary disturbances of serine availability', *Molecular Genetics and Metabolism*, 124(3), pp. 204–209.

Fischer, D., Schabhüttl, M., Wieland, T., Windhager, R., Strom, T. M. and Auer-Grumbach, M. (2014) 'A novel missense mutation confirms ATL3 as a gene for hereditary sensory neuropathy type 1.', *Brain*, 137(Pt 7), p. e286.

Fischmann, A., Morrow, J. M., Sinclair, C. D. J., Reilly, M. M., Hanna, M. G., Yousry, T. and Thornton, J. S. (2014) 'Improved anatomical reproducibility in quantitative lower-limb muscle MRI', *Journal of Magnetic Resonance Imaging*, 39(4), pp. 1033–1038.

Flaxman, T. E., Smith, A. J. J. and Benoit, D. L. (2014) 'Sex-related differences in neuromuscular control: Implications for injury mechanisms or healthy stabilisation strategies?', *Journal of Orthopaedic Research*, 32(2), pp. 310–317.

Fridman, V., Oaklander, A., David, W., Johnson, E., Pan, J., Novak, P., Brown, R. J. and Eichler, F. (2015) 'Natural History and Biomarkers in Hereditary Sensory Neuropathy

Type 1', *Muscle & nerve*, 51(4), pp. 489–95.

Fridman, V. and Reilly, M. M. (2015) 'Inherited Neuropathies', *Semin Neurol*, 35(4), pp. 407–23.

Fridman, V., Suriyanarayanan, S., Novak, P. and David, W. (2019) 'Randomized trial of L - serine in patients with hereditary sensory and autonomic neuropathy type 1', *Neurology*, 92(4), pp. e359–e370.

Fu, X.-M., Wang, P. and Zhu, B. T. (2011) 'Characterization of the Estradiol-Binding Site Structure of Human Protein Disulfide Isomerase (PDI)', *PLoS ONE*, 6(11), p. e27185.

Gable, K. (2000) 'Tsc3p Is an 80-Amino Acid Protein Associated with Serine Palmitoyltransferase and Required for Optimal Enzyme Activity', *Journal of Biological Chemistry*, 275(11), pp. 7597–7603.

Gable, K., Gupta, S. D., Han, G., Niranjanakumari, S., Harmon, J. M. and Dunn, T. M. (2010) 'A disease-causing mutation in the active site of serine palmitoyltransferase causes catalytic promiscuity', *Journal of Biological Chemistry*, 285(30), pp. 22846–22852.

Gable, K., Han, G., Monaghan, E., Bacikova, D., Natarajan, M., Williams, R. and Dunn, T. M. (2002) 'Mutations in the yeast LCB1 and LCB2 genes, including those corresponding to the hereditary sensory neuropathy type I mutations, dominantly inactivate serine palmitoyltransferase.', *The Journal of biological chemistry*, 277(12), pp. 10194–200.

Gagliostro, V., Casas, J., Caretti, A., Abad, J. L., Tagliavacca, L., Ghidoni, R., Fabrias, G. and Signorelli, P. (2012) 'Dihydroceramide delays cell cycle G1/S transition via activation of ER stress and induction of autophagy', *International Journal of Biochemistry and Cell Biology*, 44(12), pp. 2135–2143.

García de Yébenes Prous, M. J., Salvanés, F. R. and Ortells, L. C. (2008) 'Responsiveness of Outcome Measures', *Reumatología Clínica (English Edition)*, 4(6), pp. 240–247.

Garofalo, K., Penno, A., Schmidt, B. P., Lee, H., Frosch, M. P., Eckardstein, A. Von, Brown,

R. H., Hornemann, T. and Eichler, F. S. (2011) ‘Oral l -serine supplementation reduces production of neurotoxic deoxysphingolipids in mice and humans with hereditary sensory autonomic neuropathy type 1’, *The Journal of Clinical Investigation*, pp. 14–16.

Geraldes, R., de Carvalho, M., Santos-Bento, M. and Nicholson, G. (2004) ‘Hereditary sensory neuropathy type 1 in a Portuguese family-electrodiagnostic and autonomic nervous system studies.’, *Journal of the neurological sciences*, 227(1), pp. 35–8.

Gess, B., Baets, J., De Jonghe, P., Reilly, M., Pareyson, D. and Young, P. (2015) ‘Ascorbic acid for the treatment of Charcot-Marie-Tooth disease (Review)’, *Cochrane Database of Systematic Reviews*, (12).

Geuna, S., Raimondo, S., Ronchi, G., Scipio, F. Di, Tos, P., Czaja, K. and Fornaro, M. (2009) ‘Histology of the peripheral nerve and changes occurring during nerve regeneration’, *International Review of Neurobiology*. 1st edn. Elsevier Inc., 87(09), pp. 27–46.

Glover, G. H. and Schneider, E. (1991) ‘Three-Point Dixon Technique for True Water / Fat Decomposition with Bo Inhomogeneity Correction’, *Magnetic resonance in medicine*, 18, pp. 371–383.

Gorden, D. L. *et al.* (2015) ‘Biomarkers of NAFLD progression: a lipidomics approach to an epidemic’, *Journal of Lipid Research*, 56(3), pp. 722–736.

Görlach, A., Bertram, K., Hudecova, S. and Krizanova, O. (2015) ‘Calcium and ROS: A mutual interplay’, *Redox Biology*, 6, pp. 260–271.

Gould, T. and Oppenheim, R. (2011) ‘Motor Neuron Trophic Factors : Therapeutic Use in ALS ?’, *Brain Res Rev*, 67(1–2), pp. 1–39.

Guelly, C. *et al.* (2011) ‘Targeted high-throughput sequencing identifies mutations in atlastin-1 as a cause of hereditary sensory neuropathy type I.’, *American journal of human genetics*, 88(1), pp. 99–105.

Güntert, T., Hänggi, P., Othman, A., Suriyanarayanan, S., Sonda, S., Zuellig, R. A., Hornemann, T. and Ogunshola, O. O. (2016) ‘1-Deoxysphingolipid-induced

neurotoxicity involves N-methyl-D-aspartate receptor signaling', *Neuropharmacology*, 110, pp. 211–222.

Gururaj, C., Federman, R. and Chang, A. (2013) 'Orm proteins integrate multiple signals to maintain sphingolipid homeostasis.', *The Journal of biological chemistry*, 288(28), pp. 20453–63.

Hall, A. K. (2006) 'Rodent sensory neuron culture and analysis.', *Current protocols in Neurosci*, Chapter 3(Unit 3), p. 19.

Han, C., Huang, J. and Waxman, S. (2016) 'Sodim channel Nav1.8: Emerging links to human disease', *Neurology*, 86(5), pp. 473–83.

Han, G., Gable, K., Yan, L., Natarajan, M., Krishnamurthy, J., Gupta, S. D., Borovitskaya, A., Harmon, J. M. and Dunn, T. M. (2004) 'The topology of the Lcb1p subunit of yeast serine palmitoyltransferase.', *The Journal of biological chemistry*, 279(51), pp. 53707–16.

Han, G., Gupta, S. D., Gable, K., Niranjanakumari, S., Moitra, P., Eichler, F., Brown, R. H., Harmon, J. M. and Dunn, T. M. (2009) 'Identification of small subunits of mammalian serine palmitoyltransferase that confer distinct acyl-CoA substrate specificities.', *Proceedings of the National Academy of Sciences of the United States of America*, 106(20), pp. 8186–91.

Han, S., Lone, M. a, Schneiter, R. and Chang, A. (2010) 'Orm1 and Orm2 are conserved endoplasmic reticulum membrane proteins regulating lipid homeostasis and protein quality control.', *Proceedings of the National Academy of Sciences of the United States of America*, 107(13), pp. 5851–6.

Hanada, K. (2003) 'Serine palmitoyltransferase, a key enzyme of sphingolipid metabolism', *Biochimica et Biophysica Acta (BBA) - Molecular and Cell Biology of Lipids*, 1632(1–3), pp. 16–30.

Hanada, K., Hara, T. and Nishijima, M. (2000) 'Purification of the serine palmitoyltransferase complex responsible for sphingoid base synthesis by using affinity peptide chromatography techniques.', *The Journal of biological chemistry*, 275(12), pp. 8409–15.

Handel, A. E., Chintawar, S., Lalic, T., Whiteley, E., Vowles, J., Giustacchini, A., Argoud, K., Sopp, P., Nakanishi, M., Bowden, R., Cowley, S., Newey, S., Akerman, C., Ponting, C. P. and Cader, M. Z. (2016) 'Assessing similarity to primary tissue and cortical layer identity in induced pluripotent stem cell-derived cortical neurons through single-cell transcriptomics', *Human Molecular Genetics*, 25(5), pp. 989–1000.

Hannun, Y. a and Obeid, L. M. (2008) 'Principles of bioactive lipid signalling: lessons from sphingolipids.', *Nature reviews. Molecular cell biology*, 9(2), pp. 139–50.

Harding, A. E. and Thomas, P. K. (1980) 'The clinical features of hereditary motor and sensory neuropathy types I and II', *Brain*, 103, pp. 259–280.

Hartfield, E. M., Yamasaki-Mann, M., Ribeiro Fernandes, H. J., Vowles, J., James, W. S., Cowley, S. A. and Wade-Martins, R. (2014) 'Physiological characterisation of human iPS-derived dopaminergic neurons', *PLoS ONE*, 9(2), p. e87388.

Hashimoto, R., Koike, H., Takahashi, M., Ohyama, K., Kawagashira, Y., Iijima, M. and Sobue, G. (2015) 'Uncompacted myelin lamellae and nodal ion channel disruption in POEMS syndrome', *Journal of Neuropathology and Experimental Neurology*, 74(12), pp. 1127–1136.

Hicks, E. (1922) 'Hereditary perforating ulcer of the foot', *Lancet*, pp. 319–21.

Higa, A., Taouji, S., Lhomond, S., Jensen, D., Fernandez-Zapico, M. E., Simpson, J. C., Pasquet, J.-M., Schekman, R. and Chevet, E. (2014) 'Endoplasmic Reticulum Stress-Activated Transcription Factor ATF6 Requires the Disulfide Isomerase PDIA5 To Modulate Chemoresistance', *Molecular and Cellular Biology*, 34(10), pp. 1839–1849. Available at: http://mcb.asm.org/cgi/doi/10.1128/MCB.01484-13.

Hojjati, M. R., Li, Z. and Jiang, X.-C. (2005) 'Serine palmitoyl-CoA transferase (SPT) deficiency and sphingolipid levels in mice.', *Biochimica et biophysica acta*, 1737(1), pp. 44–51. Available at: http://www.ncbi.nlm.nih.gov/pubmed/16216550 (Accessed: 1 January 2015).

Hornemann, T., Alecu, I., Hagenbuch, N., Zhakupova, A., Cremonesi, A., Gautschi, M., Jung, H. H., Meienberg, F., Bilz, S., Christ, E., Baumgartner, M. R. and Hochuli, M. (2018) 'Disturbed sphingolipid metabolism with elevated 1-deoxysphingolipids in

glycogen storage disease type I – A link to metabolic control', *Molecular Genetics and Metabolism*, 125(1–2), pp. 73–78.

Hornemann, T., Penno, A. and von Eckardstein, A. (2008) 'The accumulation of two atypical sphingolipids cause hereditary sensory neuropathy type 1 (HSAN1)', *Chem Phys Lipids*, 154S, p. S62.

Hornemann, T., Penno, A., Richard, S., Nicholson, G., van Dijk, F. S., Rotthier, A., Timmerman, V. and von Eckardstein, A. (2009) 'A systematic comparison of all mutations in hereditary sensory neuropathy type I (HSAN I) reveals that the G387A mutation is not disease associated.', *Neurogenetics*, 10(2), pp. 135–43.

Hornemann, T., Penno, A., Rütti, M. F., Ernst, D., Kivrak-Pfiffner, F., Rohrer, L. and von Eckardstein, A. (2009) 'The SPTLC3 subunit of serine palmitoyltransferase generates short chain sphingoid bases.', *The Journal of biological chemistry*, 284(39), pp. 26322–30.

Hornemann, T., Richard, S., Rütti, M. F., Wei, Y. and von Eckardstein, A. (2006) 'Cloning and initial characterization of a new subunit for mammalian serine-palmitoyltransferase.', *The Journal of biological chemistry*, 281(49), pp. 37275–81.

Hornemann, T., Wei, Y. and von Eckardstein, A. (2007) 'Is the mammalian serine palmitoyltransferase a high-molecular-mass complex?', *The Biochemical journal*, 405(1), pp. 157–64.

Houlden, H., King, R., Blake, J., Groves, M., Love, S., Woodward, C., Hammans, S., Nicoll, J., Lennox, G., O'Donovan, D. G., Gabriel, C., Thomas, P. K. and Reilly, M. M. (2006) 'Clinical, pathological and genetic characterization of hereditary sensory and autonomic neuropathy type 1 (HSAN I).', *Brain : a journal of neurology*, 129(Pt 2), pp. 411–25.

Husted, J. a, Cook, R. J., Farewell, V. T. and Gladman, D. D. (2000) 'Methods for assessing responsiveness: a critical review and recommendations.', *Journal of clinical epidemiology*, 53(5), pp. 459–468.

Hyung, S., Yoon Lee, B., Park, J. C., Kim, J., Hur, E. M. and Francis Suh, J. K. (2015) 'Coculture of Primary Motor Neurons and Schwann Cells as a Model for in Vitro

Myelination', *Scientific Reports*, 5, p. 15122.

Indo, Y. (2001) 'Molecular Basis of Congenital Insensitivity to Pain With Anhidrosis (CIPA): Mutations and Polymorphisms in TRKA (NTRK1) Gene Encoding the Receptor Tyrosine Kinase for Nerve Growth Factor', 471, pp. 462–471.

Indo, Y., Tsuruta, M., Hayashida, Y. and Karim, M. (1996) 'Mutations in the TRKA/NGF receptor gene in patients with congenital insensitivity to pain with anhidrosis', *Nature Genetics*, 13(4), pp. 485–8.

Jenkins, B. A. and Lumpkin, E. A. (2017) 'Developing a sense of touch', *Development*, 144(22), pp. 4078–4090.

Jeong, N., Shin, Y. and Jung, J. (2013) 'Neuropathic pain in hereditary peripheral neuropathy', *J Exerc Rehabil*, 9(4), pp. 397–9.

Jiménez-Rojo, N., Sot, J., Busto, J. V, Shaw, W. a, Duan, J., Merrill, A. H., Alonso, A. and Goñi, F. M. (2014) 'Biophysical Properties of Novel 1-Deoxy-(Dihydro)ceramides Occurring in Mammalian Cells.', *Biophysical journal*, 107(12), pp. 2850–9.

Johnson, N. E., Heatwole, C., Creigh, P., McDermott, M. P., Dilek, N., Hung, M., Bounsanga, J., Tang, W., Shy, M. E. and Herrmann, D. N. (2018) 'The Charcot–Marie–Tooth Health Index: Evaluation of a Patient-Reported Outcome', *Annals of Neurology*, 84(2), pp. 225–233.

Jun, B. K., Chandra, A., Kuljis, D., Schmidt, B. P. and Eichler, F. S. (2015) 'Substrate Availability of Mutant SPT Alters Neuronal Branching and Growth Cone Dynamics in Dorsal Root Ganglia', *The Journal of Neuroscience*, 35(40), pp. 13713–13719.

Kanda, T. (2013) 'Biology of the blood – nerve barrier and its alteration in immune mediated neuropathies', *Journal of Neurology, Neurosurgery & Psychiatry*, 84, pp. 208–212.

Kanemura, S., Okumura, M., Yutani, K., Ramming, T., Hikima, T., Appenzeller-Herzog, C., Akiyama, S. and Inaba, K. (2016) 'Human ER Oxidoreductin-1-α (Ero1α) undergoes dual regulation through complementary redox interactions with protein-disulfide isomerase', *Journal of Biological Chemistry*, 291(46), pp. 23952–23964.

Khaminets, A., Heinrich, T., Mari, M., Grumati, P., Huebner, A. K., Akutsu, M., Liebmann, L.,

Stolz, A., Nietzsche, S., Koch, N., Mauthe, M., Katona, I., Qualmann, B., Weis, J., Reggiori, F., Kurth, I., Hübner, C. A. and Dikic, I. (2015) 'Regulation of endoplasmic reticulum turnover by selective autophagy', *Nature*, 522(7556), pp. 354–358.

King, R. (2013) *Microscopic anatomy:normal structure*. *Handbook of Clinical Neurology*. 1st edn. Edited by S. G and K. C. Elsevier B.V.

Kiya, T., Kawamata, T., Namiki, A. and Yamakage, M. (2011) 'Role of satellite cell-derived l-serine in the dorsal root ganglion in paclitaxel-induced painful peripheral neuropathy', *Neuroscience*, 174, pp. 190–199.

Klein, C. J. *et al.* (2011) 'Mutations in DNMT1 cause hereditary sensory neuropathy with dementia and hearing loss.', *Nature genetics*, 43(6), pp. 595–600.

Klein, R. (1994) 'Role of neurotrophins in mouse neuronal development', *FASEB J*, 10, pp. 738–44.

Kok, J. W., Nikolova-Karakashian, M., Klappe, K., Alexander, C. and Merrill, A. H. (2002) 'Dihydroceramide Biology', *Journal of Biological Chemistry*, 272(34), pp. 21128–21136.

Kornak, U. *et al.* (2014) 'Sensory neuropathy with bone destruction due to a mutation in the membrane-shaping atlastin GTPase 3', *Brain*, 137(3), pp. 683–692.

Kornmann, B. (2013) 'The molecular hug between the ER and the mitochondria', *Current Opinion in Cell Biology*, 25(4), pp. 443–448.

Kramer, R., Bielawski, J., Kistner-Griffin, E., Othman, A., Alecu, I., Ernst, D., Kornhauser, D., Hornemann, T. and Spassieva, S. (2015) 'Neurotoxic 1-deoxysphingolipids and paclitaxel-induced peripheral neuropathy', *FASEB J*, 29(11), pp. 4461–4472.

Kranz, P., Neumann, F., Wolf, A., Classen, F., Pompsch, M., Ocklenburg, T., Baumann, J., Janke, K., Baumann, M., Goepelt, K., Riffkin, H., Metzen, E. and Brockmeier, U. (2017) 'PDI is an essential redox-sensitive activator of PERK during the unfolded protein response (UPR)', *Cell Death and Disease*, 8(8), p. e2986.

Kugathasan, U. *et al.* (2019) 'Development of MRC Centre MRI calf muscle fat fraction protocol as a sensitive outcome measure in Hereditary Sensory Neuropathy Type 1',

Journal of Neurology, Neurosurgery and Psychiatry, 90, pp. 895–906.

Kurth, I., Pamminger, T., Hennings, J. C., Soehendra, D., Huebner, A. K., Rotthier, A., Baets, J., Senderek, J., Topaloglu, H., Farrell, S. a, Nürnberg, G., Nürnberg, P., De Jonghe, P., Gal, A., Kaether, C., Timmerman, V. and Hübner, C. a (2009) 'Mutations in FAM134B, encoding a newly identified Golgi protein, cause severe sensory and autonomic neuropathy.', *Nature genetics*, 41(11), pp. 1179–81.

Lafrenie, R. G. *et al.* (2004) 'Identification of a Novel Gene (HSN2) Causing Hereditary Sensory and Autonomic Neuropathy Type II through the Study of Canadian Genetic Isolates', *Am. J. Hum. Genet*, 74, pp. 1064–1073.

Lallemend, F. and Ernfors, P. (2012) 'Molecular interactions underlying the specification of sensory neurons', *Trends in Neurosciences*, 35(6), pp. 373–381.

Laurà, M., Hutton, E. J., Blake, J., Lunn, M. P., Fox, Z., Pareyson, D., Solari, A., Radice, D., Koltzenburg, M. and Reilly, M. M. (2014) 'Pain and small fiber function in charcot-marie-tooth disease type 1A', *Muscle and Nerve*, 50(3), pp. 366–371.

Lauria, G. (2005) 'Skin biopsy in the diagnosis of peripheral neuropathies', *Practical neurology*, 5, pp. 92–99.

Lauria, G., Dacci, P., Lombardi, R., Cazzato, D., Porretta-Serapiglia, C., Taiana, M., Sassone, J., Dalla Bella, E., Rinaldo, S., Lettieri, C., Eleopra, R. and Devigili, G. (2015) 'Side and time variability of intraepidermal nerve fiber density.', *Neurology*, 84(23), pp. 2368–2371.

Lawson, B. Y. S. N. and Waddell, P. J. (1991) 'Soma neurofilament immunoreactivity is related to cell size and fibre conduction velocity in rate primary sensory neurons', *Journal of Physiology*, 435, pp. 41–63.

Leanza, L., Managò, A., Zoratti, M., Gulbins, E. and Szabo, I. (2016) 'Pharmacological targeting of ion channels for cancer therapy: In vivo evidences', *Biochimica et Biophysica Acta - Molecular Cell Research*, 1863(6), pp. 1385–1397.

Lee, G., Kim, H., Elkabetz, Y., Al Shamy, G., Panagiotakos, G., Barberi, T., Tabar, V. and Studer, L. (2007) 'Isolation and directed differentiation of neural crest stem cells

derived from human embryonic stem cells', *Nature Biotechnology*, 25(12), pp. 1468–1475.

Lee, G., Papapetrou, E. P., Kim, H., Chambers, S. M., Tomishima, M. J., Fasano, C. a, Ganat, Y. M., Menon, J., Shimizu, F., Viale, A., Tabar, V., Sadelain, M. and Studer, L. (2009) 'Modelling pathogenesis and treatment of familial dysautonomia using patient-specific iPSCs.', *Nature*, 461(7262), pp. 402–6.

Lee, G., Ramirez, C. N., Kim, H., Zeltner, N., Liu, B., Radu, C., Bhinder, B., Kim, Y. J., Choi, I. Y., Mukherjee-Clavin, B., Djaballah, H. and Studer, L. (2012) 'Large-scale screening using familial dysautonomia induced pluripotent stem cells identifies compounds that rescue IKBKAP expression', *Nature Biotechnology*, 30(12), pp. 1244–1248.

Leipold, E. *et al.* (2013) 'A de novo gain-of-function mutation in SCN11A causes loss of pain perception.', *Nature genetics*, 45(11), pp. 1399–404.

Leonardis, L., Auer-Grumbach, M., Papić, L. and Zidar, J. (2012) 'The N355K atlastin 1 mutation is associated with hereditary sensory neuropathy and pyramidal tract features.', *European journal of neurology*, 19(7), pp. 992–8.

Lewin, G. R., Lisney, S. J. W. and Mendell, L. M. (1992) 'Neonatal Anti-NGF Treatment Reduces the Aδ- and C-Fibre Evoked Vasodilator Responses in Rat Skin: Evidence That Nociceptor Afferents Mediate Antidromic Vasodilatation', *European Journal of Neuroscience*, 4(12), pp. 1213–1218.

Lewis, R. A., Li, J., Fuerst, D. R., Shy, M. E. and Krajewski, K. (2003) 'Motor unit number estimate of distal and proximal muscles in Charcot-Marie-Tooth disease', *Muscle and Nerve*, 28(2), pp. 161–167.

Lewis, R. a, McDermott, M. P., Herrmann, D. N., Hoke, A., Clawson, L. L., Siskind, C., Feely, S. M. E., Miller, L. J., Barohn, R. J., Smith, P., Luebbe, E., Wu, X. and Shy, M. E. (2013) 'High-dosage ascorbic acid treatment in Charcot-Marie-Tooth disease type 1A: results of a randomized, double-masked, controlled trial.', *JAMA neurology*, 70(8), pp. 981–7.

Lindahl, A. J., Lhatoo, S. D., Campbell, M. J., Nicholson, G. and Love, S. (2006) 'Late-onset

hereditary sensory neuropathy type I due to SPTLC1 mutation: autopsy findings.', *Clinical neurology and neurosurgery*, 108(8), pp. 780–3.

Linn, S. C., Kim, H. S., Keane, E. M., Andras, L. M., Wang, E. and Merrill, A. H. (2001) 'Regulation of de novo sphingolipid biosynthesis and the toxic consequences of its disruption.', *Biochemical Society transactions*, 29(Pt 6), pp. 831–5.

Liu, M. L., Zang, T. and Zhang, C. L. (2016) 'Direct Lineage Reprogramming Reveals Disease-Specific Phenotypes of Motor Neurons from Human ALS Patients', *Cell Reports*, 14(1), pp. 115–128.

Liu, Y. and Ma, Q. (2011) 'Generation of somatic sensory neuron diversity and implications on sensory coding', *Current Opinion in Neurobiology*, 21, pp. 52–60.

Lone, M. A., Santos, T., Alecu, I., Silva, L. C. and Hornemann, T. (2019) '1-Deoxysphingolipids', *Biochimica et Biophysica Acta - Molecular and Cell Biology of Lipids*, 1864(4), pp. 512–521.

Longo, C. a, Tyler, D. and Mallampalli, R. K. (1997) 'Sphingomyelin metabolism is developmentally regulated in rat lung.', *American journal of respiratory cell and molecular biology*, 16(5), pp. 605–12.

Lowther, J., Naismith, J. H., Dunn, T. M. and Campopiano, D. J. (2012) 'Structural, mechanistic and regulatory studies of serine palmitoyltransferase.', *Biochemical Society transactions*, 40(3), pp. 547–54.

Lund, R. J., Närvä, E. and Lahesmaa, R. (2012) 'Genetic and epigenetic stability of human pluripotent stem cells', *Nature Reviews Genetics*, 13(10), pp. 732–744.

Mahley, R. W. (2016) 'Central nervous system lipoproteins: ApoE and regulation of cholesterol metabolism', *Arteriosclerosis, Thrombosis, and Vascular Biology*, 36(7), pp. 1305–1315.

Malin, S. a, Davis, B. M. and Molliver, D. C. (2007) 'Production of dissociated sensory neuron cultures and considerations for their use in studying neuronal function and plasticity.', *Nature protocols*, 2(1), pp. 152–60.

Mandon, E. C., Echten, G., Birk, R., Schmidt, R. R. and Sandhoff, K. (1991) 'Sphingolipid

biosynthesis in cultured neurons. Down-regulation of serine palmitoyltransferase by sphingoid bases', *European Journal of Biochemistry*, 198(3), pp. 667–674.

Mandon, E. C., Ehses, I., Rother, J., Echten, G. Van and Sandhoffg, K. (1992) 'Subcellular Localization and Membrane Topology Serine of Palmitoyltransferase , 3-Dehydrosphinganine Reductase , and Sphinganine N-Acyltransferase in Mouse Liver', *J Biol Chem*, 267(16), pp. 11144–8.

Mannil, M. *et al.* (2014) 'Selected items from the Charcot-Marie-Tooth (CMT) Neuropathy Score and secondary clinical outcome measures serve as sensitive clinical markers of disease severity in CMT1A patients.', *Neuromuscular disorders*, 24, pp. 1003–1017.

Marchi, S., Patergnani, S., Missiroli, S., Morciano, G., Rimessi, A., Wieckowski, M. R., Giorgi, C. and Pinton, P. (2017) 'Mitochondrial and endoplasmic reticulum calcium homeostasis and cell death', *Cell Calcium*, 69, pp. 62–72.

Mardinoglu, A., Agren, R., Kampf, C., Asplund, A., Uhlen, M. and Nielsen, J. (2014) 'Genome-scale metabolic modelling of hepatocytes reveals serine deficiency in patients with non-alcoholic fatty liver disease', *Nature Communications*, 5(May 2013), pp. 1–11.

Marin, R. and Diaz, M. (2018) 'Estrogen interactions with lipid rafts related to neuroprotection. Impact of brain ageing and menopause', *Frontiers in Neuroscience*, 12(Mar), pp. 1–18.

Marmigère, F. and Ernfors, P. (2007) 'Specification and connectivity of neuronal subtypes in the sensory lineage', *Nature Reviews Neuroscience*, 8(2), pp. 114–127.

Marshall, L. L., Stimpson, S. E., Hyland, R., Coorssen, J. R. and Myers, S. J. (2014) 'Increased lipid droplet accumulation associated with a peripheral sensory neuropathy', *Journal of Chemical Biology*, 7(2), pp. 67–76.

Marsick, B., San Miguel-Ruiz, J. and Letourneau, P. (2012) 'Activation of ERM mediates attractive growth cone guidance through regulation of growth cone actin and adhesion receptors', *J Neuroscience*, 32(1), pp. 282–296.

Matsuda, S., Kobayashi, N., Wakisaka, H., Saito, S. and Saito, K. (2000) 'Morphological Transformation of Sensory Ganglion Neurons and', *Biomedical Reviews*, 11(January), pp. 39–52.

McArthur, J. C., Stocks, E. A., Hauer, P., Cornblath, D. R. and Griffin, J. W. (1998) 'Epidermal Nerve Fiber Density', *Archives of Neurology*, 55(12), pp. 1513–1520.

McCampbell, A., Truong, D., Broom, D. C., Allchorne, A., Gable, K., Cutler, R. G., Mattson, M. P., Woolf, C. J., Frosch, M. P., Harmon, J. M., Dunn, T. M. and Brown, R. H. (2005) 'Mutant SPTLC1 dominantly inhibits serine palmitoyltransferase activity in vivo and confers an age-dependent neuropathy.', *Human molecular genetics*, 14(22), pp. 3507–21.

McCoy, E., Taylor-Blake, E., Street, S., Pribisko, A., Zheng, J. and Zylka, M. (2014) 'Peptidergic CGRP alpha primary sensory neurons encode heat and itch and tonically suppress sensitivity to cold', *Neuron*, 78(1), pp. 138–151.

McDermott, L. A., Weir, G. A., Themistocleous, A. C., Segerdahl, A. R., Blesneac, I., Baskozos, G., Clark, A. J., Millar, V., Peck, L. J., Ebner, D., Tracey, I., Serra, J. and Bennett, D. L. (2019) 'Defining the Functional Role of Na V 1.7 in Human Nociception', *Neuron*, 101(5), pp. 905–919.

Mead, S. *et al.* (2013) 'A Novel Prion Disease Associated with Diarrhea and Autonomic Neuropathy', *New England Journal of Medicine*, 369(20), pp. 1904–1914.

Merkies, I. S. J. and Lauria, G. (2006) '131st ENMC international workshop: selection of outcome measures for peripheral neuropathy clinical trials 10-12 December 2004, Naarden, The Netherlands.', *Neuromuscular disorders*, 16(2), pp. 149–56.

Merkies, I. S. J., Lauria, G. and Faber, C. G. (2012) 'Outcome measures in peripheral neuropathies: requirements through statements.', *Current opinion in neurology*, 25(5), pp. 556–63.

Mertens, J., Paquola, A. C. M., Ku, M., Hatch, E., Böhnke, L., Ladjevardi, S., McGrath, S., Campbell, B., Lee, H., Herdy, J. R., Gonçalves, J. T., Toda, T., Kim, Y., Winkler, J., Yao, J., Hetzer, M. W. and Gage, F. H. (2015) 'Directly Reprogrammed Human Neurons Retain Aging-Associated Transcriptomic Signatures and Reveal Age-

Related Nucleocytoplasmic Defects', *Cell Stem Cell*, 17(6), pp. 705–718.

Micallef, J. *et al.* (2009) 'Effect of ascorbic acid in patients with Charcot-Marie-Tooth disease type 1A: a multicentre, randomised, double-blind, placebo-controlled trial.', *Lancet neurology*, 8(12), pp. 1103–1110.

Middel, B. and van Sonderen, E. (2002) 'Statistical significant change versus relevant or important change in (quasi) experimental design: some conceptual and methodological problems in estimating magnitude of intervention-related change in health services research.', *International journal of integrated care*, 2(December), p. e15.

Miller, J. D., Ganat, Y. M., Kishinevsky, S., Bowman, R. L., Liu, B., Tu, E. Y., Mandal, P. K., Vera, E., Shim, J. W., Kriks, S., Taldone, T., Fusaki, N., Tomishima, M. J., Krainc, D., Milner, T. A., Rossi, D. J. and Studer, L. (2013) 'Human iPSC-based modeling of late-onset disease via progerin-induced aging', *Cell Stem Cell*, 13(6), pp. 691–705.

Mizisin, A. P. and Weerasuriya, A. (2011) 'Homeostatic regulation of the endoneurial microenvironment during development , aging and in response to trauma , disease and toxic insult', *Acta Neuropathol*, 121, pp. 291–312.

Molenaar, D. S., de Haan, R. and Vermeulen, M. (1995) 'Impairment, disability, or handicap in peripheral neuropathy: analysis of the use of outcome measures in clinical trials in patients with peripheral neuropathies.', *Journal of Neurology, Neurosurgery & Psychiatry*, 59(2), pp. 165–169.

Morrow, J. M., Sinclair, C. D. J., Fischmann, A., Machado, P. M., Reilly, M. M., Yousry, T. A., Thornton, J. S. and Hanna, M. G. (2015) 'MRI biomarker assessment of neuromuscular disease progression: a prospective observational cohort study', *The Lancet Neurology*, 4422(15), pp. 1–13.

Muller, F. J., Schuldt, B. M., Williams, R., Mason, D., Altun, G., Papapetrou, E. P., Danner, S., Goldmann, J. E., Herbst, A., Schmidt, N. O., Aldenhoff, J. B., Laurent, L. C. and Loring, J. F. (2011) 'A bioinformatic assay for pluripotency in human cells', *Nature Methods*, 8(4), pp. 315–317.

Murphy, S. M., Ernst, D., Wei, Y., Laurà, M., Liu, Y.-T., Polke, J., Blake, J., Winer, J.,

Houlden, H., Hornemann, T. and Reilly, M. M. (2013) ‘Hereditary sensory and autonomic neuropathy type 1 (HSANI) caused by a novel mutation in SPTLC2.’, *Neurology*, 80(23), pp. 2106–2111.

Murphy, S. M., Herrmann, D. N., McDermott, M. P., Scherer, S. S., Shy, M. E., Reilly, M. M. and Pareyson, D. (2011) ‘Reliability of the CMT neuropathy score (second version) in Charcot-Marie-Tooth disease.’, *Journal of the peripheral nervous system*, 16(3), pp. 191–8.

Mwinyi, J., Boström, A., Fehrer, I., Othman, A., Waeber, G., Marti-Soler, H., Vollenweider, P., Marques-Vidal, P., Schiöth, H. B., Von Eckardstein, A. and Hornemann, T. (2017) ‘Plasma 1-deoxysphingolipids are early predictors of incident type 2 diabetes mellitus’, *PLoS ONE*, 12(5), pp. 1–12.

Myers, S. J., Malladi, C. S., Hyland, R. A., Bautista, T., Boadle, R., Robinson, P. J. and Nicholson, G. A. (2014) ‘Mutations in the SPTLC1 protein cause mitochondrial structural abnormalities and endoplasmic reticulum stress in lymphoblasts.’, *DNA and cell biology*, 33(7), pp. 399–407.

Nagiec, M. M., Baltisberger, J. A., Wells, G. B., Lester, R. L. and Dickson, R. C. (1994) ‘The LCB2 gene of Saccharomyces and the related LCBJ gene encode subunits of serine palmitoyltransferase , the initial enzyme in sphingolipid synthesis’, *Proc. Natl. Acad. Sci.*, 91(August), pp. 7899–7902.

Nélaton M (1852) ‘Affection singuliere des os du pied’, *Gazette des Hopitaux Civils et Militaires*, 4, p. 13.

Nicholson, G. A. a, Dawkins, J. L. L., Blair, I. P. P., Auer-Grumbach, M., Brahmbhatt, S. B. B. and Hulme, D. J. J. (2002) ‘Hereditary Sensory Neuropathy Type I: Haplotype Analysis Shows Founders in Southern England and Europe’, *The American Journal of Human Genetics*, 69(3), pp. 655–659.

Nicholson, G., Dawkins, J. and Blair, I. (1996) ‘The gene for hereditary sensory neuropathy type I (HSN–I) maps to chromosome 9q22. 1–q22. 3’, *Nat Genet*, 13(1), pp. 101–104.

Okumura, M., Kadokura, H. and Inaba, K. (2015) ‘Structures and functions of protein

disulfide isomerase family members involved in proteostasis in the endoplasmic reticulum', *Free Radical Biology and Medicine*, 83, pp. 314–322.

Oswald, M. C. W., West, R. J. H., Lloyd-Evans, E. and Sweeney, S. T. (2015) 'Identification of dietary alanine toxicity and trafficking dysfunction in a Drosophila model of hereditary sensory and autonomic neuropathy type 1', *Human Molecular Genetics*, 24(24), pp. 6899–6909.

Othman, a, Rütti, M. F., Ernst, D., Saely, C. H., Rein, P., Drexel, H., Porretta-Serapiglia, C., Lauria, G., Bianchi, R., von Eckardstein, a and Hornemann, T. (2012) 'Plasma deoxysphingolipids: a novel class of biomarkers for the metabolic syndrome?', *Diabetologia*, 55(2), pp. 421–31.

Othman, A., Benghozi, R., Alecu, I., Wei, Y., Niesor, E., Von Eckardstein, A. and Hornemann, T. (2015) 'Fenofibrate lowers atypical sphingolipids in plasma of dyslipidemic patients: A novel approach for treating diabetic neuropathy?', *Journal of Clinical Lipidology*, 9(4), pp. 568–575.

Othman, A., Bianchi, R., Alecu, I., Wei, Y. and Porretta-serapiglia, C. (2015) 'Lowering Plasma 1-Deoxysphingolipids Improves Neuropathy in Diabetic Rats', *Diabetes*, 64(3), pp. 1035–45.

Othman, A., Saely, C. H., Muendlein, A., Vonbank, A., Drexel, H., von Eckardstein, A. and Hornemann, T. (2015) 'Plasma 1-deoxysphingolipids are predictive biomarkers for type 2 diabetes mellitus', *BMJ Open Diabetes Research and Care*, 3(1), pp. 1–9.

Owen, D. E. and Egerton, J. (2012) 'Culture of dissociated sensory neurons from dorsal root ganglia of postnatal and adult rats', *Methods Mol Biol,* 846, pp. 179–187.

Parakh, S. and Atkin, J. D. (2015) 'Novel roles for protein disulphide isomerase in disease states: a double edged sword?', *Frontiers in Cell and Developmental Biology*, 3(May), pp. 1–11.

Parakh, S., Spencer, D. M., Halloran, M. A., Soo, K. Y. and Atkin, J. D. (2013) 'Redox regulation in amyotrophic lateral sclerosis', *Oxidative medicine and cellular longevity*, 2013, p. 408681.

Pareyson, D., Reilly, M. M., Schenone, A., Fabrizi, G. M., Cavallaro, T., Santoro, L., Vita, G., Quattrone, A., Padua, L., Gemignani, F., Visioli, F., Laurà, M., Radice, D., Calabrese, D., Hughes, R. a C. and Solari, A. (2011) 'Ascorbic acid in Charcot-Marie-Tooth disease type 1A (CMT-TRIAAL and CMT-TRAUK): a double-blind randomised trial.', *The Lancet. Neurology*, 10(4), pp. 320–8.

Pareyson, D., Saveri, P. and Pisciotta, C. (2017) 'New developments in Charcot-Marie-Tooth neuropathy and related diseases', *Current Opinion in Neurology*, 30(5), pp. 471–480.

Pareyson, D., Scaioli, V. and Laura, M. (2006) 'Clinical and Electrophysiological Aspects of Charcot-Marie-Tooth Disease', *NeuroMolecular Medicine*, 8(1–2), pp. 3–22.

Passage, E., Norreel, J. C., Noack-Fraissignes, P., Sanguedolce, V., Pizant, J., Thirion, X., Robaglia-Schlupp, A., Pellissier, J. F. and Fontés, M. (2004) 'Ascorbic acid treatment corrects the phenotype of a mouse model of Charcot-Marie-Tooth disease', *Nature Medicine*, 10(4), pp. 396–401.

Patani, R. (2016) 'Generating Diverse Spinal Motor Neuron Subtypes from Human Pluripotent Stem Cells', *Stem Cells Int*, 2016, p. 1036974.

Patzkó, Á., Bai, Y., Saporta, M. A., Katona, I., Wu, X., Vizzuso, D., Feltri, M. L., Wang, S., Dillon, L. M., Kamholz, J., Kirschner, D., Sarkar, F. H., Wrabetz, L. and Shy, M. E. (2012) 'Curcumin derivatives promote Schwann cell differentiation and improve neuropathy in R98C CMT1B mice', *Brain*, 135(12), pp. 3551–3566.

Penno, A., Reilly, M. M., Houlden, H., Laurá, M., Rentsch, K., Niederkofler, V., Stoeckli, E. T., Nicholson, G., Eichler, F., Brown, R. H., von Eckardstein, A. and Hornemann, T. (2010) 'Hereditary sensory neuropathy type 1 is caused by the accumulation of two neurotoxic sphingolipids.', *The Journal of biological chemistry*, 285(15), pp. 11178–87.

Perri, E. R., Thomas, C. J., Parakh, S., Spencer, D. M. and Atkin, J. D. (2016) 'The Unfolded Protein Response and the Role of Protein Disulfide Isomerase in Neurodegeneration', *Frontiers in Cell and Developmental Biology*, 3(January), pp. 1–17.

Petropoulos, I. N., Ponirakis, G., Khan, A., Almuhannadi, H., Gad, H. and Malik, R. A. (2018) 'Diagnosing diabetic neuropathy: Something old, something new', *Diabetes and Metabolism Journal*, 42(4), pp. 255–269.

Pfau, D. B., Krumova, E. K., Treede, R. D., Baron, R., Toelle, T., Birklein, F., Eich, W., Geber, C., Gerhardt, A., Weiss, T., Magerl, W. and Maier, C. (2014) 'Quantitative sensory testing in the German Research Network on Neuropathic Pain (DFNS): Reference data for the trunk and application in patients with chronic postherpetic neuralgia', *Pain*. International Association for the Study of Pain, 155(5), pp. 1002–1015.

Piscosquito, G., Reilly, M. M., Schenone, A., Fabrizi, G. M., Cavallaro, T., Santoro, L., Manganelli, F., Vita, G., Quattrone, A., Padua, L., Gemignani, F., Visioli, F., Laurà, M., Calabrese, D., Hughes, R. A. C., Radice, D., Solari, A. and Pareyson, D. (2015) 'Responsiveness of clinical outcome measures in Charcot-Marie-Tooth disease', *European Journal of Neurology*, 22(12), pp. 1556–1563.

Preston, D. and Shapiro, B. (2005) *Electromyography and Neuromuscular Disorders*. Second. Elsevier

Priestley, J. V, Michael, G. J., Averill, S., Liu, M. and Willmott, N. (2002) 'Regulation of nociceptive neurons by nerve growth factor and glial cell line derived neurotrophic factor', *Canadian Journal of Physiology and Pharmacology*, 80(5), pp. 495–505.

Rajabally, Y. and Cavanna, A. (2015) 'Health related quality of life in chronic neuropathies: A systematic review', *J Neurological Sciences*, 348, pp. 18–23.

Rautenstrauss B, Neitzel B, M. C. et al (2009) 'Late onset hereditary sensory neuropathie type 1 (HSN1) caused by a p.C133R missense mutation in SPTLC1', *J Periph Nerv Syst*, 14(Supplement), pp. 124–5.

Reilly, M. M., Shy, M. E., Muntoni, F. and Pareyson, D. (2010) '168th ENMC International Workshop: outcome measures and clinical trials in Charcot-Marie-Tooth disease (CMT).', *Neuromuscular disorders*, 20(12), pp. 839–46.

Reinhold, A. K. and Rittner, H. L. (2020) 'Characteristics of the nerve barrier and the blood dorsal root ganglion barrier in health and disease', *Experimental Neurology*,

327(January), p. 113244.

Rivière, J.-B. *et al.* (2011) 'KIF1A, an axonal transporter of synaptic vesicles, is mutated in hereditary sensory and autonomic neuropathy type 2.', *American journal of human genetics*, 89(2), pp. 219–30.

Roach, K. E. (2006) 'Measurement of Health Outcomes: Reliability, Validity and Responsiveness', *Journal of Prosthetics and Orthotics*, 18(6), pp. P8–P12.

Rodriguez-Cuenca, S., Barbarroja, N. and Vidal-Puig, A. (2015) 'Dihydroceramide desaturase 1, the gatekeeper of ceramide induced lipotoxicity', *Biochimica et Biophysica Acta - Molecular and Cell Biology of Lipids*, 1851(1), pp. 40–50.

Rolke, R., Magerl, W., Campbell, K. A., Schalber, C., Caspari, S., Birklein, F. and Treede, R.-D. (2006) 'Quantitative sensory testing: a comprehensive protocol for clinical trials.', *European journal of Pain*, 10, pp. 77–88.

Rossor, A. M., Evans, M. R. B. and Reilly, M. M. (2015) 'A practical approach to the genetic neuropathies', *Practical Neurology*, 15(3), pp. 187–198.

Rossor, A. M., Polke, J. M., Houlden, H. and Reilly, M. M. (2013) 'Clinical implications of genetic advances in charcot-marie-tooth disease', *Nature Reviews Neurology*, 9(10), pp. 562–571.

Rotta, L. N., Da Silva, C. G., Perry, M. L. and Trindade, V. M. (1999) 'Undernutrition decreases serine palmitoyltransferase activity in developing rat hypothalamus.', *Annals of nutrition & metabolism*, 43(3), pp. 152–8.

Rotthier, A., Auer-Grumbach, M., Janssens, K., Baets, J., Penno, A., Almeida-Souza, L., Van Hoof, K., Jacobs, A., De Vriendt, E., Schlotter-Weigel, B., Löscher, W., Vondráček, P., Seeman, P., De Jonghe, P., Van Dijck, P., Jordanova, A., Hornemann, T. and Timmerman, V. (2010) 'Mutations in the SPTLC2 subunit of serine palmitoyltransferase cause hereditary sensory and autonomic neuropathy type I.', *American journal of human genetics*, 87(4), pp. 513–22.

Rotthier, A., Baets, J., Timmerman, V. and Janssens, K. (2012) 'Mechanisms of disease in hereditary sensory and autonomic neuropathies.', *Nature reviews. Neurology*,

8(2), pp. 73–85.

Rotthier, A., Baets, J., De Vriendt, E., Jacobs, A., Auer-Grumbach, M., Lévy, N., Bonello-Palot, N., Kilic, S. S., Weis, J., Nascimento, A., Swinkels, M., Kruyt, M. C., Jordanova, A., De Jonghe, P. and Timmerman, V. (2009) 'Genes for hereditary sensory and autonomic neuropathies: a genotype-phenotype correlation.', *Brain*, 132(Pt 10), pp. 2699–711.

Rotthier, A., Penno, A., Rautenstrauss, B., Auer-Grumbach, M., Stettner, G. M., Asselbergh, B., Van Hoof, K., Sticht, H., Lévy, N., Timmerman, V., Hornemann, T. and Janssens, K. (2011) 'Characterization of two mutations in the SPTLC1 subunit of serine palmitoyltransferase associated with hereditary sensory and autonomic neuropathy type I.', *Human mutation*, 32(6), pp. E2211-25.

Roussel, B. D., Kruppa, A. J., Miranda, E., Crowther, D. C., Lomas, D. A. and Marciniak, S. J. (2013) 'Endoplasmic reticulum dysfunction in neurological disease', *The Lancet Neurology*, 12(1), pp. 105–118.

Sadjadi, R., Reilly, M. M., Shy, M. E., Pareyson, D., Laura, M., Murphy, S., Feely, S. M. E., Grider, T., Bacon, C., Calabrese, D. and Burns, T. M. (2014) 'Psychometrics evaluation of Charcot-Marie-Tooth Neuropathy Score (CMTNSv2) second version , using Rasch analysis', *Journal of the Peripheral Nervous System*, 19, pp. 192–196.

Sakai, K., Shimba, K., Kotani, K. and Jimbo, Y. (2017) 'A co-culture microtunnel technique demonstrating a significant contribution of unmyelinated Schwann cells to the acceleration of axonal conduction in Schwann cell-regulated peripheral nerve development', *Integrative Biology*, 9(8), pp. 678–686.

Salcedo, M., Cuevas, C., Alonso, J. L., Otero, G., Faircloth, G., Fernandez-Sousa, J. M., Avila, J. and Wandosell, F. (2007) 'The marine sphingolipid-derived compound ES 285 triggers an atypical cell death pathway', *Apoptosis*, 12(2), pp. 395–409.

Sánchez, A. M., Malagarie-Cazenave, S., Olea, N., Vara, D., Cuevas, C. and Díaz-Laviada, I. (2008) 'Spisulosine (ES-285) induces prostate tumor PC-3 and LNCaP cell death by de novo synthesis of ceramide and PKCζ activation', *European Journal of Pharmacology*, 584(2–3), pp. 237–245.

Sandelius, Å., Zetterberg, H., Blennow, K., Adiutori, R., Malaspina, A., Laura, M., Reilly, M. M. and Rossor, A. M. (2018) 'Plasma neurofilament light chain concentration in the inherited peripheral neuropathies', *Neurology*, 90(6), pp. e518–e524.

Sandoe, J. and Eggan, K. (2013) 'Opportunities and challenges of pluripotent stem cell neurodegenerative disease models', *Nature Neuroscience,* 16(7), pp. 780–789.

Saporta, M. A., Dang, V., Volfson, D., Zou, B., Xie, X. S., Adebola, A., Liem, R. K., Shy, M. and Dimos, J. T. (2015) 'Axonal Charcot-Marie-Tooth disease patient-derived motor neurons demonstrate disease-specific phenotypes including abnormal electrophysiological properties', *Experimental Neurology,* 263, pp. 190–199.

Schöffski, P., Dumez, H., Ruijter, R., Miguel-Lillo, B., Soto-Matos, A., Alfaro, V. and Giaccone, G. (2011) 'Spisulosine (ES-285) given as a weekly three-hour intravenous infusion: Results of a phase i dose-escalating study in patients with advanced solid malignancies', *Cancer Chemotherapy and Pharmacology*, 68(6), pp. 1397–1403.

Schwartzentruber, J. *et al.* (2018) 'Molecular and functional variation in iPSC-derived sensory neurons', *Nature Genetics*, 50(1), pp. 54–61.

Scorrano, L., Oakes, S. A., Opferman, J. T., Cheng, E. H., Sorcinelli, M. D., Pozzan, T. and Korsmeyer, S. J. (2003) 'BAX and BAK Regulation of Endoplasmic Reticulum Ca 2+ : A Control Point for Apoptosis', 300(April), pp. 135–140.

Scroggs, R. S., Todorovic, S. M., Anderson, E. G. and Fox, A. P. (1994) 'Variation in IH, IIR, and ILEAK between acutely isolated adult rat dorsal root ganglion neurons of different size.', *Journal of neurophysiology*, 71(1), pp. 271–9.

Sereda, M. W., Meyer Zu Hörste, G., Suter, U., Uzma, N. and Nave, K. A. (2003) 'Therapeutic administration of progesterone antagonist in a model of Charcot-Marie-Tooth disease (CMT-1A)', *Nature Medicine*, 9(12), pp. 1533–1537.

Shi, Y., Inoue, H., Wu, J. C. and Yamanaka, S. (2017) 'Induced pluripotent stem cell technology: A decade of progress', *Nature Reviews Drug Discovery*, 16(2), pp. 115–130.

Shy, M. E., Blake, J., Krajewski, K., Fuerst, D. R., Laura, M., Hahn, a F., Li, J., Lewis, R. a

and Reilly, M. (2005) ‘Reliability and validity of the CMT neuropathy score as a measure of disability.’, *Neurology*, 64(7), pp. 1209–14.

Shy, M. E., Chen, L., Swan, M. E. R., Taube, B. R., Krajewski, K. M., Herrmann, M. D., Lewis, R. A. and Mcdermott, M. P. (2008) ‘Neuropathy progression in Charcot-Marie-Tooth disease type 1A’, *Neurology*, 70, pp. 378–383.

Simmen, T., Lynes, E. M., Gesson, K. and Thomas, G. (2010) ‘Oxidative protein folding in the endoplasmic reticulum: Tight links to the mitochondria-associated membrane (MAM)’, *Biochimica et Biophysica Acta - Biomembranes*, 1798(8), pp. 1465–1473.

Simovic, D. and Weinberg, D. H. (1997) ‘Terminal latency index in the carpal tunnel syndrome’, *Muscle and Nerve*, 20(9), pp. 1178–1180.

Sisková, Z., Mahad, D. J., Pudney, C., Campbell, G., Cadogan, M., Asuni, A., O’Connor, V. and Perry, V. H. (2010) ‘Morphological and functional abnormalities in mitochondria associated with synaptic degeneration in prion disease’, *American Journal of Pathology*, 177(3), pp. 1411–1421.

Slaugenhaupt, S. a., Blumenfeld, A., Gill, S. P., Leyne, M., Mull, J., Cuajungco, M. P., Liebert, C. B., Chadwick, B., Idelson, M., Reznik, L., Robbins, C. M., Makalowska, I., Brownstein, M. J., Krappmann, D., Scheidereit, C., Maayan, C., Axelrod, F. B. and Gusella, J. F. (2001) ‘Tissue-Specific Expression of a Splicing Mutation in the IKBKAP Gene Causes Familial Dysautonomia’, *The American Journal of Human Genetics*, 68(3), pp. 598–605.

Smith, M. and Wilkinson, S. (2017) ‘ER homeostasis and autophagy.’, *Essays in biochemistry*, 61(6), pp. 625–635.

Soares Moretti, A. I. and Martins Laurindo, F. R. (2017) ‘Protein disulfide isomerases: Redox connections in and out of the endoplasmic reticulum’, *Archives of Biochemistry and Biophysics*, 617, pp. 106–119.

Solari, a, Laurà, M., Salsano, E., Radice, D. and Pareyson, D. (2008) ‘Reliability of clinical outcome measures in Charcot-Marie-Tooth disease.’, *Neuromuscular disorders*, 18(1), pp. 19–26.

Soldner, F. and Jaenisch, R. (2012) 'iPSC Disease Modeling', *Science*, 338(6111), pp. 1155–1156.

Sousa-Valente, J., Andreou, A. P., Urban, L. and Nagy, I. (2014) 'Transient receptor potential ion channels in primary sensory neurons as targets for novel analgesics', *British Journal of Pharmacology*, 171(10), pp. 2508–2527.

Spring, P. J., Kok, C., Nicholson, G. a, Ing, A. J., Spies, J. M., Bassett, M. L., Cameron, J., Kerlin, P., Bowler, S., Tuck, R. and Pollard, J. D. (2005) 'Autosomal dominant hereditary sensory neuropathy with chronic cough and gastro-oesophageal reflux: clinical features in two families linked to chromosome 3p22-p24.', *Brain*, 128(Pt 12), pp. 2797–810.

Steiner, R., Saied, E. M., Othman, A., Arenz, C., Maccarone, A. T., Poad, B. L. J., Blanksby, S. J., von Eckardstein, A. and Hornemann, T. (2016) 'Elucidating the chemical structure of native 1-deoxysphingosine', *Journal of Lipid Research*, 57(7), pp. 1194–1203.

Stifani, N. (2014) 'Motor neurons and the generation of spinal motor neuron diversity', *Frontiers in Cellular Neuroscience*, 8(October), pp. 1–22.

Stimpson, S. E., Coorssen, J. R. and Myers, S. J. (2014) 'Mitochondrial protein alterations in a familial peripheral neuropathy caused by the V144D amino acid mutation in the sphingolipid protein, SPTLC1', *Journal of Chemical Biology*, 8(1), pp. 25–35.

Stirling, J., Curry, A. and Eyden, B. (eds) (2013) *Diagnostic Electron Microscopy. A Practical Guide to Interpretation and Technique*. Wiley

Stockmann-Juvala, H. and Savolainen, K. (2008) 'A review of the toxic effects and mechanisms of action of fumonisin B1.', *Hum. Exp. Toxicol,* 27(11), pp. 799–809.

Studer, L., Vera, E. and Cornacchia, D. (2015) 'Programming and Reprogramming Cellular Age in the Era of Induced Pluripotency', *Cell Stem Cell*, 16(6), pp. 591–600.

Sun, Y., Lim, Y., Li, F., Liu, S., Lu, J.-J., Haberberger, R., Zhong, J.-H. and Zhou, X.-F. (2012) 'ProBDNF collapses neurite outgrowth of primary neurons by activating RhoA.', *PloS one*, 7(4), p. e35883.

Suriyanarayanan, S., Auranen, M., Toppila, J., Paetau, A., Shcherbii, M., Palin, E., Wei, Y., Lohioja, T., Schlotter-Weigel, B., Schön, U., Abicht, A., Rautenstrauss, B., Tyynismaa, H., Walter, M. C., Hornemann, T. and Ylikallio, E. (2016) 'The Variant p.(Arg183Trp) in SPTLC2 Causes Late-Onset Hereditary Sensory Neuropathy', *NeuroMolecular Medicine*, 18(1), pp. 81–90.

Suriyanarayanan, S., Othman, A., Dräger, B., Schirmacher, A., Young, P., Mulahasanovic, L., Hörtnagel, K., Biskup, S., von Eckardstein, A., Hornemann, T. and Lone, M. A. (2019) 'A Novel Variant (Asn177Asp) in SPTLC2 Causing Hereditary Sensory Autonomic Neuropathy Type 1C', *NeuroMolecular Medicine*, 21(2), pp. 182–191.

Taberner, F. J., Fernández-Ballester, G., Fernández-Carvajal, A. and Ferrer-Montiel, A. (2015) 'TRP channels interaction with lipids and its implications in disease', *Biochimica et Biophysica Acta - Biomembranes*, 1848(9), pp. 1818–1827.

Takahashi, K., Tanabe, K., Ohnuki, M., Narita, M., Ichisaka, T., Tomoda, K. and Yamanaka, S. (2007) 'Induction of Pluripotent Stem Cells from Adult Human Fibroblasts by Defined Factors', *Cell*, 131(5), pp. 861–872.

Takahashi, K. and Yamanaka, S. (2006) 'Induction of Pluripotent Stem Cells from Mouse Embryonic and Adult Fibroblast Cultures by Defined Factors', *Cell*, 126(4), pp. 663–676.

Takahashi, K. and Yamanaka, S. (2016) 'A decade of transcription factor-mediated reprogramming to pluripotency', *Nature Reviews Molecular Cell Biology*, 17(3), pp. 183–193.

Tang, Y., Liu, M.-L., Zang, T. and Zhang, C.-L. (2017) 'Direct Reprogramming Rather than iPSC-Based Reprogramming Maintains Aging Hallmarks in Human Motor Neurons', *Frontiers in Molecular Neuroscience*, 10(November), pp. 1–13.

Tapia, N. and Schöler, H. R. (2016) 'Molecular Obstacles to Clinical Translation of iPSCs', *Cell Stem Cell*, 19(3), pp. 298–309.

Themistocleous, A. C., Ramirez, J. D., Serra, J. and Bennett, D. L. H. (2014) 'The clinical approach to small fibre neuropathy and painful channelopathy.', *Practical neurology*, 14(6), pp. 368–379.

Triplett, J., Nicholson, G., Sue, C., Hornemann, T. and Yiannikas, C. (2019) 'Hereditary sensory and autonomic neuropathy type IC accompanied by upper motor neuron abnormalities and type II juxtafoveal retinal telangiectasias', *Journal of the Peripheral Nervous System*, 24, pp. 224–229.

Tsibris, J. C., Hunt, L. T., Ballejo, G., Barker, W. C., Toney, L. J. and Spellacy, W. N. (1989) 'Selective inhibition of protein disulfide isomerase by estrogens.', *The Journal of biological chemistry*, 264(24), pp. 13967–70.

Tucker, B. a, Rahimtula, M. and Mearow, K. M. (2006) 'Laminin and growth factor receptor activation stimulates differential growth responses in subpopulations of adult DRG neurons.', *The European journal of neuroscience*, 24(3), pp. 676–90.

Ubogu, E. E. (2013) 'The molecular and biophysical characterization of the human blood-nerve barrier: Current concepts', *Journal of Vascular Research*, 50(4), pp. 289–303.

Uncini, A. and Vallat, J. M. (2018) 'Autoimmune nodo-paranodopathies of peripheral nerve: The concept is gaining ground', *Journal of Neurology, Neurosurgery and Psychiatry*, 89(6), pp. 627–635.

Vance, J., Speer, M., Stajich, J., West, S., Wolpert, C., Gaskel, P., Lennon, F., Tim, R. and Rozear, M. (1996) 'Misclassification and Linkage of Hereditary Sensory and Autonomic Neuropathy Type 1 as Charcot-Marie- Tooth Disease, Type 2B', *Am. J. Hum. Genet.*, 59, pp. 258–260.

Vanhecke, D., Graber, W. and Studer, D. (2008) 'Chapter 9 Close-to-Native Ultrastructural Preservation by High Pressure Freezing', *Methods in Cell Biology*, 88(08), pp. 151–164.

Verhamme, C., de Haan, R. J., Vermeulen, M., Baas, F., de Visser, M. and van Schaik, I. N. (2009) 'Oral high dose ascorbic acid treatment for one year in young CMT1A patients: a randomised, double-blind, placebo-controlled phase II trial.', *BMC medicine*, 7, p. 70.

Verhoeven, K., Coen, K., De Vriendt, E., Jacobs, a., Van Gerwen, V., Smouts, I., Pou-Serradell, a., Martin, J.-J., Timmerman, V. and De Jonghe, P. (2004) 'SPTLC1 mutation in twin sisters with hereditary sensory neuropathy type I', *Neurology*,

62(6), pp. 1001–1002.

Verhoeven, K., De Jonghe, P., Coen, K., Verpoorten, N., Auer-Grumbach, M., Kwon, J. M., FitzPatrick, D., Schmedding, E., De Vriendt, E., Jacobs, A., Van Gerwen, V., Wagner, K., Hartung, H.-P. and Timmerman, V. (2003) 'Mutations in the small GTP-ase late endosomal protein RAB7 cause Charcot-Marie-Tooth type 2B neuropathy.', *American journal of human genetics*, 72(3), pp. 722–7.

Vetrugno, R., Liguori, R., Cortelli, P. and Montagna, P. (2003) 'Sympathetic skin response: basic mechanisms and clinical applications.', *Clinical autonomic research*, 13(4), pp. 256–70.

Vilar, E., Grünwald, V., Schöffski, P., Singer, H., Salazar, R., Iglesias, J. L., Casado, E., Cullell-Young, M., Baselga, J. and Tabernero, J. (2012) 'A phase I dose-escalating study of ES-285, a marine sphingolipid-derived compound, with repeat dose administration in patients with advanced solid tumors', *Investigational New Drugs*, 30(1), pp. 299–305.

Vincent, A. E., Ng, Y. S., White, K., Davey, T., Mannella, C., Falkous, G., Feeney, C., Schaefer, A. M., McFarland, R., Gorman, G. S., Taylor, R. W., Turnbull, D. M. and Picard, M. (2016) 'The Spectrum of Mitochondrial Ultrastructural Defects in Mitochondrial Myopathy', *Scientific Reports*, 6(July), pp. 1–12.

Wainger, B. J., Buttermore, E. D., Oliveira, J. T., Mellin, C., Lee, S., Saber, W. A., Wang, A. J., Ichida, J. K., Chiu, I. M., Barrett, L., Huebner, E. A., Bilgin, C., Tsujimoto, N., Brenneis, C., Kapur, K., Rubin, L. L., Eggan, K. and Woolf, C. J. (2015) 'Modeling pain in vitro using nociceptor neurons reprogrammed from fibroblasts', *Nature Neuroscience*, 18(1), pp. 17–24.

Walter, P. and Ron, D. (2011) 'the Unfolded Protein Response ':, *Science*, 334(6059), pp. 1081–6.

Ware, J., Kosinski, M., Bjorner, J., Turner-Bowker, D., Gandek, B. and Maruish, M. (2007) *User's Manual fo rthe SF-36v2TM Health Survey*. Edited by 2nd. Lincoln, RI,QualityMetrid Incorporated

Wei, J., Yerokun, T., Leipelt, M., Haynes, C., Radhakrishna, H., Momin, A., Kelly, S., Park,

H., Wang, E., Carton, J., Uhlinger, D. and Merrill, A. (2009) ‘Serine palmitoyltransferase subunit 1 is present in the endoplasmic reticulum, nucleus and focal adhesions and functions in cell morphology’, *Biochim Biophys Acta*, 1791(8), pp. 746–756.

Wei, N., Pan, J., Pop-Busui, R., Othman, A., Alecu, I., Hornemann, T. and Eichler, F. S. (2014) ‘Altered sphingoid base profiles in type 1 compared to type 2 diabetes’, *Lipids in Health and Disease*, 13(1), pp. 2–5.

Weiss, B. and Stoffel, W. (1997) ‘Human and Murine Serine-Palmitoyl-CoA Transferase. Cloning, Expression and Characterization of the Key Enzyme in Sphingolipid Synthesis’, *European Journal of Biochemistry*, 249(1), pp. 239–247.

Willis, T. A. *et al.* (2013) ‘Quantitative Muscle MRI as an Assessment Tool for Monitoring Disease Progression in LGMD2I: A Multicentre Longitudinal Study’, *PLoS ONE*, 8(8), pp. 6–12.

Wilson, E. R., Bernadett, K., Kugathasan, U., Clark, A. J., Bennett, D. L. H., Abramov, A., Reilly, M. M. and Greensmith, L. (2017) ‘2017 Peripheral Nerve Society Meeting July 8-12, 2017 Sitges, Barcelona, Spain’, in *Journal of the Peripheral Nervous System*, p. 409.

Wilson, E. R., Kugathasan, U., Abramov, A. Y., Clark, A. J., Bennett, D. L. H., Reilly, M. M., Greensmith, L. and Kalmar, B. (2018) ‘Hereditary sensory neuropathy type 1-associated deoxysphingolipids cause neurotoxicity , acute calcium handling abnormalities and mitochondrial dysfunction in vitro’, *Neurobiology of Disease*, 117(May), pp. 1–14.

Woolf, C. J. and Ma, Q. (2007) ‘Nociceptors--noxious stimulus detectors.’, *Neuron*, 55(3), pp. 353–64.

World Health Organisation (2013) ‘A practical Manual for using the International Classification of Functioning, Disability and Health’, *World Health Organisation, 2013*, (October).

Wozniak, M., Young, P. and Gess, B. (2015) ‘P188. Gender-dependent differences in a cohort of Charcot-Marie-tooth (CMT) patients’, *Clinical Neurophysiology*.

International Federation of Clinical Neurophysiology, 126(8), pp. e167–e168.

Wu, Y., Whiteus, C., Xu, C. S., Hayworth, K. J., Weinberg, R. J., Hess, H. F. and De Camilli, P. (2017) 'Contacts between the endoplasmic reticulum and other membranes in neurons', *Proceedings of the National Academy of Sciences*, 114(24), pp. E4859–E4867.

Yard, B. a, Carter, L. G., Johnson, K. a, Overton, I. M., Dorward, M., Liu, H., McMahon, S. a, Oke, M., Puech, D., Barton, G. J., Naismith, J. H. and Campopiano, D. J. (2007) 'The structure of serine palmitoyltransferase; gateway to sphingolipid biosynthesis.', *Journal of molecular biology*, 370(5), pp. 870–86.

Ye, Y., Dang, D., Viet, C. T., Dolan, J. C. and Schmidt, B. L. (2012) 'Analgesia targeting IB4-positive neurons in cancer-induced mechanical hypersensitivity.', *The journal of pain* 13(6), pp. 524–31.

Young, G. T., Gutteridge, A., Fox, H. D. E., Wilbrey, A. L., Cao, L., Cho, L. T., Brown, A. R., Benn, C. L., Kammonen, L. R., Friedman, J. H., Bictash, M., Whiting, P., Bilsland, J. G. and Stevens, E. B. (2014) 'Characterizing human stem cell-derived sensory neurons at the single-cell level reveals their ion channel expression and utility in pain research', *Molecular Therapy*, 22(8), pp. 1530–1543.

Yuan, J., Matsuura, E., Higuchi, Y., Hashiguchi, A., Nakamura, T., Nozuma, S., Sakiyama, Y., Yoshimura, A., Izumo, S. and Takashima, H. (2013) 'Hereditary sensory and autonomic neuropathy type IID caused by an SCN9A mutation.', *Neurology*, 80(18), pp. 1641–9.

Zhao, L., Spassieva, S., Gable, K., Gupta, S. D., Shi, L.-Y., Wang, J., Bielawski, J., Hicks, W. L., Krebs, M. P., Naggert, J., Hannun, Y. A., Dunn, T. M. and Nishina, P. M. (2015) 'Elevation of 20-carbon long chain bases due to a mutation in serine palmitoyltransferase small subunit b results in neurodegeneration', *Proceedings of the National Academy of Sciences*, 112(42), pp. 12962–12967.

Zitomer, N. C., Mitchell, T., Voss, K. a, Bondy, G. S., Pruett, S. T., Garnier-Amblard, E. C., Liebeskind, L. S., Park, H., Wang, E., Sullards, M. C., Merrill, A. H. and Riley, R. T. (2009) 'Ceramide synthase inhibition by fumonisin B1 causes accumulation of 1-

deoxysphinganine: a novel category of bioactive 1-deoxysphingoid bases and 1-deoxydihydroceramides biosynthesized by mammalian cell lines and animals.', *The Journal of biological chemistry*, 284(8), pp. 4786–95.

Zuellig, R. A., Hornemann, T., Othman, A., Hehl, A. B., Bode, H., Güntert, T., Ogunshola, O. O., Saponara, E., Grabliauskaite, K., Jang, J.-H. H., Ungethuem, U., Wei, Y., von Eckardstein, A., Graf, R. and Sonda, S. (2014) 'Deoxysphingolipids, novel biomarkers for type 2 diabetes, are cytotoxic for insulin-producing cells.', *Diabetes*, 63(4), pp. 1326–39.